Transcriptional Checkpoint Response *SET* in Motion: Role for miR-106b-5p and H3K36me3 in Regulating E2F-Dependent Transcription



Submitted for the degree of *Doctor of Philosophy*

MRC Oxford Institute for Radiation Oncology

Michaelmas Term 2021

Linda van Bijsterveldt

University College, University of Oxford

Declaration

The material presented in this thesis is entirely my own, except where work that formed part of jointly-authored publications, which are listed below, has been included.

van Bijsterveldt, L., Durley, S. C., Maughan, T. S., & Humphrey, T. C. (2021). The Challenge of Combining Chemo- and Radiotherapy with Checkpoint Kinase Inhibitors. *Clinical Cancer Research*, *27*(4), 937 LP – 962. https://doi.org/10.1158/1078-0432.CCR-20-3358.

Winchester, L., van Bijsterveldt, L., Dhawan, A., Wigfield, S., Triantafyllidis, C., Haider, S., McIntyre, A., Humphrey, T.C., Harris, A.L., & Buffa, F.M. (2021). Dicer-to-Argonaute switch controls biogenesis of oncogenic miRNA. *BioRxiv*, 2021.08.30.458145. https://doi.org/10.1101/2021.08.30.458145.

Where it concerns already published materials (or materials deposited on the *BioRxiv* preprint server), collaborative contributions have been explicitly indicated in the figure legends. I confirm that permission to reproduce any figures or tables was obtained from co-authors and that, where reference to the work of others was made, appropriate credit has been given.

This work has not been previously submitted, either partially or in full, for a qualification at this University or for a qualification at any other institution. In accordance with the Medical Sciences Division guidelines, this thesis does not exceed 50,000 words (exclusive of bibliography, appendices, figures, and tables).

Signed: Linda van Bijsterveldt

Date: 25 November 2021

Abstract

Linda van Bijsterveldt
University College
Michaelmas Term 2021

Doctor of Philosophy
Department of Oncology
University of Oxford

Non-coding RNAs are key regulators of mammalian gene expression, and their dysregulation has frequently been associated with tumourigenesis. Understanding how non-coding RNAs, and specifically miRNAs, contribute towards the aggressive nature of breast tumours by serving oncogenic or tumour suppressive roles, may help identify novel molecular biomarkers or therapeutic targets.

This thesis seeks to identify genetic drivers of altered miRNA biogenesis in breast tumours. Integrated analysis of genomic and transcriptomic data revealed recurrent amplification-dependent overexpression of *AGO2* and its interacting partner, *PABPC1.* The analysis of mature: precursor miRNA ratios showed that *AGO2* copy number amplification results in the preferential maturation of oncogenic miRNA species, including of the miR-106b/25 cluster, which promoted the silencing of known breast cancer-associated genes, such as *E2F1*, *SETD2*, and *CDKN1A*, during cancer evolution. Elevated miR-106b-5p expression caused premature S-phase entry, and both miR-106b-5p and p21 therefore demonstrated utility as prognostic markers for sensitivity to WEE1 kinase inhibition, which targets *SETD2*-deficient cancers.

Furthermore, this thesis presents an integrated analysis of miRNA-mRNA expression profiles in the response to ionising radiation and hydroxyurea treatment. This approach revealed that the early transcriptomic response to DNA damage and replication stress is universal and involves the inhibition of cell cycle progression through miR-124-3p-mediated downregulation of cytoskeletal genes. Furthermore, I identified a role for miRNAs in controlling the epigenome

in response to external stresses, such as via the miR-7704-KDM6B axis, and further confirmed the regulation of SETD2-dependent H3K36me3 by miR-106b-5p, thereby providing a functional link between miRNAs and regulation of cell cycle progression.

In the final chapter, I built on emerging evidence showing that sustained E2F-dependent transcription is required for replication stress tolerance, primarily to prevent the generation of DNA damage under low nucleotide pool conditions. Here, I established a role for SETD2-dependent H3K36 trimethylation in facilitating E2F-target gene expression in S-phase. Loss of *SETD2* caused reduced E2F1-binding to its target genes, as well as expression defects in a number of canonical E2F-transcripts, including *CDT1*, *CDC6*, and *MCM2-7.* Furthermore, E2F- and p53- gene expression changes following hydroxyurea-induced replication fork stalling were accompanied by global ATR/CHK1-dependent H3K36 trimethylation changes on the promoter regions of target genes. Taken together, these findings establish a central role for both miRNAs and SETD2-dependent H3K36me3 in the replication stress checkpoint and highlight a novel pathway through which SETD2 exerts its tumour suppressive effects.

Acknowledgements

I would like to express my sincere gratitude to my supervisor, Dr. Timothy Humphrey, for his academic supervision throughout my doctorate. He has fostered my scientific curiosity and encouraged me to drive my research projects forward. I am thankful for the learning and training opportunities he has provided during my time in Oxford.

I wish to thank all past and present members of the Humphrey group for their support, general collegiality, and insightful discussions. Special thanks to Dr. Sovan Sarkar, who showed me the ropes of scientific research, made the lab a much more enjoyable place to work, helped me source reagents from various (obscure) places in the department, excitedly discussed science with me at conferences, meetings, and over lunch time, and gave me honest and critical feedback that helped shape my thesis. I am also grateful to Dr. Sam Durley and Dr. Asmita Sharda for providing such timely and useful feedback on my written work.

This project relied heavily on collaborations with other groups and individuals based at the University of Oxford. Special thanks to all collaborators, including, but not limited to, Francesca Buffa, Andrew Dhawan, Charalampos Triantifyllidis, Nick Proudfoot, Gwendal Dujardin, Michael Tellier, Adrian Harris, Esther Bridges, and Simon Carr for their feedback, advice, and scientific contributions.

Outside of the lab, I wish to thank my parents, my grandfather, and my sister, Inge, and my friends, old and new, for their unconditional support. Their integrity, dedication, and their encouragement have cultivated a curiosity and strong desire to learn. Lastly, thank you, Julian. Thank you for your enduring compassion, encouragement, and love.

Linda van Bijsterveldt, November 2021

List of Figures

Figure 1.1 Schematic of CDK-cyclin waves in mammalian cells

Figure 1.2 Cell cycle control and DNA damage checkpoints work cooperatively to maintain genome stability

Figure 1.3 Combination therapy targets common cell cycle mutations in cancer

Figure 1.4 DICER-dependent and -independent miRNA biogenesis pathways in cancer

Figure 1.5 Cartoon illustrating known SETD2 protein domains (AA 1404-2564)

Figure 2.1 Map of the SETD2 FL (Full-Length)-GFP plasmid

Figure 2.2 Map of the SETD2 ΔSRI-GFP plasmid

Figure 2.3 Overview of library construction for miRNA- and mRNA sequencing

Figure 3.1 Somatic mutation frequency of miRNA biogenesis genes in TCGA-BRCA

Figure 3.2 Mean copy number gain/amplification frequency at genomic locations encoding miRNA biogenesis genes in TCGA-BRCA

Figure 3.3 Boxplots showing the relationship between *ADAR*, *AGO2*, *DHX9*, *MAPKAPK2*, *TARBP1* and *PAPBPC1* mRNA expression (y-axis) versus copy number value (x-axis)

Figure 3.4 Copy number profiles for 1904 cases in METABRIC

Figure 3.5 Correlation (Spearman rho) between copy number and mRNA levels of miRNA biogenesis genes in METABRIC

Figure 3.6 *AGO2* amplification is inversely correlated with *DICER1* levels in TCGA-BRCA

Figure 3.7 HCC1806 cells harbour amplification-dependent *AGO2* overexpression

Figure 3.8 Impact of siRNA-mediated AGO2 depletion on cellular survival of HCC1806 cells

Figure 3.9 Microarray profiling reveals AGO2-driven expression of a subset of miRNAs

Figure 3.10 Quantification of miR-106b-5p expression levels across a panel of BC cell lines

Figure 3.11 Plots of the correlation between *AGO2* copy number, *AGO2* mRNA, *MCM7* mRNA, and miR-106b-5p levels in a panel of BC cell lines

Figure 3.12 Correlation between *AGO2* copy number and mature: immature miR-106b levels in a panel of BC cell lines

Figure 3.13 Inhibition of AGO2 in HCC1806 cells points to preferential miRNA maturation

Figure 3.14 *MCM7* and *E2F1* expression levels following AGO2 and/or DICER1 knockdown in HCC1806 cells

Figure 3.15 AGO2 regulates miRNA maturation in JIMT-1 cells in the absence of *DICER1*

Figure 3.16 Expression of *DICER1*, *AGO2*, miR-106-3p, miR-106b-5p, and miR-93-5p in *DICER1* diploids, shallow deleted and deep deleted cases in TCGA-BRCA

Figure 3.17 *AGO2* copy number variation versus *TP53* mutation in TCGA-BRCA

Figure 4.1 miR-106b-5p expression levels in BC tumours compared to paired normal adjacent tissue (TCGA-BRCA)

Figure 4.2 Association of miR-106b-5p expression levels with expression of the major hormone and growth factor receptors, ER, PR, and HER2

Figure 4.3 miR-106b-5p expression is positively correlated with advanced tumour stage and metastases

Figure 4.4 Kaplan-Meier Survival Plots for miR-106b-5p expression in METABRIC and TCGA-BRCA TNBC cohorts

Figure 4.5 Inhibition of miR-106b-5p reduces the proliferative capacity of MDA-MB-453 and MDA-MB-468 cells

Figure 4.6 3D spheroid growth of MDA-MB-468, HCC70, and BT-549 cells transfected with either anti-miR-106b-5p or a non-targeting antisense oligonucleotide

Figure 4.7 Quantification of *SETD2* and *RRM2* expression levels across a panel of BC cell lines

Figure 4.8 Plots of expression correlation between *SETD2* mRNA, *E2F1* mRNA, *RRM2* mRNA and miR-106b-5p levels in a panel of BC cell lines

Figure 4.9 Western blot analysis of H3K36me3 and p21 protein levels in U2OS cells transfected with a non-targeting control miRNA or miR-106b-5p mimic

Figure 4.10 Western blot analysis of RRM2 protein levels and AZD1775-sensitivity in U2OS cells transfected with a non-targeting control miRNA or miR-106b-5p mimic

Figure 4.11 AZD1775 activity in a panel of BC cell lines

Figure 4.12 UCN-01 and VE-822 activity in a panel of BC cell lines
Figure 4.13 Immunoblot analyses of the the histone mark H3K36me3 in a panel of BC cell lines
Figure 4.14 AZD1775-sensitivity correlates with miR-106b-5p levels in a panel of BC cell lines
Figure 4.15 miR-106b-5p and miR-93-5p levels modify the effects of AZD1775 treatment in HCC1806 cells
Figure 4.16 qRT-PCR analysis showing changing expression of E2F1 after transfection of anti-miR-93-5p or anti-miR-106b-5p in HCC1806 cells
Figure 4.17 Dose-response curves for *RB*-mutated BT-549 cells transfected with a non-targeting control or anti-miR-106b-5p, exposed to increasing concentrations of AZD1775 or VE-822 for 72 hours
Figure 4.18 qRT-PCR analysis showing the changing expression of E2F1 after miR-93-5p or miR-106b-5p transfection in T47D and MDA-MB-453 cells
Figure 4.19 Western Blot analysis of MCM7, PCNA, E2F1, and H3K36me3 protein levels in T47D and MDA-MB-453 cells transfected with a non-targeting control miRNA or miR-106b-5p mimic
Figure 4.20 miR-106b-5p overrides the AZD1775-induced checkpoint in MCF10A cells and accelerates S-phase progression
Figure 4.21 S-phase-dependent cell cycle effects of anti-miR-106b-5p oligonucleotides in AZD1775-treated BT-549 or HCC1806 cells
Figure 4.22 Anti-miR-106b-5p treatment causes a permanent G_1-arrest in MCF-7 cells
Figure 4.23 Knockdown of CDKN1A sensitised *SETD2*-proficient and -deficient U2OS cells to WEE1 inhibitor treatment
Figure 4.24 Knockdown of CDKN1A increases the S-phase population in *SETD2* KO U2OS cells treated with AZD1775
Figure 4.25 Combination of p21 and WEE1 inhibition for treatment of *SETD2*-deficient cancer cells
Figure 5.1 Quality of isolated RNA was analysed using the Agilent 2100 Bioanalyser
Figure 5.2 Gel electrophoresis of total RNA extracted from HCC1806 cells
Figure 5.3 Highly expressed microRNAs in HCC1806 cells
Figure 5.4 Scatter plots of the differential expression levels of microRNAs between the control, 2 hours post-IR (T2) and 6 hours post-IR (T6) HCC1806 samples

Figure 5.5 Differential microRNA expression, with fold difference between $\log_2$ normalised expression in A) control and T2 (2 hours post-IR treatment) and B) control and T6 (6 hours post-IR treatment) HCC1806 cells plotted versus $-\log_{10}$ P-value (n=2)

Figure 5.6 Elevated miR-7704 expression in response to γ-irradiation in HCC1806 cells

Figure 5.7 Differential mRNA expression, with fold difference between $\log_2$ normalised expression in A) control and T2 (2 hours post-IR treatment) and B) control and T6 (6 hours post-IR treatment) HCC1806 cells plotted versus $-\log_{10}$ P-value (n=2)

Figure 5.8 Venn diagram depicting common up- and downregulated DEGs in HCC1806 cells 2 hours post-IR (T2) and 6 hours post-IR (T6)

Figure 5.9 Upregulated miRNAs 2-hours post-IR target cell cycle kinases WEE1 and SIK1

Figure 5.10 hsa-miR-93-3p and hsa-miR-93-5p expression in HCC1806 cells decrease following irradiation (10 Gy dose), in contrast to miR-106b-3p and miR-106b-5p levels, which show increased expression

Figure 5.11 *SETD2*, *E2F1* and *MCM7* expression levels in response to γ-irradiation treatment in HCC1806 cells

Figure 5.12 Knockdown of SETD2 sensitises U2OS cells to ionising radiation

Figure 5.13 Differential microRNA expression, with fold difference between $\log_2$ normalised expression in control and hydroxyurea (2 mM) treated HCC1806 cells plotted versus $-\log_{10}$ P-value (n=2)

Figure 5.14 Differential mRNA expression, with fold difference between $\log_2$ normalised expression in control and hydroxyurea (2 mM) treated HCC1806 cells plotted versus $-\log_{10}$ P-value (n=2)

Figure 5.15 Upregulated miRNAs 4 hours post-HU treatment with their target-mRNAs

Figure 5.16 Expression changes of hsa-miR-124-3p-target genes involved in Microtubule Cytoskeleton Organisation following HU- or IR-treatment

Figure 5.17 Upregulation of miR-93-3p in response to hydroxyurea treatment

Figure 5.18 E2F-dependent transcription in response to hydroxyurea treatment

Figure 6.1 Downregulated genes in the *SETD2*-depleted cells were enriched for molecular functions, such as transcription factor binding

Figure 6.2 TFEA for down- and upregulated DEGs in *SETD2* CRISPR KO U2OS cells

Figure 6.3 E2F-target genes are downregulated in *SETD2* CRISPR KO U2OS cells when compared to *SETD2* WT U2OS cells

Figure 6.4 Knockdown of SETD2 in synchronised T98G cells was confirmed using WB for H3K36me3

Figure 6.5 ChIP-qPCR analysis of E2F1 occupancy on *CDC6*, *CDT1,* and *MCM2* promoters in T98G cells treated with siNT or siSETD2 using IgG or anti-E2F1 antibodies

Figure 6.6 Levels of H3K36me3 peak at the G_1-to-S transition and decrease in S-phase

Figure 6.7 Transcriptional response to HU-induced replication stress

Figure 6.8 SETD2 and inactivation of E2F6 are required for expression of E2F-dependent transcripts

Figure 6.9 Expression of wild-type SETD2 restores H3K36me3 levels and expression of E2F1 and its target genes

Figure 6.10 ATR inhibitor (VE-822) treatment partly impairs HU-induced checkpoint signalling in U2OS cells

Figure 6.11 Meta-analysis of reads density for mNUC-seq H3 signal over gene bodies

Figure 6.12 SETD2 facilitates the transcriptional checkpoint response to HU-induced replication stress in an ATR-dependent manner

Figure 6.13. Transcriptional response to replication stress is dependent on ATR signalling

Figure 6.14 H3K36me3 induction in response to replication stress in S-phase is dependent on ATR- and CHK1-signalling

Figure 6.15 FACS analysis of synchronised T98G cells treated with 2 mM HU, 2 μM VE-822, or both for 4 hours

Figure 6.16 Expression changes of E2F- and p53-target genes in response to HU and/or ATR inhibitor treatment in the presence and absence of *SETD2*

Figure 6.17 mNUC-seq signal of H3K36me3/H3 on *RRM2B* and *CDKN1A* gene loci of HU-, VE822-, or HU- and VE822-treated samples compared to control

Figure 6.18 ATR inhibition causes H3K36me3 re-distribution and subsequent expression changes

Figure 6.19 Graphical Abstract: Role for SETD2 in The Transcriptional Checkpoint Response

List of Tables

Table 3.1 Spearman's correlation statistics of CNA and mRNA expression of miRNA biogenesis genes that were amplified in >50 % of TCGA- BRCA cases

Table 3.2 List of miRNAs associated with *AGO2* expression across two independent invasive breast cancer cohorts

Table 3.3 List of miRNAs that were significantly positively associated with *AGO2* expression in the TCGA-BRCA cohort, when comparing the mature: precursor ratio

Table 4.1 Expression correlation of hsa-miR-106b-5p and *SETD2* across 13 cancer types

Table 5.1. Top 5 most upregulated miRNAs 2 hours post-IR (T2 vs control)

Table 5.2 Top 5 most upregulated miRNAs 6 hours post-IR (T6 vs control)

Table 5.3. Top 5 most upregulated miRNAs 4 hours post-HU (T4 vs control)

Abbreviations

AA	Amino Acid
AGO2	Argonaute 2
AS	Alternative Splicing
ATM	Ataxia Telangiectasia Mutated
ATR	Ataxia Telangiectasia and Rad3-related protein
ATRi	ATR inhibition
BRCA	Breast Invasive Carcinoma
BrdU	Bromodeoxyuridine
CCLE	Cancer Cell Line Encyclopaedia
ccRCC	Clear Cell Renal Cell Carcinoma
CDC2	Cell Division Cycle 2
CDC6	Cell Division Cycle 6
CDK	Cyclin-Dependent Kinase
CDKN1A	Cyclin-dependent Kinase Inhibitor 1A Gene
CDT1	Chromatin licensing and DNA replication factor 1
ChEA	ChIP Enrichment Analysis
CHK1	Checkpoint Kinase 1
CHK2	Checkpoint Kinase 2
ChIP	Chromatin Immunoprecipitation
CKI	Cyclin-Dependent Kinase Inhibitor
CMG	Cdc45–MCM–GINS
CN	Copy Number
CNA	Copy Number Amplification
CNV	Copy Number Variation
COSMIC	Catalogue of Somatic Mutations in Cancer
CTD	C-Terminal Domain
CtIP	C-Terminal-binding protein Interacting Protein
DGCR8	DiGeorge Syndrome Critical Region 8
DDK	Dbf4-dependent Cdc7 kinase
DDR	DNA Damage Response
DNA	Deoxyribonucleic Acid
DEG	Differentially Expressed Gene
DMSO	Dimethyl Sulfoxide
DNMT3B	*De Novo* DNA Methyltransferase 3b
dNTP	Deoxyribonucleotide Triphosphate
DSB	Double-Strand Break
ER	Oestrogen Receptor
FACS	Fluorescence-Activated Single Cell Sorting
FBS	Foetal Bovine Serum
FC	Fold Change
FDR	False Discovery Rate
FL	Full-Length
FOXM1	Forkhead Box M1
FPKM	Fragments Per Kilobase Million
GISTIC	Genomic Identification of Significant Targets in Cancer
GMNN	Geminin DNA Replication Inhibitor
GO	Gene Ontology
GSEA	Gene-Set Enrichment Analysis

Gy	Gray
H3K36me3	Histone 3 Lysine 36 Trimethylation
HER2	Human Epidermal Growth Factor Receptor 2
hnRNP	Heterogeneous Nuclear Ribonucleoprotein
HRR	Homologous Recombination Repair
HU	Hydroxyurea
IC_{50}	Half-maximal Inhibitory Concentration
IR	Ionising Radiation
KDM4A	Histone Lysine Demethylase 4A
KO	Knockout
LEDGF	Lens Epithelium Derived Growth Factor
LFC	Log2-Fold Change
MBF	MCB-Binding Factor
MCM	Minichromosome Maintenance Complex
METABRIC	Molecular Taxonomy of Breast Cancer International Consortium
MMEJ	Microhomology-mediated End Joining
mNUC-seq	Mono-Nucleosome Sequencing
MRN	Mre11/Rad50/Nbs1
mRNA	Messenger RNA
miRNA	MicroRNA
NGS	Next-Generation Sequencing
NHEJ	Non-Homologous End-Joining
NT	Non-Targeting
OS	Overall Survival
PBS	Phosphate Buffered Saline
PCNA	Proliferating Cell Nuclear Antigen
PI	Propidium Iodide
PLK1/2	Polo-Like Kinase 1/2
PR	Progesterone Receptor
Pre-miRNA	Precursor microRNA
Pre-RC	Pre-Replication Complex
Pri-miRNA	Primary microRNA
qPCR	Quantitative Polymerase Chain Reaction
RB	Retinoblastoma
RF	Replication Fork
RISC	RNA-Induced Silencing Complex
RNA	Ribonucleic Acid
RNA-seq	RNA-sequencing
RNAPII	RNA Polymerase II
RNR	Ribonucleotide Reductase
RRM2	Ribonucleotide Reductase regulatory subunit 2
RPA	Replication Protein A
RPKM	Reads Per Kilobase (of Transcript) Million (Mapped Reads)
SAC	Spindle Assembly Checkpoint
SD	Standard Deviation
SDL	Synthetic Dosage Lethality
SEM	Standard Error of the Mean
SETD2	SET Domain Containing 2
SHI	SETD2-hnRNP Interaction Domain
siRNA	Small Interfering RNA

ssDNA	Single-Stranded DNA
SNP	Single Nucleotide Polymorphism
SRI	Set2 Rpb1 Interacting Domain
sRNA-seq	Small RNA-sequencing
TCGA	The Cancer Genome Atlas
TES	Transcription End Site
TF	Transcription Factor
TFEA	Transcription Factor Enrichment Analysis
TNBC	Triple-Negative Breast Cancer
TP53	Tumour Protein 53
TPM	Transcripts Per Million
TRBP	Trans-activation-responsive RNA-Binding Protein
TSG	Tumour Suppressor Gene
TSS	Transcription Start Site
UTR	Untranslated Region
WEE1i	WEE1 kinase inhibition
WT	Wild-type
XPO5	Exportin 5

Table of Contents

Chapter 1 ..... ***1***

1.1 Cell Cycle Control in Cancer 1

1.2 The Eukaryotic Cell Cycle 1
- 1.2.1 Cyclins and Cyclin-Dependent Kinases 2
- 1.2.2 The Restriction Point of the Cell Cycle and Dynamics of the RB-E2F Pathway 4
- 1.2.3 Regulation of Mammalian DNA Replication 6
- 1.2.4 G_2/M transition and the role of WEE1 kinase 8

1.3 Cell Cycle Checkpoints 11
- 1.3.1 Cell Cycle Checkpoints and DNA Double-Strand Break (DSB) Repair 11
- 1.3.2 Cellular Response to Replication Stress 13

1.4 Dysregulation of the Cell Cycle in Breast Cancer 15
- 1.4.1 Therapeutic Opportunities in Breast Cancer 16

1.5 MicroRNA-mediated Gene Regulation in Cancer 20
- 1.5.1 Genomic Organisation and Canonical Biogenesis of Mammalian MicroRNAs 21
- 1.5.2 Mechanisms of miRNA Dysregulation in Cancer 25
- 1.5.3 The polycistronic miR-106b/25 cluster 26

1.6 Post-Translation Histone Modifications 28
- 1.6.1 Structure and Function of the SETD2 methyltransferase 29
- 1.6.2 Biological Roles of SETD2 32
- 1.6.3 SETD2 and H3K36me3 in Cancer 33
- 1.6.4 Targeting *SETD2*-deficient Cancers 34

1.7 Thesis Aims 36

Chapter 2 ..... ***39***

2.1 Genomic and Transcriptomic Analyses of Clinical Datasets 39

2.2 Cancer Cell Line Encyclopaedia (CCLE) Data and Analyses 40

2.3 Tissue Culture 40
- 2.3.1 Revival of Frozen Cell Lines 40
- 2.3.2 Cell Line Maintenance 41
- 2.3.3 Cryopreservation of Cell Lines 41

2.4 Cell Lines 42
- 2.4.1 Cell Cycle Synchronisation 42

2.5 Gene Silencing 42
- 2.5.1 Transfection of siRNAs, miRNA mimics, or miRNA inhibitors 42
- 2.5.2 Plasmid Transfection 43

2.6 Protein Detection by Western Blotting 45
- 2.6.1 Sample Collection for Western Blotting 45
- 2.6.2 Western Blotting 45
- 2.6.2 Antibodies 46

2.7 Drugs and Inhibitors 46

2.7.1 Ionising Radiation....47
2.8 Cellular Survival Assays....47
2.8.1 Clonogenic Survival Assay....47
2.8.2 Resazurin Assay for Cell Viability....48
2.8.3 Spheroid Formation Assay....48
2.9 Cell Cycle Analysis by Flow Cytometry....49
2.10 Quantification of microRNAs....49
2.10.1 Small RNA isolation....49
2.10.2 Quantitative Reverse Transcription Polymerase Chain Reaction (qRT-PCR) for miRNA expression....50
2.10.3 MicroRNA Microarray....50
2.11 Quantification of mRNAs....51
2.11.1 mRNA isolation....51
2.11.2 qRT-PCR for mRNA expression....51
2.12 Chromatin Immunoprecipitation (ChIP)....54
2.13 miRNA- and mRNA-sequencing using Illumina....55
2.13.1 Sample Collection....55
2.13.2 miRNA sequencing library preparation....56
2.13.3 mRNA sequencing (RNA-seq) library preparation....56
2.13.4 Illumina Sequencing....57
2.13.5 Statistical Analysis for miRNA Sequencing....58
2.13.6 Statistical Analysis For mRNA Sequencing....58
2.14 mNUC-seq sample preparation....59
2.14.1 Statistical Analysis for mNUC-sequencing....59
2.15 Gene Ontology (GO) and Pathway Enrichment Analysis....60
2.16 Graphical Display of Results and Statistical Analysis....61
***Chapter 3*....62**
3.1 Introduction....62
3.2 Recurrent Alterations of miRNA Biogenesis Genes in Breast Cancer....64
3.3 *AGO2* Amplification is Inversely Correlated with *DICER1* Deletion....73
3.4 *AGO2* Amplification is Associated with Overexpression of *OncomiR* Families....75
3.5 AGO2 Silencing in *AGO2*-Amplified HCC1806 Cells Supports Selective miRNA Maturation....79
3.6 Correlation Between *AGO2* and miR-106b-5p Levels in a Panel of Breast Cancer Cell Lines....82
3.7 Inhibition of AGO2 in HCC1806 Cells Confirms Preferential Maturation of the miR-106b/25 Cluster....86
3.8 Mapping the Synthetic Dosage Lethality Network of *AGO2*-Amplified Cancers....90
3.9 Conclusion....92

Chapter 4 ..... ***94***

4.1 Introduction 94

4.2 The Clinicopathological Significance of miR-106b-5p in Breast Cancer 96

4.3 MicroRNA-106b-5p Regulates Cellular Proliferation of Breast Cell Lines 100

4.4 MicroRNA-106b-5p Negatively Regulates *SETD2* in 6 Cancer Types 103

4.5 Relation Between miR-106b-5p, *SETD2*, and *RRM2* Expression in Breast Cancer 105

4.6 MicroRNA-106b-5p Regulates p21 and RRM2 Protein Levels in U2OS Cells 108

4.7. ATR, WEE1, and CHK1 Inhibitor-Treatment Reduce Proliferation in Breast Cancer Cell Lines 111

4.8 MiR-106b-5p Expression Levels Correlate with WEE1 Inhibitor-Sensitivity 112

4.9 Inhibition of miR-106b-5p and miR-93-5p Results in Increased E2F-Mediated Transcription and Altered AZD1775-sensitivity 115

4.10 MiR-106b-5p and MiR-93-5p Regulate E2F1 mRNA and Protein Levels in T47-D and MDA-MB-453 Cells 119

4.11 MiR-106b-5p Affects Cell Cycle Progression and Regulates WEE1i-induced Replicative Catastrophe 121

4.12 Relationship Between p21 Levels and AZD1775-sensitivity in *SETD2*-proficient and -deficient cells 126

4.13 Conclusion 130

Chapter 5 ..... ***133***

5.1 Introduction 133

5.2 Extraction and Quality Control of RNA samples 134

5.3 Sequencing and Annotation of miRNAs in HCC1806 Cells 136

5.4 Impact of γ-irradiation on the Transcriptomic Profile of HCC1806 cells 137

5.4.1 Changes in Global miRNA Expression in Response to γ-Irradiation 137

5.4.2 Changes in Global mRNA Expression in Response to γ-Irradiation 144

5.4.3 miRNA Target Transcript Predictions in Response to γ-Irradiation 149

5.4.4 Roles of SETD2 and the miR-106b/25 Cluster in Response to γ-Irradiation 152

5.5 Impact of Hydroxyurea on the Transcriptomic Profile of HCC1806 Cells 157

5.5.1 Changes in Global miRNA Expression in Response to Hydroxyurea 157

5.5.2 Changes in Global mRNA Expression in Response to Hydroxyurea 159

5.5.3 MicroRNA Target Transcript Predictions in Response to Hydroxyurea 162

5.5.4 Roles of SETD2 and the miR-106b/25 Cluster in the Replication Stress Response 165

5.6 Chapter Discussion 168

Chapter 6 ..... ***171***

6.1 Introduction 171

6.2 SETD2-depletion Causes Altered Transcription Factor Binding 173

6.3 Loss of SETD2 Causes Reduced Expression of E2F-dependent Transcripts 176
6.4 SETD2-dependent H3K36me3 Mediates E2F1-binding to its Target Genes in G_1 178
6.5 SETD2 and H3K36me3 Levels Peak Prior to Entry into S-phase 180
6.6 SETD2 Mediates E2F1-Target Expression in Response to Replication Stress 183
6.7 Complementation of *SETD2* KO U2OS Cells with SETD2-FL cDNA Restores H3K36me3 and E2F1 Expression Levels 186
6.8 HU-induced Replication Stress Causes a Global Re-distribution of Total H3 and H3K36me3 Levels 187
6.9 H3K36me3 Re-distribution and E2F-dependent Transcription Following HU is Dependent on Intra-S checkpoint Signalling 191
6.10 ATR and CHK1 Inhibition Prevent Expression of H3K36me3 in Response to Replication Stress 193
6.11 E2F- and p53-Target Gene Expression Requires ATR-dependent H3K36me3 195
6.12 Conclusion 200

Chapter 7 ..... ***204***

7.1 Non-canonical miRNA Biogenesis Pathways and Oncogenic MicroRNA Production in Breast Cancer 204
7.2 miR-106b-5p Levels Predict the Response to WEE1 inhibition 206
7.3 Conserved Role for SETD2-dependent H3K36me3 in The Transcriptional Checkpoint Response 208
7.4 Future Directions 209

Bibliography ***211***

Chapter 1
Introduction

1.1 Cell Cycle Control in Cancer

Sustained proliferative signalling, which drives uncontrolled progression through the growth-and-division cycle, is an important hallmark of cancer and lies at the heart of tumourigenesis as a pathological process (Hanahan & Weinberg, 2000; Hanahan & Weinberg, 2011; Matthews, Bertoli, & de Bruin, 2021). Loss of control over cellular proliferation is driven by genetic alterations that promote premature entry into S-phase, where DNA replication takes place, or those that prevent programmed cell death and compromise cell cycle exit (Matthews et al., 2021).

For proper cell division, each stage of the cell cycle must be passed through in the correct order and in timely fashion, and cells therefore have strict control over completion of all the necessary processes at various signalling checkpoints (Figure 1.2). These cell cycle checkpoints preclude cells from progressing through the cell cycle in the presence of, for instance, damaged or under-replicated DNA (Kastan & Bartek, 2004). Loss of checkpoint control can lead to increased genome instability and mutagenesis (Hanahan & Weinberg, 2000; Hanahan & Weinberg, 2011; Matthews et al., 2021).

1.2 The Eukaryotic Cell Cycle

Production of two cells from one requires duplication of the genetic material and organelles that compose each cell. The process of DNA synthesis is limited to several hours in S-phase and requires the temporally ordered expression, assembly, and activation of many proteins at the origins of DNA replication (Pasero & Schwob, 2000). After successful completion of DNA replication, cells enter G_2-phase in preparation for mitosis, which is when the in S-phase

duplicated chromosomes become segregated and the cell divides into two genetically identical daughter cells. Cellular proliferation therefore depends on progression through four distinct cell cycle phases – Gap 1 (G_1), DNA synthesis (S), Gap 2 (G_2), and Mitosis (M) (Howard & Pelc, 1953; Mitchison, 1971). Eukaryotes have an additional gap phase (G_0) in which cells go into a state of quiescence.

1.2.1 Cyclins and Cyclin-Dependent Kinases

In eukaryotes, progression through the cell cycle is tightly regulated by correct assembly and activation of cyclin-dependent serine/threonine kinases (CDKs) (Cooper & Hausman, 2007; Malumbres, 2014). To date, numerous CDKs have been identified and of these at least four play an important role in cell cycle regulation. CDK2, CDK4 and CDK6 are active during G_0- and G_1-phase, CDK2 during S-phase, and CDK1 during mitosis (Harper & Brooks, 2004; Malumbres, 2014; van den Heuvel & Harlow, 1993).

The CDK subunit on its own has no detectable kinase activity and therefore requires binding of positive regulatory subunits known as cyclins (Morgan, 1995; Pines, 1995). The sequential accumulation of cyclins is tightly controlled by elaborate transcriptional networks, as well as by post-translational mechanisms such as ubiquitin-dependent proteolysis. In turn, CDK/cyclin complex-mediated phosphorylation events control cell-cycle transcription and mediate the transition into the next phase of the cell cycle at several key "checkpoints" (Hartwell & Weinert, 1989). These key "checkpoints", namely at the G_1-to-S, G_2-to-M, and M-to-G_1 transition (during spindle assembly), coincide with three main transcriptional waves (Figure 1.1).

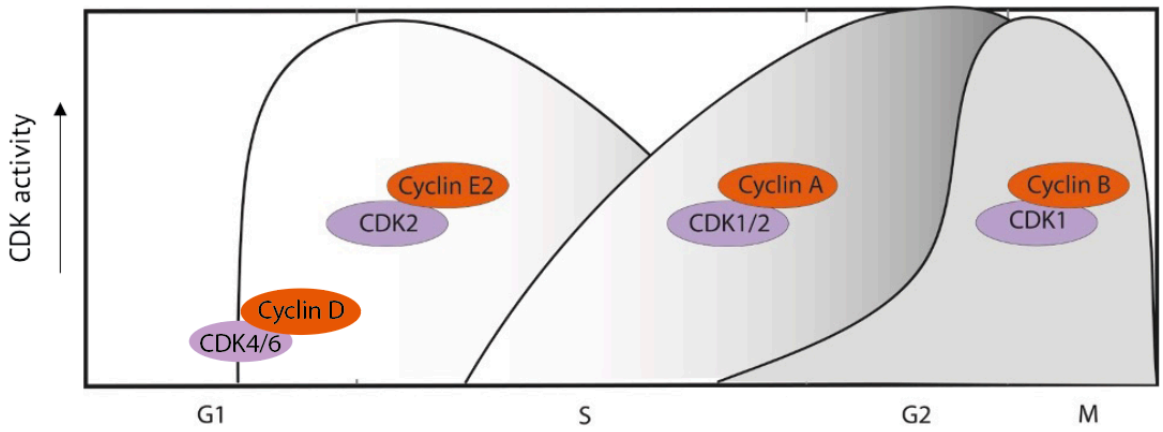

Figure 1.1. ***Schematic of CDK-cyclin waves in mammalian cells.*** *CDK/cyclin-mediated phosphorylation events regulate cell-cycle transcription and promote ordered progression through the cell cycle. Transcriptional waves are shown in grey.*

In addition to regulation of CDK activity via a series of direct phosphorylation and dephosphorylation events through WEE1 and CDC25, respectively (Section 1.2.4), progression through the cell cycle is controlled by two families of cell cycle inhibitory proteins, called CDK inhibitors (CKIs) (Sherr & Roberts, 1995). Inhibitor of CDK4 (INK4) family members, INK4A (p16), INK4B (p15), INK4C (p18), and INK4D (p19), inhibit cyclin D by competing for binding to CDK4/6 in early G_1 (reviewed in Ortega, Malumbres, & Barbacid, 2002). The second family, called the CDK interacting protein/kinase inhibitory protein (Cip/Kip) family, includes $p21^{CIP1}$, $p27^{KIP1}$, and $p57^{KIP2}$. Binding of Cip and Kip proteins modulates the kinase activity of CDK-cyclin complexes, in particular CDK1 and CDK2 complexes, to varying degrees (reviewed in Besson, Dowdy, & Roberts, 2008). Furthermore, p27 facilitates cyclin-activating kinase (CAK)-dependent phosphorylation of the T-loop in CDK4, which is required for CDK4/6 activity at the G_1/S transition (Guiley et al., 2019). The interdependence of CDK activity and cell cycle-regulated transcription creates a regulatory network that together determines the order and timing of the cell cycle (Simmons Kovacs, Orlando, & Haase, 2008).

1.2.2 The Restriction Point of the Cell Cycle and Dynamics of the RB-E2F Pathway

To enter the cell cycle from quiescence, cells must progress from G_1 into S-phase via the restriction point, which is when the cell commits to DNA synthesis and no longer requires extracellular growth factors (Pardee, 1974). The mitogen-dependent progression from quiescence to and through the restriction point is governed by the tumour suppressor gene (TSG) retinoblastoma-associated protein (*RB1*), whose gene product, RB, undergoes CDK-mediated changes in its phosphorylation status throughout the cell cycle. Because the antigrowth circuit converges onto RB, many human cancers are characterised by *RB*-deficiency, typically as a result of homozygous deletion (Knudsen & Zacksenhaus, 2018).

According to the classical view of cell cycle entry, D-type cyclins (primarily cyclin D1, but also D2 and D3) are induced in response to mitogenic signals and drive the transition from quiescence into the proliferative state (Baldin, Lukas, Marcote, Pagano, & Draetta, 1993; Lew, Dulić, & Reed, 1991; Stallaert et al., 2021; Xiong, Connolly, Futcher, & Beach, 1991). Increased expression levels of the D-type cyclins in mid-G_1, which bind and activate their catalytic partners CDK4 and CDK6, cause RB and the other RB-like proteins, p130 and p107, to be phosphorylated (Kato, Matsushime, Hiebert, Ewen, & Sherr, 1993; Narasimha et al., 2014) (Figure 1.2). When RB is in its unphosphorylated state in quiescent cells, it binds the transactivation domain of the E2F transcription factors (E2F1-3) to inhibit their transcriptional activity (Hiebert, Srikumar, Chellappan, Horowitz, & Nevins, 1992; Weintraub, Prater, & Dean, 1992). Increased mono-phosphorylation of RB by the cyclin D–CDK4/6 complex reduces inhibitory control of the E2F transcription factor family and increases the expression of oxidative phosphorylation genes, thereby altering the metabolic state of the cell (Sanidas et al., 2019). Additionally, reduced inhibition of the E2F transcription factors by RB initiates a positive feedback loop, promoting transcription of the E-type cyclins, cyclin E1 and E2, just

prior to the G_1/S transition, which subsequently activates CDK2 and other proteins, driving cells into a decision window to commit to a new round of DNA replication (Geng et al., 1996; Harbour, Luo, Dei Santi, Postigo, & Dean, 1999; Matthews et al., 2021). Therefore, phosphorylation and inactivation of RB is commonly used to define the boundary between arrested cells (in G_0) and actively proliferating cells undergoing cell cycle commitment (in G_1) (Stallaert et al., 2021).

The final event driving cell cycle commitment, aside from increased E2F-dependent transcription, is the inactivation of G_1-specific APC/C complexes, which function to degrade S-phase proteins, including A-type cyclins, during G_1. Increased cyclin E-CDK2 activity in late G_1 stimulates the destruction of the APC^{Cdh1} subunit, thereby switching off APC/C and enabling initiation of S-phase (Cappell, Chung, Jaimovich, Spencer, & Meyer, 2016). The inactivation of APC/C subsequently allows cyclin A to accumulate as S-phase begins, to replace cyclin E to form the cyclin A-CDK2 complex, which maintains Rb phosphorylation through to mitosis (Coverley, Laman, & Laskey, 2002; Dulic, Lees, & Reed, 1992). Therefore, only when E2F-dependent transcription is active and APC^{Cdh1} is inactive, a cell can pass the commitment point and successfully complete DNA replication (Matthews et al., 2021).

It is important to note that the mechanism of G_1/S transcriptional activation is highly conserved from yeast to humans (Cross, Buchler, & Skotheim, 2011). In *Schizosaccharomyces pombe*, transcription of genes involved in the G_1/S transition, which includes the gene encoding the large subunit of ribonucleotide reductase (*cdc22*), is facilitated by the transcription factor complex MBF (MCB-binding factor). MBF is the functional homologue of mammalian E2F, and is switched off by the co-repressor proteins Nrm1 and Yox1 in S-phase (Caetano, Klier, & Bruin, 2011; de Bruin et al., 2006).

1.2.3 Regulation of Mammalian DNA Replication

DNA replication in eukaryotes is initiated from multiple sites across the genome, called origins of replication (reviewed in Prioleau & MacAlpine, 2016). Activation of replication origins proceeds via a tightly controlled two-step mechanism consisting of origin licensing (step 1) and subsequent replication initiation (step 2). Firstly, at the end of a growth-and-division cycle (in late mitosis), when CDK activity drops, origins can become licensed to start a new round of replication. Secondly, DNA replication is initiated from a subset of preassembled origins. To ensure complete genome duplication, eukaryotic cells license many more origins in G_1 than are fired during each round of replication (Demczuk et al., 2012; Jackson & Pombo, 1998). Furthermore, even though the activation of early-replication regions is synchronised at the onset of S-phase, other genomic regions, organised into different initiation zones, are activated at different times during S-phase to ensure that each genomic region is replicated only once during each cell cycle. Spatial and temporal regulation of replication is orchestrated by a combination of histone marks, nuclear architecture, and chromatin accessibility (Van Rechem *et al.*, 2021; reviewed in Vouzas & Gilbert, 2021).

Origin licensing, which involves unwinding of double-stranded DNA at the origins of replication, takes place from mitosis and through G_1 and involves loading of the minichromosome maintenance complex 2-7 (*MCM2-7*) helicases onto the chromatin. The loading of MCM2-7 complexes to form the pre-replicative complex (pre-RC) is regulated by multiple loading factors, such as Cell Division Cycle 6 (*CDC6*) and Chromatin licensing and DNA replication factor 1 (*CDT1*) (reviewed in Symeonidou, Taraviras, & Lygerou, 2012). MCM2-7 helicases loaded onto origins of replication remain inactive until the G_1/S transition, when the combined activities of Dbf4-dependent Cdc7 kinase (DDK) and CDKs trigger replication initiation through MCM2-7-phosphorylation and formation of two active CMG

(Cdc45–MCM–GINS) helicases (Boos, Frigola, & Diffley, 2012; Costa et al., 2011). These active CMG complexes translocate along ssDNA, away from the replication origins with 3' to 5' directionality, forming the basis of the active replisome (Fu et al., 2011; Ilves, Petojevic, Pesavento, & Botchan, 2010). Excess MCMs can either remain inactive or dormant until removed by passing replication forks, or can be "fired" to maintain DNA replication rates in the presence of under-replicated DNA, also referred to as replication stress (Ge, Jackson, & Blow, 2007). The replisome is disassembled upon ubiquitylation of the CMG complex by SCF^{Dia2} and subsequent association of the Cdc48/p97 segregase, only when two replication forks from opposite directions converge during termination (Dewar, Budzowska, & Walter, 2015; Maric, Maculins, De Piccoli, & Labib, 2014).

Formation of the pre-RC complex in G_1 is driven by cyclin E-CDK2, which completes RB hyperphosphorylation, enabling the release of the activating E2F transcription factors (TFs), E2F1-3 (Harbour et al., 1999; Lundberg & Weinberg, 1998; Pagano et al., 1993) (Figure 1.2). The activating E2F TFs allow for timely regulation of pre-RC assembly, as they facilitate transcription and subsequent recruitment of *CDT1, CDC6*, and *MCM2-7*, as well as expression of the catalytic subunit of ribonucleotide reductase (*RRM2*), which supplies the building blocks for DNA replication (Bertoli, Skotheim, & De Bruin, 2013; Coverley et al., 2002; Johnson & Schneider-Broussard, 1998). Once in S-phase, the cyclin A-CDK2 complex activates DNA synthesis by replication complexes that are already assembled and prevents repeated initiation through inhibition of new replication complex assembly (Coverley et al., 2002; Deegan & Diffley, 2016; Katsuno et al., 2009).

1.2.4 G_2/M transition and the role of WEE1 kinase

Of the numerous CDKs, CDK1, also termed cell division cycle protein 2 (CDC2), is responsible for the transition through G_2 and into mitosis (Norbury, Blow, & Nurse, 1991) (Figure 1.2). The catalytic activity of the cyclin B1-CDK1 complex, which becomes more active through S-phase and reaches peak activity before nuclear envelope breakdown, is the main trigger of mitotic entry and initiation of prophase as a result of phosphorylation of over a thousand CDK substrates (Dephoure et al., 2008; Gavet & Pines, 2010; Pines & Hunter, 1989). One target of the cyclin B1-Cdk1 complex is the transcription factor Forkhead Box M1 (FOXM1) (Major, Lepe, & Costa, 2004). Phosphorylation of FOXM1 by CDK1 creates a docking site for Polo-Like Kinase 1 (PLK1) binding (Fu et al., 2008). Upon binding, PLK1 directly phosphorylates FOXM1 to promote its transcriptional activity and induce expression of key mitotic regulators necessary to complete cell division (Fu et al., 2008). During normal DNA replication, the checkpoint kinase Ataxia Telangiectasia and Rad3-related protein (ATR) is activated to block this FOXM1-mediated switch until S-phase ends, and completion of DNA replication is therefore tightly coupled with mitotic onset (Saldivar et al., 2018).

Activity of the CDK1–cyclin B complex is directly restricted until the cell approaches mitosis by phosphorylation events through WEE1 and MYT1, which catalyse inhibitory tyrosine-15 and threonine-14 phosphorylation in the ATP-binding domain of CDK1/2, respectively, rendering those CDKs inactive (Figure 1.2) (Liu, Stanton, Wu, & Piwnica-Worms, 1997; McGowan & Russell, 1993; Nurse & Thuriaux, 1980; Parker & Piwnica-Worms, 1992). Even though both WEE1 and MYT1 can phosphorylate CDK1, WEE1 is essential for normal cell cycle progression and checkpoint activation, whereas MYT1 is thought to have a more prominent role during checkpoint recovery (Chow & Poon, 2012). Inhibitory phosphorylation can be reversed by the phosphatase CDC25, the human protein responsible for

dephosphorylation of the tyrosine-15 residue of CDK1 at the G_2/M border, in the absence of DNA damage (Parker & Piwnica-Worms, 1992). Studies have shown that the replacement of the endogenous CDK1 with a non-phosphorylatable variant ($CDK1^{T14A/Y15F}$) was embryonically lethal in mice and led to mitotic events in S-phase (Szmyd et al., 2018). Hence, control over the balance of CDC25-WEE1 regulation of CDK1 activity is essential for establishing and maintaining both the intra-S and G_2/M checkpoints (Figure 1.2).

As cells exit mitosis, they face the proliferation-quiescence decision: they can either progress directly into G_1 with sustained RB phosphorylation, or exit the cell cycle into a state of quiescence following the loss of RB phosphorylation (Stallaert et al., 2021). In each daughter cell, this fate decision was found to be controlled primarily by a bifurcation in CDK2 activity, determined by the balance between cyclin D and p21 expression (Spencer et al., 2013; Stallaert et al., 2021). Therefore, when the inhibitory action of $p21^{CIP1}$ persists directly after mitosis, as is the case in the presence of DNA damage or altered mitogen signalling, postmitotic daughter cells are thought to exit the cell cycle with low CDK activity and enter a transient G_0-like state (Spencer et al., 2013; Stallaert et al., 2021).

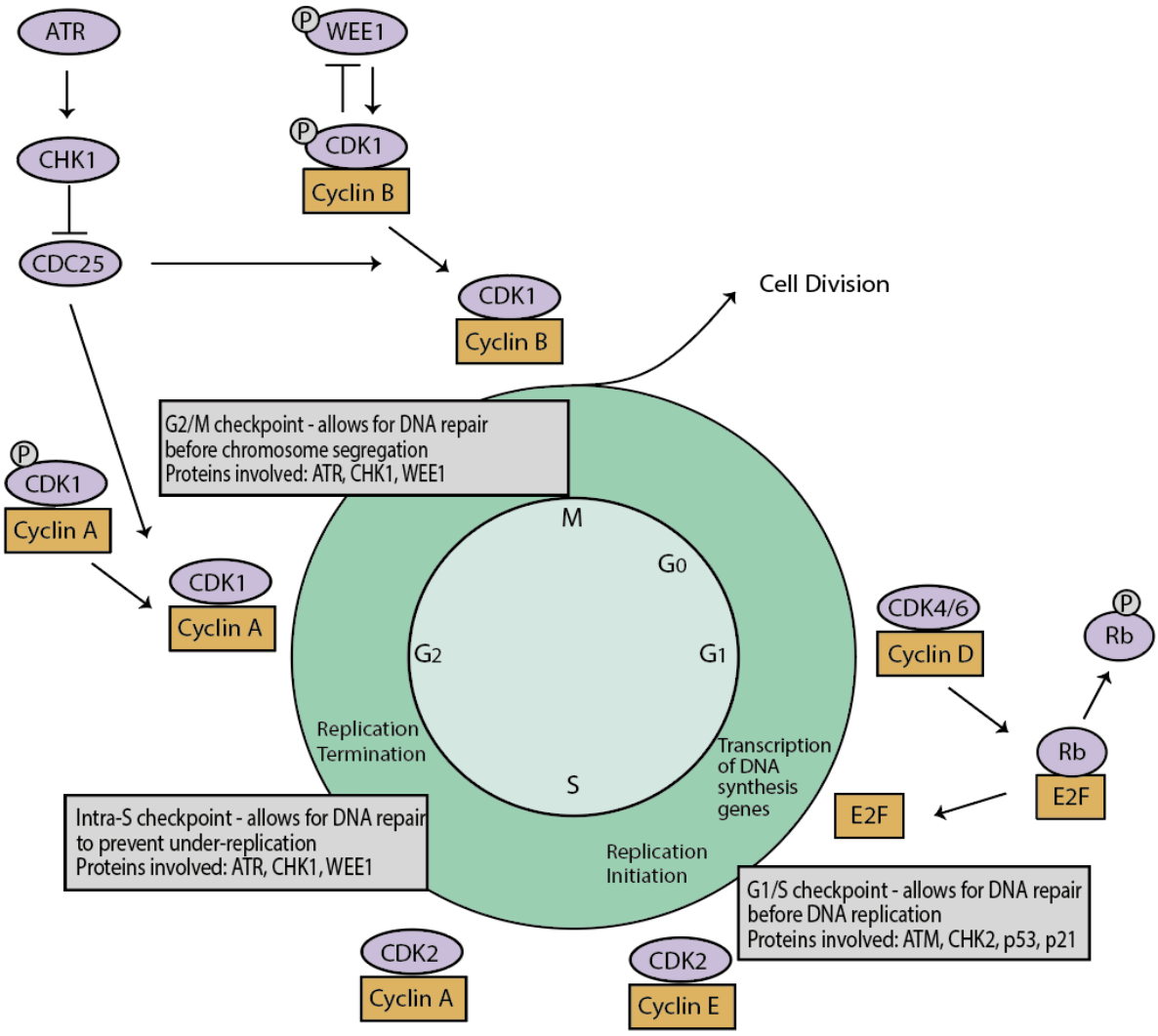

Figure 1.2. ***Cell cycle control and DNA damage checkpoints work cooperatively to maintain genome stability.*** *According to the classical model of cell cycle control, D-type cyclins and CDK4 or CDK6 regulate events in early G_1 phase, cyclin E-CDK2 triggers S-phase, cyclin A-CDK2 regulates the completion of S-phase, and cyclin B-CDK1 is responsible for mitosis. In the presence of replication stress or DNA damage, three checkpoints, including the G_1/S, intra-S and G_2/M checkpoints, are responsible for the restriction of CDK activity to halt cell cycle progression and promote DNA repair. Figure reprinted from Clinical Cancer Research, with permission from AACR.*

Section 1.3.1 – 1.3.4 are based on the following publication:

van Bijsterveldt, L., Durley, S. C., Maughan, T. S., & Humphrey, T. C. (2021). **The Challenge of Combining Chemo- and Radiotherapy with Checkpoint Kinase Inhibitors.** *Clinical Cancer Research*, *27*(4), 937 LP – 962. https://doi.org/10.1158/1078-0432.CCR-20-3358.

1.3 Cell Cycle Checkpoints

1.3.1 Cell Cycle Checkpoints and DNA Double-Strand Break (DSB) Repair

In the presence of replication stress during S-phase (Section 1.3.2), or a DNA break during interphase, cell cycle progression is restrained by different checkpoint kinases, including ATR and Ataxia Telangiectasia Mutated (ATM), WEE1, and checkpoint kinases 1 (CHK1) and 2 (CHK2) (Figure 1.2). Damaged DNA can be propagated during S-phase and mitosis, and therefore, cell cycle arrest occurs either (1) prior to S-phase entry (G_1/S checkpoint) to prevent cells from replicating DNA damage, (2) in S-phase (intra-S checkpoint) to protect and restart stalled replication forks, or (3) prior to mitotic entry (G_2/M checkpoint) to allow for repair of DNA prior to chromosome segregation. Activation of these different DNA damage response (DDR) checkpoints ensures genome integrity by pausing the cell cycle and allowing for repair to take place, or in the case of unrepairable DNA damage, by promoting programmed cell death (Ciccia & Elledge, 2010; O'Connell, Walworth, & Carr, 2000). The severity of the damage often dictates the choice of cell fate. Even though the G_1/S, intra-S, and G_2/M checkpoints respond to different stimuli, activation of either one of these signalling cascades results in inhibition of CDK activity, either directly or through p53-dependent induction of the CDK inhibitor p21 (Bunz et al., 1998). Other mechanisms, however, are distinct because different sets of kinases, CDK-cyclin complexes, and DNA repair proteins are activated in the G_1- and G_2-phases of the cell, respectively.

The DNA damage checkpoint is activated in response to DNA double-strand breaks (DSBs), which can form either as a result of exposure to exogenous agents, such as chemicals or radiation, or through endogenous processes, such as metabolic processes or unresolved DNA replication stress (Section 1.3.2). DNA DSBs generated in G_1 only undergo repair via non-homologous end-joining (NHEJ), which involves ligation of two broken DNA ends, bypassing the need for a repair template (Chiruvella, Liang, & Wilson, 2013). NHEJ-mediated repair is initiated by Ku70/80 heterodimer and DNA-PKcs binding to DSBs, which phosphorylate several NHEJ factors to promote DNA end tethering and DNA end alignment and ligation (Graham, Walter, & Loparo, 2016; Hussmann et al., 2021). As this process requires only minor nucleolytic processing and therefore does not generate significant amounts of replication protein A (RPA)-coated ssDNA (Jazayeri et al., 2005), the DNA damage checkpoint (G_1/S) is believed to be controlled primarily by ATM rather than ATR. ATM phosphorylates a large number of substrates in the presence of a DSB (Bensimon et al., 2010), including downstream effector kinase CHK2 and the transcription factor p53 (Mak, 2000), which can induce either reversible (quiescence) or irreversible (senescence) cell cycle arrest, or programmed cell death (apoptosis).

Additionally, both the ATM-CHK2 and ATR-CHK1 axes contribute to establishment and maintenance of the intra-S and G_2/M checkpoints. This is, in part, because ATM- and Mre11/Rad50/Nbs1 (MRN)-dependent DNA break end-resection, which is essential for both repair of DSBs and restart of stalled replication forks via homologous recombination repair (HRR), generates ssDNA, which serves as a platform for RPA binding and signalling (Adams, Medhurst, Dart, & Lakin, 2006; Jazayeri et al., 2005; Myers & Cortez, 2006). This extended RPA-ssDNA signal subsequently allows for ATR recruitment, via its partner protein ATRIP (Zou & Elledge, 2003). Activation of these intra-S checkpoint proteins, including ATR and its downstream effector kinase CHK1, can subsequently counteract CDC7 and CDK2 kinase

activity at origins of replication, thereby limiting replication origin activity in the presence of DNA damage and replication stress (Moiseeva et al., 2017; Moiseeva et al., 2019; Petermann, Woodcock, & Helleday, 2010).

In addition to regulation of the intra-S and G_2/M checkpoints by the ATR-CHK1 axis, CDK1 activity is also tightly controlled by WEE1 kinase activity (Elbæk, Petrosius, & Sørensen, 2020). WEE1 is necessary to prevent cells from entering mitosis before DNA replication has been completed, which would result in mitotic catastrophe (Elbæk et al., 2020). A role for WEE1 in regulating checkpoint activation and genome integrity was confirmed by pre-clinical studies, where conditional *Wee1* heterozygous deletion in mice caused cells to progress into mitosis while still undergoing DNA replication, resulting in accumulation of DNA damage, elevated genomic instability and, ultimately, in enhanced proliferation and tumour development (Vassilopoulos et al., 2014).

1.3.2 Cellular Response to Replication Stress

As previously discussed, both the ATM-CHK2 and ATR-CHK1 axes contribute to establishment and maintenance of the intra-S checkpoint, which inhibits the accumulation of cyclin A/B–CDK1/2 activity to block late-origin firing and mitotic entry (Section 1.3.1). The intra-S-checkpoint is activated not only in response to DNA DSBs, but also when the CMG helicase and the DNA polymerase are uncoupled as a result of impediments to replication fork (RF) progression, leaving large strands under-replicated DNA exposed (McGowan & Russell, 2004; Zeman & Cimprich, 2014). This slowing or stalling of replication fork progression, leading to exposure of ssDNA, is also referred to as replication stress (Zeman & Cimprich, 2014). Replication stress can be attributed to many different factors, most notably aberrant replication origin firing, collision of the replication and transcription machineries, defective nucleotide metabolism, reactive oxygen radicals, and factors blocking replication fork

progression, such as chemical modifications of the template, or the tight binding of enzymatic complexes to DNA (Kotsantis, Petermann, & Boulton, 2018).

Aside from inhibiting late-origin firing, ATM and ATR can also stabilise ongoing and stalled replication forks and prevent the formation of replication stress-induced DNA DSBs (Lopes et al., 2001). Firstly, ATM and ATR can promote MRN-dependent repair of collapsed replication forks, as well as polymerase ε reloading, which is necessary for replication restart (Trenz, Smith, Smith, & Costanzo, 2006). Further, ATR phosphorylates and selectively destabilises human exonuclease 1 in response to stalled DNA replication, which has an important role in DNA recombination and repair (El-Shemerly, Hess, Pyakurel, Moselhy, & Ferrari, 2008). It is thus important to note that replication stress is not DNA damage, and that the main function of the replication stress checkpoint is to prevent DNA damage formation.

Additionally, the DNA replication stress checkpoint also coordinates the checkpoint transcriptional response, and maintains high levels of G_1-S transcription to prevent genome instability during replication stress (Bertoli, Klier, McGowan, Wittenberg, & De Bruin, 2013; Chu et al., 2007; Oliveira, Harris, Brazauskas, Bruin, & Smolka, 2012; Travesa et al., 2012). In mammalian cells, this mechanism involves CHK1-mediated phosphorylation, inactivation of the transcriptional repressor E2F6, and consequently, high levels of E2F-dependent transcription in S-phase, including proteins that prevent RF collapse and DNA damage, those that allow replication to resume after the arrest (e.g., CtIP and RAD51), and those that allow for deoxynucleotide triphosphate (dNTP) production for DNA synthesis (e.g., *RRM2*) (Bertoli, Klier, McGowan, et al., 2013; Choi & Kim, 2019).

1.4 Dysregulation of the Cell Cycle in Breast Cancer

Breast cancer is the most commonly diagnosed cancer in females and accounts for 11.6% of total cancer-related deaths (Allemani et al., 2015; Bray et al., 2018). Mutations in tumour suppressor genes such as *BRCA1*, *BRCA2*, *CDH1*, and *TP53*, are considered to be the major drivers in approximately 10% of breast cancer cases (reviewed in Shiovitz & Korde, 2015). However, the majority of breast cancer cases are driven by multiple, low-penetrant mutations that act cumulatively and alter the functioning of two major signalling pathways: 1) the p16–cyclin D1–CDK4–RB pathway, which drives S-phase entry through changes in the processing of mitogenic signalling before the onset of replication; and 2) the DNA damage checkpoints, which upon mutation allow for the propagation of damaged DNA by preventing p53/p21-mediated cell cycle exit.

For instance, overexpression of cyclin D1, cyclin D3, or both was found to be very common in invasive and *in situ* breast carcinomas (Gillett et al., 1994; Weinstat-Saslow et al., 1995). Oestrogen Receptor (ER) signalling activates the *CCND1* promoter (Kenny et al., 1999) and cyclin D1 overexpression can therefore occur independently of *CCND1* gene amplification in many ER-positive breast cancers (Gillett et al., 1994). In contrast with ER-positive luminal cancer, basal-like triple-negative breast cancers (TNBC) are characterised by *RB*-deficiency and cyclin E1 overexpression (Treré et al., 2009; Zhao et al., 2019). Both *RB*-deficiency and *CCND1* or *CCNE1* amplification induce E2F-dependent transcription, which promotes S-phase entry and DNA replication initiation, and these genetic alterations therefore compromise the ability of the cell to induce quiescence in the pre-replicative phase.

Additionally, breast cancer pathogenesis is frequently accelerated by genomic alterations that underlie DNA damage checkpoint deficiency. *TP53* (Tumour Protein 53) is the most frequently

mutated gene in breast cancer (30%) and renders cancer cells unable to initiate quiescence, senescence, or programmed cell death in the presence of unrepairable DNA damage (Shahbandi, Nguyen, & Jackson, 2020). Other mutations that affect cell cycle control in response to DNA damage have also been identified in breast tumours. For instance, germ-line *ATM* heterozygosity occurs in about 1% of the population and causes a 5- to 9-fold increase in risk of breast cancer in women (Swift, Morrell, Massey, & Chase, 2010). Further, loss of *ATM* expression was significantly associated with aggressive breast cancer and a higher mitotic index (Abdel-Fatah et al., 2014), probably due to the high rate of *ATM* copy number variation (391 of 852 analysed specimens in The Catalogue of Somatic Mutations in Cancer (*COSMIC))* (Bamford et al., 2004). *ATM* is located on the long arm of chromosome 11 (11q23.1) as are many other DDR components, such as *MRE11*, *CHK1* and the histone variant H2AX. Loss of heterozygosity at 11q is commonly observed in breast cancer (Laake et al., 1999), so many of these genes often display co-deletion with *ATM*.

The main functions of the other cell cycle checkpoints, including the replication stress and spindle assembly checkpoint (SAC), discussion of which is beyond the scope of this thesis, remain essential in tumour cells. Mutations in those pathways, which function to prevent mitotic entry and exit in the presence of replication stress or incomplete spindle assembly, respectively, are therefore not frequently observed in cancers (Matthews et al., 2021).

1.4.1 Therapeutic Opportunities in Breast Cancer

The genetic alterations discussed above promote S-phase entry and compromise the ability of cancer cells to initiate cell cycle exit. However, they also create enhanced dependency on the remaining intra-S and mitotic checkpoints for the preservation of genome integrity, and therefore reveal a clinical vulnerability that can be exploited for therapeutic purposes. Over the past decade, several new targeted therapies have emerged alongside surgery, radiotherapy, and

chemotherapy for the treatment of human tumours. Clinical implementation of ATR, CHK1, and WEE1 checkpoint kinase inhibitors (van Bijsterveldt, Durley, Maughan, & Humphrey, 2021) and CDK4/6 inhibitors (O'Leary, Finn, & Turner, 2016) has allowed for tumour targeting with improved effectiveness and lower drug-related toxicity in non-cancerous cells.

Radiotherapy and the majority of chemotherapeutics either directly damage the DNA or target basic cellular and metabolic processes that cause indirect DNA damage, both leading to checkpoint activation. Therefore, combining chemotherapeutics or radiotherapy with compounds targeting (intact) intra-S and mitotic checkpoint kinases are predicted to have favourable clinical outcomes based on the rationale that tumour cells lacking any functional checkpoints will not be able to arrest the cell cycle and repair DNA damage. This irreversible damage results in replicative catastrophe or is taken through into mitosis, where tumour cells undergo programmed cell death (Koniaras, Cuddihy, Christopoulos, Hogg, & O'Connell, 2001). Several druggable targets have been identified that can be inhibited to disrupt the intra-S and mitotic checkpoints (reviewed in Brandsma et al., 2017; Lin, McNeely and Beckmann, 2017; Smith et al., 2020; Gorecki, Andrs, & Korabecny, 2021).

Targeted cell death by combination therapies occurs through two main pathways: replicative and mitotic catastrophe, although they are not necessarily mutually exclusive. First, ATR, CHK1, and WEE1 play an important role in regulating CDK activity within the intra-S checkpoint (Poli et al., 2012; Saldivar et al., 2018). Inhibition of these checkpoint kinases therefore leads to higher CDK activity and elevated replication origin firing in S-phase (Moiseeva et al., 2017), thereby increasing the cellular demand for dNTPs. Moreover, ATR, CHK1, and WEE1 are critical for dNTP production in response to replication stress (Koppenhafer, Goss, Terry, & Gordon, 2020) through promoting the synthesis (Zhang, Jones,

Martin, Caplen, & Pommier, 2009), activation, and stabilization (D'Angiolella et al., 2012; Pfister et al., 2015) of ribonucleotide reductase (RNR). Thus, their inactivation can lead to under-replication, and depending on the mutational background, replicative catastrophe (Anda, Rothe, Boye, & Grallert, 2016; Beck et al., 2010; Saldivar et al., 2018; Toledo et al., 2013).

Second, regions of under-replicated DNA can be taken through into mitosis, where mitotic catastrophe is induced through chromosome mis-segregation or delayed cell death occurs after micronucleation (reviewed in Vitale et al., 2011). Inhibiting the DDR through abrogation of the damage induced G_2/M checkpoint, either via CDC25A stabilization by CHK1 or ATR inhibition, or via CDK1 re-activation through WEE1 inhibition, poses additional cytotoxicity (Kohn, Ruth, Brown, Livingstone, & Eastman, 2002; Wang, Decker, & Sebolt-Leopold, 2003). As cells subjected to G_2/M checkpoint inhibition cannot downregulate CDK1 activity, they enter mitosis and attempt to perform chromosome segregation with extensive DNA damage, ultimately leading to mitotic catastrophe and cell death (Figure 1.3).

Several examples of this have been taken into pre-clinical and clinical trials, including for various breast cancer subtypes. For example, integration of high throughput drug screening data and molecular tumour profiling from The Cancer Genome Atlas (TCGA) predicted AZD1775, a WEE1 inhibitor, to be the most effective drug in TNBC, mostly in patients with *TP53* mutations, followed by AZD7762, a CHK1 & CHK2 inhibitor (Gruener et al., 2021). High cyclin E expression levels in TNBC have previously been shown to predict increased sensitivity to WEE1 kinase inhibition (WEE1i) (Chen et al., 2018) (NCT03253679). Furthermore, co-administration of AZD1775 with standard-of-care paclitaxel was able to inhibit tumour growth and increase survival *in vitro* and in a xenograft mouse model of TNBC (Gruener et al., 2021), probably due to prolonged mitotic arrest following a combination of

these drugs (Lewis et al., 2017). In the recent FOCUS4-C clinical trial, AZD1175 monotherapy improved progression free survival in *RAS/TP53*-mutant colorectal cancer (Seligmann et al., 2021), suggesting that WEE1i treatment could also be a promising approach for TNBC management, as monotherapy, in combination with radiotherapy or other chemotherapeutic agents, or even in combination with other DDR inhibitors (Kong & Mehanna, 2021).

Similarly, another study reported synergy between AZD1775, the WEE1 inhibitor, and ATR inhibition (ATRi) in TNBC cells due to impaired DNA damage repair and excessive replication stress, ultimately leading to increased DNA damage and mitotic catastrophe. Dual inhibition of WEE1 and ATR inactivated RAD51-mediated HRR, which produced selective synthetic lethality and further sensitised TNBC cells to cisplatin (Bukhari et al., 2019; Jin et al., 2018).

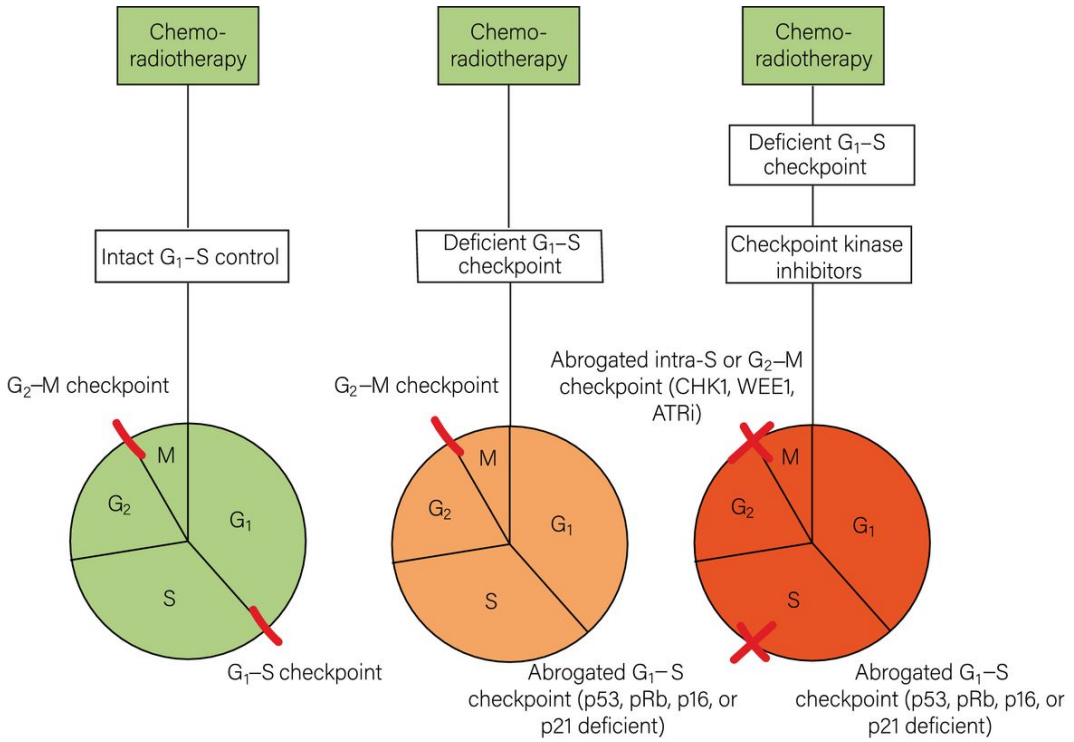

Figure 1.3. ***Combination therapy targets common cell cycle mutations in cancer.*** *Combination therapies target cancer cells that have lost one of the major cell cycle checkpoints, typically the G_1/S checkpoint, due to the inactivation of endogenous inhibitors (p16 or p21 family) or p53-mediated changes, ultimately leading to aberrant CDK activity and inactivation of RB (and E2F-mediated transcription). By inducing exogenous damage or replication stress in these cells, using chemoradiotherapy agents, and simultaneously targeting the intra-S or G_2/M checkpoints, cancer cells are unable to efficiently repair damage, prematurely enter mitosis, and undergo cell death. Figure reprinted from Clinical Cancer Research, with permission from AACR.*

1.5 MicroRNA-mediated Gene Regulation in Cancer

MicroRNAs (miRNAs) comprise a large family of small ~20-22 nucleotide non-coding RNAs that regulate protein-encoding genes via messenger RNA (mRNA) decay and translational repression (Lagos-Quintana, Rauhut, Lendeckel, & Tuschl, 2001). Numerous TSGs are under control of miRNA regulation, and various miRNA-mRNA pairs have therefore been associated with cancer phenotypes and hallmarks across tissue types (Dhawan, Scott, Harris, & Buffa, 2018).

In the majority of cases, miRNA-mRNA interactions are mediated by the miRNA seed region, a 6- to 8-nucleotide-long fragment at the 5'-end of the miRNA that typically binds to the 3' untranslated region (UTR) of the cytosolic target-mRNA (reviewed in Bartel, 2009). Each microRNA therefore has the potential to target hundreds of mRNAs that harbour seed region complementary sites (Lai, 2002; Lim et al., 2005), with estimates indicating that up to 60 percent of the protein-coding genes in the human genome is under miRNA control (Friedman, Farh, Burge, & Bartel, 2009). The fate of target-mRNAs depends on the degree of base-pairing complementarity between the mRNA molecule and the 'seed' region, where perfect complementarity between the seed region of the miRNA and the mRNA targets the transcript for AGO2-mediated degradation, whereas imperfect combination causes translational repression (Krol, Loedige, & Filipowicz, 2010; Vasudevan, Tong, & Steitz, 2007). The importance of miRNAs as master regulators of gene expression is further highlighted by the high percentage of cancers that bear single nucleotide polymorphisms (SNPs) in mature miRNA sequences or 3' UTR regions of mRNAs that alter miRNA-mRNA binding and processing, rendering these transcripts insensitive to miRNA-mediated regulation (Ziebarth, Bhattacharya, & Cui, 2012).

Numerous studies have demonstrated that RNA species, and miRNAs in particular, are dysregulated in human cancer. MicroRNAs could therefore be useful tools for tumour classification, diagnosis, prediction of treatment response, and prognosis (Peng & Croce, 2016). The adaptation of next-generation sequencing (NGS) techniques, such as small RNA sequencing (sRNA-seq), have allowed for the profiling of miRNAs in tumour and adjacent healthy tissues and revealed that each cancer type possesses a distinct miRNA expression signature (Stahlhut & Slack, 2013). This provides a strong basis for the classification of tumours according to their tissue of origin based on their miRNA signature (Rosenfeld et al., 2008), and as such recent efforts have been made to associate distinct miRNA patterns with breast cancer molecular subtypes and hormone receptor status (Farazi et al., 2014). Numerous miRNAs were found to be upregulated in breast cancer (Dvinge et al., 2013), and those that can act as oncogenes, for instance by downregulating TSGs, are generally termed '*oncomiRs*'. Currently, there are 1,917 annotated human miRNA precursor genes and mature miRNAs (http://www.mirbase.org/index.shtml), which use the assignment of miR-XXX-5p and miR-XXX-3p for mature miRNA sequences derived from the 5' and 3' arms of the mature miRNA hairpin duplex, respectively (miRBase 22.1 release, October 2018) (Griffiths-Jones, Grocock, van Dongen, Bateman, & Enright, 2006).

1.5.1 Genomic Organisation and Canonical Biogenesis of Mammalian MicroRNAs

Many miRNA-coding sequences are located within or overlap with annotated genes for mRNAs or other RNAs, often referred to as "host genes". Intronic or intergenic miRNAs located within the host gene, in the same orientation, may be co-transcribed along with the primary transcript through the same promoter. Debranched intronic primary miRNAs can be excised out by Drosha, a process that is thought to precede splicing, and a single transcript can thus give rise to both a mature miRNA and mRNA (Morlando et al., 2008). The presence of a miRNA sequence within an intron does, however, not necessitate co-regulation of the miRNA

with the host gene, as miRNA processing or alternative promoter usage can also affect mature miRNA levels (Baskerville & Bartel, 2005). Alternatively, miRNAs can be expressed as separate transcriptional units, which may encode a single microRNA hairpin precursor or clusters of multiple precursors (Corcoran et al., 2009).

MiRNA genes are transcribed by RNA Polymerase II (RNAPII), or occasionally RNA Polymerase III, to produce large primary miRNA (pri-miRNA) transcripts that are 5' capped and contain a 3' polyadenylated tail (Borchert, Lanier, & Davidson, 2006; Cullen, 2004; Lee et al., 2004). Following transcription, long pri-miRNAs are cleaved into ~85-nucleotide stem–loop structures called precursor miRNAs (pre-miRNAs) by the microprocessor complex, consisting of RNA-binding protein DiGeorge Syndrome Critical Region 8 (DGCR8) and Drosha, a member of the RNase III enzyme family (reviewed in Lee et al., 2002). DGCR8 functions as a molecular anchor to promote the fidelity of Drosha-mediated cleavage of stem loops (Filippov, Solovyev, Filippova, & Gill, 2000), which are embedded in the primary transcripts, thus determining the identity of both the 3' and 5' arm of the mature miRNA (Han et al., 2006).

Pre-miRNAs are subsequently exported from the nucleus by Ran/GTP/Exportin 5 (XPO5) and further processed by another multiprotein complex, including Argonaute 2 (AGO2), RNase III enzyme Dicer, and TRBP (trans-activation-responsive RNA-binding protein), into an unstable ~20–22-nucleotide miRNA/miRNA* duplex, where the passenger strand is designated miRNA*. This transient double-stranded miRNA duplex is unwound, after which a single guide strand (mature miRNA) is incorporated into the miRNA-containing ribonucleoprotein (miRNP) complex and the passenger strand (miRNA*) is degraded (Kwak & Tomari, 2012). Which strand is retained depends on the relative thermodynamic stability of the two ends of

the duplex intermediate (Khvorova, Reynolds, & Jayasena, 2003). The guide miRNA, associated with AGO2, is subsequently incorporated into a protein complex termed RNA-induced silencing complex (RISC), which subsequently tethers to (partly) complementary sequence motifs in target-mRNAs (Figure 1.4A) (Meister et al., 2004) The human genome contains eight AGO-family proteins, of which AGO2 is the only protein with RNA endonuclease cleavage activity and therefore the main effector of miRNA-mediated silencing (Hutvagner & Simard, 2008).

Alternatively, primary miRNA transcripts can be processed into mature miRNAs via a number of non-canonical pathways (Graves & Zeng, 2012). For example, pri-miRNAs of mirtron genes (i.e., intronic miRNA precursors) can be processed into pre-miRNAs by the splicing machinery, in a Drosha-independent way (Ruby, Jan, & Bartel, 2007). Similarly, some mature miRNAs are produced in a DICER-independent manner; instead, the pre-miRNA becomes loaded into Argonaute where it is cleaved to generate an intermediate 3′ end, which is then further trimmed (Cheloufi, Dos Santos, Chong, & Hannon, 2010; Kim, Kim, & Kim, 2016) (Figure 1.4B).

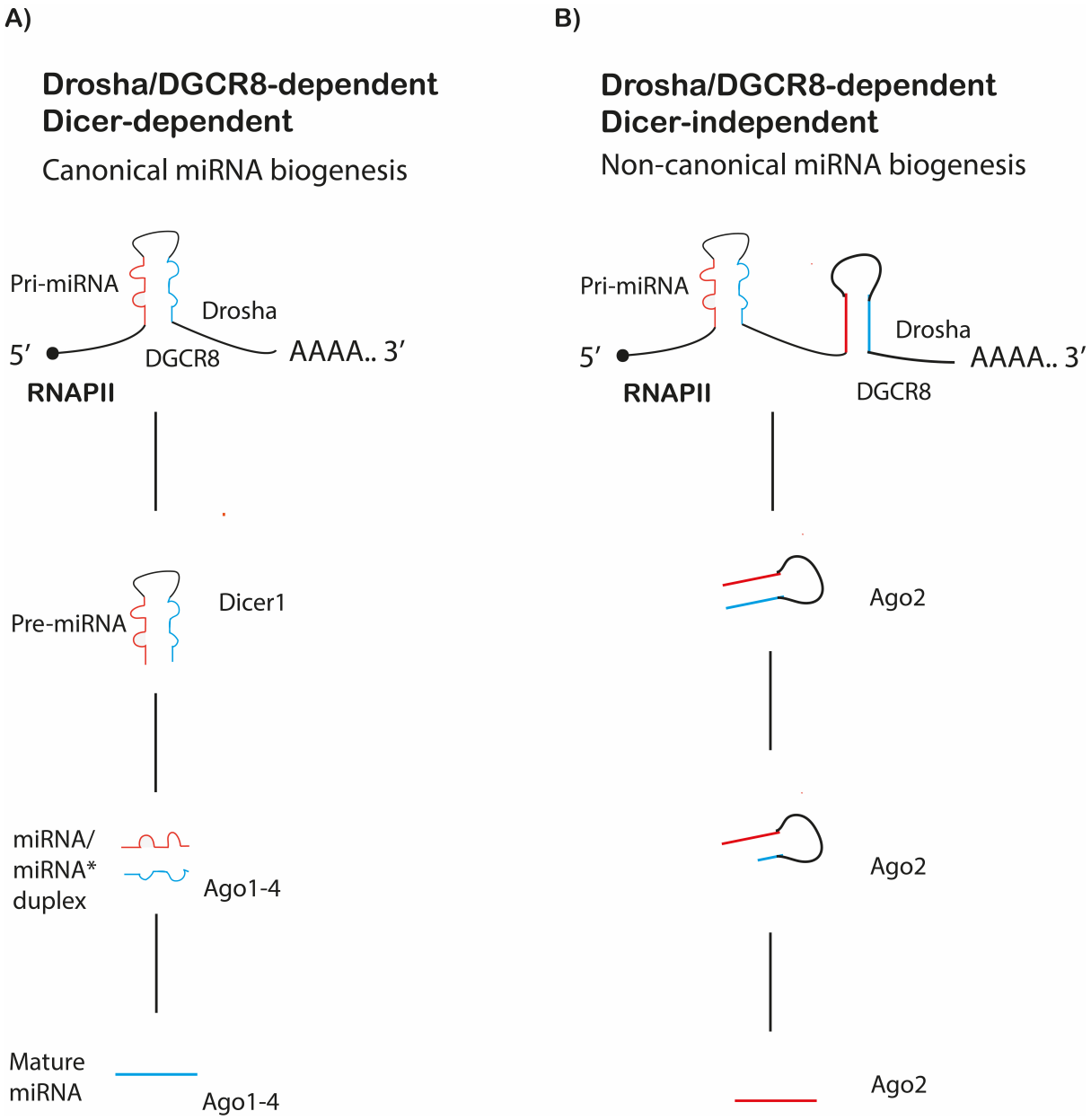

Figure 1.4. ***DICER-dependent and -independent miRNA biogenesis pathways in cancer.*** *A) Canonical miRNAs are transcribed by RNAPII to generate primary miRNA transcripts. Pri-miRNAs are cleaved into 85 nt stem-loop structures called pre-miRNAs by DGCR8 and DROSHA. Pre-miRNAs are exported to the cytoplasm, where the RNase III enzyme DICER cleaves towards the terminal loop end to generate miRNA/miRNA* duplexes. One of the duplex strands is preferentially retained in Ago1-4 to form the functional RNA-induced silencing complex. B). In non-canonical biogenesis, the pre-miRNA is directly incorporated into Ago2. Adapted from: (Yang and Lai, 2011).*

1.5.2 Mechanisms of miRNA Dysregulation in Cancer

Dysregulation of miRNA expression in cancer can occur through multiple mechanisms, including amplification or deletion of the sequence, epigenetic changes (including promoter methylation), alterations in miRNA biogenesis pathways or widespread transcription factor-mediated changes (reviewed in Gulyaeva & Kushlinskiy, 2016). Below, I provide a summary of important mechanistic aspects of miRNA dysregulation:

1) **Genetic alterations.** Approximately 50% of all human miRNA genes are located at fragile sites (chromosomal regions that are particularly prone to breaking) or within cancer-associated genomic regions, and consequently, miRNA expression can vary as a function of DNA copy number changes (Calin et al., 2004; Di Leva, Garofalo, & Croce, 2014; Zhang et al., 2006). Recent studies have additionally identified a number of miRNA genes and hotspots that are frequently overmutated across cancer types (Urbanek-Trzeciak et al., 2020).
2) **Epigenetic alterations.** Comprehensive mapping of human miRNA genes revealed that ~50% of miRNA loci were associated with CpG islands, CpG dinucleotide-dense regions that are subject to DNA methylation changes (Hsieh, 1994; Weber, Stresemann, Brueckner, & Lyko, 2007). DNA methylation plays a critical role in controlling gene expression, and consequently, DNA hypomethylation was shown to upregulate the expression of specific *oncomiR* species (Iorio et al., 2007; Saito et al., 2006; Scott, Mattie, Berger, Benz, & Benz, 2006).
3) **Alterations in miRNA biogenesis pathways.** MicroRNA expression levels can also be modulated as a consequence of defects or changes in the miRNA biogenesis machinery (Thomson et al., 2006). Reduced biogenesis efficiency and decreased global mature miRNA levels have previously been associated with mutations in exportin-5 (*XPO5*) (Melo et al., 2010) and *SMAD2, SMAD4*, and *DICER1* (Urbanek-

Trzeciak et al., 2020). Furthermore, genomic data revealed that a high number of malignancies display frequent loss of one allele of *DICER1* (via hemizygous deletion), a key RNase III endonucleases in miRNA maturation (Kumar et al., 2009; Zhang et al., 2006). Mouse models of cancer harbouring deletion of a single copy of *Dicer1* exhibited impaired miRNA processing (Kumar et al., 2009).

4) **Transcriptional control of miRNA(s) cluster(s).** MicroRNA expression is tightly controlled by different transcription factors, either constitutively or under specific conditions, and as such, altered miRNA expression in cancer can be attributed to dysregulation of key transcription factors (Peng & Croce, 2016). For example, c-Myc, which is frequently amplified or overexpressed in cancers, activates expression of the oncogenic miR-17–92 cluster (O'Donnell, Wentzel, Zeller, Dang, & Mendell, 2005).

1.5.3 The polycistronic miR-106b/25 cluster

The polycistronic miR-106b/25 cluster of miRNAs is located on chromosome 7 (7q22.1), in the 13th intron of the *MCM7* gene, and comprises three miRNA species: miR-106b, miR-93, and miR-25 (reviewed in Mehlich, Garbicz, & Włodarski, 2018). Individual miRNAs from the miR-106b/25 polycistron are generated from one long pri-miRNA transcript, which shares a promoter with its host gene, *MCM7*. Therefore, upregulation of the miR-106b/25 polycistron is strongly associated with amplification and overexpression of *MCM7* (Kan et al., 2009). Although *MCM7* and miR-106b/25 are often co-expressed through their shared modes of regulation, recent studies have identified novel mechanisms that can lead to discordance between the expression of the mature miRNAs and their host gene, *MCM7* (Mehlich et al., 2018). For instance, the miR-106b/25 polycistron can be transcribed independently of *MCM7*

in breast cancer cells, through a separate promoter which is induced by TGF-β and c-jun signalling (Gong et al., 2013; Ramalingam et al., 2014).

Expression of *MCM7* is cell cycle-regulated, and expression of the miR-106b5/25 cluster is therefore, in parallel with its host gene, under control of the E2F1 and E2F3 transcription factors (Brosh et al., 2008; Bueno et al., 2010; Petrocca et al., 2008). In turn, miR-106b and miR-93 can negatively regulate *E2F1* expression by targeting its 3' UTR in gastric cancer, establishing a miRNA-directed negative feedback loop, where the balance of E2F1 activity ultimately mediates cell fate decisions (i.e., induction of cellular proliferation or apoptosis, as excessive accumulation of E2F transcription factors results in pro-apoptotic activity) (Brosh et al., 2008; Petrocca et al., 2008; Shalgi, Lieber, Oren, & Pilpel, 2007).

The miR-106b/25 cluster of miRNAs is also under control of the damage-inducible transcription factor p53, and a decrease in miRNA expression was observed in human breast cancer specimens that harbour wild-type (WT) p53 when compared with those that harbour mutant forms of p53 (Brosh et al., 2008). Transcriptional activation by the MYC/E2F axis in *MYC*-driven cancers, or loss of the tumour suppressor protein p53, therefore results in overexpression of the miR-106b/25 cluster of miRNAs in breast tumours, where it can regulate multiple targets to change breast cancer characteristics, including the capability for migration, invasion, and proliferation (Li et al., 2017; Mehlich et al., 2018). Clustered miRNA genes demonstrate a high degree of sequence homology and functional cooperation but can still be differentially associated with patient prognosis, metastatic potential, and survival. For instance, miR-106b, but not miR-93 or miR-25, was identified as part of a so-called "hub RNA" regulating TNBC and TNBC-associated metastasis (Banerjee, Kalyani Yabalooru, & Karunagaran, 2020).

Changes in levels of circulating miRNAs in blood plasma and serum do not only predict prognosis but can also provide useful insights with regards to therapy response as many miRNAs are involved in regulating the drug resistance of tumour cells by targeting genes related to cell proliferation, cell cycle checkpoints, DNA damage repair, and apoptosis (Gottesman, 2002; Si, Shen, Zheng, & Fan, 2019). As an example, miRNAs from the miR-106b/25 cluster have been implicated in the regulation of chemosensitivity. Doxorubicin-resistant cells displayed significantly elevated miR-93 expression, which targets *PTEN* and thereby enhances the activity of the phosphatidylinositol-3 kinase (PI3K)/Akt pathway, implicated in drug resistance (Chu et al., 2017; Li et al., 2017). Finally, microRNAs can also function as "switches" in response to stress to allow cells to adapt to transient changes in their microenvironment. MicroRNAs from the miR-106b/25 cluster play an important role in response to mitogenic signalling, and their expression is thought to prevent replicative stress upon S-phase entry (Bueno et al., 2010).

1.6 Post-Translation Histone Modifications

Genomic DNA in eukaryotic cells is bound by histones, a family of evolutionarily conserved proteins that compact the DNA into condensed chromatin through creation of a DNA fibre (Kornberg, 1974). Nucleosomes, the repeating unit of chromatin, contain two copies of each of the four highly conserved alkaline core histones (H2A, H2B, H3 and H4) and approximately 147-149 base pairs of double-stranded DNA (Horn & Peterson, 2002; Luger, Mäder, Richmond, Sargent, & Richmond, 1997). Modifications that occur on amino acid (AA) side chains in the N-terminal tails that protrude from the surface of each histone octamer can alter nucleosome packing density through regulation of DNA-histone interactions and interactions between acidic histone domains of neighbouring nucleosomes (Arya & Schlick, 2009; Ruthenburg, Li, Patel, & David Allis, 2007). Chromatin density can also be regulated by chromatin remodellers and the incorporation of histone variants (reviewed in Venkatesh &

Workman, 2015). Together, those mechanisms of regulation determine the higher order structure of the chromatin, creating an equilibrium between active euchromatin (less condensed) and silent heterochromatin (highly condensed) domains (Horvath, Bailey, Locke, & Eichler, 2001). Both variations in packing densities and dynamic histone modifications allow for differences in the accessibility of transcription start sites (TSS) to RNAPII and transcription factors, and changes in chromatin compaction thus underlie altered expression of genes and other genetic elements (Horn & Peterson, 2002; Jiang & Pugh, 2009).

Two very well-characterised histone modifications include methylation of lysine (K) and arginine (R) residues of histone H3 or H4 by methyltransferases. Lysine methyltransferases transfer a S-adenosyl-L-methionine group to the ε-nitrogen of the target lysine residue, thereby generating mono-, di-, or tri-methylated states (me1, me2, and me3, respectively) (reviewed in Smith & Denu, 2009). Addition or removal of a methyl group does not alter the charge of the amino acid side chain and its function is therefore thought to be predominantly mediated by recruitment of so-called 'reader' complexes that contain a methyl-lysine-binding motif (reviewed in Musselman, Khorasanizadeh, & Kutateladze, 2014). Generally, H3K4 and H3K36 trimethylations are associated with euchromatin, whereas H3K9, H3K27 and H3K79 trimethylations mark heterochromatin (Black, Van Rechem, & Whetstine, 2012).

1.6.1 Structure and Function of the SETD2 methyltransferase

The tumour suppressor SET-domain-containing (SETD2) protein is the major histone methyltransferase catalysing histone H3 lysine 36 trimethylation (H3K36me3) in somatic mammalian cells (Edmunds, Mahadevan, & Clayton, 2008). In meiotic cells, H3K36me3 is catalysed by a different methyltransferase, PDRM9 (Eram et al., 2014). *PDRM9* expression is

normally restricted to germ cells, however, and therefore less likely to play a role during cancer development (Hayashi, Yoshida, & Matsui, 2005).

The human SETD2 protein consists of 2,564 AAs and has a predicted molecular weight of 287.5 kDa. To date, four conserved functional domains have been identified in SETD2, including a tryptophan (WW) domain, a Set2 Rpb1 (RNAPII) interacting domain (SRI), the SETD2-hnRNP Interaction domain (SHI), and the Set2 domain itself, which consists of the associated with SET (AWS), SET and Post-SET motifs (Bhattacharya, Levy, et al., 2021; Edmunds et al., 2008; Rebehmed, Revy, Faure, De Villartay, & Callebaut, 2014). The catalytic SET domain is a sequence of 130 AAs, originally named after the Drosophila genes "Suppressor of Variegation, Enhancer of Zeste and Trithorax" (Jenuwein, Laible, Dorn, & Reuter, 1998). By virtue of its catalytic domain, SETD2 transfers a methyl group from S-adenosyl-L-methionine to di-methylated lysine residue of the histone H3 tail to generate H3K36me3 (Edmunds et al., 2008) (Figure 1.5).

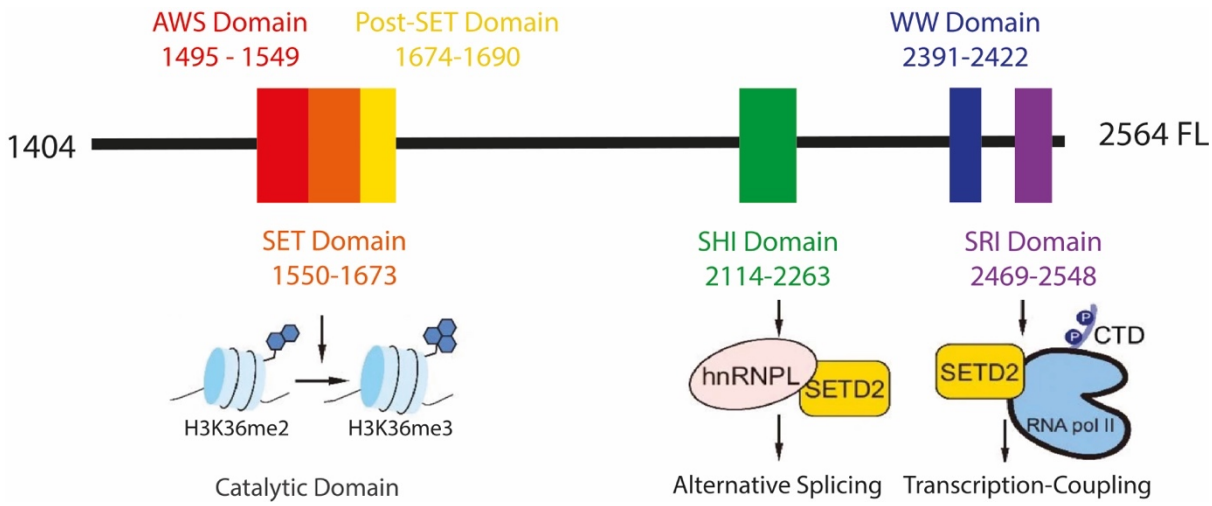

Figure 1.5. ***Cartoon illustrating known SETD2 protein domains (AA 1404-2564).*** *Coloured regions represent known SETD2 protein domains (red, orange, and yellow: AWS associated with SET, SET (Su(var)3–9, Enhancer-of-zeste and Trithorax), and post-SET domain; green: SHI (SETD2-hnRNP) domain; blue: WW domain; purple: SRI (Set2 Rpb1-interacting) domain). Adapted fro*m: *(Xiao et al., 2021).*

The SRI domain is highly conserved from yeast to humans (Rebehmed et al., 2014) and preferentially binds the elongating form of RNAPII, as revealed by its high affinity to both the serine 2- and serine 5- phosphorylated C-terminal domain (CTD) tail of the largest Rpb1 subunit of RNAPII (Kizer et al., 2005; Li, Howe, Anderson, Yates, & Workman, 2003). Hence, SETD2 catalyses, co-transcriptionally, H3K36 trimethylation via its association with elongating RNAPII (Sun et al., 2005), resulting in higher levels of H3K36me3 downstream of the first exons of actively transcribed genes (Bannister et al., 2005; Li et al., 2003; Shilatifard, 2006).

H3K36me3 is not only a hallmark of active transcription, but also has a role in preventing spurious transcription initiation through recruitment of the FACT histone chaperone complex (Carvalho et al., 2013). Loss of SETD2 causes loss of nucleosome occupancy (H2B) in active genes, leading to an increased RNAPII occupancy and formation of cryptic transcripts at intragenic sites (Carvalho et al., 2013). Recent studies have additionally revealed a role for H3K36me3 and histone acetylation in regulating polymerase pausing, and H3K36me3 may therefore also function as a speed control for transcriptional elongation (Zhang, Cavallaro, & Hebenstreit, 2021).

Further, SETD2 and H3K36me3 can also influence transcription through other mechanisms. Firstly, H3K36me3 can bind the PWWP domain of *de novo* DNA methyltransferase b (DNMT3b), to target accurately DNA methylation to cytosine residues in CpG-dense regions within actively transcribing gene bodies to prevent spurious transcription initiation events (Baubec et al., 2015; Neri et al., 2017). Secondly, H3K36me3 was found to participate in cross talk with other histone marks, and loss of H3K36me3 therefore leads not only to a failure in

establishing the correct DNA methylome, but also to invasion of H3K4me3 and H3K27me3 into former H3K36me3 territories (Q. Xu et al., 2019).

1.6.2 Biological Roles of SETD2

SETD2 has been shown to participate in divergent biological processes (Xiao et al., 2021), including regulation of DNA methylation (Baubec et al., 2015), cryptic transcription (Carvalho et al., 2013), DNA repair (Aymard et al., 2014; Li et al., 2013; Pfister et al., 2014; Sundarraj, Taylor, Kriegsheim, & Pradeepa, 2017), pre-mRNA splicing (Bhattacharya, Wang, et al., 2021; Sorenson et al., 2016), and chromosome segregation via its modulation of tubulin proteins (Park et al., 2016).

SETD2 has an important role in maintaining genome stability through facilitating both HRR of DNA DSBs and DNA mismatch repair (MMR), which corrects erroneous insertions, deletions, and mis-incorporation of bases that arise during DNA replication and recombination. Specifically, H3K36me3 is important for HRR in actively transcribing regions of the genome (Aymard et al., 2014; Pfister et al., 2014; Sundarraj et al., 2017). Loss of SETD2-dependent H3K36 trimethylation abolishes binding of Lens Epithelium Derived Growth Factor (LEDGF), also referred to as p75, to sites of DNA damage (Daugaard et al., 2012; Pfister et al., 2014). Reduced levels of LEDGF lead to impaired recruitment of the C-terminal binding protein interacting protein (CtIP) and other DNA repair proteins (e.g., PARP1), causing subsequent defects in DNA-end resection (Daugaard et al., 2012; Pfister et al., 2014; Sundarraj et al., 2017). Unresected DSBs cannot rely on HRR for efficient repair and cells therefore have to use alternative and often more error-prone mechanisms of repair, such as NHEJ and/or microhomology-mediated end-joining (MMEJ) (Pfister et al., 2014).

Secondly, SETD2 also has an important role in regulating alternative splicing (AS), both in fission yeast and mammalian cells. In *S. cerevisiae*, faithful mRNA splicing was shown to depend on association of the Set2 SRI domain with the RNAPII CTD, suggesting that Set2 may act co-transcriptionally to recruit splicing factors (Sorenson et al., 2016). Deletion of Set2 did indeed result in decreased splicing efficiency across the genome, partly due to endogenous intron retention (Sorenson et al., 2016). In mammalian cells, studies have similarly found that H3K36me3 can regulate mRNA splicing. SETD2 can engage RNA-binding proteins such as the heterogeneous ribonucleoproteins (hnRNPs) through its SHI domain to couple transcription with RNA splicing (Bhattacharya, Levy, et al., 2021; Bhattacharya, Wang, et al., 2021). Constitutive exons, but not alternative exons and introns, are preferentially enriched with H3K36me3 (Kolasinska-Zwierz et al., 2009), where it facilitates exon definition through recruitment of the splicing regulator polypyrimidine tract-binding protein (PTB) via the chromatin binding MORF-related gene (MRG15) (Kolasinska-Zwierz et al., 2009; Luco et al., 2010).

Finally, epigenomic features can also regulate replication timing. Modulation of the H3K36/H3K9-specific histone demethylase, KDM4A, for instance, can alter replication patterns, especially in mid-S-phase (Van Rechem et al., 2021).

1.6.3 SETD2 and H3K36me3 in Cancer

SETD2 and H3K36me3 are frequently lost in clear cell renal cell carcinoma (ccRCC) patients (Duns et al., 2010), and biallelic inactivation of *SETD2* is strongly linked with larger tumour size, advanced disease stage, and elevated risk of carcinoma-related death (Hakimi et al., 2013; Ho et al., 2015; Liu et al., 2015). According to the COSMIC database, *SETD2* is ranked fourth in the top-20 most commonly mutated genes in ccRCC with 11% of samples bearing mutations,

only preceded by *VHL* (46%), *PBRM1* (31%), and *BAP1* (12%) (http://cancer.sanger.ac.uk/cosmic). Multi-region exome sequencing revealed that H3K36me3 levels were significantly reduced in a subset (~20%) of primary ccRCC tumour cells (Ricketts & Linehan, 2014), consistent with recent clinical reports indicating that mutations of the *SETD2* gene occur in up to 12% of early stage ccRCC cases (Liu et al., 2015). Notably, however, H3K36me3-positive nuclei were further reduced in metastatic ccRCC (with 60%), suggesting that SETD2 methyltransferase activity is progressively impeded during RCC tumour progression (Ho et al., 2015). Recent studies have additionally found that loss of *SETD2* facilitates the transition from c-MYC–driven polycystic kidney disease (PKD) to ccRCC by promoting epithelial-to-mesenchymal transition and tumourigenesis through the hyperactivation of Wnt/β-catenin signalling (Rao et al., 2021), reinforcing the notion that SETD2 is an important tumour suppressor in renal cancer. Interestingly, *SETD2* mRNA and protein levels can also be downregulated in ccRCC at a post-transcriptional level via miR-106b-5p-mediated degradation (Xiang et al., 2015).

Tumour cells bearing frameshift or missense mutations in *SETD2* completely lack trimethylated H3K36 (Gerlinger et al., 2012), and although under-expression and mutation of *SETD2* is most commonly found in kidney cancer, mutations in and loss of *SETD2* have also been reported in a wide range of other tumour types, including lung cancer (Jin et al., 2021; Walter et al., 2017), stromal tumours (Huang et al., 2016), glioma (Fontebasso et al., 2013), leukaemia (Zhu et al., 2014), and breast cancer (Al Sarakbi et al., 2009).

1.6.4 Targeting *SETD2*-deficient Cancers

Synthetic lethality approaches seek to exploit the aberrant genetics associated with cancer development (e.g., gene mutation, deletion of amplification of gene *A*) by targeting a second

(unlinked) gene partner (gene *B*) with a drug, where only the combined impact of these alterations causes cellular death (reviewed in Guarente, 1993). This approach is therapeutically advantageous over the use standard anti-cancer agents, in that their enhanced selectivity towards tumours cells can limit cytotoxic side effects.

H3K36me3-deficient cancers can be targeted by exploiting a synthetic lethal interaction with WEE1 inhibition (WEE1i) (Pfister et al., 2015). In addition to a checkpoint function for WEE1 at the G_2/M transition, as described in Section 1.3.1, WEE1 also plays an important role in regulating CDK activity and replication dynamics during S-phase (Beck et al., 2012; Booher, Holman, & Fattaey, 1997). Loss of WEE1 causes reduced inhibitory tyrosine-15 phosphorylation on both CDK1 and CDK2 and subsequent hyperactivation of CDK activity during S-phase (Gu, Rosenblatt, & Morgan, 1992). Hyperactive CDK activity during DNA synthesis leads to unscheduled origin firing and subsequent RPA exhaustion, nucleotide pool depletion and reduced replication fork progression (Beck et al., 2012).

Furthermore, hyperactivation of CDK1 and CDK2 following WEE1i also leads to degradation of RRM2, the catalytic subunit of RNR (D'Angiolella et al., 2012). RNR catalyses the rate-limiting step of the formation of deoxyribonucleotides, the precursors of DNA synthesis, by direct reduction of the corresponding ribonucleotides (Elledge, Zhou, & Allen, 1992). Elevated CDK activity in the presence of AZD1775 causes increased phosphorylation of RRM2 at threonine 33, which exposes the CY motif (residues 49-51 of RRM2) for Cyclin F recognition, thereby promoting RRM2 ubiquitination and degradation via the SCF-Cyclin F complex (D'Angiolella et al., 2012; Pfister et al., 2015). *SETD2*-deficient cells display lower *RRM2* transcript levels and can therefore be preferentially targeted with AZD1775 as dNTP pools reach critically low levels (Pfister et al., 2015).

Despite the complex responses initiated by the cell to stabilise and restart perturbed replication forks, persistent replication stress can provoke catastrophic widespread fork collapse (reviewed in Zeman & Cimprich, 2014). Fork collapse involves dissociation of the replisome and the formation of a DNA DSB at the site of the stalled replication fork, in an ATR, MUS81, and Bloom's syndrome-associated (BLM) helicase-dependent manner (Shimura et al., 2008). Reduced intracellular dNTP pools in *SETD2*-deficient cells following WEE1 inhibition similarly cause stalled replication forks to collapse into transient DSBs. Therefore, cell death resulting from loss of *SETD2* and WEE1 inhibition is primarily caused by excessive DNA damage, and ultimately, cell death by replicative catastrophe (Pai et al., 2019; Pfister et al., 2015).

1.7 Thesis Aims

1.7.1 Understanding the Role of miRNA Biogenesis Pathways in *oncomiR* Production

MicroRNA abundance can be dysregulated at the transcriptional level, through increased or reduced transcription of precursor miRNAs, or as a result of modified miRNA processing, which alters the rate or efficiency at which mature miRNAs are produced and can bind to their target transcripts. In Chapter 3, the aim is to better understand the interplay between these two mechanisms of miRNA regulation during cancer evolution, and to further elucidate how genomic alterations contribute to oncogenic miRNA production, especially of the miR-106b/25 cluster of miRNAs.

1.7.2 Exploring a Role for miR-106b-5p as Biomarker for WEE1-inhibitor sensitivity

We know that genetic alterations causing early entry into S-phase, such as mutation of *TP53*, or elevated (intrinsic) replication stress, such as *RAS* gain-of-function, cause cells to display enhanced sensitivity to WEE1 kinase inhibitor treatment (Seligmann et al., 2021). In Chapter

4, I explore the utility of miR-106b-5p as a WEE1i sensitivity biomarker in breast cancer cells through evaluating the associations between miR-106b-5p levels and activity of the RB/E2F-pathway, which drives S-phase entry. Furthermore, I investigate the clinical parameters associated with miR-106b-5p overexpression and explore whether miR-106b-5p plays a role in regulating tumour growth.

1.7.3 Understanding Differential Expression Changes of Early-Response Genes and miRNAs to Ionising Radiation and Hydroxyurea Treatment

Cells have evolved a range of mechanisms to distinguish between, and deal with, damages from different sources (Blackford & Jackson, 2017). We do not know, however, how miRNAs might regulate the differential activation of various cell cycle checkpoints in response to stress (e.g., hydroxyurea) or DNA damage (e.g., ionising radiation). In Chapter 5, I aim to identify specific DNA damage- or replication stress-inducible miRNAs and shine some light on their roles in regulating the cellular stress response by identifying miRNA-mRNA pairs which may be relevant for the regulation of cell cycle progression. Moreover, I further characterise roles for SETD2 and the miR-106b/25 cluster of miRNAs in response to both IR and HU treatment.

1.7.4 Understanding the Role of SETD2-dependent H3K36me3 in the Transcriptional Checkpoint Response

Studies in fission yeast have shown a role for Set2-dependent H3K36 methylation in promoting MluI cell-cycle box (MCB) binding factor (MBF)-complex-dependent transcription, including that of the large RNR subunit *cdc22* (Pai et al., 2017). This mechanism of transcriptional activation is important at the G_1/S transition, but also in response to genotoxic stress to prevent the formation of replication stress-induced DNA damage. In the final chapter, I ask whether the role for SETD2-dependent H3K36 trimethylation in facilitating E2F-dependent cell cycle

transcription is conserved across species. Furthermore, I ask whether SETD2-dependent maintenance of E2F-mediated transcription in S-phase is dependent on the replication stress checkpoint and therefore test the relationship between ATR/CHK1-activation and global H3K36me3 distribution.

Chapter 2
Materials and Methods

2.1 Genomic and Transcriptomic Analyses of Clinical Datasets

Genomic and transcriptomic data from 1,098 Breast Invasive Carcinoma (BRCA) samples were downloaded from TCGA (https://portal.gdc.cancer.gov/projects/TCGA-BRCA) (Koboldt et al., 2012). Specifically, this dataset contained 1,079 samples with complete genomic (genotyping array) and transcriptomic (RNA-sequencing and miRNA-sequencing) data. Individual patient files containing RSEM (RNA-Seq by Expectation-Maximization) normalised read counts (Illumina HiSeq) for mRNA expression were downloaded (Li & Dewey, 2011), $\log_2$ transformed and combined into a single matrix. Genes expressed in fewer than 25% of clinical samples were removed from further analysis. Putative copy number (CN) calls were determined using GISTIC 2.0 (Genomic Identification of Significant Targets in Cancer) (Mermel et al., 2011) and comprised a list of predicted segments with a CN status between 0 – 6 (normal diploid CN = 2). Genes were considered amplified if CN > 2 and the full region of the gene was located within the amplicon segment.

The METABRIC (Molecular Taxonomy of Breast Cancer International Consortium) clinical cohort contained 1,992 cancer and 144 normal tissue samples (Curtis et al., 2012). Pre-processed METABRIC files were downloaded from the European Genome-Phenome Archive (EGA) (Study ID: EGAS00000000083), summarised and quantile-normalised. Probe to gene-level mapping was performed by keeping the most variable (standard deviation, SD) probe. Log_2 scaled data was used for differential expression analysis. Copy number data from segmented genomic regions was obtained from the original publication and processed to create gene-by-patient $\log_2$ ratios and calls profiles (Curtis et al., 2012). In the METABRIC dataset, genes were considered amplified when their amplification frequency (cut-off = 0.128) was 40

times higher than the estimated average mutation rate (=0.031), which was calculated by assessing the amplification frequency for permutations of 43 random genes (n=1000).

Correlation analyses of copy number and genome-wide miRNA and mRNA expression, or mRNA expression and genome-wide miRNA expression were performed using Spearman's coefficient tests. P-values were corrected for multiple testing using the FDR (False Discovery Rate) method (Benjamini & Hochberg, 1995). The cBioPortal for Cancer Genomics (http://cbioportal.org) was used to visualise these two datasets (Cerami et al., 2012; Gao et al., 2013).

2.2 Cancer Cell Line Encyclopaedia (CCLE) Data and Analyses

Gene-level copy number (Affymetrix SNP6) and mRNA expression data (CCLE_expression_full.csv, Affymetrix U133 Plus 2.0) of the Broad-Novartis Cancer Cell Line Encyclopaedia (CCLE) (Barretina et al., 2012) were collected from the cBioPortal for Cancer Genomics (Cerami et al., 2012; Gao et al., 2013). Copy number variations of segmented genomic regions were normalised against the cell line's background ploidy. Amplification of a gene was defined as > 1 of the ploidy-corrected copy number. Expression levels were expressed as $\log_2(TPM + 1)$ (Transcripts per Million) values.

2.3 Tissue Culture

2.3.1 Revival of Frozen Cell Lines

Cell lines stored in liquid nitrogen were rapidly thawed at 37 °C for 2 minutes. Cells were washed with complete media to remove dimethyl sulfoxide (DMSO) from the freezing media and pelleted by centrifugation at 1,300 rpm for 5 minutes. The supernatant was removed, the

cell pellet resuspended in 5 ml complete media and the cell suspension transferred to a T25 cell culture flask.

2.3.2 Cell Line Maintenance

MCF10A cells were cultured in DMEM /F12 Ham's Mixture supplemented with 5% horse serum (Life Technologies), epidermal growth factor (EGF) 20 ng/ml (Peprotech), insulin 10μg/ml (Sigma), hydrocortisone 0.5 mg/ml (MP Biomedicals UK), cholera toxin 100 ng/ml (Sigma), 100 units/ml penicillin (Sigma), and 100 μg/ml streptomycin (Sigma). BT-549, HCC1806, HCC70, and T-47D cells were cultured in RPMI-1640 medium supplemented with 10% v/v foetal bovine serum (FBS, Sigma), 100 units/ml penicillin (Sigma), and 100 μg/ml streptomycin (Sigma). All other cell lines were maintained in complete media consisting of Dulbecco's Modified Eagle's Medium (DMEM) supplemented with 10% v/v foetal bovine serum (FBS, Sigma), penicillin (100 units/mL, Sigma), and streptomycin (0.1 mg/mL, Sigma) at 37°C in a humidified atmosphere containing 5% CO_2. Culture media were changed every 2-4 days, while cells were passaged, when 70% confluence was reached, at a split ratio of 1:8-1:10 using 0.25% (w/v) Trypsin-EDTA (Life Technologies) for 5 minutes at 37°C. Exposure of cell cultures to hypoxia (1% O_2) was undertaken in an *In vivo2* Hypoxia Work Station (Ruskin Technologies, Pencoed, UK) in parallel with cells maintained in normoxic conditions (21% O_2).

2.3.3 Cryopreservation of Cell Lines

Log-phase growing cells were rinsed with phosphate buffered saline (PBS) and trypsinised using 0.25% (w/v) Trypsin-EDTA (Life Technologies) for 5 minutes at 37°C. 1 x 10^6 cells were spun down at 500 g for 5 minutes and re-suspended in 1 ml freezing media (FBS supplemented with 10% (v/v) DMSO. The cell suspension (1 mL aliquots) was transferred to

a cryovial and frozen at -80 °C overnight before being transferred into liquid nitrogen (vapor phase) for long-term storage.

2.4 Cell Lines

The U2OS (human osteosarcoma) cell line was obtained from ATCC (ATCC number HTB-96). The U2OS *SETD2* CRISPR knockout (KO) cell line was generated by Dr Sovan Sarkar and Dr Sophia Pfister using the CRISPR-Cas9 technology as previously described (Pfister et al., 2015). The target sequence of the chimeric gRNA scaffold was ACTCTGATCGTCGCTACCAT (first exon of *SETD2*). MCF7 and MDA-MB-231 (ER-/PR-/HER2-) breast cancer cell lines were obtained from A. Ryan, MDA-MB-453, MDA-MB-468, BT474, BT549, SKBR3, HCC1806 and T47D cell lines were kind gifts from A. Harris. T98G cells were derived from human glioblastoma and obtained from the lab of Dr Rob De Bruin. MCF10A cells were obtained from ATCC (ATCC number CRL-10317). JIMT-1 (ACC-589) was obtained from Deutsche Sammlung von Mikroorganismen und Zellkulturen (DSMZ). HCC70 cells were obtained from ATCC (ATCC number *ATCC* CRL-2315).

2.4.1 Cell Cycle Synchronisation

Synchronisation of T98G cells in quiescence was achieved by culturing cells in serum-free DMEM for 72 hours. Cells were released from G_0-G1 arrest by addition of complete media.

2.5 Gene Silencing

2.5.1 Transfection of siRNAs, miRNA mimics, or miRNA inhibitors

All small-interfering RNAs (siRNAs) (12 nM final concentration) or miRNA mimics/inhibitors (25 nM final concentration) were delivered to cells using Lipofectamine RNAiMAX Transfection Reagent (Invitrogen) according to the manufacturer's instructions.

RNA-lipid complexes were prepared directly inside the wells, after which cells and serum free medium (Opti-MEM, Reduced Serum Medium) were added (reverse transfection). Medium was replaced 16-20 hours after transfection.

The target sequences of the siRNAs used in this project are listed below:

Non-targeting (NT) siRNA: proprietary sequence of supplier (Qiagen)

siSETD2#3 (si#3) (Dharmacon): GAAACCGUCUCCAGUCUGU

siSETD2#5 (si#5) (Dharmacon): UAAAGGAGGUAUAUCGAAU

siE2F6 (Custom): AAGGAUUGUGCUCAGCAGCUG (Oberley, Inman, & Farnham, 2003)

siCDKN1A (ON-TARGETplus SMARTpool, Dharmacon): L-003471

siDICER1 (ON-TARGETplus SMARTpool, Dharmacon): L-003483

siAGO2 (ON-TARGETplus SMARTpool, Dharmacon): L-004639

The target sequences of the microRNA hairpin inhibitor used in this project are listed below:

miRIDIAN microRNA hsa-miR-106b-5p Mature microRNA sequence:

UAAAGUGCUGACAGUGCAGAU (mimic): C-300649

miRIDIAN microRNA mimic negative control #1: CN-001000-01

miRIDIAN microRNA Hairpin Inhibitor Negative Control #2: CN-002000-01

miRIDIAN hsa-miR-106b-5p hairpin inhibitor (Dharmacon): IH-300649

miRIDIAN hsa-miR-93-5p hairpin inhibitor (Dharmacon): IH-300512

2.5.2 Plasmid Transfection

The SETD2 FL-GFP and SETD2 ΔSRI-GFP plasmids were obtained from Jerry Workman's research group (Bhattacharya, Levy, et al., 2021). Cells were seeded in a 6-well plate (4 x 10^5 per well) overnight prior to transfection. Plasmid DNA (2 μg) was transfected into cells using

jetPRIME (Polyplus) according to manufacturer's instructions. The medium was replaced 16 hours after transfection and the cells were allowed to recover for another 24 hours. The plasmids used in this study are listed below:

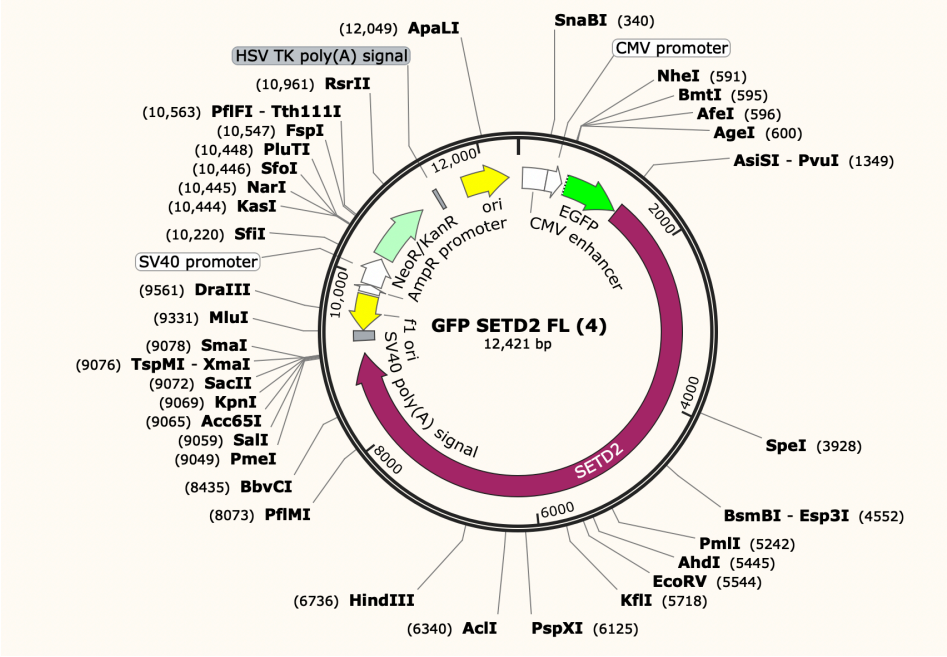

Figure 2.1. ***Map of the SETD2 FL (Full-Length)-GFP plasmid****. Map of the 12,421 bp vector with CMV promoter, GFP reporter gene, and kanamycin resistance marker.*

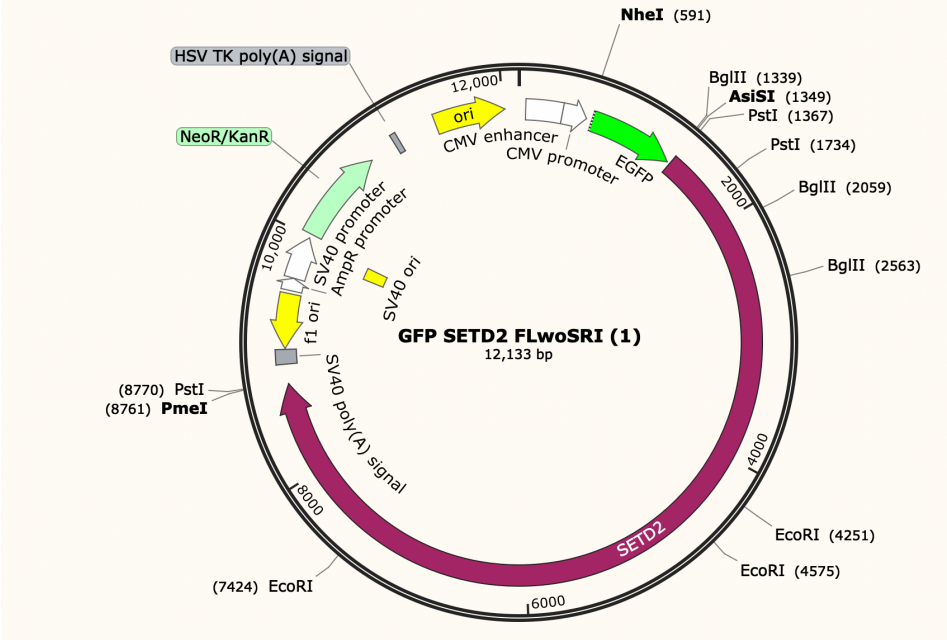

Figure 2.2. ***Map of the SETD2 ΔSRI-GFP plasmid****. Map of the 12,133 bp vector with CMV promoter, GFP reporter gene, and ampicillin resistance marker.*

2.6 Protein Detection by Western Blotting

2.6.1 Sample Collection for Western Blotting

Cells were washed with PBS, harvested, and lysed in lysis buffer (50 mM Tris HCl pH 7.5, 150 mM NaCl, 1% Triton X-100) supplemented with 1:50 fresh protease inhibitor cocktail and 1:100 fresh phosphatase inhibitor cocktail (1mM NaOVa; 10mM NaF; 10mM NaPyrophosphate) for 10 minutes on ice. Cell lysates were sonicated using the Bioruptor (Diagenode) at high intensity for 15 s on/10 s off cycles for 5 rounds. Lysates were centrifuged at 17,000 g for 10 minutes at 4 °C to pellet cellular debris. The supernatant was subsequently transferred to a fresh Eppendorf tube and protein concentrations were quantified by the Bradford Protein Assay using the Pierce Coomassie Plus Assay Reagent.

2.6.2 Western Blotting

25-35 µg of protein was mixed with the NuPAGE LDS loading buffer (Invitrogen) and the reducing agent dithiothreitol (DTT) (3: 1 ratio). Samples were denatured by boiling for 3-5 minutes at 95 °C. Then, the different protein samples (using anti- α-GAPDH/β-Tubulin antibody as loading control) were separated onto a pre-cast 3-8% or 4-12% NuPAGE Tris-Acetate gel (Invitrogen) followed by transfer onto a polyvinylidene fluoride (PVDF) membrane (0.45 µm pore size) (Invitrogen) according to the manufacturer's instructions. After transfer, residual binding sites on the membranes were blocked with 4% skimmed milk, or Bovine Serum Albumin (BSA) for histone proteins, in PBS-$T_{0.05}$ for 45-60 minutes at room temperature and probed with the appropriate primary antibodies at 4 °C overnight (5% BSA in TBS-Tween Buffer, pH 7.4). The membranes were washed three times with PBS-$T_{0.05}$, followed by incubation with horseradish peroxidase-conjugated (HRP)-conjugated secondary antibodies (1:4000) for 1 hour at room temperature. Antibody reactivity was visualised with the Pierce ECL Western Blotting Substrate (Thermo Scientific) using the ChemiDoc™ MP

Imaging System (Bio-Rad) as per the manufacturer's instructions. The relevant bands were scanned and quantified using ImageLab Software 5.2.1. Blots were either stripped and re-probed, or washed in PBS, wrapped in cling film and stored at -20°C.

2.6.2 Antibodies

Targets of the primary antibodies used for western blotting are as follows: β-Actin (Abcam, 1:4000, ab6276), Argonaute 2 (Cell Signalling Technology, 1:1000, 2897), Apoptosis Cocktail (pro/p17-caspase-3, cleaved caspase-3, cleaved-PARP, cleaved-actin) (Abcam, 1:500, ab136812), ATR (Cell Signalling Technology, 1:500, 2790), phospho-ATR (Ser428) (Cell Signalling Technology, 1:500, 2853), Chk1 (2G1D5) (Cell Signalling Technology, 1:1000, 2360), phospho-Chk1(S317) (Cell Signalling, 1:1000, 2344), cyclin E2 (Cell Signalling Technology, 1:1000, 4132), Dicer (Santa Cruz Biotechnology, 1:1000, H-212), E2F1 (Santa Cruz Biotechnology, 1:1000, sc-193), GAPDH (Novus, 1:4000), phospho-γ-H2AX(Ser139) (1:1000, Upstate, 05-636), H3K36me3 (Abcam, 1:1000, ab9050), Histone H3 (Abcam, 1:4000, ab1791), p21 Waf1/Cip1 (12D1) (Cell Signalling Technology, 1:1000, 2947), MCM2 (Cell Signalling Technology, 1:2000, 4007S), MCM7 (Santa Cruz Biotechnology, 1:1000, sc-9966), p53R2 (Abcam, 1:1000, ab8105), PCNA (Santa Cruz Biotechnology, 1:1000, 2586), R2/RRM2 (Santa Cruz Biotechnology, 1:1000, sc-10844), phospho-RB (Ser807/811) (Cell Signalling Technology, 1:1000, 9308), phospho-RPA32(Ser33) (Bethyl Laboratories, 1:1000, A300-246A), SETD2 (D5T1Q) (Cell Signalling Technology, 1:500, 23486), α-Tubulin (Sigma, 1:2000, T5168). Secondary Alexa Fluor antibodies were purchased from Invitrogen.

2.7 Drugs and Inhibitors

Hydroxyurea powder (Sigma) was reconstituted in sterile water. All other inhibitors were prepared in 100% DMSO at a concentration of 10 mM and stored at -80 °C. All stock solutions

were aliquoted and stored at -20 °C until use, and dilutions of the drugs for treatment of cells were made using DMSO and/or complete culture media.

WEE1 inhibitor: AZD1775 (MK-1775) (Axon Medchem)

CHK1 inhibitor: UCN-01 (Sigma-Aldrich)

ATR inhibitor: VE-822 (Axon Medchem)

P21 inhibitor: UC2288 (Merck Chemicals)

2.7.1 Ionising Radiation

Cells were exposed to the indicated Gray (Gy) of ionising radiation (IR) using a ^{137}caesium source (Gamma-Service Medical GmbH) at a dose rate of 1.3 Gy/min. Cells were left to recover in a 5% CO_2 incubator at 37°C for the indicated recovery times. For the sequencing experiments, cells were collected at times 0 (untreated), 2, and 6 hours after exposure.

2.8 Cellular Survival Assays

2.8.1 Clonogenic Survival Assay

48 hours after siRNA transfection, cells were seeded in 6-well plates at low densities (600-800 cells per well) and allowed to attached overnight at 37 °C. Culture media were subsequently replaced with media containing DMSO or the appropriate concentrations of the desired inhibitors or DNA damaging agents. Colonies were washed with PBS and stained with Brilliant Blue R Concentrate (Sigma) for 1 hour with gentle shaking after 7-10 days of culturing. Colonies consisting of > 50 cells were counted using a colony counter (GelCount, Oxford Optronix, Oxford, UK). Plating efficiency (PE) and Surviving Fraction (SF) were calculated according a previously published protocol (Franken, Rodermond, Stap, Haveman, & van Bree, 2006).

2.8.2 Resazurin Assay for Cell Viability

Equal numbers of cells were seeded in triplicate in 96-well plates (Corning, Flat-Bottom) 24 hours prior to inhibitor treatment. At the desired time point after treatment (between 48-96 hours), culture medium was removed and fresh complete medium without phenol red, containing 10 µg/ml resazurin (Sigma), was added to each well. Resazurin is a nonfluorescent dye that can be converted via a redox reaction to a red fluorescent compound, resorufin, by living cells. The fluorescent signal is thus proportional to the number of living cells and was measured with a POLARstar Omega plate reader (BMG Labtech GmbH, Ortenberg, Germany) with excitation at 544 nm, emission at 590 nm, and gain 1000 after 2 hours of incubation at 37°C. The average of the values of the triplicate 'blank' wells were subtracted from all other wells and normalised to the average of the control-treated wells (DMSO or dH_2O). For drug treatment experiments, the IC_{50} was defined as the concentration of drug that reduces viability by 50%.

2.8.3 Spheroid Formation Assay

Cells grown as a monolayer were detached with trypsin (48 hours post-siRNA transfection) to generate a single cell suspension. The cell suspension was diluted to 2.5 x 10^4 cells per ml of ice-cold medium. We plated at a total of 5000 cells per spheroid. The Matrigel Basement Matrix (reconstituted basement membrane BD Biosciences, Bedford, MA 734-1100) was thawed overnight (on ice) and added to the cell suspension with ice-cold pipette tips at a final concentration of 2.5%. A volume of 200 µl of this cell suspension was added to each well of an Ultra-Low Cluster 96-well plate (COSTAR 7007) with a round bottom. The spheroid formation was initiated by centrifugation of the plates at 1000 g for 10 min. The plates were incubated under standard cell culture conditions at 37° C, 5% CO_2 in humidified incubators. After 10 days of growth, images were taken. The area of the spheroid was measured using

ImageJ Open-Source Software (http://imagej.nih.gov/ij/) as previously described (Leek, Grimes, Harris, & McIntyre, 2016).

2.9 Cell Cycle Analysis by Flow Cytometry

Cells were incubated in media containing 20 μM bromodeoxyuridine (BrdU) for 30 minutes at 37 °C and then collected by trypsinisation and fixed in ice-cold excess 70% ethanol for a minimum of 30 minutes. Cells were centrifuged at 250 g for 5 minutes and incubated in 1 ml of HCl containing 0.1 mg/ml pepsin, to denature double-stranded DNA and digest nuclear proteins. Cells were washed once in 2 ml PBS and centrifuged at 350 g for 5 minutes, followed by a wash with 1 ml PBS containing 2% FBS and 0.5% Tween. Cell pellets were resuspended in 100 μl PBS containing 2% FBS (Blocking Buffer) and 2 μl anti-BrdU monoclonal antibody (1:50 dilution, BD clone 44, cat. no. 347580) and incubated for 90 minutes at room temperature, mixing every 30 minutes. Cells were washed twice with blocking buffer and incubated with 100 μl 2 PBS containing 2% FBS and 0.5 μl Alexa Fluor 488 secondary antibody (1:200 dilution, Life Technologies) for 60 minutes at room temperature in the dark. Cells were washed with PBS and resuspended in 0.5 ml PBS containing 10 μl propidium iodide (PI) and 10 μl RNAse (Invitrogen). Samples were analysed by Fluorescence-Activated Single Cell Sorting (FACS) scan (Beton Dickinson).

2.10 Quantification of microRNAs

2.10.1 Small RNA isolation

Small RNAs were isolated using the mirVana miRNA Isolation Kit (Ambion, Thermo Fisher Scientific) following the manufacturer's instructions.

2.10.2 Quantitative Reverse Transcription Polymerase Chain Reaction (qRT-PCR) for miRNA expression

MicroRNA expression levels were determined using TaqMan™ Advanced miRNA Assays (Life Technologies) according to the manufacturer's instructions. The following miRNA assay were used: hsa-miR-25-3p (Assay ID: 477994), hsa-miR-25-5p (Assay ID: 478786), hsa-miR-93-3p (Assay ID: 478209), hsa-miR-93-5p (Assay ID: 478210), hsa-miR-106b-3p (Assay ID: 477866), hsa-miR-106b-5p (assay ID: 478412), and endogenous controls hsa-423-5p (Assay ID: 478090), hsa-miR-16-5p (Assay ID: 477860), hsa-miR-5787 (Assay ID: 480167), hsa-miR-29c-3p (Assay ID: 479229), and hsa-miR-191-5p (Assay ID: 477952). Reference microRNAs were chosen based on their stable expression across sample groups in microarray data obtained from HCC1806 cells (Section 2.10.3) or previously published literature. These 5 normalisation candidates (hsa-423-5p, hsa-miR-16-5p, hsa-miR-5787, hsa-miR-29c-3p, and hsa-miR-191-5p) were first investigated by qRT-PCR to ascertain stability across several breast cancer cell lines, both in the presence and absence of miRNA processing factors DICER1 and AGO2. Conditions for miRNA amplification were as follows: 30 minutes at 16°C, 30 minutes at 42°C, and a final step of 5 minutes at 85°C. Quantitative real time PCR was then performed using the Taqman Universal PCR Master Mix (434437) following the manufacturer's instructions using a 7500 Fast Real-Time PCR System (Applied Biosystems).

2.10.3 MicroRNA Microarray

HCC1806 cells were transfected with a non-targeting control siRNA or an siRNA targeting AGO2. miRNA was extracted using the Qiagen miRNA extraction kit, according to manufacturer's instructions. We obtained four biological replicates for each condition. MicroRNA expression profiles were obtained using the Human 8x60K Array (V.21 with spike-in probes) (Agilent Technologies, Santa Clara, California, USA). Probe Level Signal Data

(Raw Data) was Quantile Normalised. The *Limma* R package was used to performed differential expression analysis, where microRNAs with adjusted p-values lower than 0.05 were considered significantly regulated (Ritchie et al., 2015). Benjamini and Hochberg method was used to correct for multiple testing (Benjamini & Hochberg, 1995).

2.11 Quantification of mRNAs

2.11.1 mRNA isolation

Total RNA was purified from cell pellets with the RNeasy mini kit (Qiagen). RNA concentration and A260/A280 ratio were determined using a Nanodrop, ND-1000 spectrophotometer (Thermo Scientific).

2.11.2 qRT-PCR for mRNA expression

Purified total RNA (1 µg) was reverse transcribed using the Superscript II First Strand Synthesis Supermix for qRT-PCR kit (Invitrogen), according to the manufacturer's instructions. Reactions were carried out in triplicate for each target transcript using the 7500 Fast Real-Time PCR Detection System (Applied Biosystems). Each reaction contained 20 ng cDNA, 200 nM of each primer (Fw and Rev), 10 µl water, and 12.5 µl Absolute Blue quantitative Polymerase Chain Reaction (qPCR) SYBR low ROX Mix (Thermo Scientific, 4385612). qPCR settings were as follows: initialisation at 95 ºC for 15 min, followed by 45 cycles of denaturation at 95 ºC for 15 seconds, annealing at 60 ºC for 30 seconds, and extension at 72 ºC for 30 seconds. The comparative CT method was applied for quantification of gene expression, and values were normalised against *ACTINB* as control. Differences in expressed genes were identified using the Mann–Whitney U test where P-values ≤0.05 were considered significant.

The following primers were used:

ACTINB Fw	5’-AAGAGCTATGAGCTGCCTGA-3’
ACTINB Rev	5’-TACGGATGTCAACGTCACAC-3’
AGO2 Fw	5’-GTCTCTGAAGGCCAGTTCCA-3’
AGO2 Rev	5’-ATAGAGGCCTCACGGATGG-3’
CCNB1 Fw	5’-TTCTGGATAATGGTGAATGGAC-3’
CCNB1 Rev	5’-ATGTGGCATACTTGTTCTTGAC-3’
CCNE2 Fw	5’-AAGGAGCGGGACACCATGA-3’
CCNE2 Rev	5’-ACGGTCACGTTTGCCTTCC-3’
CDC6 Fw	5’-TGTTCTCCTCGTGTAAAAGCC-3’
CDC6 Rev	5’-GGGGAGTGTTGCATAGGTTGT-3’
CDT1 Fw	5’-CGGTGGACGAGGTTTCCAG-3’
CDT1 Rev	5’-CTGCCGGGGTGGATTTCTT-3’
CTIP Fw	5’- CTGCTTAGCACAATACCTGGAA-3’
CTIP Rev	5’- CTCAACTCTGCAGCTGTATGGA-3’
DICER1 Fw	5’-TTAACCTTTTGGTGTTTGATGAGTGT-3’
DICER1 Rev	5’-GGACATGATGGACAATTTTCACA-3’
E2F1 Fw	5’-GCCACTGACTCTGCCACCATAG-3’
E2F1 Rev	5’-CTGCCCATCCGGGACAAC-3’
E2F2 Fw	5’-CGTCCCTGAGTTCCCAACC-3’
E2F2 Rev	5’-GCGAAGTGTCATACCGAGTCTT-3’
E2F3 Fw	5’-AGCGGTCATCAGTACCTCTCAG-3’
E2F3 Rev	5’-TGGTGAGCAGACCAAGAGACGT-3’
GMNN Fw	5’-ACATCTACAACTTCCAGCCCT-3’
GMNN Rev	5’-TCCGTTTTTCTGCCACTTCCT-3’

MCM2 Fw	5’-CCGTGACCTTCCACCATTTGA-3’
MCM2 Rev	5’-GGTAGTCCCTTTCCATGCCAT-3’
MCM7 Fw	5’-CCTACCAGCCGATCCAGTCT-3’
MCM7 Rev	5’-CCTCCTGAGCGGTTGGTTT-3’
PCNA Fw	5’-GTGGAGAACTTGGAAATGGAA-3’
PCNA Rev	5’-ACCGTTGAAGAGAGTGGAGTG-3’
PLK2 Fw	5’- GACCCTATGGGACTCCTCTTT-3’
PLK2 Rev	5’- GTATGCCTTAGCCTGTTCTGG-3’
Pre-miR-25 Fw	5’-GTGTTGAGAGGGCGGAGACTT-3’
Pre-miR-25 Rev	5’-TCAGACCGAGACAAGTGCA-3’
Pre-miR-93 Fw	5’-AAGTGCTGTTCGTGCAGG-3’
Pre-miR-93 Rev	5’-CTCGGGAAGTGCTAGCTCA-3’
Pre-miR-106b Fw	5’-TGGAGCAGCAAGTACCCACAGT-3’
Pre-miR-106b Rev	5’-GCTGACAGTGCAGATAGTGGTC-3’
RB1 Fw	5’-GACCCAGAAGCCATTGAAATCT-3’
RB1 Rev	5’-GGTGTGCTGGAAAAGGGTCC-3’
RBL1 Fw	5’-GGAGTGCTAAGAGGAGACTGTTTGG-3’
RBL1 Rev	5’-ATAGGAACCAGTGTGATTTCTCCAG-3’
RRM2 Fw	5’-TTTAAAGGCTGCTGGAGTGAGG-3’
RRM2 Rev	5’-GCAGCTGCTTTAGTTTTCGGCT-3’
SETD2 Fw	5’-CCTGGGGAATTCAACCCTGC-3’
SETD2 Rev	5’-ATGTTTCAGGTTCAGGGGGAG-3’

2.12 Chromatin Immunoprecipitation (ChIP)

Cells were grown in 10-cm dishes and transfected with siRNA constructs as described in Section 2.5. Formaldehyde (1% final concentration) was added for 10 minutes at room temperature to allow for DNA-protein cross-linking. Glycine was added (125 mM final concentration) and incubated for 5 minutes with gentle shaking to terminate the reaction. Cell culture medium was then aspirated, the cells were rinsed twice with ice-cold PBS, scraped, and collected in PBS. The cell suspension was centrifuged at 500 g for 10 minutes and the supernatant removed. The pellets were re-suspended in 500 µl SDS lysis buffer (1% SDS, 5 mM EDTA, 50 mM Tris-HCl, pH 8.0, protease inhibitor) and transferred to new 1.5 ml Eppendorf tubes. The cell suspensions were sonicated at 4°C to generate sheared, soluble chromatin with an average fragment size of 700 bp, and then pelleted. The DNA sizes were analysed by diluting 5 µl of the supernatant in 5 µl of TE buffer (1 mM EDTA, 10 mM Tris-HCl, pH 8.0), adding 2 µl of Pronase (Merck), incubating the mix at 42°C for 2 hours, and visualising it on a 1% agarose gel. 1/10 of each sample was stored as "ChIP Input" control, while the remaining supernatant was transferred to new tubes and topped up with 2500 µl dilution buffer (1% Triton-X100, 2 mM EDTA, 20 mM Tris-HCl, pH 8.0, 150 mM NaCl, protease inhibitor). Protein A/G Magnetic Beads, blocked with BSA for 4 hours, were added and rotated at 4°C for 4 hours to pre-clear the mixtures. Next, they were centrifuged, and the supernatant was transferred to new tubes. These supernatant fractions were subjected to chromatin immunoprecipitation with 5 µg of E2F1 or IgG antibody at 4°C overnight. Next, the beads were washed sequentially with 1) buffer TSE-I (0.1% NP-40, 1% Triton X-100, 2 mM EDTA, 20 mM Tris-HCl pH 8.0, and 150 mM NaCl), 2) buffer TSE-II (0.1% NP-40, 1% Triton X-100, 2 mM EDTA, 20 mM Tris-HCl pH 8.0, 500 mM NaCl), 3) buffer III (250 mM LiCl, 1% NP-40, 1% sodium deoxycholate, 1 mM EDTA, 10 mM Tris-HCl pH 8.0) and twice in TE buffer, for 10 minutes each. Proteins were then eluted with 120 µl elution buffer (1% SDS, 10

mM EDTA, 50 mM Tris-HCl pH 8.0, 0.5 mg/ml RNase A) beads and transferred to new 1.5 ml tubes. Elution buffer was also added to the input samples. Samples were incubated at 65°C overnight to reverse cross-linkage. The DNA was purified from the samples using a PCR purification kit (Qiagen) according to the manufacturer's instructions. The purified DNA was prepared for quantitative real-time PCR (qPCR) using the 7500 Fast Real-Time PCR System (Applied Biosystems). We used *ACTINB* primers as previously described (Takahashi, Rayman, & Dynlacht, 2000).

The primer sequences used in the qPCR were:

CDC6 Fw primer: 5'- GGCCTCACAGCGACTCTAAGA-3'

CDC6 Rev primer: 5'- CTCGGACTCACCACAAGC-3'

MCM2 Fw primer: 5'- TCACGTGAACCACTTTTCGC-3'

MCM2 Rev primer: 5'- CCAGGTCAGTGGTAGGTAGG-3'

CDT1 Fw primer: 5'- GGTAACACAGTACAGCCCTCGC-3'

CDT1 Rev primer: 5'- GCGAAACTCGCCGCGCTTGG-3'

2.13 miRNA- and mRNA-sequencing using Illumina

2.13.1 Sample Collection

HCC1806 cells were treated with 2 mM hydroxyurea (HU) for 4 hours or exposed to 10 Gray (Gy) of ionising radiation (IR) using a ^{137}caesium source (Gamma-Service Medical GmbH) at a dose rate of 1.3 Gy/min. Cells were left to recover in a 5% CO_2 incubator at 37°C for 2- or 6-hours post-IR treatment. Control and treated cells were harvested using scraping and maintained on ice prior to RNA isolation. Total RNA was purified from cell pellets with the RNeasy mini kit (Qiagen). A total amount of 3 µg and 6 µg of RNA per sample, measured using the Qubit 2.0 Fluorometer (Life Technologies, USA) was used as input material for the

cDNA library preparation for mRNA sequencing and small RNA sequencing, respectively. There were two biological replicates available for each treatment condition. RNA quality was visualised using Agarose Gel Electrophoresis, and RNA quantification was performed using the 2100 Bioanalyser (Agilent Technologies).

2.13.2 miRNA sequencing library preparation

Small RNA library preparation and Illumina sequencing was performed by technical staff at Novogene Co Ltd, using the NEB Next® Multiplex Small RNA Library Prep Set for Illumina® (Set 1, E7300) with modified adaptors and primers compatible with the NovaSeq sequencing platform. Small RNA size selection was performed using a 15% urea-TBE gel (Invitrogen) for 1 hour at 200 V, from a total of 6 μg of RNA per sample. The library size was assessed using a DNA 1000 chip and the Agilent 2100 Bioanalyser (Agilent Technologies) and accurately quantified using Q-PCR.

2.13.3 mRNA sequencing (RNA-seq) library preparation

Following Quality Control (Section 2.12.1), mRNA was enriched using oligo(dT) beads. Ribosomal RNA was removed using the Epicentre Ribo-zero™ rRNA Removal Kit (Epicentre, USA) according to the manufacturer's instructions, and rRNA free residue was cleaned up by ethanol precipitation. Next, sequencing libraries were generated using the NEBNext® Ultra™ RNA Library Prep Kit for Illumina® (NEB, USA) following manufacturer's recommendations. Briefly, mRNA fragmentation was carried out using a fragmentation buffer. First-strand cDNA was synthesised using random hexamer primers, after which a custom second-strand synthesis buffer (Illumina), with dNTPs, RNaseH, and DNA Polymerase I was added to initiate the second-strand synthesis. Remaining overhangs were converted into blunt ends via exonuclease/polymerase activities. After adenylation of 3' ends of DNA fragments

and ligation of the sequencing adaptors, the double-stranded cDNA library was size selected and enriched using PCR, with Phusion High-Fidelity DNA polymerase, Universal PCR primers and Index (ATCACG) Primer. Finally, library quality was assessed on the Agilent Bioanalyser 2100 system and concentrations were quantified using qPCR.

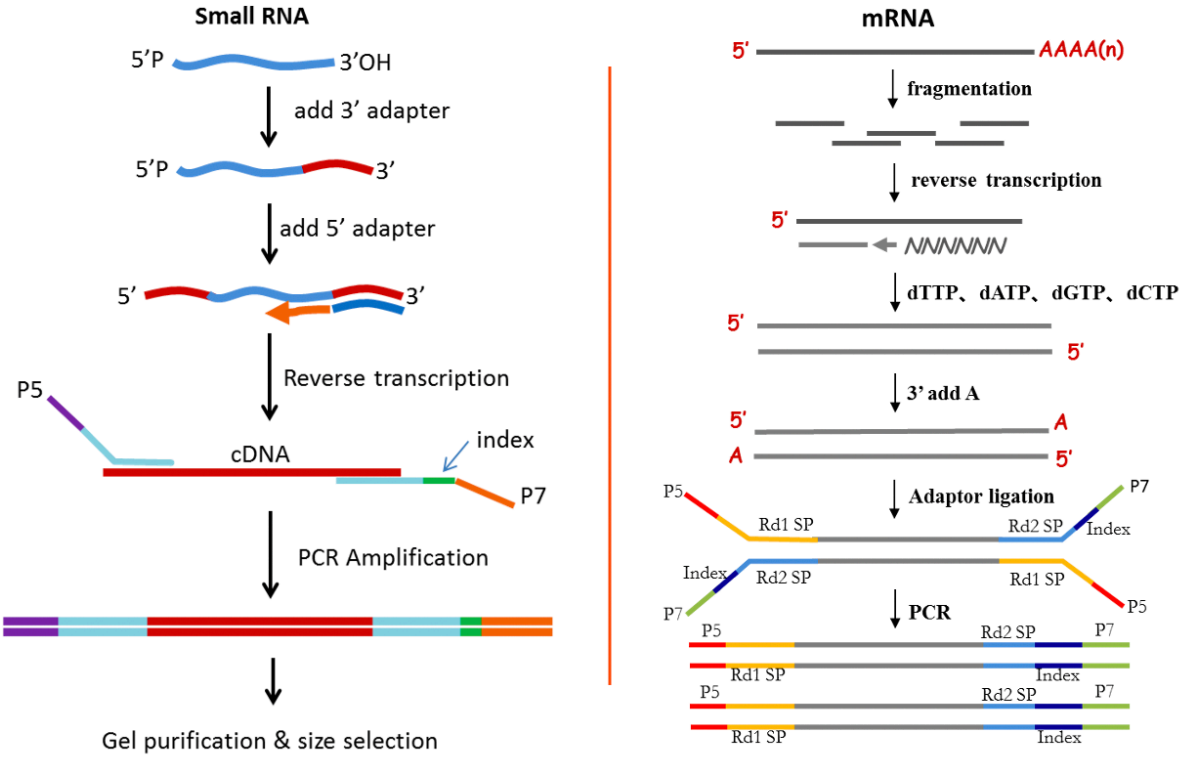

Figure 2.3. ***Overview of library construction for miRNA- and mRNA sequencing.*** *Workflow Charts were obtained from Novogene Company Ltd.*

2.13.4 Illumina Sequencing

cDNA libraries for mRNA were sequenced on the Illumina NovaSeq 6000 platform with paired-end (2 x 150 nucleotides) reads (Q30>80%) and yielded an average of 27 million reads per sample. Small RNA sequencing experiments were performed on Illumina NovaSeq 6000 with single-end 50 nt reads (Q30>85%) and yielded an average of 21 million reads per sample. All sequencing was outsourced to Novogene Ltd.

2.13.5 Statistical Analysis for miRNA Sequencing

3' adapter trimming was performed using *Reaper* in R (Davis, van Dongen, Abreu-Goodger, Bartonicek, & Enright, 2013) . Post-trimmed reads were screened for quality, specificity of mapping, and contaminant sequences using FASTQC (http://www.bioinformatics.babraham.ac.uk/projects/fastqc/). The cleaned sequence files (FASTA) were scanned against all known human miRbase hairpin precursor sequences using the Chimira web interface from the EBI institute (Vitsios & Enright, 2015). The obtained miRNA expression data (counts) and their associated modifications were downloaded. Downstream differential expression analysis was performed using the *DESeq2* R package (Love, Huber, & Anders, 2014) . *DESeq2* employs a negative binomial distribution to identify genes with significant expression differences while explicitly accounting for differences in the total number of reads for each sample and differences in expression noise for low- versus highly expressed genes. Gene target prediction of microRNA was done with *miRNAtap* from Bioconductor package, which includes the prediction algorithms of DIANA, Miranda, PicTar, TargetScan and miRDB (Pajak and Simpson, 2021).

2.13.6 Statistical Analysis For mRNA Sequencing

The GEO accession number for the raw mRNA-sequencing data is: GSE182775. Adapter trimming was performed using *Trimmomatric* (Version 0.30) (Bolger, Lohse, & Usadel, 2014) and reads below 36 bases long were dropped. Quality control was performed with FastQC (http://www.bioinformatics.babraham.ac.uk/projects/fastqc/). Mapping and gene level quantification were performed using *Kallisto* version 0.46.2 (index build with GRCh38-Ensembl 96 Archive, April 2019), giving a mean mapping rate of 86% (N. L. Bray, Pimentel, Melsted, & Pachter, 2016). *Tximport* was used to summarise the transcript levels counts and abundances to gene levels counts (Soneson, Love, & Robinson, 2016). The reads were mean-

normalised using predicted size factors. Finally, the *DESeq2* method was used for differential analysis of mRNA count data.

2.14 mNUC-seq sample preparation

Mono-nucleosome sequencing (mNUC-seq) was performed as previously described (Nojima et al., 2018). Using 100 ∼500 ng of DNA, libraries were made using the NEBNext Ultra II DNA Library Prep Kit for Illumina (NEB) manual. 5∼9 cycles of PCR were used to amplify the library. Deep sequencing (Hi-Seq 4000, Illumina) was performed by Novogene Company Ltd as described above (GEO accession number: GSE182055).

2.14.1 Statistical Analysis for mNUC-sequencing

mNUC-seq data (n=2) were processed as follows: adapters were trimmed with *Cutadapt* version 1.18 (Martin, 2011) in paired-end mode with the following parameters: --minimum-length 10 -q 15, 10 -j 16 -a AGATCGGAAGAGCACACGTCTGAACTCCAGTCA. Trimmed reads were mapped to the human reference genome (version GRCh38.p13) with STAR version 2.7.3a (Dobin et al., 2013) and the parameters: --runThreadN 16 --readFilesCommand gunzip -c -k –alignIntronMax 1 --limitBAMsortRAM 20000000000 --outSAMtype BAM SortedByCoordinate. *SAMtools* version 1.9 (Li et al., 2009) was used to retain the accurately mapped reads and to remove PCR duplicates. Reads mapping to the DAC Exclusion List Regions (accession: ENCSR636HFF) were removed with *BEDtools* version 2.29.2 (Quinlan & Hall, 2010). *SAMtools* was used to subsample all the samples to 28 million properly mapped paired-end reads. FPKM (Fragments Per Kilobase of transcript per Million mapped reads)-normalised bigwig files were created with *deepTools* version 3.4.2 bamCoverage tool with the parameters -bs 10 -p max –e --normalizeUsing RPKM (Reads Per Kilobase (of Transcript) Million (Mapped Reads)) (Ramírez et al., 2016).

Peak calling was performed with MACS version 2.2. (Zhang et al., 2008) and the following options: callpeak -t Treatment.bam -c Input.bam -n Name_OutputFolder -f BAMPE -g 2.9e9 -q 0.01 --bdg --call-summits --nomodel --extsize 200. MACS bdgdiff was then used to compare the different treatments (HU, VE-822 or HU + VE-822) to the control condition. Only genes found to be present in both biological replicates per treatment condition were considered to be associated with an increased H3K36me3 signal.

Metagene profiles of genes scaled to the same length were generated with the *Deeptools2* computeMatrix tool with a bin size of 10 bp. Plotting data was obtained with plotProfile –outFileNameData tool. Graphs representing the (H3 – total histone H3) signal were created with GraphPad Prism Version 8.4.2. Metagene profiles are shown as the average of two biological replicates.

2.15 Gene Ontology (GO) and Pathway Enrichment Analysis

To classify the functions of differentially expressed genes (DEGs), we performed Gene Ontology (GO) Enrichment and Transcription Factor Enrichment Analyses (TFEA) using the web interface ShinyGO v0.66 (Ge, Jung, Jung, & Yao, 2020). Pathway analyses were performed using the hypergeometric test and both adjusted p-values and fold enrichment, which is defined as the percentage of queried genes belonging to a pathway, divided by the corresponding percentage in the background, were reported. Statistically significant overrepresented GO terms or pathways were represented as hierarchical clustering trees. Pathways with many shared genes were clustered together and dot sizes indicate the degree of statistical significance (ShinyGO version 0.66, http://bioinformatics.sdstate.edu/go/).

2.16 Graphical Display of Results and Statistical Analysis

For all statistical analysis and graphical display, GraphPad Prism Version 8.4.2 (www.graphpad.com) was used. All statistical analyses between two comparison groups were carried out using unpaired two-tailed *t*-tests, and one- or two-way ANOVAs were performed as mentioned in the figure legends. *P* values refer to: ***$P < 0.001$, **$P < 0.01$, *$P < 0.05$, $^{ns}P > 0.05$. Quantitative data was presented as mean ± standard error of the mean (SEM).

Chapter 3

Multi-Omics Profiling Identifies a Dicer-to-Argonaute Switch Controlling Biogenesis of Oncogenic miRNAs, including the miR-106b/25 Cluster

Chapter 3 is based on the following publication:

Winchester, L., van Bijsterveldt, L., Dhawan, A., Wigfield, S., Triantafyllidis, C., Haider, S., McIntyre, A., Humphrey, T.C., Harris, A.L., Buffa, F.M. (2021). **Dicer-to-Argonaute switch controls biogenesis of oncogenic miRNA.** *BioRxiv*, 2021.08.30.458145. https://doi.org/10.1101/2021.08.30.458145

*Any contributions from colleagues, such as diagrams or statistical analyses, are explicitly referenced in the figure legends, with their names and contributions indicated

3.1 Introduction

As previously described (Section 1.5), miRNAs are 18-22 nucleotide long single-stranded RNA molecules that bind to and subsequently regulate, post-transcriptionally, the expression levels of a large number of target-mRNAs. In cancer, miRNAs act as negative regulators of various TSGs, including *PTEN* and *DNMT3A* (Dhawan et al., 2018). Recurrent miRNA-TSG interactions can therefore contribute to malignant transformation, and consequently, miRNA dysregulation has been commonly associated with the hallmarks of cancer (Dhawan et al., 2018; Jacobsen et al., 2013; Krol et al., 2010).

Previous studies have shown that miRNAs with recurrent target relationships, i.e., those that are found consistently across cancer types, are frequently dysregulated by somatic genetic and epigenetic alterations (Jacobsen et al., 2013). Moreover, some miRNAs are dysregulated because of changes in transcription of the genes in which they are embedded in (Chang et al., 2008). However, an alternative – and not as well-understood – mechanism by which miRNA abundance can be dysregulated, is through alterations in miRNA biogenesis pathways, which function to convert primary miRNA (pri-miRNA) transcripts into mature miRNAs. These

alterations can change the rate or efficiency at which mature functional miRNAs are produced, whilst the production of the pri-miRNA transcript remains unchanged.

Even though aberrant expression levels of components of the miRNA processing machinery have previously been implicated in tumourigenesis, and an alternative AGO2-dependent, DICER-independent miRNA biogenesis pathway has been reported (Kim et al., 2016), the relative contributions of each of these processing steps (Figure 1.4) to global miRNA dysregulation in breast cancer remains unclear. Understanding how the interplay between these two mechanisms of miRNA regulation, with on the one hand altered transcription of the pri-miRNA, and on the other hand, altered miRNA biogenesis, contributes to the pathology of cancer is crucial, and could help improve and identify novel therapeutic approaches.

Recent work by Dr. Andrew Dhawan, Dr. Laura Winchester, and Dr. Simon Wigfield demonstrated that *AGO2* amplification was frequently associated with hypoxia in multiple clinical cohorts, causing a shift towards the production of oncogenic miRNA (manuscript under review) (Winchester et al., 2021). In this chapter, I extended this analysis further, and utilised exome- and whole genome sequencing data from TCGA and METABRIC projects to identify putative drivers of altered miRNA biogenesis in breast cancer. We identified frequent gene amplification of *AGO2* and AGO2-interacting protein, *PAPBC1,* across clinical cohorts and demonstrated significant co-occurrence of *AGO2* copy number amplification or gain with *DICER1* mutation and deletion. Next, I asked whether *AGO2*-amplified cells demonstrated altered precursor and mature miRNA expression profiles and explored whether these changes were caused by altered transcription of the pri-miRNA, or by altered miRNA maturation, as measured by the ratio of precursor to mature miRNA *in vitro*. These results demonstrated an

important role for non-canonical AGO2-driven alternative miRNA biogenesis in the production of oncogenic miRNAs, which could be exploited for therapeutic purposes.

3.2 Recurrent Alterations of miRNA Biogenesis Genes in Breast Cancer

First, we selected 43 components of the canonical mammalian miRNA biogenesis machinery for analysis (Kim, Han, & Siomi, 2009; Krol et al., 2010; Meister, 2013). These genes were selected by Dr. Laura Winchester, following a thorough literature review of miRNA biogenesis pathways, and listed in a table with the relevant references described in the DPhil thesis of Dr. Andrew Dhawan (Dhawan, 2018).

To identify somatic mutation frequencies across these 43 miRNA biogenesis genes, I took advantage of publicly available whole exome sequencing data for 1,079 primary breast tumours generated as part of The Cancer Genome Atlas Breast Invasive Carcinoma (TCGA-BRCA) project (Koboldt et al., 2012). To investigate possible drivers of altered miRNA biogenesis, we used a previously published approach, which relies on ranking the observed mutations in a given genomic element based on recurrence, followed by statistical comparison of the frequency of mutation (over-mutation) in these genetic elements with the expected background mutation rate (Campbell et al., 2020).

The average tumour mutational burden (TMB), defined as the number of non-synonymous mutations per megabase (Mb) of tumour tissue DNA, in TCGA-BRCA (n=1,079) was 2.73 Mut/Mb. Furthermore, we found a mutation level with a mean frequency of 0.45% and standard deviation (SD) of 0.40% in genomic regions encoding miRNA biogenesis proteins (43 genes) (Figure 3.1). The average mutation rate for miRNA biogenesis genes did not significantly differ

from the expected background mutation rate per tumour (in TCGA-BRCA, two-sided proportion test, p-value = 1.0000).

As shown in Figure 3.1, the most frequently mutated genes included *PIWIL1* (1.72%), which belongs to a subfamily of Argonaute proteins that bind small RNAs (PIWI-interacting RNAs, piRNAs) (Tian, Simanshu, Ma, & Patel, 2011), *CNOT1* (1.52%), a mediator of mRNA degradation by miRNAs (Mathys et al., 2014), *TARBP1,* a double-stranded RNA (dsRNA) binding protein that forms part of the RISC (Chendrimada et al., 2005), and *TNRC6A* (also known as GW182), which provides a docking platform through which deadenylase complexes gain access to the poly(A) tail of miRNA targets to promote their deadenylation and degradation (Braun, Huntzinger, Fauser, & Izaurralde, 2011).

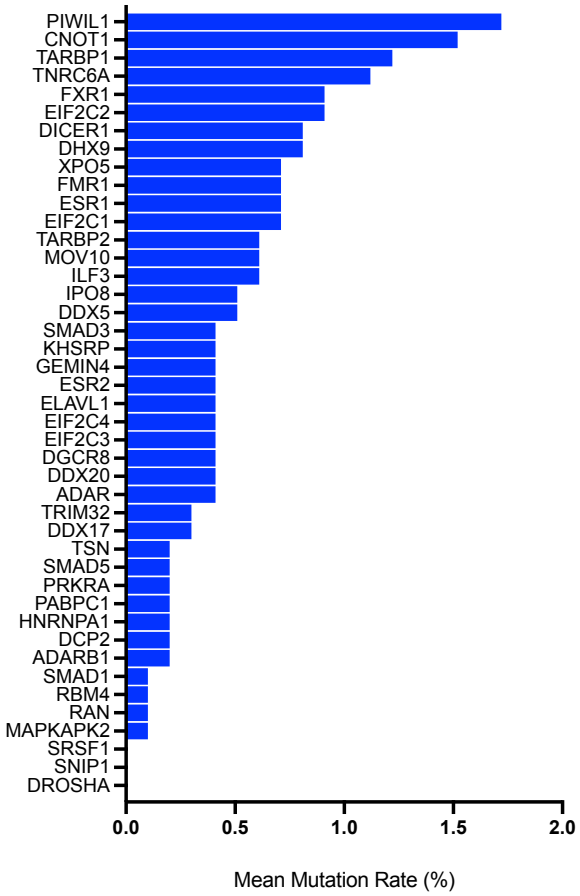

Figure 3.1. ***Somatic mutation frequency of miRNA biogenesis genes in TCGA-BRCA.*** *Data are expressed as percentages (0-100%) of TCGA-BRCA cohort (n=1,079).*

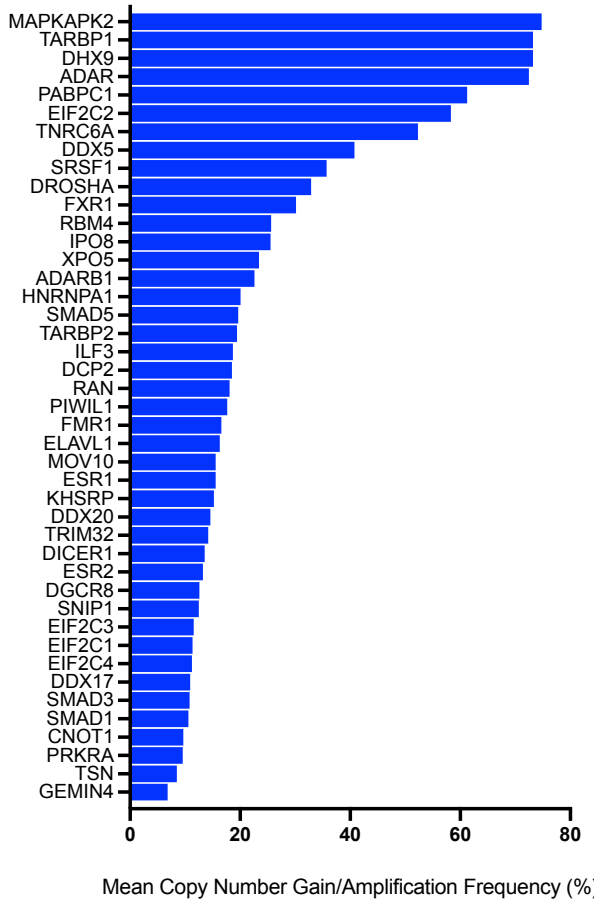

Figure 3.2. ***Mean copy number gain/amplification frequency at genomic locations encoding miRNA biogenesis genes in TCGA-BRCA.*** *Data are expressed as percentages (0-100%) of TCGA-BRCA cohort (n=1,079).*

In accordance with previous work demonstrating that many miRNA biogenesis genes were located within common fragile sites and thus commonly amplified or deleted in cancer (Calin et al., 2004; Zhang et al., 2006), I identified frequent copy number variations (CNVs) in miRNA biogenesis genes in the TCGA-BRCA dataset. Copy number deletion of genomic regions encoding miRNA biogenesis proteins was rare, but observed in some cases, such as for *CNOT1, DCP2, GEMIN4,* and *DICER1*, with 1.40%, 0.65%, 0.84%, and 0.47% of TCGA-BRCA cases harbouring a homozygous/deep deletion, respectively. Copy number amplification (CNA) or gain of miRNA biogenesis genes was more commonly observed, with the average CNA or copy number gain frequency in miRNA biogenesis genes ranging from 7% (*GEMIN4*) to 74% (*MAPKAPK2*), with *EIF2C2 (AGO2) (58%), PABPC1 (61%), ADAR, DHX9, TARBP1,* and *MAPKAPK2* amplified in over half of breast cancer cases (Figure 3.2).

To distinguish between passenger alterations (i.e., random alterations that do not confer a growth or survival advantage) and driver alterations, copy number and mRNA expression correlation analysis was performed for those miRNA biogenesis genes that harboured CNA or copy number gain in >50% of samples in TCGA-BRCA (Figure 3.2). Oncogenic gene driver alterations, i.e., those that propel cancer initiation and progression, are selected for during cancer evolution and therefore associated with enhanced phenotypes. Therefore, one could predict that genomically amplified miRNA biogenesis genes that display corresponding mRNA overexpression play important roles during tumourigenesis (Ohshima et al., 2017).

For the six genes that showed frequent (>50%) copy number gain or amplification (Figure 3.2), putative copy number variations (CNVs) (using the provided Genomic Identification of Significant Targets in Cancer (GISTIC) calls (Mermel et al., 2011)) were plotted against mRNA expression estimates (Li & Dewey, 2011) (Figure 3.3.). Next, Pearson's correlation analysis between copy number and mRNA expression was performed to identify those CNA events that resulted in gene upregulation (Spearman's $\rho > 0.3$, $q < 10\text{-}3$). This analysis revealed that the six most-commonly amplified miRNA biogenesis genes in breast cancer showed a strong copy number versus gene expression correlation (Table 3.1 and Figure 3.3).

Table 3.1. ***Spearman's correlation statistics of CNA and mRNA expression of miRNA biogenesis genes that were amplified in >50 % of TCGA-BRCA cases.*** *Shown are the correlation coefficients (Rho) for the TCGA-BRCA dataset, with their p- and q-values.*
**This analysis was performed with the help of A. Dhawan and F. Buffa.*

	Rho	***p-value***	***q-value***
PABPC1	0.647	1.15E-119	8.02E-119
EIF2C2	0.644	2.32E-118	8.13E-118
TARBP1	0.511	1.09E-67	1.91E-67
ADAR	0.487	1.21E-60	1.69E-60
MAPKAPK2	0.477	6.23E-58	7.27E-58
DHX9	0.321	1.84E-25	1.84E-25

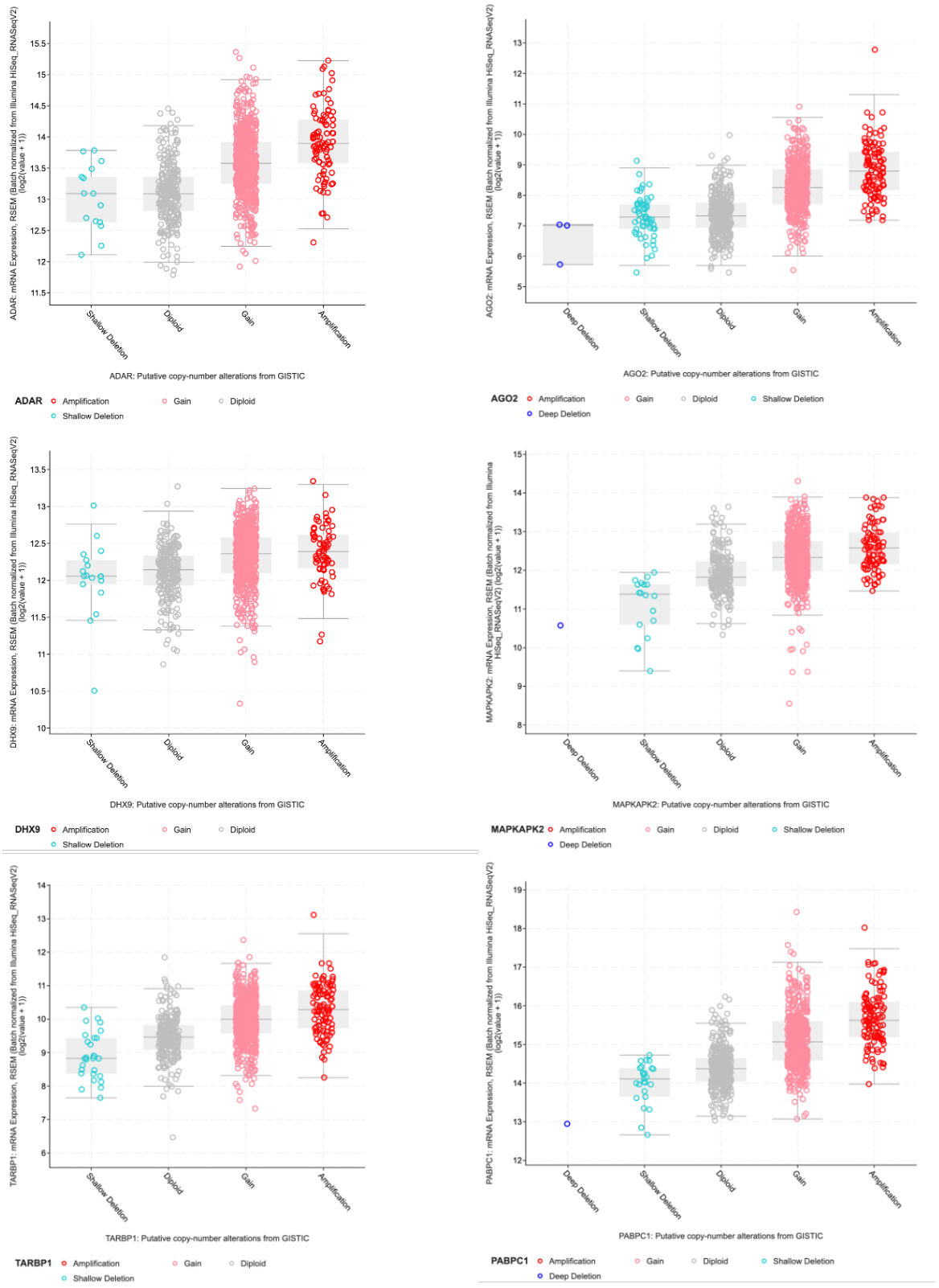

Figure 3.3. ***Boxplots showing the relationship between ADAR, AGO2, DHX9, MAPKAPK2, TARBP1, and PAPBPC1 mRNA expression (y-axis) versus copy number value (x-axis).*** *Data was obtained from TCGA-BRCA dataset (n=1,079) (cBioPortal). Expression values were shown as the $\log_2$ of (RSEM (RNA-Seq by Expectation-Maximization) +1). Possible GISTIC scores are -2 = Deep (homozygous) deletion; -1 = Shallow (hemizygous) deletion; 0 = neutral/diploid; 1 = gain (low copy); 2 = high level amplification.*

Two genes, *EIF2C2 (AGO2)* and *PABPC1*, which is an AGO2-interacting protein with a role in promoting miRNA inhibition efficiency (Zhang et al., 2015), demonstrated very strong amplification-dependent overexpression (Spearman's $\rho > 0.6$) (Akoglu, 2018). More moderate relationships between copy number and mRNA expression, with Pearson's correlation coefficients between 0.3 and 0.6, were identified for *TARBP1,* which provides a platform for RISC assembly and recruitment of AGO2 to miRNA or siRNA (Chendrimada et al., 2005), *ADAR*, which is responsible for regulating miRISC loading and miRNA target inhibition via RNA editing (Nishikura, 2015), *MAPKAPK2,* and *DHX9,* which is a RNA helicase that aids the processing of primary miRNA transcripts (Kawai & Amano, 2012). Together, this data suggested that amplification-dependent overexpression of genes involved in the AGO2-dependent miRNA biogenesis pathway frequently occurs in breast tumours.

Next, we assessed whether the genomic landscape for miRNA biogenesis pathways observed in the TCGA-BRCA dataset, including genomic CNA of these six putative driver genes, could be cross-validated in the breast cancer METABRIC dataset. To do this, we used samples for which matched transcriptomic and genomic Copy Number Variation (CNV) data were available (n=1904) (Curtis et al., 2012). Our analysis in the METABRIC dataset confirmed frequent CNA or gain of miRNA biogenesis genes, including *MAPKAPK2, DHX9, TARBP1, ADAR, PABPC1,* and *EIF2C2 (AGO2)* (Figure 3.4), in accordance with our findings in the TCGA-BRCA dataset, and additionally, *SRSF1* and *DDX5,* which both have a role in recognising and processing the stem region of specific pri-miRNAs, resulting in enhanced cleavage by Drosha (Fukuda et al., 2007; Wu et al., 2010).

Furthermore, we observed several clusters that demonstrated distinct CNV patterns (Figure 3.4), mostly, but not completely, reflecting common or near-genomic locations. For instance,

AGO family members 1, 3 and 4, located on chromosome 1, shared a similar CNA correlation profile; whereas AGO2, located on chromosome 8, showed a markedly different profile. Exceptions to these regional clustering patterns were identified for *PABPC1* and *AGO2* CNA, whose copy number amplifications were highly clustered and correlated (this gene pair's CN profiles (Spearman's $\rho = 0.90$, p-value $< 2.2 \times 10^{-16}$) (Figure 3.4) despite their genomic locations not being immediately proximal, with the former on the 8q22 and the latter on the 8q24 amplicon. This suggests that CNA of these two genes is co-selected for.

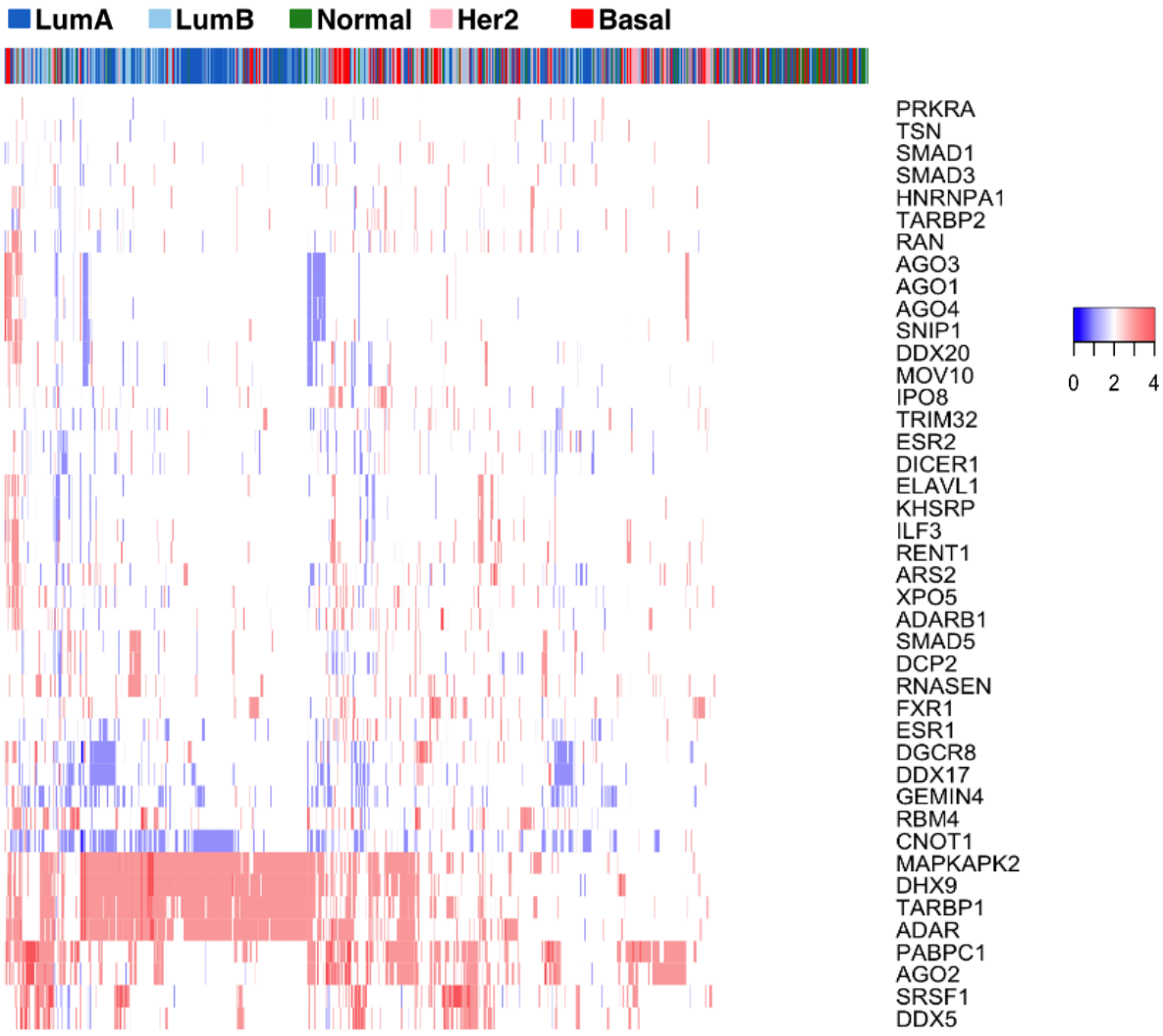

Figure 3.4. ***Copy number profiles for 1904 cases in METABRIC.*** *Cases (columns) and miRNA biogenesis genes (rows) were visually clustered using hierarchical clustering. PAM50 classification is colour coded and shown at the top. *Heatmap was generated by A. Dhawan.*

To identify overlapping drivers of oncogenic miRNA biogenesis between the TCGA-BRCA and METABRIC datasets, we repeated the correlation analysis between copy number and mRNA levels of miRNA biogenesis genes in the METABRIC cohort and identified genes that demonstrated consistent amplification-dependent overexpression across cohorts.

To this end, we used a resampling analysis with randomly selected (x1000 times) sets of 43 genes across the genome (same number as the gene set of miRNA biogenesis genes) and found that for the majority (20/43) of miRNA biogenesis genes, the correlation between amplification and expression levels was significantly greater than expected by chance alone (mean Spearman's $\rho = 0.12$ across these genes, p-value =1.5e-05). Furthermore, using Cox survival analysis, we found that amplification and overexpression of *DDX5* (Hazard Ratio (HR) = 1.6, p-value = 0.0012), *AGO2* (HR = 1.4, p-value = 0.014), *PABPC1* (HR = 1.4, p-value = 0.0058) and *SRSF1* (HR = 1.3, p-value = 0.040) were associated with poor outcome in the METABRIC dataset.

Finally, we identified *AGO2* and *PABPC1* as top candidate drivers, as they were highly amplified and concordantly over-expressed genes across both cohorts. The association of amplification and over-expression of both *AGO2* and *PABPC1* with poor prognosis in the METABRIC cohort further suggests that the synergistic action between *AGO2* and *PABPC1* plays an important role during cancer development.

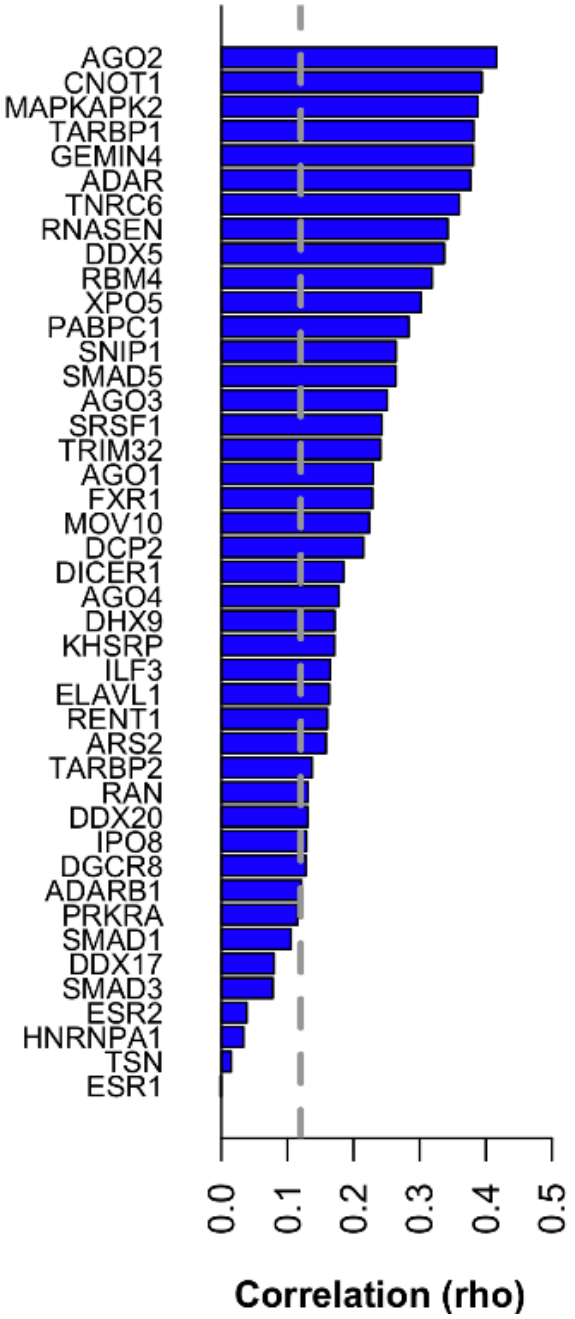

Figure 3.5. ***Correlation (Spearman rho) between copy number and mRNA levels of 43 miRNA biogenesis genes in METABRIC****. Dotted line represents the average correlation obtained when resampling (x1000) random sets of 50 genes across the genome. Genes are ranked from highest to lowest correlation to show strongest amplification effect.*

**Correlation analysis was performed by A. Dhawan.*

3.3 *AGO2* Amplification is Inversely Correlated with *DICER1* Deletion

Normally, miRNAs are sequentially processed by two RNase III enzymes, Drosha and Dicer (Treiber, Treiber, & Meister, 2018). However, there have also been reports of miRNA biogenesis pathways that bypass DICER and instead rely on AGO2 for accurate miRNA processing and maturation, such as for miR-451 production (Kretov et al., 2020). Even though DICER-independent miRNA maturation is thought to lead to markedly reduced mature miRNA levels (Kim et al., 2016), global miRNA expression defects can be partly rescued by AGO2 overexpression (Kretov et al., 2020).

Therefore, I further explored the relationship between *AGO2* and *DICER1* in breast cancer samples, using both transcriptomic and genomic data. Exploration of the TCGA-BRCA dataset revealed that more *AGO2*-amplified cases than expected by chance alone harboured a *DICER1* deletion (Figure 3.6A). Similarly, we observed reduced *DICER1* mRNA levels, either because of somatic mutations or as a consequence of epigenetic changes, in samples that harboured *AGO2* gain or amplification (Figure 3.6C). Furthermore, mRNA expression levels of *AGO2* were increased in cases harbouring *DICER1* shallow or deep deletions when compared to diploid cases (Figure 3.6B). However, the opposite was not observed, i.e., there was no enrichment for *DICER1* copy number amplifications in *AGO2* deleted cases, suggesting DICER and AGO2 do not functionally compensate for one another (Figure 3.6A). These results, taken together, suggest a genomic switch from a DICER-dependent to AGO2-dependent, DICER-independent, miRNA processing in breast cancer.

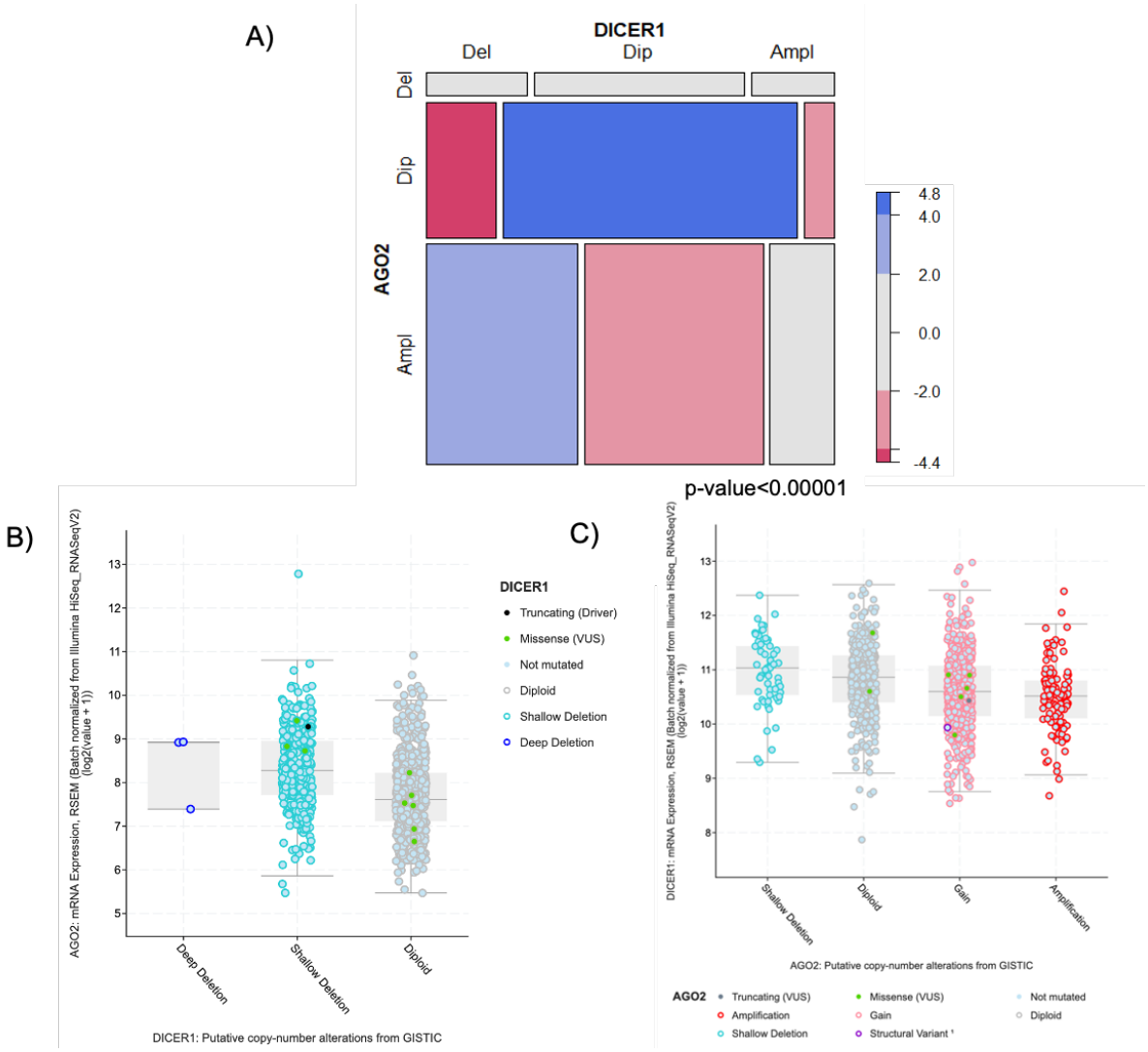

Figure 3.6. ***AGO2 amplification is inversely correlated with DICER1 levels in TCGA-BRCA.*** *A) Mosaic plot of copy number alterations is shown for AGO2 and DICER1. GISTIC calls: Del=Deep or Shallow Deletions, Dip=Diploids, Ampl=Gain or Amplification. Pearson Residuals are colour coded (the sign, positive or negative, indicates whether the observed frequency is higher or lower than expected, with the magnitude indicating the degree of departure). B) AGO2 mRNA expression in DICER1 deleted versus diploid cases. C) DICER1 mRNA expression in AGO2 amplified versus diploid cases. Expression values were shown as the* $\log_2$ *of (RSEM (RNA-Seq by Expectation-Maximization) +1).*

3.4 *AGO2* Amplification is Associated with Overexpression of *OncomiR* Families

Because *AGO2* and *PABPC1* were identified as putative cancer drivers, we were interested in further elucidating the miRNA profiles associated with amplification of this pathway in breast cancer. The importance of Ago proteins in miRNA biogenesis is evident from previous research, and AGO2 was previously shown to play a key role regulating miRNA stability (Winter & Diederichs, 2011). *PABPC1,* however, is not involved in the production of mature miRNAs, but rather in the regulation of miRNA-mediated target inhibition efficiency (Zhang et al., 2015). Therefore, we would not expect *PABPC1* amplification or over-expression to have a global effect on miRNA abundance. Therefore, we investigated the phenotypes associated with *AGO2* amplification in breast cancer samples and asked whether AGO2 could alter miRNA abundance through its role in promoting non-canonical miRNA biogenesis.

First, we tested whether we could detect any significant associations between *AGO2* mRNA and individual miRNA expression levels across two independent breast cancer datasets (METABRIC and TCGA-BRCA). Expression of several miRNAs, including multiple members of the oncomiR-1 family, positively correlated with AGO2 expression across both datasets (Table 3.2). The oncomiR-1 family is composed of three paralogue clusters: miR-17/92, miR-106a/363 and miR-106b/25. In our analysis miR-18a, 19b, and 20a, members of the miR-17/92 cluster, and miR-93 and miR-106b, members of the miR-106b/25 cluster, were strongly positively correlated with AGO2 transcript levels (Table 3.2). We therefore suggest that these miRNAs could constitute novel drivers in *AGO2*-amplified cancers.

Table 3.2. ***List of miRNAs associated with AGO2 expression across two independent invasive breast cancer cohorts.*** *Levels of these miRNAs significantly correlated with mRNA levels of AGO2, in all two breast cancer datasets considered in this study (see methods). Correlations were calculated between mRNA and miRNA expression data and the adjusted p-value is quoted (Benjamini & Hochberg). Only patients with matched genomic (CNV), transcriptomic (both coding and non-coding mRNA) and clinical follow-up data were considered. miRNA expression data in these datasets was measured using different technologies (RNA-seq for the TCGA BRCA dataset; microarray for the METABRIC dataset), enabling us to identify robust associations.*
** This analysis was performed by A. Dhawan.*

	METABRIC (n = 1293)		**TCGA-BRCA (n = 1029)**	
	Correlation	**Adjusted p-value**	**Correlation**	**Adjusted p-value**
hsa-miR-18a	0.22	5.77E-15	0.48	8.32E-39
hsa-miR-20a	0.10	0.0003	0.25	1.10E-10
hsa-miR-93	0.27	8.74E-22	0.31	8.85E-16
hsa-miR-130b	0.11	8.54E-05	0.48	0
hsa-miR-19a	0.24	1.74E-18	0.28	2.82E-13
hsa-miR-224	0.12	1.35E-05	0.32	2.97E-17
hsa-miR-25	0.17	1.66E-09	0.28	5.49E-13
hsa-miR-106b	0.24	3.94E-18	0.49	0
hsa-miR-204	-0.12	5.54E-05	-0.13	0.0012
hsa-miR-432	-0.27	1.18E-21	-0.13	0.001212216
hsa-miR-375	-0.12	1.78E-05	-0.27	2.19E-12
hsa-let-7b	-0.35	3.00E-38	-0.22	1.30E-08
hsa-miR-10b	-0.26	4.49E-20	-0.23	2.86E-09
hsa-let-7c	-0.29	2.96E-26	-0.12	0.001842784
hsa-miR-29c	-0.26	3.88E-20	-0.32	5.18E-17
hsa-miR-195	-0.24	2.59E-18	-0.21	1.26E-07
hsa-miR-379	-0.35	5.77E-38	-0.10	0.010781664
hsa-miR-410	-0.29	4.66E-25	-0.12	0.001884708
hsa-miR-10a	-0.30	3.59E-27	-0.25	5.76E-11

To confirm that the increased abundance of select miRNAs in *AGO2*-amplified samples was indeed caused by altered miRNA processing rather than by increased, MYC-dependent or -independent transcription, we calculated the mature: precursor ratios for these miRNAs and repeated the AGO2 correlation analysis, this time using the mature: precursor ratios as a measure of miRNA abundance (Table 3.3). This revealed that the miRNA/precursor ratios for some members of the miR-106b/25 cluster, including miR-106b-3p, were significantly positively correlated (adjusted p-value < 10^{-6}) with *AGO2* amplification (Table 3.3). This supports the hypothesis that AGO2-driven miRNA expression changes occur as a result of altered miRNA processing and maturation.

Table 3.3. ***List of miRNAs that were significantly positively associated with AGO2 expression in the TCGA-BRCA cohort, when comparing the mature: precursor ratio.*** *The Bonferroni method was used to correct for multiple testing.*
** This analysis was performed by A. Dhawan.*

miRNA name	**miRNA mature: immature expression ratio vs AGO2 gene expression - adjusted P-value for positive correlation coefficient**
hsa-miR-191-3p	< 10^{-16}
hsa-miR-15b-3p	6.55E-15
hsa-miR-335-3p	1.53E-11
hsa-miR-3065-5p	3.51E-11
hsa-miR-744-3p	5.74E-11
hsa-miR-199a-3p	1.91E-10
hsa-miR-30c-5p	1.39E-09
hsa-miR-199b-3p	1.60E-09
hsa-miR-589-3p	1.80E-09
hsa-miR-185-3p	8.28E-09
hsa-miR-29b-3p	1.19E-08
hsa-miR-21-3p	5.39E-08
hsa-miR-224-5p	8.83E-08
hsa-miR-7-5p	8.83E-08
hsa-let-7a-3p	1.58E-07
hsa-miR-200c-5p	1.68E-07

hsa-miR-29a-5p	1.73E-07
hsa-miR-491-3p	2.14E-07
hsa-miR-125b-1-3p	2.97E-07
hsa-let-7g-3p	4.73E-07
hsa-miR-30e-5p	4.86E-07
hsa-miR-423-3p	6.56E-07
hsa-miR-29b-1-5p	6.93E-07
hsa-miR-431-5p	1.21E-06
hsa-let-7a-2-3p	1.30E-06
hsa-miR-330-5p	1.73E-06
hsa-miR-148b-5p	7.99E-06
hsa-miR-99b-3p	8.34E-06
hsa-let-7f-1-3p	9.15E-06
hsa-miR-125a-3p	9.84E-06
hsa-miR-340-3p	1.18E-05
hsa-miR-106b-3p	1.24E-05
hsa-miR-17-5p	2.48E-05
hsa-miR-24-3p	3.45E-05
hsa-miR-452-3p	3.75E-05
hsa-miR-377-3p	3.79E-05
hsa-let-7i-3p	4.14E-05
hsa-miR-34c-3p	5.69E-05
hsa-miR-455-3p	5.93E-05
hsa-miR-887-3p	7.66E-05
hsa-miR-497-3p	8.09E-05

3.5 AGO2 Silencing in *AGO2*-Amplified HCC1806 Cells Supports Selective miRNA Maturation

Based on our bioinformatics analysis of clinical cohorts, I next asked whether *AGO2* amplification would have a similar impact on miRNA abundance *in vitro*. I chose the HCC1806 breast cancer cell line as a pertinent model because it harbours *AGO2* (and *PAPBC1*) CNA (Figure 3.7A). We found that *AGO2* amplification (CN > 2) in HCC1806 cells was associated with its overexpression at the protein level (Figure 3.7B), making it a suitable model for further studies. Furthermore, as expression levels of DICER1 were previously shown to be reduced in hypoxic cells and tumours (van den Beucken et al., 2014), we also measured AGO2 protein levels under both normoxic and hypoxic conditions (1% O_2 for 24 hours, as shown by increased hypoxia-inducible factor (HIF-1α) expression). We found that AGO2 protein levels were not affected by hypoxia, and therefore proceeded with our analysis under normoxic conditions.

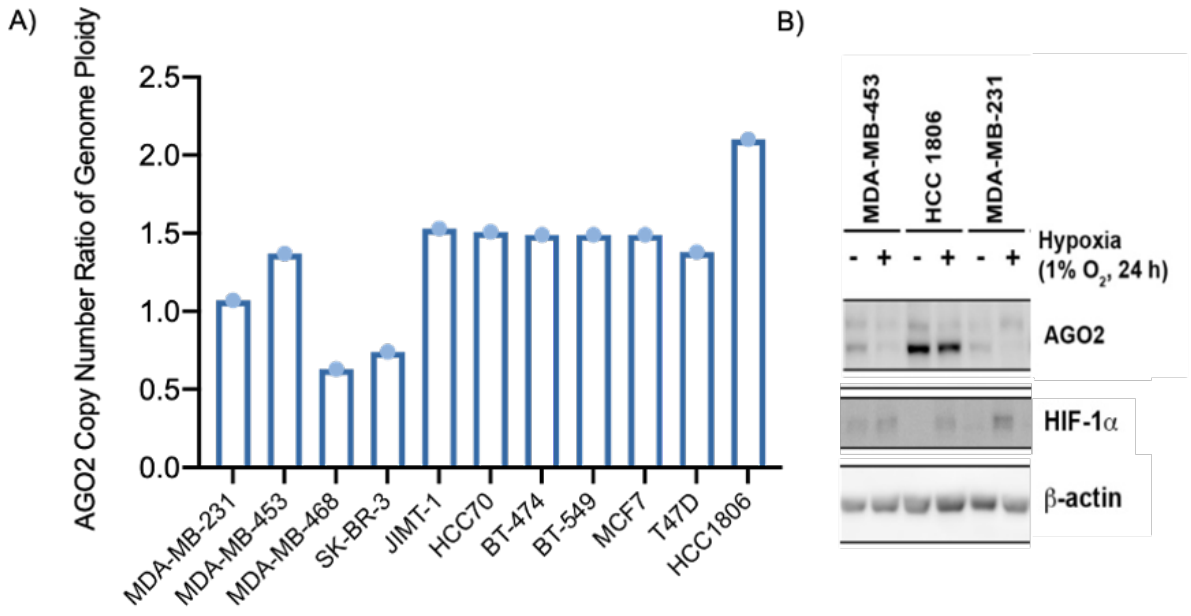

Figure 3.7. ***HCC1806 cells harbour amplification-dependent AGO2 overexpression.*** *A) The relative genomic copy number (CN) of AGO2 (normalised to ploidy). B) Expression of AGO2 in MDA-MB-453, HCC1806, and MDA-MB-231 cells by Western Blot analysis. Expression in normoxia and 24 hours of hypoxia is shown, '-' denotes normoxia, '+' denotes hypoxia (1% Oxygen, 24 hours). β-actin was used as a loading control. *The Western Blot in Figure 3.7B was performed by Simon Wigfield.*

To explore the relation between *AGO2*-amplification and miRNA expression in HCC1806 cells, AGO2 was depleted by siRNA-mediated knockdown and miRNA abundance was measured using hybridisation on miRNA microarrays.

When a clear reduction of AGO2 protein was observed in siRNA-transfected cells (Figure 3.8A), I first used colony formation assays to confirm that knockdown of AGO2 did not affect the survival of HCC1806 cells (Figure 3.8B). Moreover, as I previously identified a correlation between *AGO2* and *DICER1* levels in clinical breast cancer cohorts (Figure 3.6), I also tested DICER protein levels following siRNA-mediated depletion of AGO2, to ensure our miRNA microarray results were not confounded by altered Dicer-mediated miRNA processing. Dicer showed no change in expression following AGO2 depletion in HCC1806 cells (Figure 3.8A), and I therefore proceeded with miRNA abundance measurements.

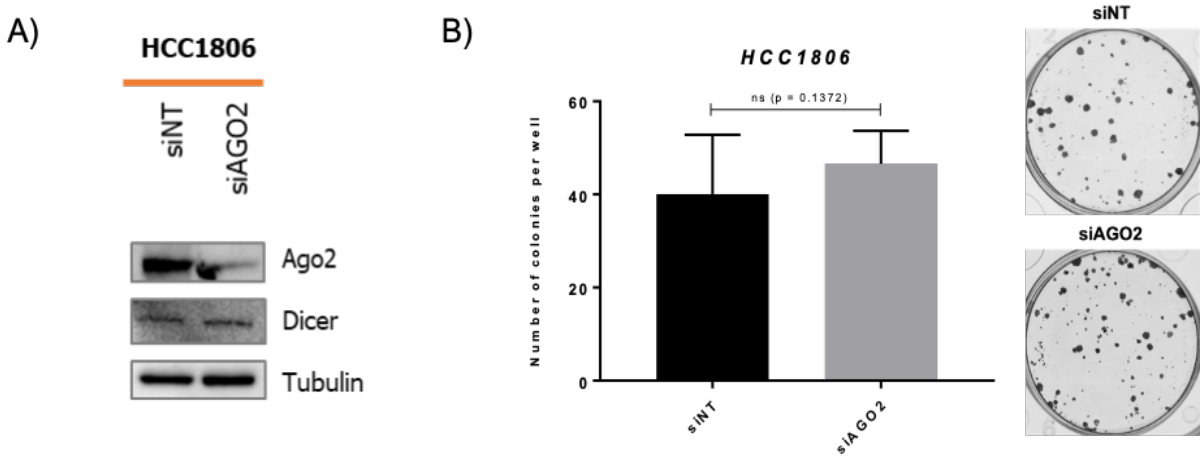

Figure 3.8. ***Impact of siRNA-mediated AGO2 depletion on cellular survival of HCC1806 cells****. A) Western blot analysis of DICER and AGO2 protein levels in HCC1806 cells to confirm AGO2 knockdown. Tubulin was used as a loading control. B) Representative colony formation assay 10 days after siNT or siAGO2 treatment (HCC1806 cells). Data points and bars represent the mean and SEM of three independent experiments. ns, not significant.*

To compare miRNA expression between *AGO2* siRNA and the non-targeting (NT) control treated HCC1806 cells, miRNA technologies and fluorescence-based detection methods were used. The Agilent miRNA microarray contains different oligonucleotide probes for each individual mature microRNA, replicated a number of times across the array surface (Wang, Ach, & Curry, 2007). Comparison of miRNA expression between the *AGO2* siRNA and siNT transfected HCC1806 cells (Figure 3.9A) confirmed that there was a striking effect on miRNA abundance following *AGO2* depletion, with a large number of miRNAs (170 probesets, targeting 114 miRNAs) differentially expressed between *AGO2*-depleted and non-targeting control-treated HCC1806 cells. Of these differentially expressed miRNAs, 131 probesets (targeting 80 miRNAs) were downregulated and 39 probesets (targeting 34 miRNAs) were upregulated in the *AGO2*-depleted cells (with respect to the control) (Figure 3.9A). Some of the most strongly differentially regulated miRNAs included both miR-93 and miR-106, members of the miR-106b/25 cluster, and members of the let-7 family of miRNAs, suggesting these miRNAs are highly expressed in *AGO2*-amplified samples (Figure 3.9B). This is in concordance with our clinical results, where we found a strong correlation between AGO2 levels and members of the oncomiR-1 family of miRNAs (Table 3.3).

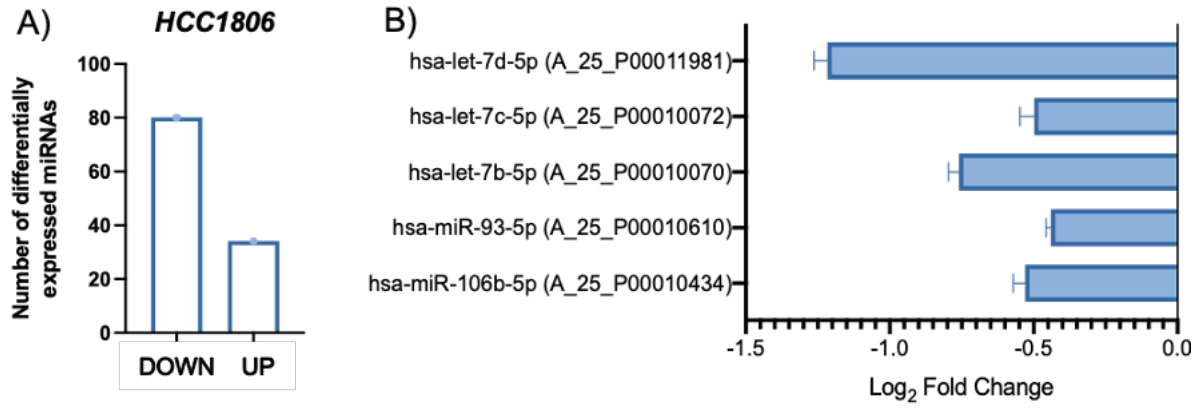

Figure 3.9. ***Microarray profiling reveals AGO2-driven expression of a subset of miRNAs.*** *A) Number of differentially expressed miRNAs in AGO2-knockdown HCC8016 cells with respect to control are shown as revealed by Agilent microarray profiling. B) Mean Log_2 Fold Changes (including probenames) of some of the most downregulated miRNAs following AGO2 depletion in HCC1806 cells.*

3.6 Correlation Between *AGO2* and miR-106b-5p Levels in a Panel of Breast Cancer Cell Lines

Next, I asked whether increased abundance of these oncogenic miRNAs, especially miR-93 and miR-106b of the miR-106b/25 cluster, could be consistently observed across *AGO2*-amplified breast cancer cell lines (Figure 3.7A). Second, I asked whether elevated expression levels of mature miRNAs of the miR-106b/25 cluster were driven by increased transcription or enhanced processing of the miR-106b-25 primary transcripts. As such, both precursor and mature miRNA levels of members of the miR-106b/25 cluster were measured in a panel of breast cancer cell lines using qRT-PCR, TaqMan™ Advanced MicroRNA Assays, and pre-existing CCLE mRNA expression data (Ghandi et al., 2019).

Mature miR-106b-5p expression levels were evaluated in a panel of 11 breast cancer cell lines and one non-tumourigenic breast epithelial cell line (MCF10A) using TaqMan™ Advanced MicroRNA Assays (Figure 3.10, Methods). Hsa-miR-423-5p and hsa-miR-16-5p were used as endogenous control miRNAs as they showed constant expression levels amongst a subset of 59 National Cancer Institute (NCI-60) cell lines (*Endogenous Controls for Real-Time Quantitation of miRNA Using TaqMan® MicroRNA Assays*, 2007). Furthermore, their abundance was not significantly correlated with *AGO2* expression levels in either the clinical datasets, or in the miRNA microarray studies (Section 3.5). Even though quantified miR-106b-5p expression levels differed slightly depending on the method of normalisation used (i.e., normalisation against miR-16-5p or miR-423-5p expression levels), the relative divergence of miR-106b-5p expression levels between cell lines was clear (Figure 3.10). Several low-miR-106b-5p expressing cell lines (including JIMT-1, which harbours a *DICER1* deep deletion, and T-47D), as well as several high-miR-106b-5p expressing cell lines (including MCF7 and HCC1806) were identified.

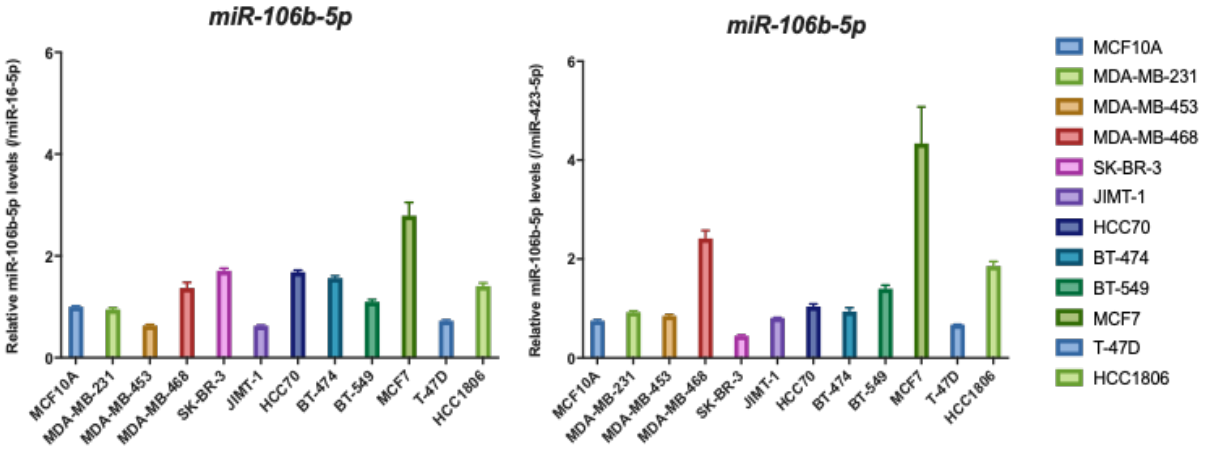

Figure 3.10. ***Quantification of miR-106b-5p expression levels across a panel of BC cell lines.*** *Reverse transcription-quantitative polymerase chain reaction (qRT-PCR) analysis (TaqMan™ Advanced miRNA Assay) of miR-106b-5p expression in a panel of breast cancer cell lines. Transcript levels were normalised to miR-423-5p and miR-16-5p expression. Data shown are from three independent experiments and expressed as mean ± 95% confidence interval (CI).*

Next, miR-106b-5p expression levels (normalised against miR-16-5p) were extracted, and Pearson's correlation analyses were performed to evaluate the strength of the relationship between mature miR-106b-5p levels and *MCM7* mRNA levels, which were obtained from published CCLE RNA-seq data (Ghandi et al., 2019). *MCM7* and the miR-106b/25 cluster share a common promoter, and one could therefore predict high concordance between *MCM7* mRNA levels and expression of the primary miR-106b miRNA transcript. Surprisingly, however, no concordance was found between *MCM7* mRNA and mature miR-106b-5p levels in this panel of BC cell lines (Spearman's $\rho = 0.004241$, p-value = ns).

Next, the relationship between *AGO2* copy number, *AGO2* mRNA, and mature miR-106b-5p miRNA levels was explored using the same method (Figure 3.11). In accordance with the role for AGO2 as a cancer driver, I identified a positive correlation between *AGO2* copy number and *AGO2* mRNA expression levels (Spearman's $\rho = 0.4537$, p-value = 0.0805). However, no linear correlation could be observed between *AGO2* copy number and mature miR-106b-5p levels, or *AGO2* mRNA levels and mature miR-106b-5p levels (Spearman's $\rho = -0.03779$ and p-

value = 0.4561, and Spearman's ρ = -0.2415 and p-value = 0.2372, respectively) (Figure 3.11). I hypothesised that the lack of correlation could be due to cell cycle-dependent changes in *MCM7* expression, as the miR-106b-25 cluster was previously shown to be maximally expressed at the G_1-to-S transition, similar to the expression pattern observed for *MCM7* (Haldar, Roy, & Banerjee, 2014). Therefore, I measured the levels of pre-miR-106b in the panel of 11 cell lines (Figure 3.12A) and calculated the ratio between mature: immature miR-106b levels. Then, the correlation analyses were repeated, now using *AGO2* copy number data and the mature miRNA/precursor ratio for miR-106b expression, thereby correcting for cell cycle differences in *MCM7* expression and co-transcription of the primary miR-106b/25 transcript.

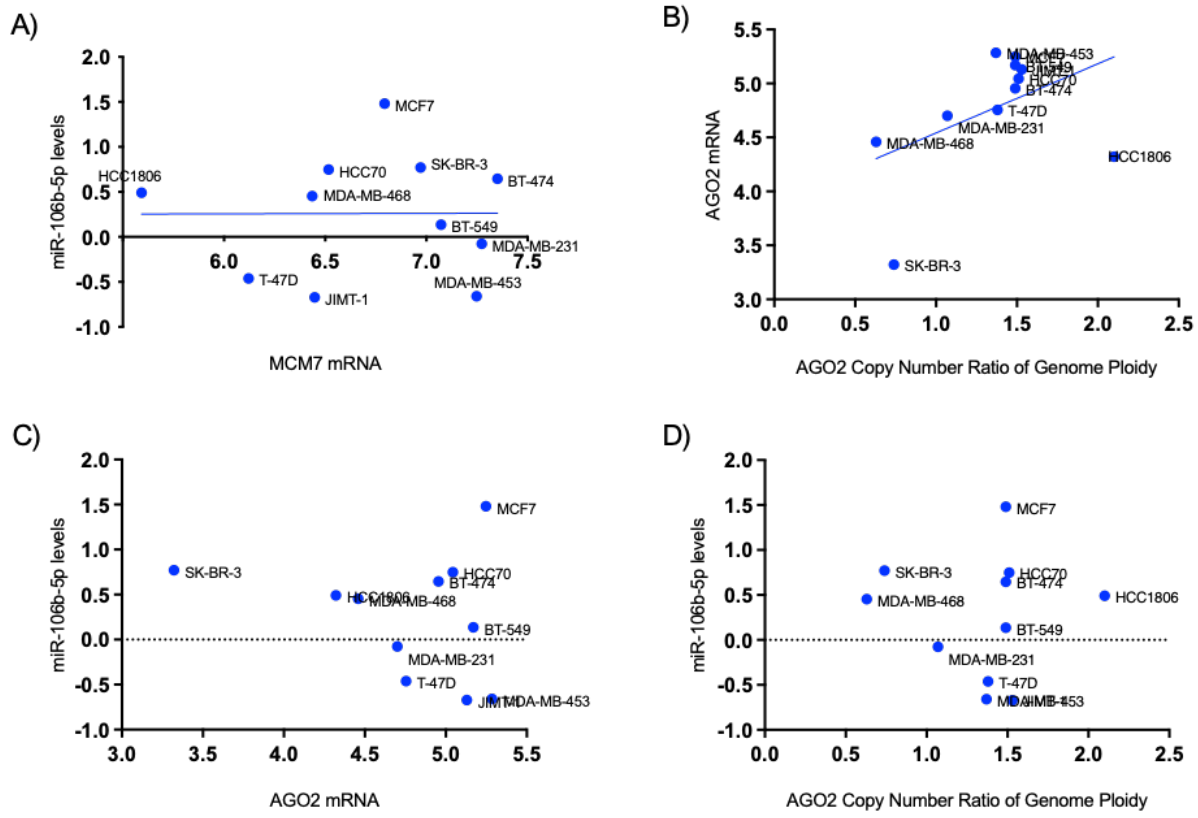

Figure 3.11. ***Plots of the correlation between AGO2 copy number, AGO2 mRNA, MCM7 mRNA, and miR-106b-5p levels in a panel of BC cell lines.*** *Scatter plots of pairwise Pearson's correlation of a) MCM7 mRNA and mature miR-106b-5p expression, b) AGO2 relative genomic copy number (CN) (normalised to ploidy) and AGO2 mRNA (Log_2 TPM, CCLE), c) AGO2 mRNA (Log_2 TPM, CCLE) and miR-106b-5p expression, and d) AGO2 relative genomic copy number (CN) (normalised to ploidy) and miR-106b-5p expression levels (n=11).*

This revealed that the miRNA/precursor ratio for miR-106b-5p was positively correlated, albeit not significantly, with *AGO2* amplification (Spearman's ρ = 0.296, p-value = 0.2114) (Figure 3.12B). Due to the low number of cell lines used in this study (n=11), and the co-existence of other genetic and epigenetic alterations, we could not establish any statistically significant relationships between AGO2 and miR-106b-5p levels. However, there was no correlation between *AGO2* copy number and mature miR-106b-5p levels (Spearman's ρ = -0.03779, p-value = ns), whereas the correlation between *AGO2* copy number and the ratio of mature miR-106b-5p (Spearman's ρ = 0.296, p-value = 0.2114) was stronger, supporting the hypothesis of increased maturation, rather than increased transcription, for miR-106b in samples harbouring *AGO2* amplification.

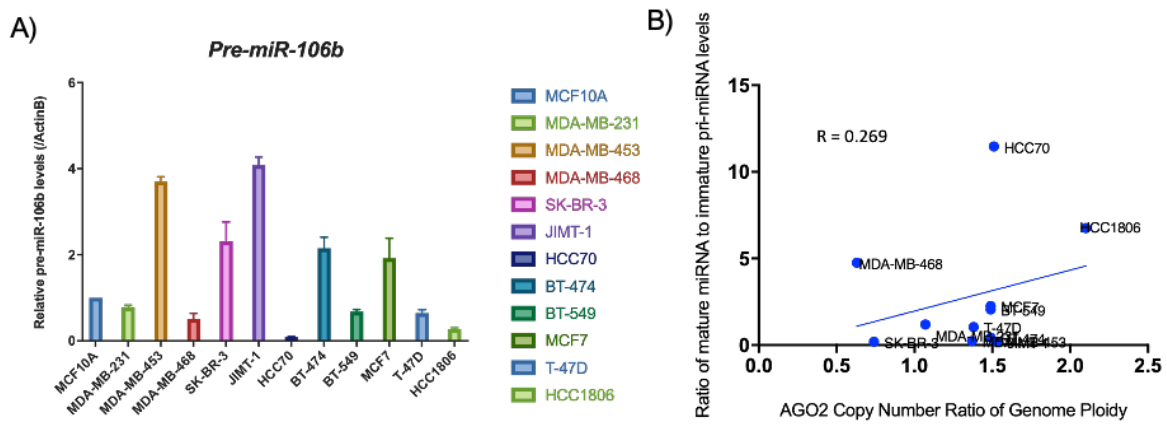

Figure 3.12. ***Correlation between AGO2 copy number and mature: immature miR-106b levels in a panel of BC cell lines.*** *A) Quantification of pre-miR-106b expression levels across a panel of BC cell lines using qRT-PCR, with expression levels normalised to Actin B. Data represented as mean ± SEM (n=3). B) Scatter plot of pairwise Pearson's correlation of AGO2 relative genomic copy number (CN) (normalised to ploidy) and the ratio of mature miR-106b-5p to precursor-miR-106b expression levels (n=11).*

3.7 Depletion of AGO2 in HCC1806 Cells Confirms Preferential Maturation of the miR-106b/25 Cluster

To validate the miRNA microarray results *in vitro* and further study the biology of *AGO2* amplification and its impact on the abundance and preferential maturation of the miR-106b/25 cluster in more detail, the levels of both the precursor and mature forms of miR-25, -93 and -106b were quantified in siNT and siAGO2-treated HCC1806 cells using qRT-PCR and TaqMan™ Advanced MicroRNA Assays, respectively. The forward and reverse primers were designed to bind within the hairpin sequence of the precursor miRNA (for primer sequences, see methods). miR-5787 was identified as the miRNA that exhibited the lowest variability across the different conditions (siNT and siAGO2) in the Agilent Microarray and was therefore used as an endogenous miRNA control for mature miRNA expression normalisation.

Knockdown of AGO2 caused a significant downregulation of mature miRNAs miR-93-5p (p-value = 0.0282) and miR-106b-3p (p-value <0.0001) (Figure 3.13A), even though levels of the miR-93/106b precursor transcripts remained unchanged in AGO2-depleted cells (Figure 3.13B). This suggests that downregulation of the miRNAs of the miR-106b-25 cluster occurs not at the pri-/pre-miRNA level, but rather at the later stages of miRNA biogenesis when pre-miRNAs get processed into mature miRNAs. miR-25-5p could not be quantified, presumably due to low expression in the HCC1806 cell line (Figure 4.12A). Knockdown of DICER1, in contrast, resulted in increased levels of miR-93/106b precursor transcripts and their corresponding mature miRNAs, in particular miR-106b-5p (Figure 3.13), suggesting that DICER1 is dispensable for miRNA maturation in *AGO2*-amplified HCC1806 cells.

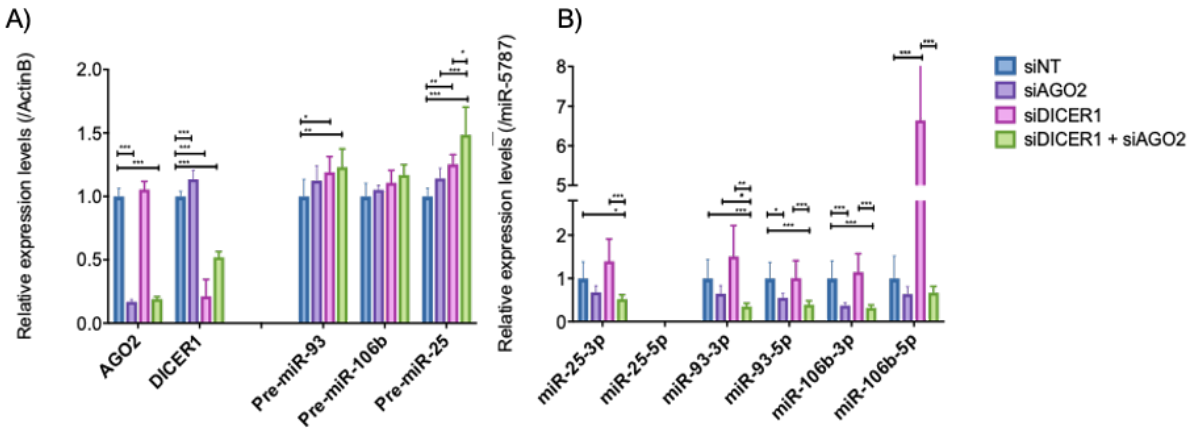

Figure 3.13. ***Depletion of AGO2 in HCC1806 cells points to preferential miRNA maturation.*** *A) Real Time PCR quantification of miR-106b/25 cluster precursors normalised to Actin B in HCC1806 transfected with siDICER1 and/or siAGO2. B) TaqMan based quantification of mature miRNAs miR-25-3p, miR-25-5p, miR-93-3p, miR-93-5p, miR-106b-3p and miR-106b-5p normalised to mitochondrial miR-5787 in HCC1806 transfected with siDICER1 and/or siAGO2. Significance calculated with a two-way ANOVA. Data shown are from three independent experiments and expressed as mean ± 95% confidence interval (CI).*

In accordance with elevated miR-106b-5p expression in cells transfected with siDICER1, we found *E2F1*, which was previously shown to be a target gene of miR-106b-5p (Petrocca et al., 2008), to be significantly downregulated in DICER1-knockdown HCC1806 cells (p-value <0.0001). We also checked expression of the host gene *MCM7* following siRNA-mediated depletion of AGO2 and DICER1, which remained unchanged (Figure 3.14).

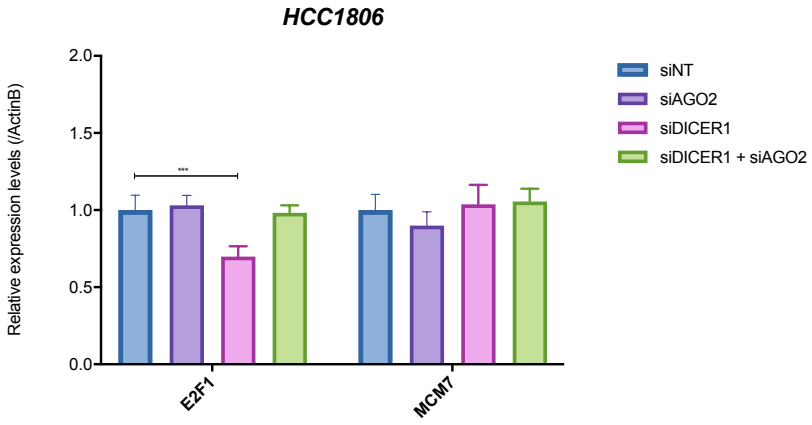

Figure 3.14. ***MCM7 and E2F1 expression levels following AGO2 and/or DICER1 knockdown in HCC1806 cells.*** *HCC1806 cells were transfected with a siRNA against AGO2 and/or DICER, and expression of E2F1 and host gene MCM7 were determined by qRT-PCR. Data shown are from three independent experiments and expressed as mean ± 95% confidence interval (CI).*

As a slight increase in *DICER1* expression levels was observed following knockdown of AGO2 in HCC1806 cells (Figure 3.13A), I wanted to ascertain our miRNA abundance measurements and conclusions were not confounded by DICER-driven changes. Therefore, the impact of AGO2 depletion on the levels of the precursor and mature miRNAs of the miR-106b-25 cluster was explored in the epithelial breast cancer cell line, JIMT-1, which harbours a *DICER1* deep deletion. In accordance with findings in HCC1806 cells, AGO2 depletion led to decreased levels of mature miRNAs miR-25-3p, miR-93-5p, and miR-106b-3p, without any changes in their corresponding precursor miRNA transcripts, providing further evidence that maturation of the miR-106b/25 cluster is AGO2-dependent and DICER1-independent (Figure 3.15).

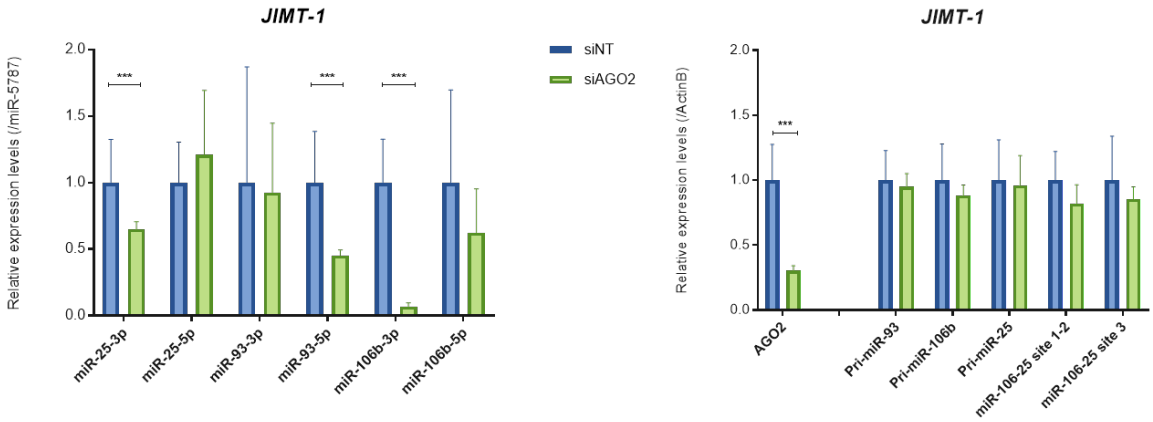

Figure 3.15. ***AGO2 regulates miRNA maturation in JIMT-1 cells in the absence of DICER1.*** *TaqMan™ Advanced miRNA assay-based quantification of mature miRNAs miR-25-3p, miR-25-5p, miR-93-3p, miR-93-5p, miR-106b-3p and miR-106b-5p normalised to mitochondrial miR-5787 and real-time PCR quantification of miR-106b/25 cluster precursors (normalised to Actin B) in JIMT-1 cells (harbouring a DICER1 deep deletion) transfected with siNT or siAGO2. Data shown are from three independent experiments and expressed as mean ± 95% confidence interval (CI).*

Finally, we validated these findings in the TCGA-BRCA dataset. We found that expression levels of miR-106b/25 cluster members miR-93-5p, miR-106b-3p and miR-106b-5p were significantly increased in samples showing elevated *AGO2* expression levels, and that this increase was accompanied by *DICER1* copy number loss (Figure 3.16).

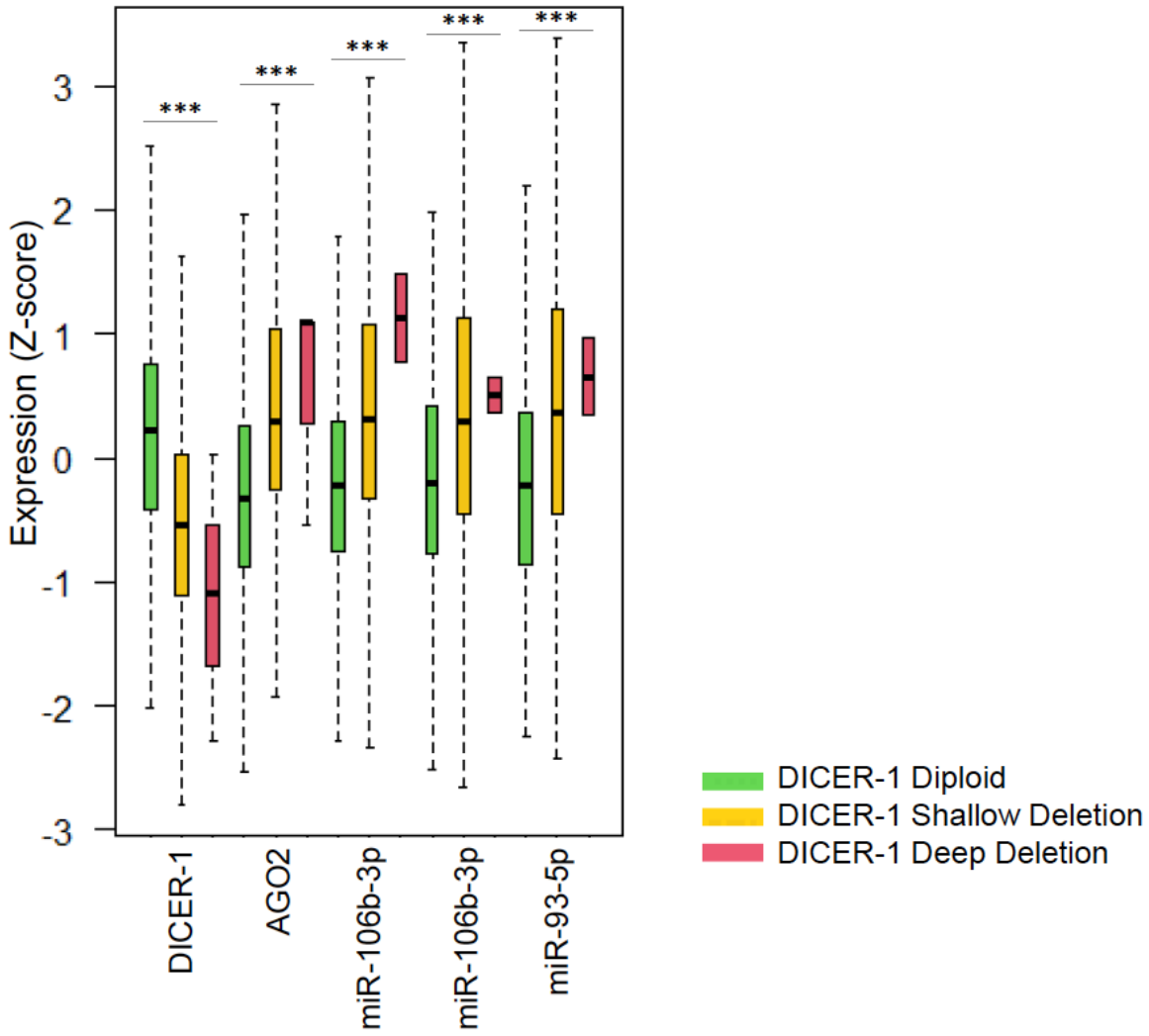

Figure 3.16. ***Expression of DICER1, AGO2, miR-106-3p, miR-106b-5p, and miR-93-5p in DICER1 diploids, shallow deleted and deep deleted cases in TCGA-BRCA*** *(z-score standardised).* ***= $p<0.00000001$, ANOVA linear model test.*

MicroRNA regulation has been often reported to differ between cell lines and clinical samples (Dvinge et al., 2013), and concordance between our findings in HCC1806 and JIMT-1 cells, as well as in the TCGA-BRCA clinical cohort, therefore strengthens the evidence for an important role for AGO2, not DICER1, in promoting oncogenic miRNA biogenesis in breast cancer.

3.8 Mapping the Synthetic Dosage Lethality Network of *AGO2*-Amplified Cancers

Given the frequency of *AGO2* CNA, we sought to identify novel methods to target the selective AGO2-dependent maturation of oncogenic miRNAs for therapeutic purposes. Even though recent efforts have been directed at the development of microRNA-specific Argonaute 2 inhibitors that block both the seed region recognition sequence and the protein's active site (Schmidt, Korb, & Abell, 2013), there are currently no clinically approved inhibitors. Hence, indirect methods of targeting *AGO2* CNA, such as through synthetic dosage lethality (SDL) Approaches (Guarente, 1993), were proposed to be more suitable.

First, we exploited two comprehensive databases containing synthetic dosage lethality pairs from a multitude of studies, the SynLethDB database (Guo, Liu, & Zheng, 2016) and the Synthetic Lethality Knowledge Graph (Zhang et al., 2021). These databases revealed two potential AGO2 SDL interaction partners: *TP53* and *BRCA1*. To confirm the SL interactions of *TP53* or *BRCA1* with *AGO2* gain or copy number amplification, we interrogated the TCGA-BRCA and METABRIC datasets. SDL interactions were defined as those for which gene *X* was altered (either through somatic mutation or a predicted deleterious mutation) in a (significantly) mutually exclusive manner to *AGO2* CNA (Srihari, Singla, Wong, & Ragan, 2015).

In both clinical datasets, we found that *TP53* mutation was more likely to co-occur with *AGO2* amplification than non-amplification. Specifically, we detected a significantly higher number of samples harbouring both *AGO2* CNA and *TP53* mutation than expected by random distribution. For instance, In the TCGA breast cancer cohort, the frequency of *TP53* mutation was 54% in cases harbouring *AGO2* CNA, but 14% in cases without *AGO2* CNA (diploid

cases), suggesting that expression of wild-type *TP53* and *AGO2* amplification are synthetic dosage lethal, or that these genetic alterations co-occur during tumourigenesis (Figure 3.17).

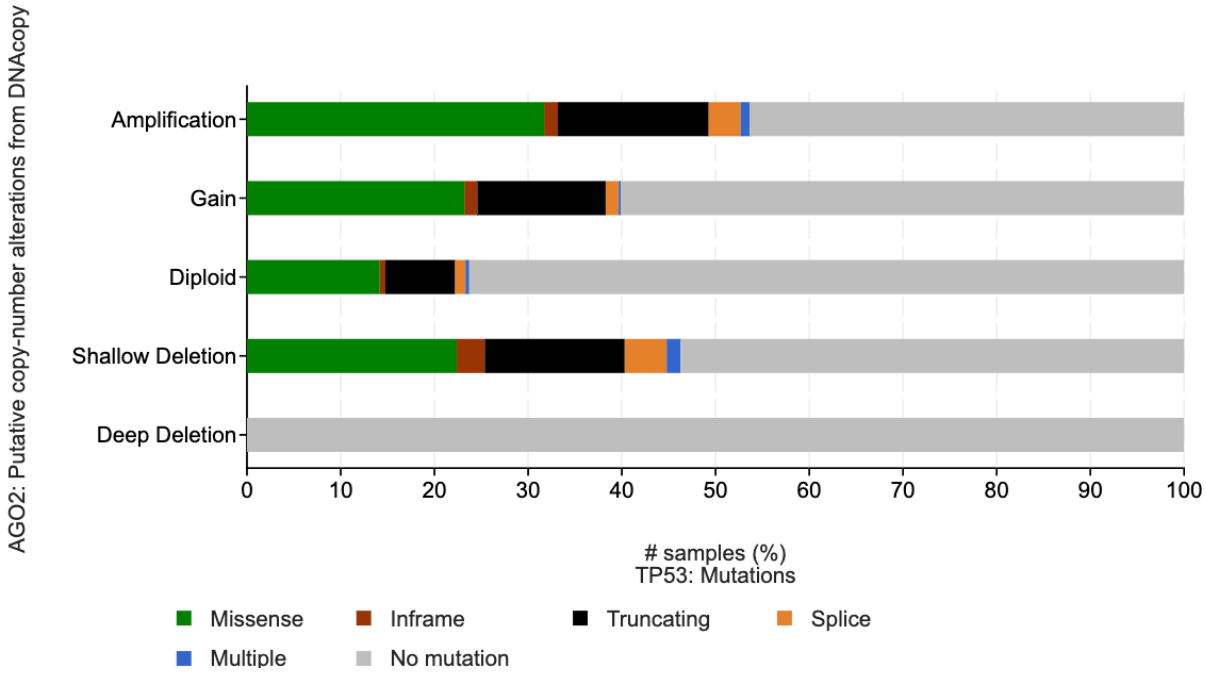

Figure 3.17. ***AGO2 copy number variation versus TP53 mutation in TCGA-BRCA*** *(n=1904).*

The frequent co-occurrence of *TP53* mutations and *AGO2* CNA across breast cancer cohorts is interesting, especially as p53, one of the most frequently mutated tumour suppressors, has been shown to interact with Ago2 to modulate the association of Ago2 with a subset of miRNAs in response to DNA damage (Krell et al., 2016). *AGO2* amplification could therefore confer advantages for tumour progression in the presence of inactivating *TP53* mutations through impairing the miRNA-mediated DNA damage response.

3.9 Conclusion

Collectively, our data shows that aberrant miRNA expression in breast cancer is primarily driven by global dysregulation of miRNA biogenesis genes, rather than by disrupted pri-miRNA transcription. Specifically, key elements of miRISC (such as *TARBP1*, *AGO2* and *PABPC1*), and miRNA editing factors (*ADAR*), were frequently amplified and concordantly over-expressed across two different breast cancer cohorts. We found that amplification and over-expression of *AGO2* promotes oncogenic miRNA production, consistent with the observation that only AGO2 was able to form the cleavage-competent miRNA induced silencing complex (Liu et al., 2004).

Silencing of AGO2 in cell lines harbouring its amplification resulted in reduced expression levels of mature miRNAs of the oncomir-1 miR-106b/25 cluster. Furthermore, I found that the ratio of mature to precursor miRNAs was increased in *AGO2*-amplified and over-expressing samples or cell lines, further supporting a role for AGO2 in promoting the selective maturation of miRNAs of the miR-106b/25 cluster. Mature miR-106b-5p levels have recently shown promise as blood-based biomarkers for minimally invasive detection of early-stage breast cancer (Sadeghi et al., 2021). Moreover, miR-106b-5p was shown be an important marker of breast cancer aggressiveness and prognosis (Farré et al., 2021), most likely because of its role in inhibiting several important tumour suppressor genes (Dhawan et al., 2018). Here, we demonstrated that *AGO2* amplification was associated with poor prognosis in the METABRIC and TCGA-TNBC cohorts, and we therefore propose an important role for *AGO2* as a cancer driver gene via its role in promoting oncogenic miRNA maturation.

Additionally, I show that the production of canonical miRNAs and the preferential maturation of oncogenic miRNAs, including of the miR-106b/25 cluster, can occur independently of

DICER1, and that amplification and over-expression of genes in the AGO2-dependent pathway frequently co-occurs with *DICER1* mutations and under-expression. Previous studies have indeed shown that Dicer is not required for RISC assembly in mammals (Betancur & Tomari, 2012), but that instead, the pre-miRNAs can be loaded into AGO2, where they are directly cleaved by the Argonaute catalytic centre to generate an intermediate 3′ end, which is then further trimmed to generate a functional mature miRNA (Cheloufi et al., 2010). It would therefore be interesting to explore whether the production of oncogenic miRNAs requires Argonaute 2 catalytic activity, as this was previously shown to allow the bypass of Dicer for miRNA production (Cifuentes et al., 2010). Even though the AGO2-mediated, DICER-independent, miRNA maturation pathway has only been recently discovered (Kim et al., 2016), we provide evidence for a switch from DICER1-dependent to -independent miRNA processing during breast cancer development.

In summary, the key findings of this chapter are:

- Amplification-dependent overexpression of *AGO2* and *PABPC1* drives oncogenic alterations in the global miRNA landscape.
- AGO2 copy number gain or amplification frequently co-occurs with loss or mutation of *DICER1* in clinical breast cancer samples.
- *AGO2*-amplification drives selective maturation of oncogenic miRNAs, in particular of the miR-106b/25 cluster, as shown by the altered ratio of precursor to mature miRNAs.
- AGO2-dependent, DICER-independent miRNA biogenesis constitutes a novel driver pathway in cancer.

Chapter 4

miR-106b-5p Promotes Cellular Growth and Predicts WEE1 Inhibitor-Sensitivity in Breast Cancer

4.1 Introduction

In the previous chapter, I have shown that *AGO2* amplification and over-expression selects for oncogenic miRNA production, especially of the miR-17/92 and miR-106b/25 polycistronic clusters. MicroRNAs have emerged as key regulatory molecules in a wide variety of cellular processes associated with cancer, including proliferation and survival, the cellular stress response, and drug resistance (Garzon, Calin, & Croce, 2009).

Because miRNAs of the oncomiR-106b/25 cluster are expressed at low levels in normal, terminally differentiated cells while they accumulate in malignant cells, they may represent ideal targets for cancer therapy (Mehlich et al., 2018). Functional characterisation of miRNAs, and specifically the miR-106b/25 cluster, is of crucial importance, as aberrant miRNA expression can silence the expression of TSGs related to cancer hallmarks (Dhawan et al., 2018). The miR-106b/25-related miR-17/92 polycistron has previously been classified as a potential human oncogene as its members can act together with c-MYC to accelerate tumour development (He et al., 2005) I therefore asked if the miR-106b/25 cluster could pose another example of an oncogenic polycistron, providing an alternative mechanism by which tumour suppressor genes can be downregulated during breast cancer development, thereby enabling tumour growth.

Here, I focus on understanding the phenotypic consequences of miR-106b-5p overexpression in breast cancer cell lines. Previous studies have shown that miR-106b-5p targets the tumour suppressor protein SETD2 to inactivate it during ccRCC progression (Xiang et al., 2015). As our group has previously demonstrated that *SETD2*-deficient cancers can be targeted with the

WEE1 inhibitor, and to a lesser extent, with ATR- or CHK1- inhibitors (Pai et al., 2019; Pfister et al., 2015), I asked whether tumour cells over-expressing miR-106b-5p would similarly display enhanced sensitivity to checkpoint kinase inhibition, as a result of reduced *SETD2* levels. On the other hand, miR-106b-5p could also alter checkpoint kinase inhibitor sensitivity through its role in regulating the checkpoint protein p21, which has previously been demonstrated to be a miR-106b-5p target in colon cancer cell lines (Ivanovska et al., 2008). As a consequence, elevated miR-106b expression was shown to override the doxorubicin-induced DNA damage checkpoint (Ivanovska et al., 2008), which can have important consequences for sensitivity to other cancer drugs. Thus, the therapeutic potential of targeting miR-106b-5p-high cancers with checkpoint kinase inhibitors needs to be thoroughly weighed and investigated against the role of miR-106b-5p in regulating tumour suppressor genes that affect both arms of the SETD2-WEE1 synthetic lethality.

To unravel some of the complexity of miRNA-based tumour regulation and give us pointers as to how we can successfully treat miR-106b-5p-driven cancers, the aims of the following chapter are:

- To investigate the clinical parameters associated with miR-106b-5p overexpression in breast cancer.
- To assess the role of miR-106b-5p in promoting tumour growth by conducting 3D spheroid growth analysis in the presence and absence of miR-106b-5p antisense oligonucleotides.
- To correlate CHK1, ATR, and WEE1 checkpoint kinase inhibitor sensitivity with miR-106b-5p expression levels.
- To study the cell cycle differences associated with the modulation of miR-106b-5p levels in breast cancer cell lines.

4.2 The Clinicopathological Significance of miR-106b-5p in Breast Cancer

An increasing number of studies have identified miRNAs as potential biomarkers for human cancer diagnosis and prognosis (reviewed in Brase *et al.*, 2010). Therefore, I was interested in understanding the role of miR-106b-5p in breast cancer and its associations with clinicopathological parameters. First, analysis of miR-106b-5p expression was performed across the TCGA pan-cancer project (Weinstein et al., 2013), which includes data from 32 human cancer types, using the starBase v3.0 Pan-Cancer miRNA Differential Expression Analysis Platform (http://starbase.sysu.edu.cn/panCancer.php) (Li, Liu, Zhou, Qu, & Yang, 2014). MiR-106b-5p was significantly overexpressed in 14 out of 32 cancer types surveyed when compared to related adjacent normal tissue samples, including in colon adenocarcinoma (COAD) (Fold Change [FC] = 27.23, FDR = 7.1E-52) and in kidney renal cell carcinoma (KIRC) (FC = 2.39, FDR = 4.1E-50). Of particular interest was breast invasive carcinoma (BRCA), where, as shown in Figure 4.1, miR-106b-5p expression in cancer tissue was significantly higher when compared to normal tissue (Fold Change = 2.51, FDR = 6.4E-36).

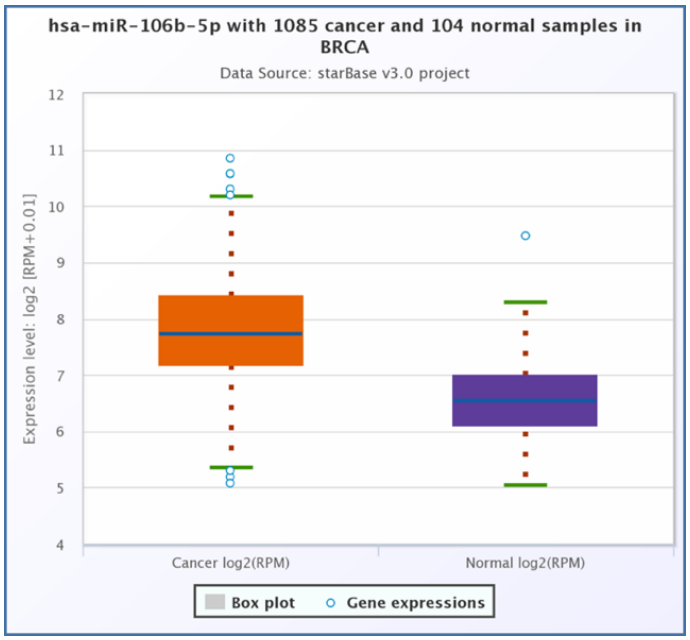

Figure 4.1. ***miR-106b-5p expression levels in BC tumours compared to paired normal adjacent tissue (TCGA-BRCA)*** *(Fold Change = 2.51, FDR = 6.4E-36). MicroRNA expression data was downloaded from the TCGA project via Genomic Data Commons Data Portal. The expression values of miRNAs from miRNA-seq data were scaled with* $log_2(RPM + 0.01)$ *(RPM =Reads Per Million).*

Breast cancer is molecularly classified based on expression of sex hormone receptors (Perou et al., 2000). Tumours expressing ER and/or the progesterone receptor (PR) are considered hormone receptor-positive breast cancers, whereas tumours that do not express ER, PR, or human epidermal growth factor receptor 2 (HER2) are triple-negative breast cancers (TNBC). Hence, I first tested whether I could observe any associations between single hormone receptor-positive, or -negative, phenotypes and miR-106b-5p levels (Figure 4.2). Interestingly, I found that for two hormone receptors (ER and PR), negative receptor status was correlated with elevated miR-106b-5p expression levels in TCGA-BRCA (Figure 4.2). Previous studies have similarly demonstrated an association between overexpression of the miR-106b/25 cluster and basal-like breast cancer, where TNBCs, defined by the absence of the ER, PR and HER2 receptors, were largely found to correspond to the basal-like tumours (87%) (de Rinaldis et al., 2013).

The associations between miR-106b-5p and clinical parameters, including tumour stage, overall survival status, and metastases in breast cancer patients, were next investigated using TCGA-BRCA data (Weinstein et al., 2013). Higher miR-106b-5p expression was positively correlated with breast tumour stage, with advanced-stage breast cancer (stages III and IV) patients showing higher miR-106b-5p expression levels than patients at early tumour stages (Figure 4.3). Furthermore, when patients were stratified based on their lymph node metastasis status, miR-106b-5p was further upregulated in the presence of tumour metastases (Figure 4.3). Collectively, these findings suggest that increased miR-106b-5p plays an important role in breast cancer progression and metastasis.

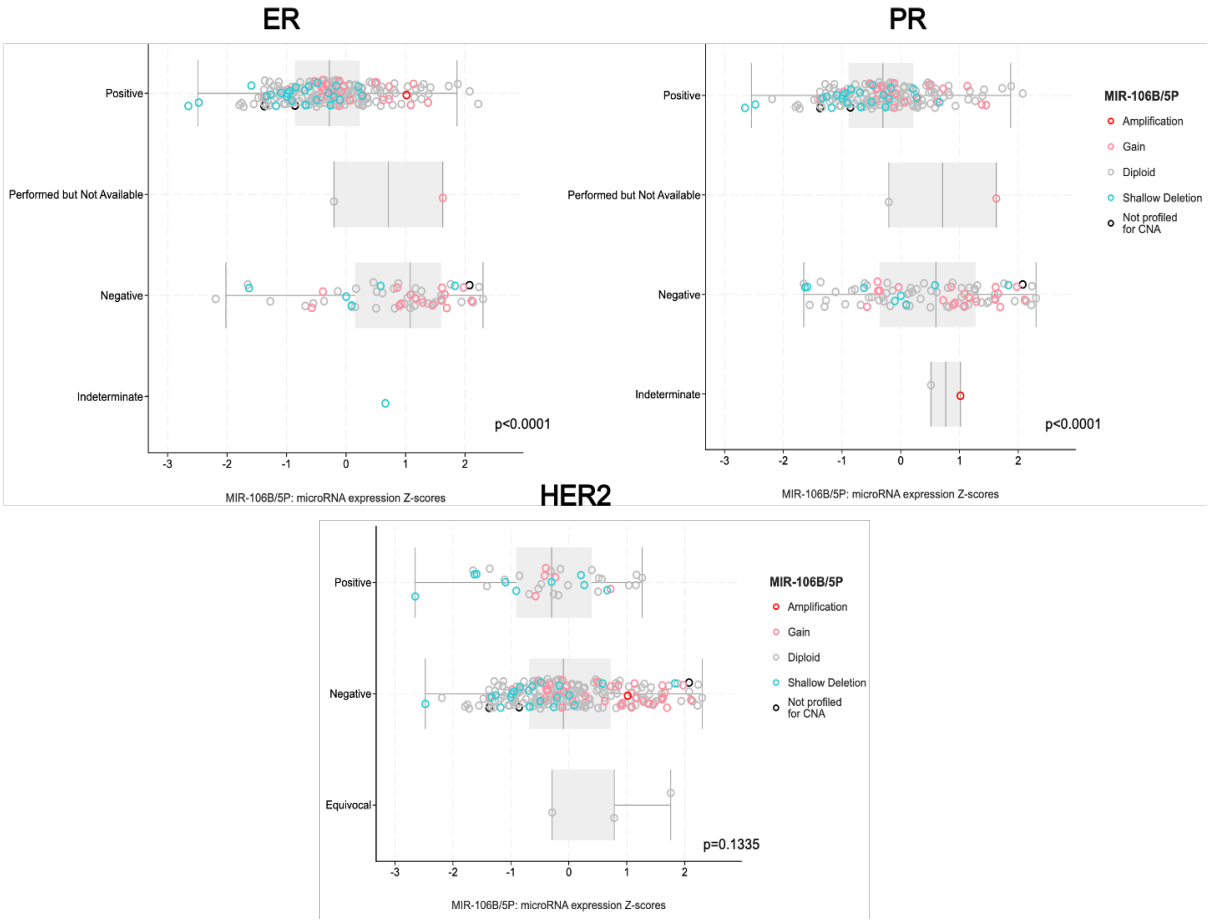

Figure 4.2. ***Association of miR-106b-5p expression levels with expression of the major hormone and growth factor receptors, ER, PR, and HER2*** *(TCGA BRCA, n=1904). P-values were calculated using the Mann-Whitney U test.*

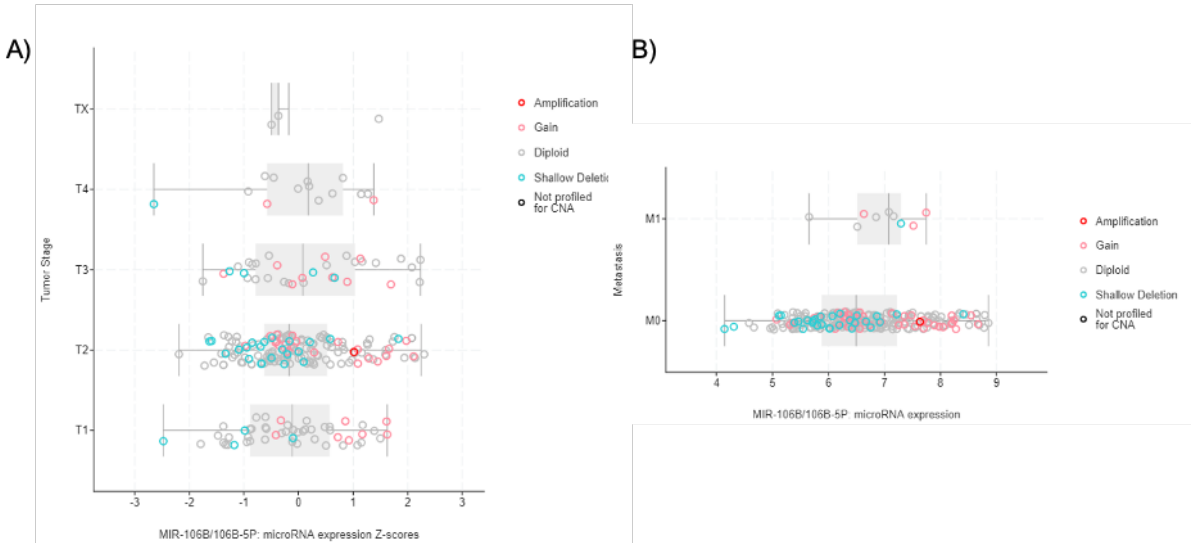

Figure 4.3. ***miR-106b-5p expression levels were positively correlated with advanced tumour stage and metastases.*** *A) miR-106b-5p expression levels (Z-scores) in different clinical stages of breast invasive carcinoma. B) miR-106b-5p expression levels (Z-scores) were elevated in patients with metastasised breast cancer.*

Considering the significant correlation between miR-106b-5p expression levels and advanced tumour stage, I asked whether miR-106b-5p expression levels were also associated with prognostic markers, such as overall survival (OS). Firstly, I tested the association between miR-106b-5p levels and prognosis in the METABRIC dataset as long-term follow-up data was available for the majority of patients (Curtis et al., 2012). Patients were divided into a low and high miR-106b-5p-expression group using the median value of its expression as a cut-off, after which the difference in survival between the two groups was evaluated by Kaplan–Meier Plots in combination with the log-rank test analysis (Bland & Altman, 2004). As shown in Figure 4.4, patients with high miR-106b-5p expression had a significantly poorer OS when compared to the group with low miRNA expression in METABRIC (p-value < 0.001).

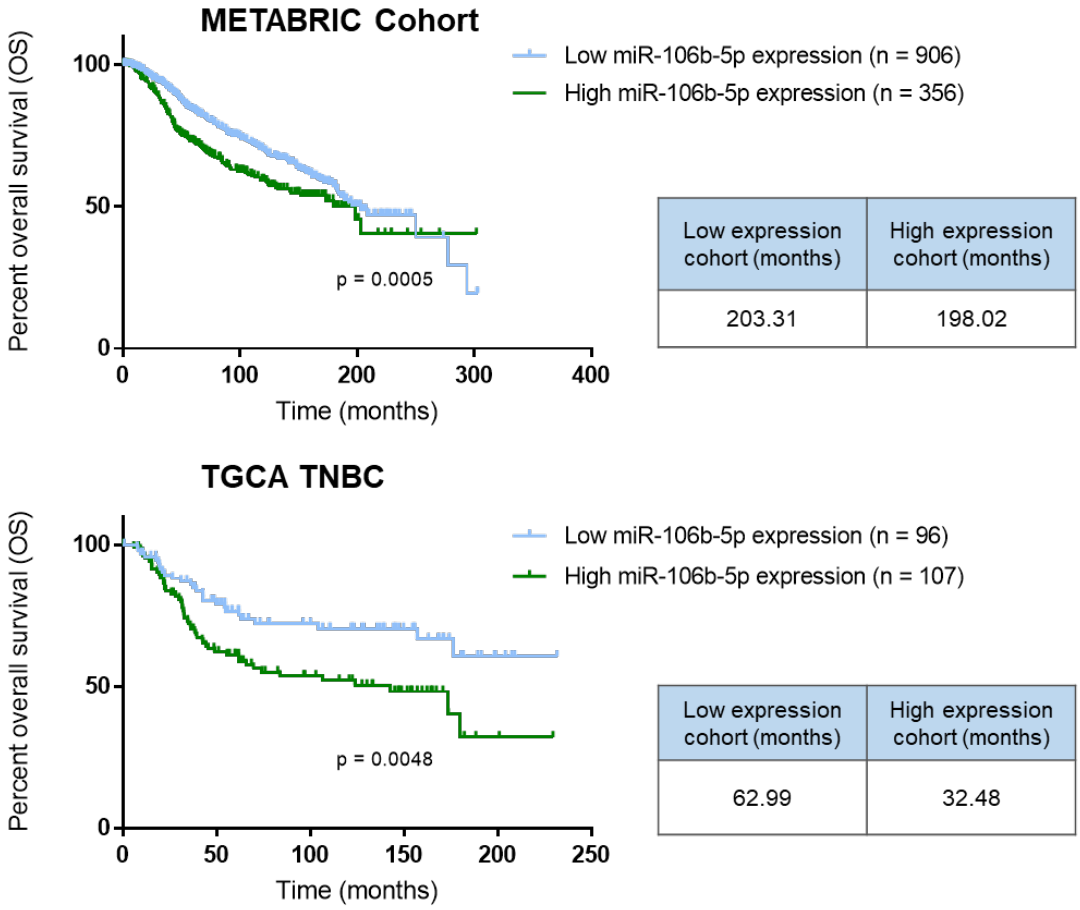

Figure 4.4. ***Kaplan-Meier Survival Plots for miR-106b-5p expression in METABRIC (n=1262) and TCGA-BRCA TNBC (n=203) cohorts.*** *The log rank test was used to compare the survival differences between low- and high-expressing cohorts. The median miR-106b-5p expression value was as a cut-off.*

Next, I also tested survival in the TCGA-BRCA cohort, with a focus on the TNBC subgroup, as they showed larger differences in miR-106b-5p levels when compared to normal tissue (Figure 4.2). In accordance with findings in the METABRIC cohort, patients expressing high miR-106b-5p levels had a significantly poorer overall survival compared to the low miR-106b-5p-expression group ($p < 0.01$) (Figure 4.4).

4.3 MicroRNA-106b-5p Regulates Cellular Proliferation of Breast Cell Lines

Because I observed a strong correlation between miR-106b-5p levels and prognostic markers in clinical samples, I asked whether modulation of miR-106b-5p levels had any significant consequences on cellular proliferation and apoptosis *in vitro*. First, I tested the effect of miR-106b-5p inhibition on cellular survival and cell death using clonogenic growth assays and western blot analysis in a low-miR-106b-5p (MDA-MB-453) and high-miR-106b-5p expressing (MDA-MB-468) cell line. MDA-MB-453 and MDA-MB-468 cells transfected with anti-miR-106b-5p oligonucleotides displayed a much-reduced cell number when compared to the control cells (Figure 4.5). Furthermore, western blot analysis of the activation of caspase 3, one of the executioner caspases whose cleavage of its many substrates leads to the downstream events of apoptosis, and PARP cleavage (Chaitanya, Alexander, & Babu, 2010) demonstrated, however, that anti-miR-93-5p or anti-miR-106b-5p treatment did not result in an increase in apoptotic signalling (Figure 4.5). This suggests that reduced proliferation was not due to increased cell death, but rather due to slower growth, perhaps because of elevated p21 levels.

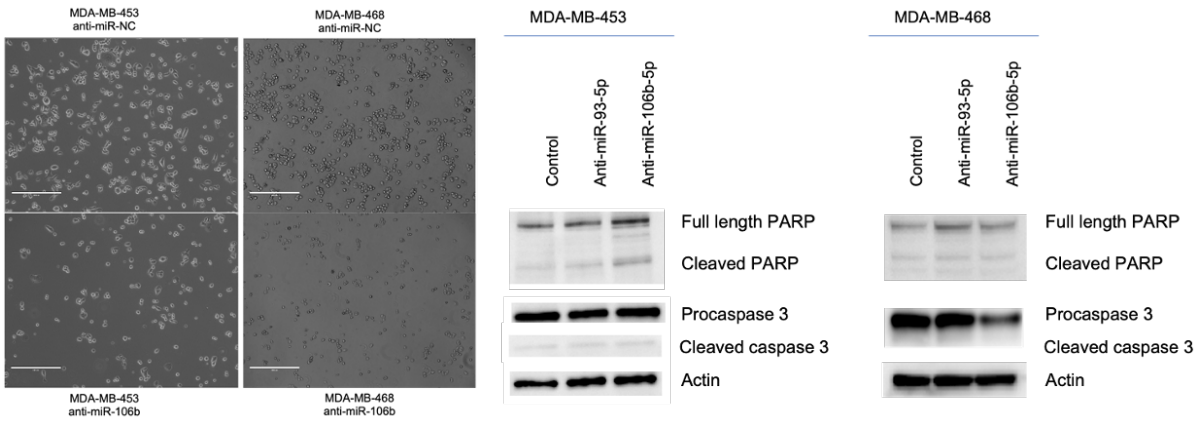

Figure 4.5. ***Inhibition of miR-106b-5p reduces the proliferative capacity of MDA-MB-453 and MDA-MB-468 cells.*** *Western blot of PARP, procaspase 3, and cleaved caspase 3 levels in MDA-MB-453 and MDA-MB-468 cell lines 72 hours after anti-miR-93-5p or anti-miR-106b-5p transfection. No cleaved caspase was detected in MDA-MN-468 cells. β-actin was used as a loading control.*

To further assess whether anti-miR-106b-5p transfection caused the TNBC cell lines MDA-MB-468, HCC70 and BT-549 to display altered growth characteristics, I measured the growth of anti-miR-NC or anti-miR-106b-5p transfected 3D tumour spheroids. This *in vitro* model was chosen because 3D spheroids mimic important features of solid tumours, such as hypoxic cores (Kunz-Schughart, Kreutz, & Knuechel, 1998). After transfection and seeding, I grew the spheroids for 6-10 days, took microscopic images every 24 hours, and measured the volume of MDA-MB-468, HCC70 and BT-549 anti-miR-NC and anti-miR-106b-5p transfected spheroids using ImageJ. I found that anti-miR-106b-5p-treated cells showed a different growth profile when compared to the control cells (Figure 4.6). Growth rates of MDA-MB-468 cells diverged beginning at 72 hours (3 days) as central necrosis appeared. After 5 days, the difference was much more apparent, and *in vitro* growth of the anti-miR-106b-5p-treated MDA-MB-468 spheroids were retarded when compared to the control-treated cells (Figure 4.6).

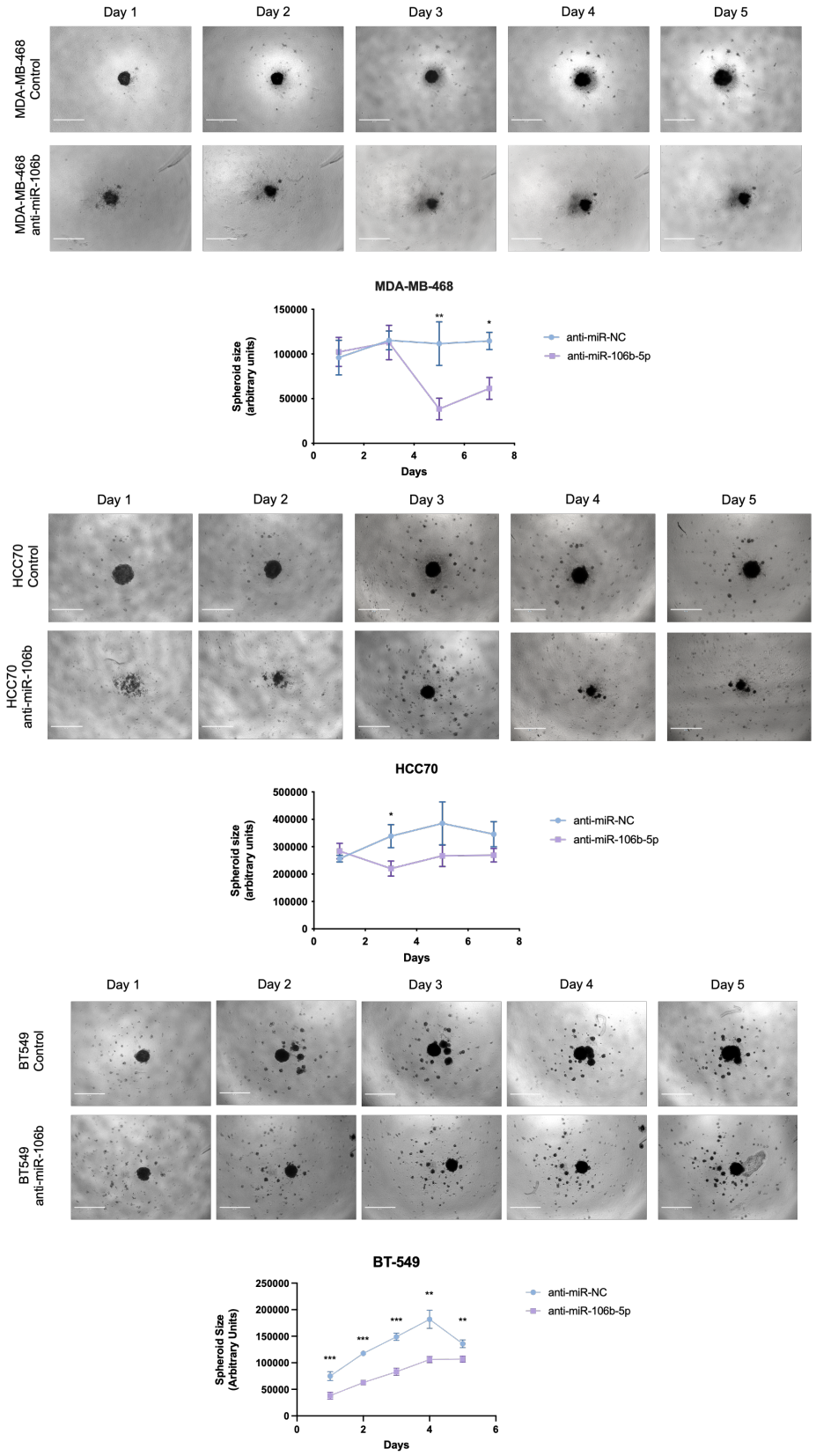

Figure 4.6. ***3D spheroid growth of MDA-MB-468, HCC70, and BT-549 cells transfected with either anti-miR-106b-5p or a non-targeting antisense oligonucleotide.*** *Representative images of 3D spheroids at the day of seeding or after 2, 3, 4, or 5 days of growth. The area of the spheroid was measured using ImageJ. Results are representative of at least three independent experiments, with an average of 10 spheroids per replicate for each condition.*

For HCC70 and BT-549 cells, a slightly different growth profile was found, as miR-106b-5p inhibition reduced the ability of HCC70 and BT-549 cells to form spheroids immediately after cell seeding. However, the two growth curves converged after 5 days, which might be explained by the transient silencing effect of miR-106b-5p targets, with mRNA-target levels recovering fully within 4-5 days of anti-miR-106b-5p transfection (Figure 4.6). These data demonstrated that inhibition of miR-106b-5p in TNBC cells slows down growth in 3D cultures, and that this might be a promising approach for future cancer therapeutics.

4.4 MicroRNA-106b-5p Negatively Regulates *SETD2* in 6 Cancer Types

Next, cBioportal v3.7.5 was used to explore the frequency of mutations and copy number alterations in *SETD2* in TCGA datasets of multiple cancer types (Gao et al., 2013; Weinstein et al., 2013). *SETD2* alterations occurred in 2 (4%) out of 56 uterine sarcoma patients, 57 (16%) out of 354 kidney renal cell carcinoma patients, 2 (1.6%) out of 123 thymoma patients, 25 (2.5%) out of 996 breast invasive carcinoma patients, and 17 (6%) out of 274 kidney renal papillary cell carcinoma patients (http://www.cbioportal.org). Despite low *SETD2* mutation rates in a number of these cancer types, we know, from our unpublished immunohistochemistry data, that a high percentage of these cancers do display loss of the histone mark H3K36me3 (Okonjo et al., manuscript in preparation). If we take breast invasive carcinoma, for instance, we observed a mutation rate of only 2.5%, whereas 23.5% of our tumour samples displayed negative or low H3K36me3 staining (Okonjo *et al.,* manuscript in preparation). To us, this suggested that mechanisms other than *SETD2* mutation can contribute to H3K36me3-deficiency.

The miRNA target prediction algorithm miRanda (John et al., 2005) predicted that the 3'-UTR of *SETD2* mRNA contained 1 putative miR-106b-5p binding site, and in accordance with this, miR-106b-5p was previously shown to negatively regulate SETD2 in renal cell carcinoma upon

binding (Xiang et al., 2015). However, the authors did not investigate whether the miRNA-mRNA interaction profile of miR-106b-5p and *SETD2* in renal cell carcinoma was distinct from that in other cancer types. Hence, I explored the correlation between miR-106b-5p and *SETD2* across 32 types of cancers (10,159 RNA-seq and 9925 miRNA-seq samples) (Table 4.1).

Indeed, I found a significant negative correlation between miR-106b-5p and *SETD2* mRNA expression levels in 6 out of 32 cancers, including uterine carcinosarcoma (Spearman's ρ = -0.238, p-value = 7.71E-2), kidney renal clear cell carcinoma (Spearman's ρ = -0.196, p-value = 6.95E-6), thymoma (Spearman's ρ = -0.19, p-value = 3.87E-2), and breast invasive carcinoma (Spearman's ρ = -0.149, p-value = 7.77E-7) (Table 4.1). This shows that in the absence of mutation, *SETD2* can alternatively be downregulated via miRNA-based mechanisms (Xiang et al., 2015), including through binding of miR-106b-5p to the 3' UTR end of *SETD2*.

Table 4.1. ***Expression correlation of hsa-miR-106b-5p and SETD2 across 13 cancer types.***

Cancer	Sample Number	Spearman's Rho	p-value	FDR
Uterine Carcinosarcoma	56	-0.238	7.71E-02	2.56E-01
Kidney Renal Clear Cell Carcinoma	517	-0.196	6.95E-06	2.98E-05
Thymoma	119	-0.19	3.87E-02	5.35E-02
Breast Invasive Carcinoma	1085	-0.149	7.77E-07	1.52E-06
Pheochromocytoma and Paraganglioma	183	-0.149	4.46E-02	1.58E-01
Kidney Renal Papillary Cell Carcinoma	289	-0.124	3.45E-02	6.41E-02
Prostate Adenocarcinoma	495	-0.09	4.57E-02	6.68E-02
Bladder Urothelial Carcinoma	408	0.143	3.82E-03	7.68E-03
Brain Lower Grade Glioma	525	0.174	6.43E-05	2.60E-04
Skin Cutaneous Melanoma	449	0.18	1.30E-04	6.43E-04
Head and Neck Squamous Cell Carcinoma	497	0.189	2.25E-05	5.37E-05
Liver Hepatocellular Carcinoma	370	0.244	2.12E-06	8.19E-06
Uveal Melanoma	80	0.308	5.48E-03	3.80E-02
Ovarian Serous Cystadenocarcinoma	376	0.409	1.24E-16	8.09E-15

4.5 Relation Between miR-106b-5p, *SETD2*, and *RRM2* Expression in Breast Cancer

Next, I tested whether the negative correlation between miR-106b-5p and *SETD2* expression levels, as found in clinical breast cancer samples, could be validated *in vitro*, using a panel of 12 breast cancer cell lines. In addition to *SETD2*, the analysis was extended to other putative miR-106b-5p target-mRNAs. MiR-106b-5p was previously shown to regulate *E2F1* mRNA levels in HEK293T cells (Trompeter et al., 2011). The transcription factor *E2F1* promotes the transcriptional activation of *RRM2*, which is the regulatory subunit of ribonucleotide reductase (RNR) (Chabes, Björklund, & Thelander, 2004; DeGregori, Kowalik, & Nevins, 1995). Therefore, as *RRM2* is under control of both SETD2 (Pfister *et al.*, 2015; Chapter 6) and E2F1 (Chabes et al., 2004; DeGregori et al., 1995), I was interested in testing whether miR-106b-5p levels were also inversely related with E2F1 and RRM2 expression levels. This is of clinical importance, as E2F1 and RRM2 are the main effectors of the synthetic lethality between loss of *SETD2* and WEE1 inhibition, and miR-106b-5p could therefore provide a novel biomarker for WEE1 inhibitor sensitivity.

In Chapter 3, I quantified mature miR-106b-5p levels in a panel of breast cancer cell lines using the Taqman™ Advanced microRNA Assay. For the same panel of cell lines, *SETD2* and *RRM2* expression data were extracted from CCLE (Ghandi et al., 2019) (Figure 4.7). *SETD2* and *RRM2* transcript levels were further validated using qRT-PCR, using 18S ribosomal RNA expression levels as an internal control (Figure 4.7). Despite a few differences between the gene expression data from CCLE and our independent qRT-PCR validation, perhaps related to quantitative changes in cells at different stages of the cell cycle, a few low-*SETD2* (e.g., SK-BR-3) and high-*SETD2* (e.g., MDA-MB-231) expressing cell lines could be identified.

Next, Pearson's correlation analyses between *SETD2* and *RRM2* mRNA levels (using CCLE RNA-seq data) and mature levels of miR-106b-5p (Ghandi et al., 2019) were performed (Figure 4.8). The correlation between *SETD2* and *RRM2* mRNA was used as a positive control, as previous studies have shown that SETD2 regulates the transcription of *RRM2* (Pfister et al., 2015). Indeed, we found that *SETD2* and *RRM2* mRNA levels were highly, and significantly, correlated (Spearman's $\rho = 0.7545$, p-value = 0.0036) in this panel of BC cell lines (Figure 4.8).

Next, the correlation between miR-106b-5p and *E2F1* or *SETD2* mRNA levels was tested. I identified negative correlations between miR-106b-5p levels and *E2F1* (Spearman's $\rho = -0.4994$, p-value = 0.0589) or miR-106b-5p and *SETD2* (Spearman's $\rho = -0.4953$, p-value = 0.0607), respectively. Similarly, a negative correlation between miR-106b-5p and *RRM2* levels (Spearman's $\rho = -0.2373$, p-value = 0.2412) was found, although the association was weaker (as evidenced by a lower correlation coefficient) than for *E2F1* and *SETD2*, possibly reflecting an indirect mode of regulation. Even though previous studies have suggested miR-106b regulates breast cell progression by suppression of PTEN (Li et al., 2017), we could not find any correlation between miR-106b-5p and *PTEN* levels in this panel of cell lines (Spearman's $\rho = -0.08484$, p-value = 0.8041) and thus decided to focus on further characterising the role of miR-106b-5p in regulating the SETD2-E2F1-RRM2 axis.

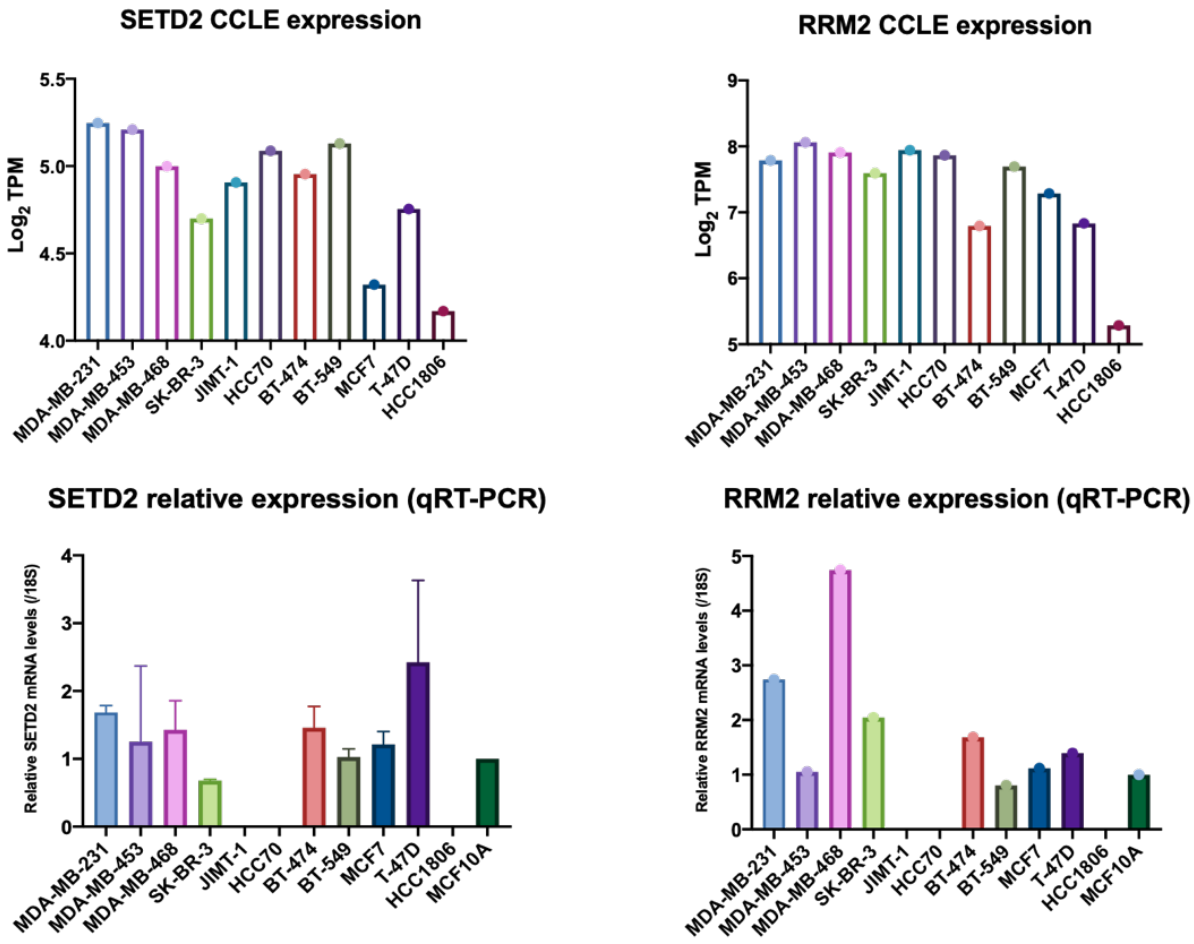

Figure 4.7. ***Quantification of SETD2 and RRM2 expression levels across a panel of BC cell lines.*** *Expression data was extracted from the CCLE RNA-sequencing database (expressed as log_2(TPM) values). qRT-PCR was used to validate these results, normalised against 18S expression levels. Data is from three independent experiments and expressed as mean ± 95% confidence interval (CI).*

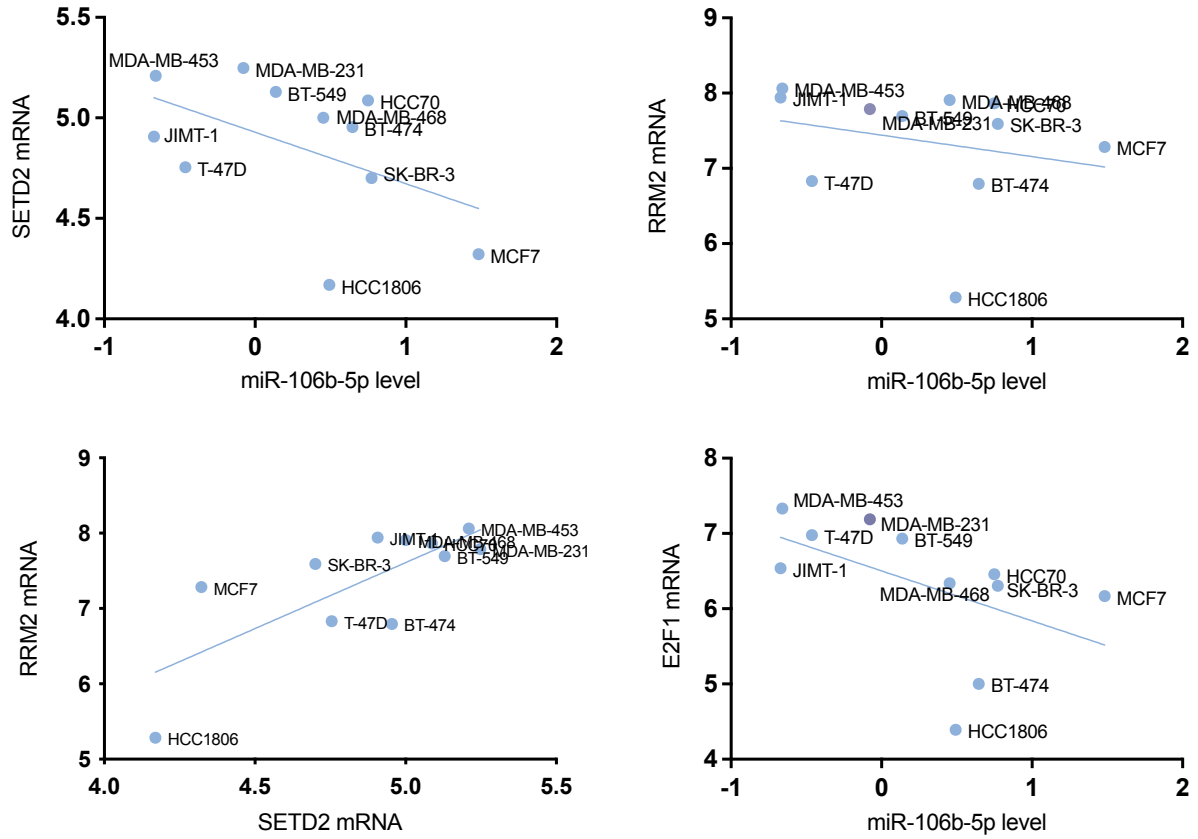

Figure 4.8. ***Plots of expression correlation between SETD2 mRNA, E2F1 mRNA, RRM2 mRNA and miR-106b-5p levels in a panel of BC cell lines.*** *Scatter plots of pairwise Pearson's correlations of A) mature miR-106b-5p levels and SETD2 mRNA levels (CCLE RNA-seq); B) mature miR-106b-5p levels and RRM2 mRNA levels (CCLE RNA-seq); C) SETD2 mRNA levels (CCLE RNA-seq) and RRM2 mRNA levels (CCLE RNA-seq); and D) mature miR-106b-5p levels and E2F1 mRNA levels (CCLE RNA-seq).*

4.6 MicroRNA-106b-5p Regulates p21 and RRM2 Protein Levels in U2OS Cells

As miR-106b-5p levels were negatively correlated with both *SETD2* and *RRM2* levels in this panel of 12 breast cancer cell lines (Figure 4.8), I wanted to demonstrate causation and asked whether increased miR-106b-5p levels could directly impact on SETD2 activity. To do this, a microRNA-106b-5p mimic was transfected into U2OS osteosarcoma cells, which has previously been shown to be an easy to manipulate cell line, with high miR-106b-5p levels (He et al., 2020). Next, the total protein was extracted, and Western Blot was performed to check for H3K36me3 levels in the absence and presence of miR-106b-5p mimics. As cyclin-dependent kinase inhibitor 1A (*CDKN1A*), or p21, has already been shown to be a target of

miR-106b-5p, p21 protein levels were used as a positive control (Figure 4.9). Despite changes in *SETD2* mRNA levels, I could not observe any apparent changes in H3K36me3 levels 48 hours after miR-106b-5p mimic transfection (Figure 4.9). I did, however, confirm a strong reduction in the levels of p21 following miR-106b-5p mimic transfection in U2OS cells (Figure 4.9).

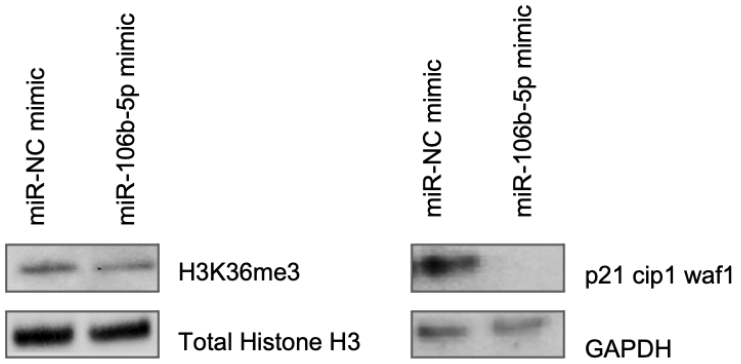

Figure 4.9. ***Western blot analysis of H3K36me3 and p21 protein levels in U2OS cells transfected with a non-targeting control miRNA or miR-106b-5p mimic.*** *GAPDH or Total Histone H3 levels were used as a loading control.*

As previously described, tumours with low levels of SETD2-dependent H3K36me3 display hypersensitivity to WEE1 inhibition by AZD1775. The synthetic lethality is manifested by low levels of RRM2 and subsequent nucleotide pool depletion (Pfister et al., 2015). Even though no changes in H3K36me3 levels were observed following the introduction of miR-106b-5p mimics, I did previously find a correlation between miR-106b-5p and *E2F1* mRNA levels (Figure 4.8). E2F1 is the transcription factor that binds to, and transcribes, *RRM2* (Chabes et al., 2004; DeGregori et al., 1995). I therefore wondered whether changing miR-106b-5p levels could impact on RRM2 protein levels, and consequently, WEE1 inhibitor sensitivity. Therefore, I tested RRM2 protein levels following miR-106b-5p mimic introduction in U2OS cells using Western Blot analysis and subsequently measured the effect of miR-106b-5p mimic introduction on AZD1775-sensitivity using the resazurin cell viability assay (Figure 4.10).

As shown in Figure 4.10, RRM2 protein levels were reduced following miR-106b-5p mimic transfection in U2OS cells, whereas levels of P53R2, which is not under control of E2F1, but rather a p53-responsive gene, remained unchanged. Furthermore, I found a small but non-significant reduction in cell viability when U2OS cells were exposed to increasing concentrations of AZD1775 (0-600 nM) in the presence of the miR-106b-5p mimic when compared to the control cells. Because U2OS cells already display high levels of miR-106b-5p (He et al., 2020) and are derived from a cancer subtype that does not show a negative correlation between miR-106b-5p and *SETD2* levels, it might not be the most suitable model to study the role of miR-106b-5p in regulating checkpoint kinase inhibitor sensitivity. Therefore, I proceeded to investigate the relationship between miR-106b-5p levels, mRNA target expression, and AZD1775-sensitivity in breast cancer cell lines.

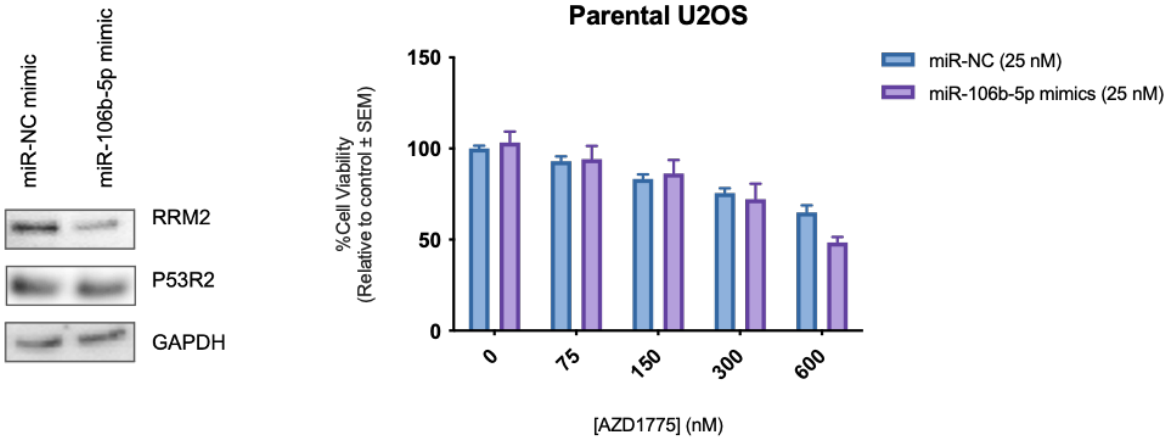

Figure 4.10 ***Western blot analysis of RRM2 protein levels in U2OS cells transfected with a non-targeting control miRNA or miR-106b-5p mimic and its associated AZD1775-sensitivity.*** *GAPDH was used as a control. Data represented as mean ± SD (n=3).*

4.7. ATR, WEE1, and CHK1 Inhibitor-Treatment Reduce Proliferation in Breast Cancer Cell Lines

First, the antiproliferative effect of the WEE1 inhibitor, AZD1775, was evaluated across a panel of 11 breast cancer cell lines and one non-tumourigenic breast epithelial cell line, MCF10A. To determine the AZD1775 IC_{50} value for each cell line, cells were treated with either DMSO or the WEE1 inhibitor (AZD1775) (dilution series of 11 concentrations from 1 µM to 0.05 nM) and subjected to a resazurin reduction assay after 72 hours to determine cell viability. Here, a number of AZD1775-sensitive cell lines, including HCC70, JIMT-1, and BT-549, were identified, as well as some AZD1775-resistant cell lines, including MCF10A (non-tumourigenic) and T47D (Figure 4.11). For a number of cell lines, such as MCF-7 and MDA-MB-231, I also tested cell viability 48 hours post-AZD1775 treatment and found that even though WEE1-inhibitor activity was slightly enhanced by prolonged exposure (i.e., after 72 hours), the sensitivity patterns were still very similar and the calculated IC_{50} values were consistent between different time-points (Figure 4.11).

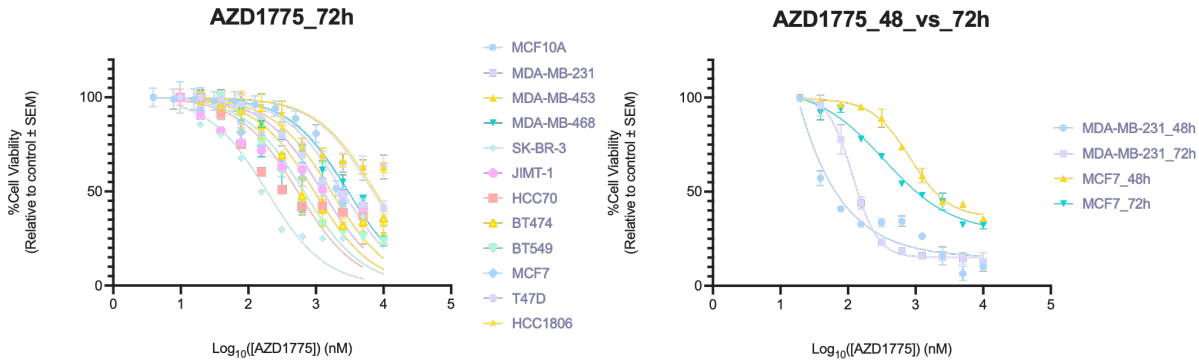

Figure 4.11 ***AZD1775 activity in a panel of BC cell lines****. A) Dose-response curves for a panel of breast cancer cell lines, exposed to increasing concentrations of AZD1775 for 72 hours. B) Dose-response curves for MDA-MB-231 and MCF-7 cells, exposed to increasing concentrations of AZD1775 for 48 or 72 hours. Data represented as mean ± SEM (n=3).*

The checkpoint kinases ATR, WEE1, and CHK1 are all involved in the replication stress response (Gorecki et al., 2021). Therefore, I also tested the sensitivity of the same panel of

breast cancer cell lines to increasing concentrations of UCN-01 (CHK1 inhibitor) and VE-822 (ATR inhibitor) (Figure 4.12). Consistent with their conserved roles in restricting CDK activity in the presence of replication stress (Gorecki et al., 2021), we found similar sensitivity patterns for AZD1775, UCN-01, and VE-822 across this panel of BC cell lines (Figure 4.11 and 4.12). Again, while T47D and MCF10A demonstrated both UCN-01 and VE-822 resistance, as for AZD1775 (Figure 4.11 and 4.12), HCC1806 cells demonstrated a very low IC_{50}, especially for VE-822.

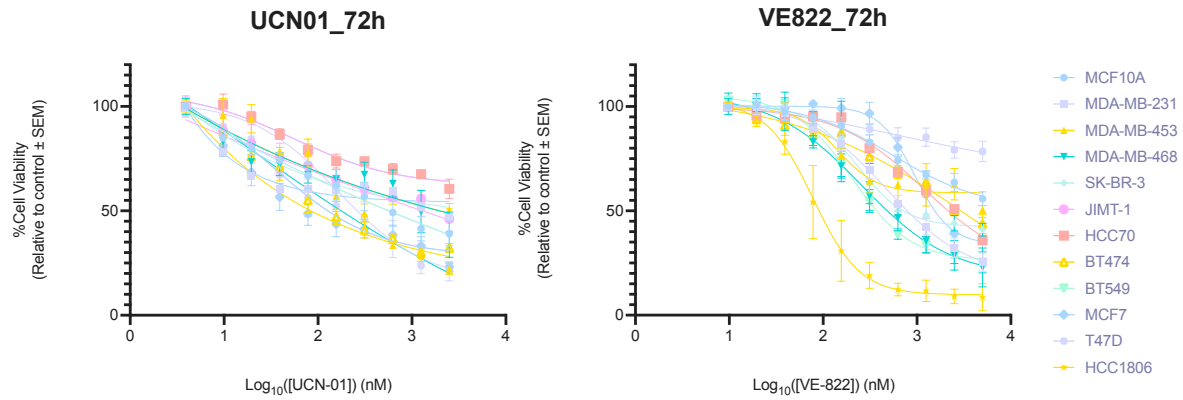

Figure 4.12. ***UCN-01 and VE-822 activity in a panel of BC cell lines****. Dose-response curves for a panel of breast cancer cell lines, exposed to increasing concentrations of UCN-01 (CHK1 inhibitor) or VE-822 (ATR inhibitor) for 72 hours. Data represented as mean ± SEM (n=3).*

4.8 MiR-106b-5p Expression Levels Correlate with WEE1 Inhibitor-Sensitivity

Next, I looked for genetic and transcriptomic predictors of WEE1, ATR, and CHK1 kinase inhibitor sensitivities in this panel of 12 breast cell lines. To identify cell line models of high-miR-106b-5p and low H3K36me3 expression, protein levels of H3K36me3 were analysed by Western Blot (Figure 4.13). Several cell lines with high levels of H3K36me3 were identified, such as MCF-7, T-47D, and MDA-MB-468. These cell lines displayed moderate to low AZD1775-sensitivity and high IC_{50} values (Figure 4.11 and 4.13), in accordance with previous findings by Pfister et al. (2015). On the contrary, cell lines with low levels of H3K36me3, such as BT-549 (Figure 4.13), displayed low AZD1775 IC_{50} values (Figure 4.14).

It is important to note that genetic alterations that disrupt cell cycle regulation have previously been shown to cause selective toxicity of WEE1 inhibitors, such as in the case of *TP53*-mutated cancers (reviewed in Kong & Mehanna, 2021). *TP53* mutations were present in 10/12 cell lines, except for MCF10A and MCF7 cells, so it is unclear to what extent high WEE1 inhibitor-sensitivity can be attributed low H3K36me3 levels or to cancer-associated mutations in p53.

Furthermore, previous studies have shown that cell lines with high c-MYC protein and *CDKN2A* (p16) deletion could accurately predict ATR- and CHK1-sensitive cell lines (Young et al., 2019). Indeed, we found lower IC_{50} values, indicating higher VE-822 and UCN-01 sensitivity, for a number of cell lines harbouring *MYC* amplification, including MCF-7 and HCC1806 cells (Figure 4.12 and 4.13) (Mean VE-822 log(IC_{50}) MYC^{amp} = 3.281, Mean log(IC_{50}) WT = 2.967, p-value = 0.1688), whereas we did not find any differences in WEE1 inhibitor sensitivity when checking for *CDKN2A* status.

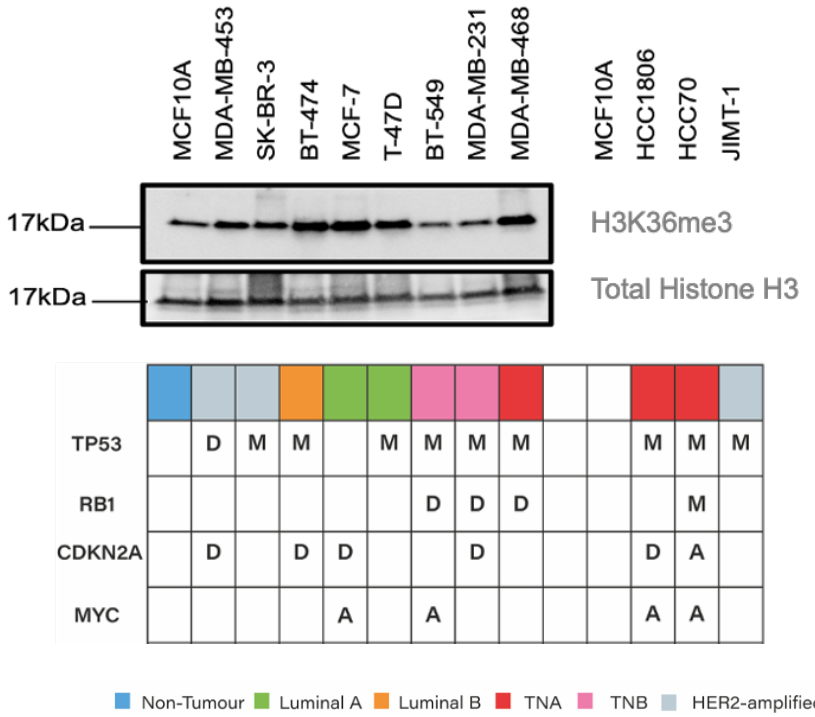

Figure 4.13. ***Immunoblot analyses of the the histone mark H3K36me3 in a panel of BC cell lines*.*** *Genomic status of indicated gene biomarkers, and the molecular subtype is shown for each cell line. Total Histone H3 levels were used as a loading control. *due to Covid-19, I was unable to determine the H3K36me3 status of HCC1806, HCC70 and JIMT-1 cells. M = Mutation, D = Deletion, A = Amplification.*

The obtained data points, as shown in Figure 4.11, were fitted to a Sigmoidal dose-response curve using GraphPad Prism in order to obtain log(IC_{50}) values for each of the 12 cell lines (Figure 4.14). Those log(IC_{50}) values, which were used as a measure of AZD1775 drug-sensitivity, were then correlated with potential biomarkers of AZD1775-sensitivity, including mature miR-106b-5p levels, *SETD2* mRNA levels, and *RRM2* mRNA levels. MiR-106b-5p levels showed a significant and negative correlation with AZD1775-sensitivity (Figure 4.14) (Spearman's $\rho = -0.5690$, p-value = 0.0339). Specifically, high levels of miR-106b-5p, such as in SK-BR3 cells, correlated with high WEE1-inhibitor sensitivity, whereas low miR-106b-5p levels, such as in MDA-MB-453 and T-47D cells, correlated with WEE1-inhibitor resistance (Figure 4.14). When Pearson's correlation analysis was performed for *RRM2* mRNA levels and log(IC_{50}) values, or for *SETD2* mRNA levels and log(IC_{50}) values, we did not find any statistically relevant relationships (Spearman's $\rho = -0.03005$, p-value = 0.4651, and Spearman's $\rho = 0.1556$, p-value = 0.3239, respectively), suggesting that miR-106b-5p levels could be a better predictor of AZD1775-sensitivity than *RRM2* expression.

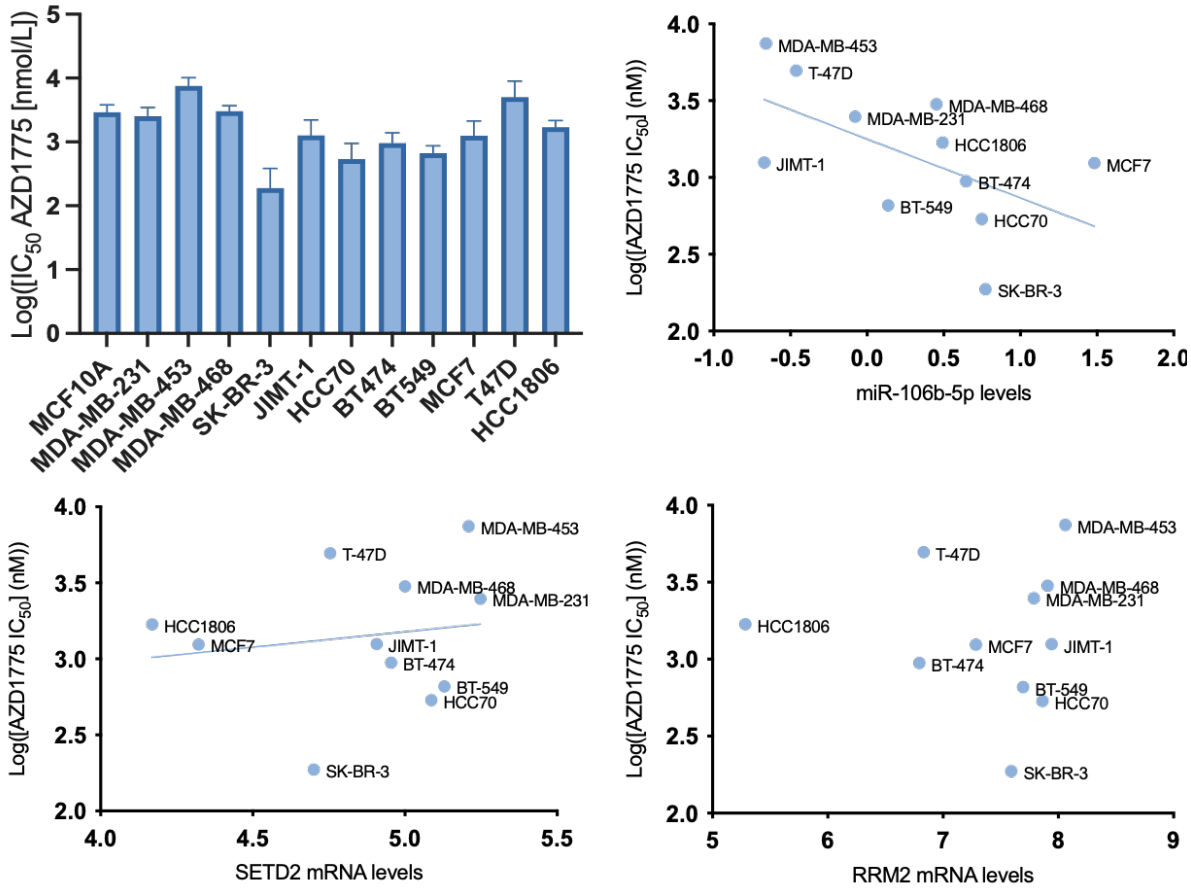

Figure 4.14. ***AZD1775-sensitivity correlates with miR-106b-5p levels in a panel of BC cell lines.*** *AZD1775 IC_{50} values of 12 BC cell lines. Mean and SEM were calculated from n ≥ 3 experiments. Scatter plots of pairwise Pearson's correlation of miR-106b-5p levels, RRM2 mRNA levels, and SETD2 mRNA levels with log(IC_{50}) values.*

4.9 Inhibition of miR-106b-5p and miR-93-5p Results in Increased E2F-Mediated Transcription and Altered AZD1775-sensitivity

Next, I assessed whether changing miR-106b-5p levels could directly impact on checkpoint kinase inhibitor sensitivity. HCC1806 cells provided a useful *in vitro* model, as this TNBC cell line displayed amplification-dependent *AGO2* overexpression, high miR-106b-5p levels, and low *SETD2* and *RRM2* expression levels (Figure 4.7).

First, anti- miR-106b-5p and anti-miR-93-5p oligonucleotides, which are single-stranded molecules showing miRNA complementarity, were used to inhibit miRNA expression *in vitro.*

Next, I evaluated whether transfection of anti-miR-93-5p or anti-miR-106b-5p oligonucleotides could alter the sensitivity profile, and corresponding IC_{50} values, of HCC1806 cells to the WEE1 (AZD1775) or ATR (VE-822) inhibitor (Figure 4.15). The dose-response curves revealed that transfection with anti-miR-93-5p or anti-miR-106b-5p oligonucleotides caused reduced WEE1-inhibitor sensitivity (Figure 4.15). Indeed, when comparing the IC_{50} values, I found that cancer cells treated with anti-miR-93-5p or anti-miR-106b-5p oligonucleotides had increased IC_{50} values when compared to the control cells ($IC_{50_AZD1775_control}$ = 789.1 nM, $IC_{50_AZD1775_anti\text{-}miR\text{-}93\text{-}5p}$ = 1180 nM, and $IC_{50_AZD1775_anti\text{-}miR\text{-}106b\text{-}5p}$ = 1379 nM) (Figure 4.15). On the contrary, antisense oligonucleotide treatment did not seem to affect the sensitivity of HCC1806 cells to ATR-inhibitor treatment (Figure 4.15). Therefore, our results suggest that miR-106b-5p levels do not only correlate with AZD1775-sensitivity, but that miR-106b-5p also plays a causal role in modulating the cellular response to WEE1 kinase inhibition in TNBC cells.

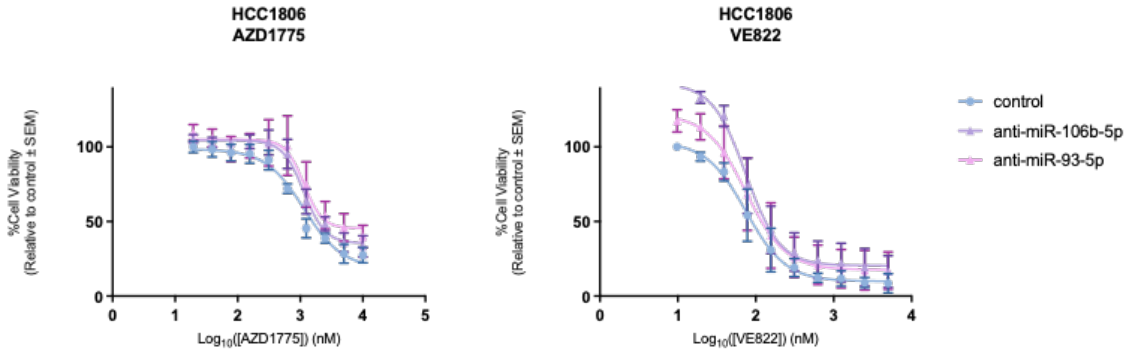

Figure 4.15. ***miR-106b-5p and miR-93-5p levels modify the effects of AZD1775 treatment in HCC1806 cells.*** *Dose-response curves for HCC1806 cells transfected with a non-targeting control, anti-miR-93-5p, or anti-miR-106b-5p, exposed to increasing concentrations of AZD1775 or VE-822 for 72 hours. Data represented as mean ± SEM (n=3).*

Next, I wanted to understand what molecular changes could underlie anti-miR-93-5p- or anti-miR-106b-5p-induced AZD1775-resistance. From previous studies, we know that both RRM2, which is under control of the E2F1 transcription factor, and SETD2 determine WEE1-inhibitor sensitivity (Pfister et al., 2015). Therefore, anti-miR-106b-5p and anti-miR-93-5p

oligonucleotides were introduced into HCC1806 cells and *SETD2*, *RRM2*, and *E2F1* expression levels were measured using qRT-PCR (Figure 4.16). Even though transfection of anti-miR-106b-5p and anti-miR-93-5p caused a slight increase in *SETD2* mRNA levels when compared to the control cells, this change was not significant (Figure 4.16). However, *E2F1* mRNA levels were significantly elevated following anti-miR-106b-5p and anti-miR-93-5p transfection compared to the control (Figure 4.16). Interestingly, elevated *E2F1* mRNA levels were accompanied by increased *RB1* mRNA levels, perhaps illustrating the importance of RB in restraining E2F1 function (Chellappan, Hiebert, Mudryj, Horowitz, & Nevins, 1991).

To test whether the increased *E2F1* mRNA levels following anti-miR-106b-5p and anti-miR-93-5p caused downstream changes in E2F-target gene expression, despite *RB1* upregulation, levels of a number of canonical E2F-targets, such as *CDC6, MCM7*, and *RRM2* were measured using qRT-PCR (Figure 4.16). Consistent with a role for E2F1 as transcriptional activator, *CDC6* and *MCM7* mRNA levels were induced following anti-miR-106b-5p treatment (Figure 4.16). Interestingly, however, *RRM2* expression levels were decreased 48 hours post- anti-miR-106b-5p and anti-miR-93-5p oligonucleotide transfection (Figure 4.16), suggesting that expression of *RRM2* might be regulated by transcription factors other than E2F1 in this cell line.

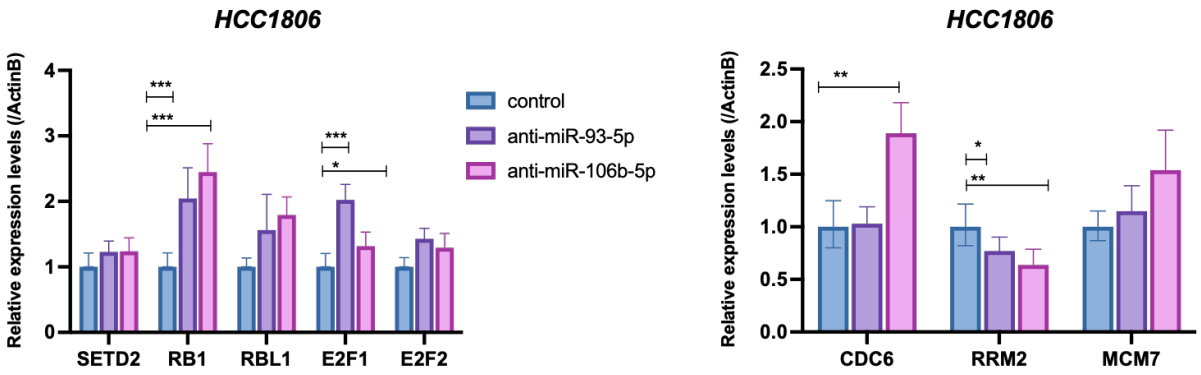

Figure 4.16. ***qRT-PCR analysis showing changing expression of E2F1 after transfection of anti-miR-93-5p or anti-miR-106b-5p in HCC1806 cells.*** *Data are expressed as mean ± 95% confidence interval (CI) (n=3). Significance calculated with a two-way ANOVA.*

Increased E2F-dependent transcription during S-phase could improve survival under low nucleotide pool conditions (DeGregori et al., 1995; Pai et al., 2019), and I therefore predicted that the altered AZD1775-sensitivity in response to anti-miR-106b-5p transfection could be attributed to RB/E2F pathway-dependent changes. Therefore, AZD1775- and VE-822-sensitivity patterns were tested in BT-549 cells, which harbour a *RB1* deletion (Figure 4.13). In several respects, the consequences of *RB1* mutations are reminiscent of ectopic overexpression of E2Fs, and any further (miRNA-mediated) increases in E2F-activity might therefore not confer any additional proliferation advantages in the presence of AZD1775. Indeed, anti-miR-106b-5p transfection did not alter AZD1775- or VE822-sensitivity in *RB*-mutated BT-549 cells (Figure 4.17), suggesting that miR-106b-5p levels might only modulate checkpoint kinase inhibitor sensitivity in cells that still have intact control over the RB/E2F pathway. Previous studies have indicated that *CDKN1A* mRNA levels were induced in *Rb* mutant tissue (Tsai et al., 1998), suggesting that elevated *E2F1* levels in this context might induce the p53 pathway to compromise WEE1i therapeutic responses.

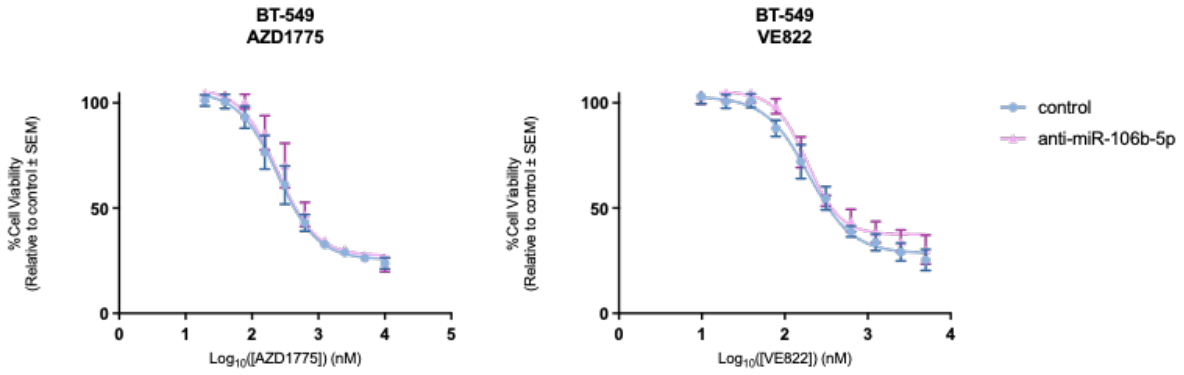

Figure 4.17. ***Dose-response curves for RB-mutated BT-549 cells transfected with a non-targeting control or anti-miR-106b-5p, exposed to increasing concentrations of AZD1775 or VE-822 for 72 hours.*** *Data represented as mean ± SEM (n=3).*

4.10 MiR-106b-5p and MiR-93-5p Regulate E2F1 mRNA and Protein Levels in T47-D and MDA-MB-453 Cells

Next, the relationship between miR-106b-5p and *E2F1* and *SETD2* levels was investigated *in vitro* using miR-106b-5p mimics. Two cell lines expressing low levels of miR-106b-5p, T47D and MDA-MB-453, were selected, miR-106b-5p mimics were transfected into these cells, and after 48 hours, both mRNA and protein expression of several predicted target genes, including *SETD2* and *E2F1*, were measured (Figure 4.18 and 4.19). MiR-106b-5p mimic introduction caused a strong and significant increase in mature miR-106b-5p levels, whereas miR-106b-3p levels remained unaffected (Figure 4.18). In accordance with our findings in HCC1806 and U2OS cells, we did not observe any significant changes in *SETD2* mRNA expression, or in levels of the histone mark H3K36me3 following miR-106b-5p mimic introduction (Figure 4.18 and 4.19). In contrast, I did identify changes in *E2F1* mRNA expression, and concomitant changes in E2F1 protein expression (Figure 4.18 and 4.19). Therefore, I can conclude that miR-106b-5p is an important regulator of E2F1 in breast cancer cell lines.

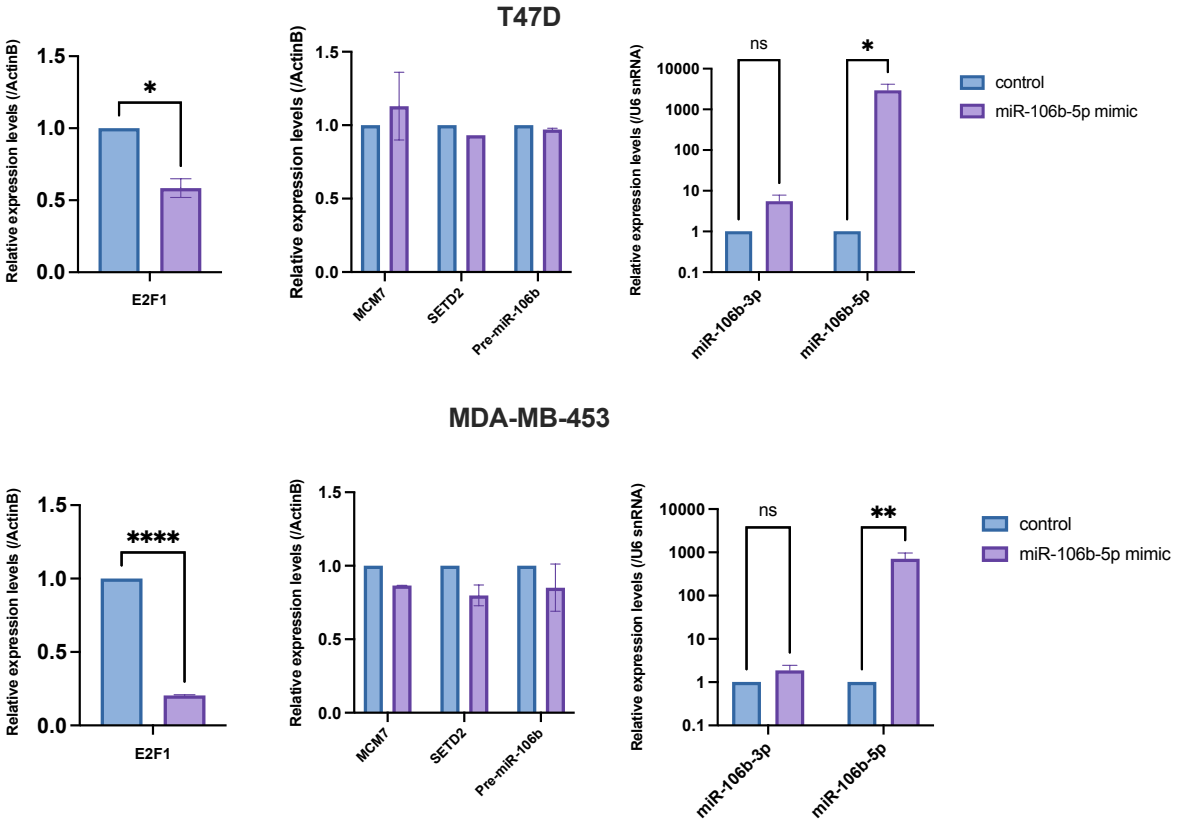

Figure 4.18. ***qRT-PCR analysis showing the changing expression of E2F1 after miR-93-5p or miR-106b-5p transfection in T47D and MDA-MB-453 cells.*** *Significance calculated with a two-way ANOVA. Data represented as mean ± SEM (n=3).*

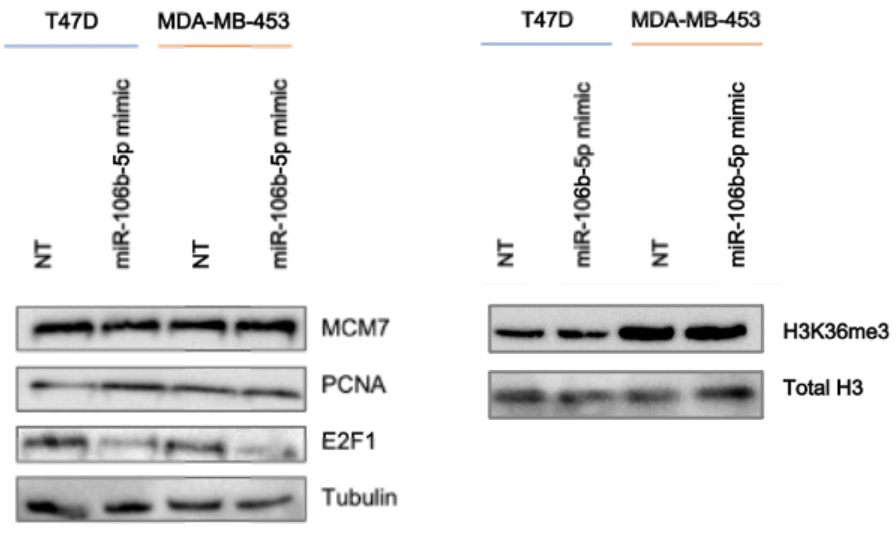

Figure 4.19. ***Western Blot analysis of MCM7, PCNA, E2F1, and H3K36me3 protein levels in T47D and MDA-MB-453 cells transfected with a non-targeting control miRNA or miR-106b-5p mimic.*** *Tubulin or Total Histone H3 levels were used as a loading control.*

4.11 MiR-106b-5p Affects Cell Cycle Progression and Regulates WEE1i-induced Replicative Catastrophe

As E2F1 is an important regulator of the G_1-to-S transition, transcribing many targets required for efficient DNA replication (DeGregori et al., 1995; Matthews et al., 2021), the effects of altered miR-106b-5p levels on DNA replication in both the absence and presence of AZD1775 were explored in several cell lines, including in (non-tumourigenic) MCF10A cells, and the malignant cell lines BT-549, HCC1806, and MCF7.

Firstly, miR-106b-5p mimics were introduced into MCF10A cells using transfection methods. 48 hours post-transfection, cells were released into medium containing DMSO (control) or AZD1775 (250 nM or 500 nM) for 48 hours, BrdU pulse-labelled for 1 hour, and assessed by flow cytometry to measure cell-cycle progression of S-phase (BrdU+ labelled) cells (Figure 4.20). AZD1775 treatment resulted in only a small percentage of MCF10A cells accumulating in non-replicating S-phase (exhibiting a DNA content between 2N and 4N, but not incorporating the synthetic nucleoside bromodeoxyuridine [BrdU]) (3.62% after treatment with 250 nM AZD1775, and 17.6% after treatment with 500 nM AZD1775). I did however observe increases in the G_1 and G_2/M populations after WEE1 inhibitor treatment, consistent with proficient checkpoint-mediated cell cycle arrest in the presence of DNA damage in non-tumourigenic cells (Figure 4.20).

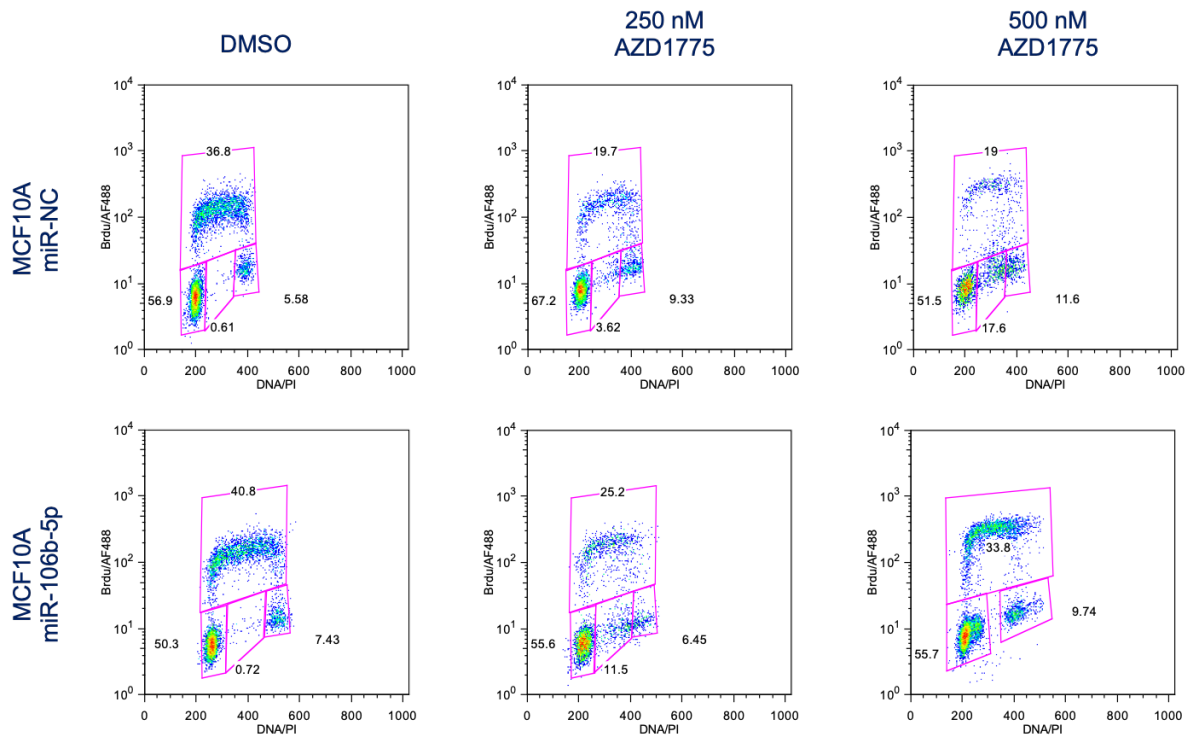

Figure 4.20. ***miR-106b-5p overrides the AZD1775-induced checkpoint in MCF10A cells and accelerates S-phase progression.*** *48 hours following DMSO or AZD1775-treatment (250 or 500 nM), control or miR-106b-5p mimic treated MCF10A cells were pulse-labelled with BrdU for 30 min and collected for cell cycle analysis. The data shown are from a single representative experiment out of three repeats. Numbers are the relative percentage of cell cycle stage.*

When the effects of miR-106b-5p mimic introduction were evaluated in MCF10A cells, I found that cells were more abundant in S-phase following miR-106b-5p mimic treatment, and that this effect became more apparent in the presence of AZD1775 (Figure 4.20), as shown by a higher percentage of BrdU+ cells after miR-106b-5p transfection when compared to the miR-NC transfected cells. This could reflect degradation of the CDK inhibitor p21 following miR-106b-5p introduction, which is functional in non-tumourigenic cells, and controls cell cycle progression in the presence of DNA damage or replication stress (Besson et al., 2008). Increased miR-106b-5p levels might therefore override G_1/S and G_2/M checkpoint control in the presence of AZD1775 (and WT *TP53*), further accelerating progression into S-phase.

Secondly, I looked at the effect of anti-miR-106b-5p oligonucleotide transfection on AZD1775-induced replicative catastrophe in HCC1806 (*RB*-wild type) and BT-549 (*RB*-mutated) cells (Figure 4.21A and B). Because anti-miR-106b-5p oligonucleotide transfection caused resistance to WEE1 inhibitor treatment in HCC1806 cells, but not BT-549 cells (Figure 4.15 and 4.17), I was interested in testing whether this was reflected in changes in the population of non-replicating cells in response to AZD1775 treatment. To this end, the distribution of cells in S-phase was determined by measuring BrdU incorporation 48 hours post-AZD1775 treatment (Figure 4.21). Consistent with our previous findings, AZD1775 treatment (300 nM) caused a chronic accumulation of BrdU- cells in S-phase – also referred to as the non-replicating S-phase population – (from 2.46% to 55.3% and from 5.46% to 27.4% in HCC1806 and BT-549 cells, respectively) (Figure 4.21A and B). This can likely be attributed to increased CDK-dependent origin firing, excessive pRPA-coated ssDNA and replicative catastrophe (Pfister et al., 2015).

Anti-miR-106b-5p transfection did not alter the cell cycles profiles of DMSO-treated (control) HCC1806 and BT-594 cells, whereas clear differences could be observed in the presence of AZD1775 (300 nM) (Figure 4.21). In HCC1806 cells, anti-miR-106b-5p transfection prevented cells from entering non-replicative catastrophe in response to AZD1775 treatment (Figure 4.21A). Instead, following anti-miR-106b-5p treatment, a larger percentage of cells remained in G_1 (44.6% in anti-miR-106b-5p + AZD1775 vs. 13.3% in anti-miR-NC+ AZD1775), and anti-miR-106b-5p treatment therefore relieved the replicative catastrophe phenotype in HCC1806 cells. This rescue could reflect increases in RB or p21 protein levels following anti-miR-106b-5p transfection (Figure 4.21C), both of which prevent cells from entering S-phase. For BT-549 cells, very few differences were observed between the cell cycle profiles of anti-miR-NC and anti-miR-106b-5p cells in the presence of AZD1775 (Figure 4.21B), which is in accordance with findings presented in Figure 4.17.

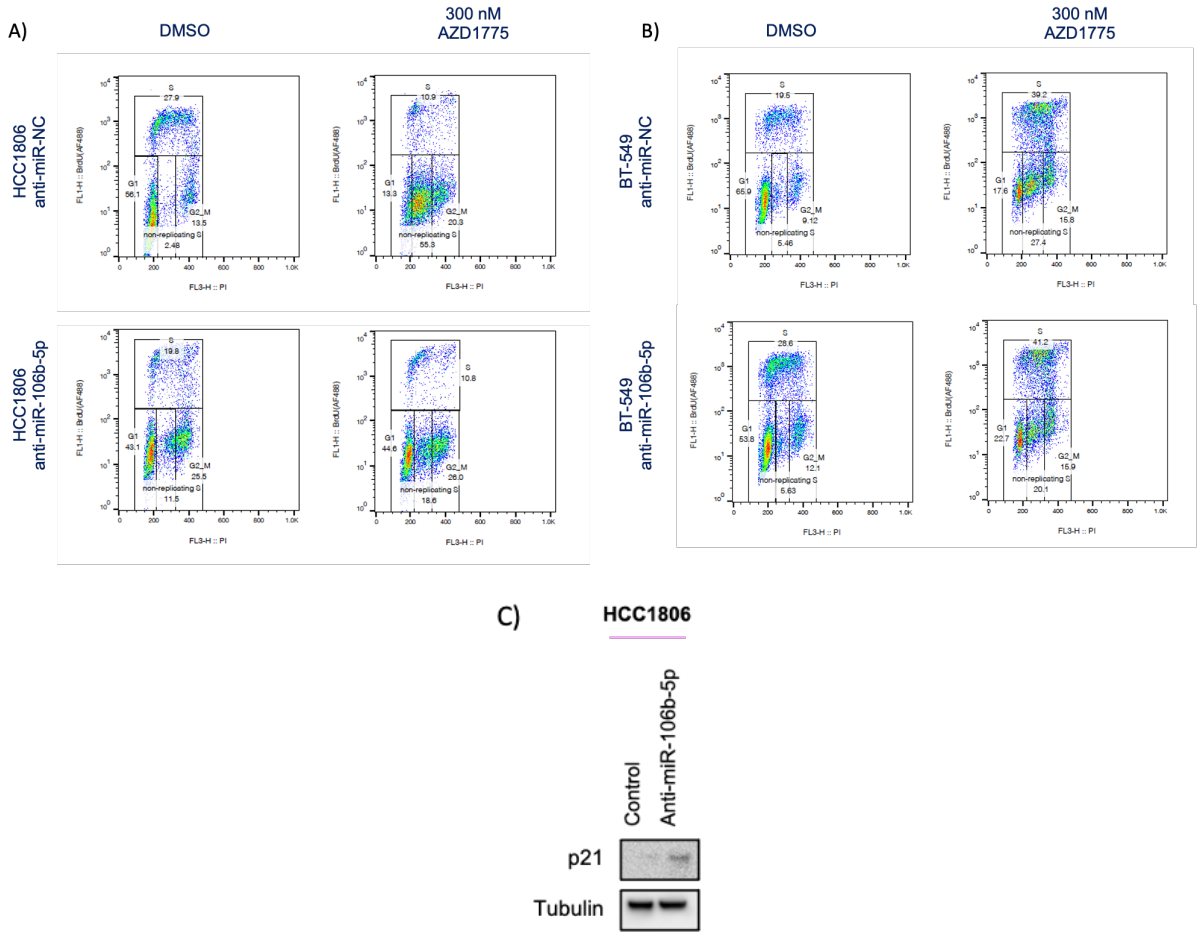

Figure 4.21. ***S-phase-dependent cell cycle effects of anti-miR-106b-5p oligonucleotides in AZD1775-treated BT-549 or HCC1806 cells.*** *A and B) 48 hours following DMSO or AZD1775-treatment (300 nM), control or anti-miR-106b-5p treated BT-549 or HCC1806 cells were pulse-labelled with BrdU for 30 min and collected for cell cycle analysis. The data shown are from a single representative experiment out of three repeats. Numbers are the relative percentage of cells in each cycle stage. C) Western Blot analysis of p21 and tubulin protein levels in HCC1806 cells transfected with non-targeting control miRNAs or anti-miR-106b-5p oligonucleotides.*

The differential response to anti-miR-106b-5p transfection in HCC1806 and BT-549 cells prompted further evaluation of miR-106b-5p's mechanism of action in different genetic backgrounds. To determine whether the anti-miR-106b-5p-induced G_1 arrest was mediated by p53-dependent signalling, I compared the cell cycle profiles of MCF-7 (*TP53*^{WT}) and HCC1806 cells (*TP53*^{MUT}, Figure 4.21) following anti-miR-106b-5p transfection and treatment with AZD1775. AZD1775-treated MCF-7 cells showed an increased S-phase population after 24 hours (40.1% after treatment with 250 nM AZD1775, and 35.1% after treatment with 500 nM

AZD1775, compared to 25.2% in the control cells) (Figure 4.22), but very few BrdU- S-phase cells, reflecting low AZD1775-sensitivity.

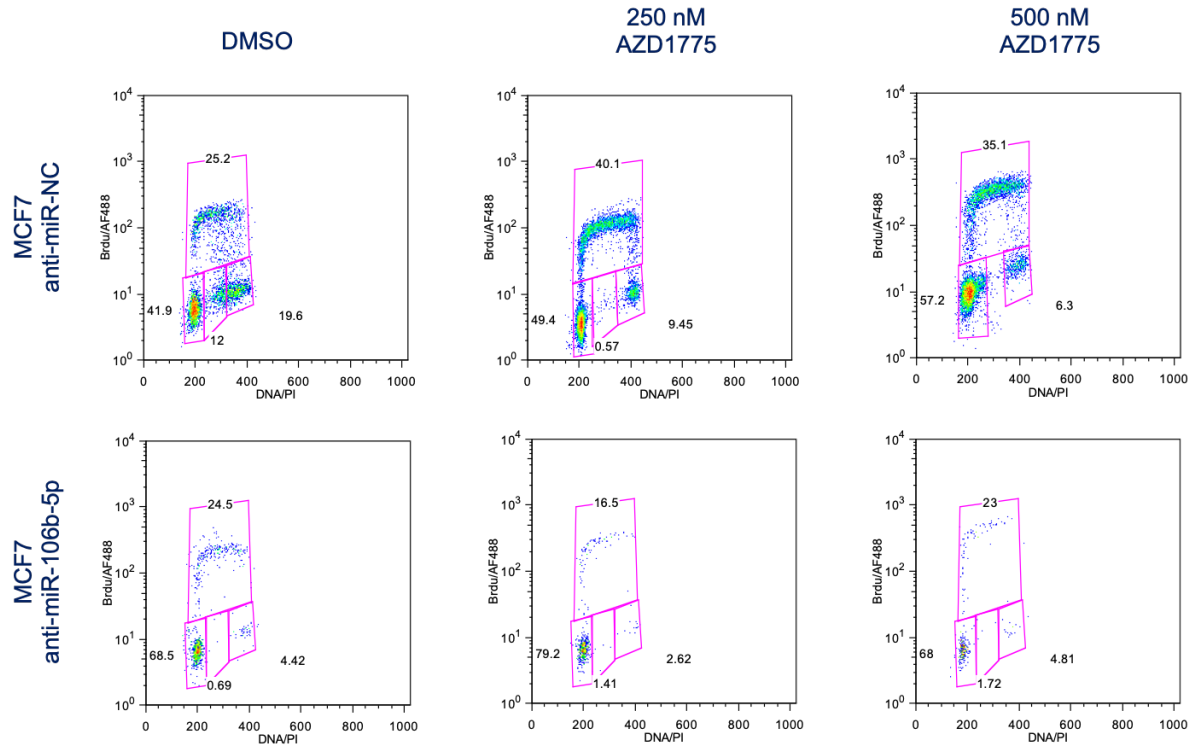

Figure 4.22. ***Anti-miR-106b-5p treatment causes a permanent G_1-arrest in MCF-7 cells.*** *MCF-7 cells were treated with AZD1775 (250 nM or 500 nM) or DMSO for 24 hours, then pulse-labelled with BrdU (10 µmol/L; 1 hour) before fixation and flow cytometry analysis. The data shown are from a single representative experiment out of three repeats. Numbers are the relative percentage of cells in each cycle stage.*

As hypothesised, MCF-7 cells transfected with an anti-miR-106b-5p oligonucleotide showed an increase in the G_1 population in the presence of DMSO (68.5% in anti-miR-106b-5p vs. 41.9% in anti-miR-NC) (Figure 4.22). Interestingly, when AZD1775 was introduced, anti-miR-106b-5p cells remained arrested in G_1 phase, even with a concentration of 500 nM, accompanied by an increase in the percentage of dead cells (Figure 4.22).

Therefore, the effects of miR-106b-5p were dependent on the genetic background. Increased miR-106b-5p levels were shown to promote DNA synthesis in non-tumourigenic cells (MCF10A). Furthermore, in cells with a functional p53-p21 axis, but not cells with defective

RB/E2F1 control, miR-106b-5p inhibition caused a G_1-arrest, and rescued DNA synthesis in the S-phase population. This anti-miR-106b-5p-induced G_1-arrest was maintained even in the presence of the WEE1 inhibitor, which is known to increase CDK activity and accelerate both S-phase and mitotic entry (Elbæk et al., 2020).

4.12 Relationship Between p21 Levels and AZD1775-sensitivity in *SETD2*-proficient and -deficient cells

Because I found that high miR-106b-5p levels caused reduced p21 protein expression, which overrode the damage-induced G_1/S checkpoint and promoted S-phase entry, I wanted to evaluate the relationship between p21 levels and WEE1 inhibitor sensitivity more directly. These experiments were performed in *SETD2* WT and *SETD2* CRISPR knockout (KO) osteosarcoma (U2OS) cell lines, as AZD1775 treatment was previously shown to induce selective killing of *SETD2* KO U2OS cells through dNTP pool depletion and accumulation of non-replicating S-phase cells (Pfister et al., 2015), and this isogenic cell line pair thus allowed for evaluation of the role of p21 in regulating WEE1i sensitivity in a clinically relevant context.

First, cell viability of *SETD2* WT and *SETD2* KO U2OS cells treated with AZD1775 was measured 48 hours after knockdown of p21 by siRNA (*siCDKN1A)* when compared with the control (siNT). Transfection of *CDKN1A* siRNA significantly reduced p21 protein expression in both cell lines (Figure 4.23A), and further sensitised both *SETD2* WT and *SETD2* KO U2OS cells to AZD1775 (Figure 4.23B).

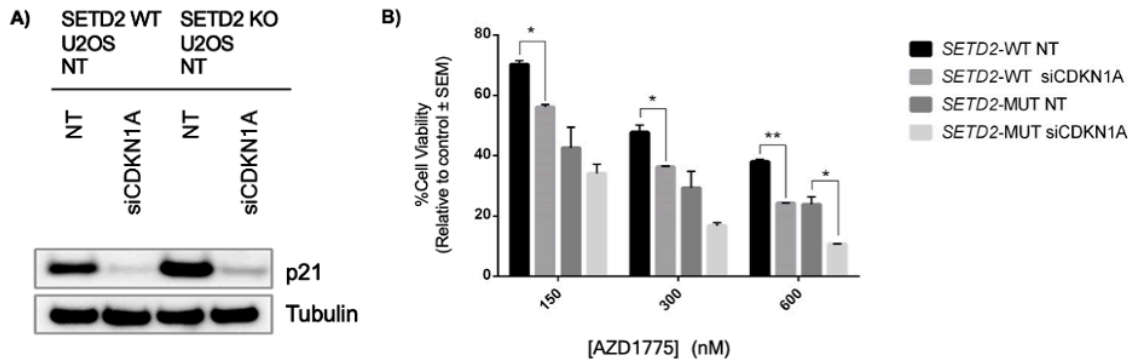

Figure 4.23. ***Knockdown of CDKN1A sensitised SETD2-proficient and -deficient U2OS cells to WEE1 inhibitor treatment.*** *A) Western Blot analysis of p21 protein levels in SETD2 WT and SETD2 CRISPR KO U2OS cells exposed to either non-targeting control siRNA or p21 siRNA. Tubulin was used as a loading control. B) Cell viability was further reduced when WEE1 inhibition was combined with p21 knockdown in SETD2 WT and SETD2 KO cells. Significance calculated with a two-way ANOVA. Data represented as mean ± SEM (n=3).*

Next, the cell cycle profiles of *SETD2* CRISPR KO cells transfected with control or *CDKN1A* siRNA were evaluated in the presence and absence of the WEE1 inhibitor, AZD1775 (Figure 4.24). Even though siCDKN1A transfection alone had a very minor effect on the cell cycle profile of *SETD2* CRISPR KO U2OS cells, depletion of p21 further increased the $BrdU^+$ and $BrdU^-$ S-phase population following 24 hours of AZD1775-treatment (15.2% increase in S-phase compared to siNT-treated *SETD2 KO* U2OS cells), in accordance with the published role for p21 in regulating the G_1/S transition (Abbas & Dutta, 2009) (Figure 4.24).

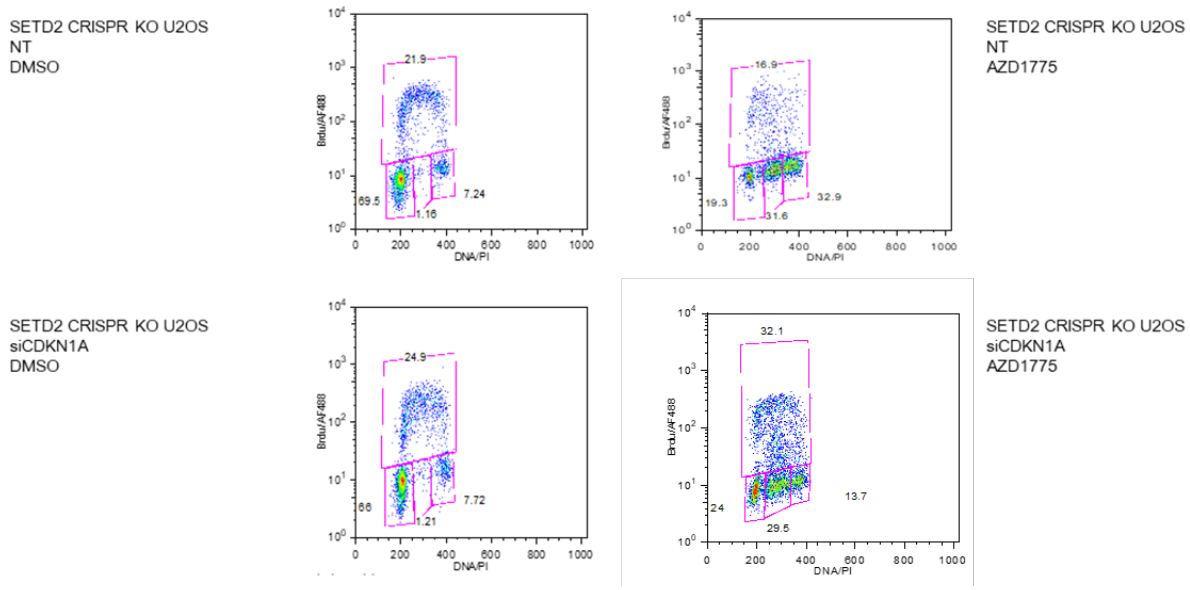

Figure 4.24. ***Knockdown of CDKN1A increases the S-phase population in SETD2 KO U2OS cells treated with AZD1775.*** *24 hr following DMSO -or AZD1775-treatment, control or siCDKN1A treated SETD2 KO U2OS cells were pulse-labelled with BrdU for 30 min and collected for cell cycle analysis. The data shown are from a single representative experiment out of three repeats. Numbers are the relative percentage of cell cycle stage.*

A pharmacological inhibitor of p21, UC2288, was previously shown to downregulate p21 on both the transcriptional and post-transcriptional level (Wettersten et al., 2013). To test whether p21 inhibitors could be applied to specifically target *SETD2*-deficient tumours, the sensitivity profiles of *SETD2* WT and *SETD2* KO U2OS cells were evaluated following UC2288 and AZD1775 exposure (Figure 4.25). In agreement with our findings following siRNA-mediated depletion of *CDKN1A*, p21 inhibition caused a small increase in the S-phase population (Figure 4.25A) and further sensitised both *SETD2* WT and *SETD2* KO U2OS cells to AZD1775, mostly at lower concentrations, showing p21 has a direct role in determining sensitivity to WEE1-inhibitor treatment (Figure 4.25B). Furthermore, we found that *SETD2* KO U2OS cells were more sensitive to p21 inhibition by UC2288 alone when compared to *SETD2* WT U2OS cells (Figure 4.25B), suggesting that p21 is a critical vulnerability in high-p21 expressing *SETD2* KO cancer cells.

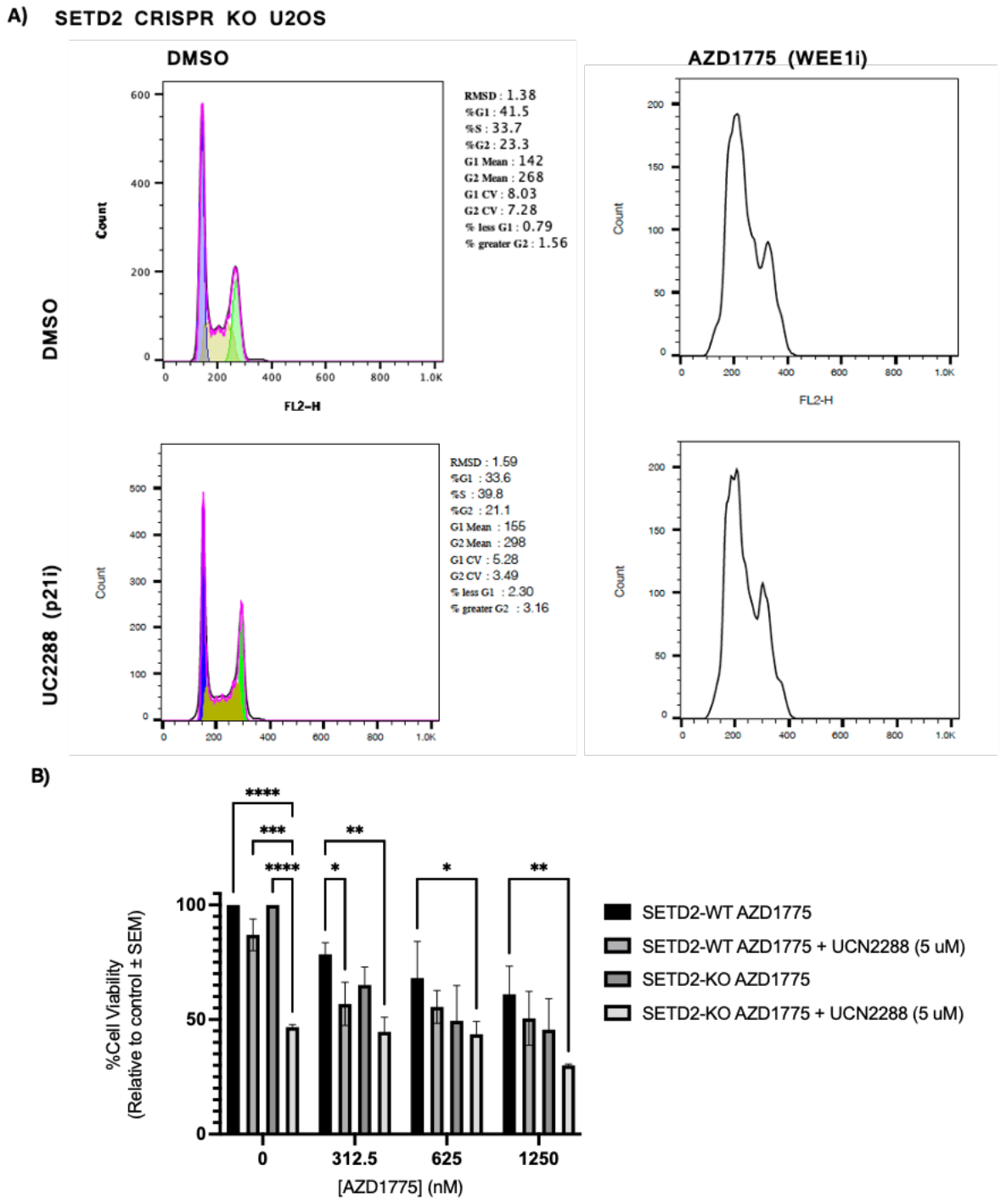

Figure 4.25. ***Combination of p21 and WEE1 inhibition for treatment of SETD2-deficient cancer cells****. A) 48 hr following DMSO, AZD1775- and/or UC2288 treatment, SETD2 KO U2OS cells were collected for cell cycle analysis. B) SETD2 WT and SETD2 CRISPR KO U2OS cells after 48h exposure to different concentrations of AZD1775 (0-10 μM) and UCC2288 (p21 inhibitor). Significance calculated with a two-way ANOVA. Data represented as mean ± SD (n=3).*

4.13 Conclusion

Dysregulation of miRNAs, including miR-106b-5p, has previously been associated with the occurrence and progression of breast cancer (Banerjee et al., 2020; Li et al., 2017). In accordance with this, I found that miR-106b-5p expression levels were significantly elevated in malignant breast tissue when compared to the adjacent healthy tissue, and that this upregulation was associated with advanced tumour stage and the formation of metastases. Furthermore, patients expressing higher levels of miR-106b-5p showed significantly poorer overall survival in both the METABRIC and TCGA-BRCA triple-negative breast cancer cohorts. The miR-17/92 polycistron was previously classified as a human oncogene as its members can act together with c-MYC to accelerate tumour development (He et al., 2005), and here, I propose a similarly oncogenic role for miR-106b/25 cluster. In line with this, transfection of antisense oligonucleotides targeting miR-106b-5p caused a G_0/G_1 arrest in HCC1806 cells and inhibited cellular proliferation in TNBC 3D spheroid models. This highlights the therapeutic potential of miR-106b inhibitors in breast cancer.

Furthermore, characterisation of a panel of 12 breast cancer cell lines also revealed high expression levels of miR-106b-5p *in vitro*, especially in TNBC cell lines. High miR-106b-5p levels resulted in reduced levels of p21, a CDK inhibitor with a key role in regulating progression through the G_1/S transition (Abbas & Dutta, 2009). Consequently, I found that both overexpression of miR-106b-5p and siRNA-mediated depletion or inhibition of p21 led to accelerated S-phase entry and increased replicative catastrophe in the presence of the WEE1 inhibitor, AZD1775. Recent clinical trials in colorectal cancer showed that AZD1775 treatment improved progression free survival in patients with RAS/TP53-mutant mCRC (Seligmann et al., 2021), due to their aberrations in DNA replication. Based on these results, one could anticipate that cells over-expressing miR-106b-5p could display a similar phenotype, because

they also harbour a G_1/S checkpoint failure, due to low p21 levels, and increased endogenous replication stress, due to impaired E2F1 signalling. Therefore, miR-106b-5p overexpressing cells might display increased reliance on the G_2/M checkpoints and thus display enhanced checkpoint kinase inhibitor sensitivity, as was found here. Alternatively, in a *TP53* wild-type or low miR-106b-5p expressing context, we propose that a combination of low doses of AZD1775 (WEE1i) and UC2288 (p21i) could be used to improve the therapeutic response of *SETD2*-deficient cells.

Finally, our data suggests that miR-106b-5p levels could provide a useful biomarker for WEE1-inibitor (AZD1775) sensitivity. Even though I did not find a correlation between miR-106b-5p levels and SETD2-dependent H3K36me3, as was previously found in ccRCC (Xiang et al., 2015), I found that high miR-106b-5p levels did correlate with reduced levels of the E2F1 transcription factor. E2F1 controls expression of numerous genes involved in DNA replication and dNTP synthesis, including *CDC6* and *RRM2* (Bertoli, Skotheim, et al., 2013; DeGregori et al., 1995). As AZD1775 is currently being investigated in more than fifty clinical trials for cancer treatment, as monotherapy or in combination with chemotherapeutic drugs and/or radiation (www.clinicaltrials.gov), finding a suitable biomarker to predict AZD1775-treatment response is crucial. MicroRNAs are particularly useful biomarkers as their expression levels can be measured in blood plasma and are therefore less invasive tools for patient stratification (Filipów & Łaczmański, 2019).

In summary, the key findings of this chapter are:

- MiR-106b-5p levels were upregulated in triple negative breast cancers compared to other subtypes and correlated with worse overall survival.
- MiR-106b-5p targets include the CDK inhibitor p21 and the transcription factor E2F1, making miR-106b-5p an important regulator of the G_1-to-S transition.
- MiR-106b-5p expression levels strongly correlated with AZD1775 IC_{50} values in a panel of breast cancer cell lines, suggesting a strong potential for miR-106b-5p as a biomarker for WEE1 inhibitor sensitivity.

Chapter 5
Characterising the Expression of Early Response Genes and MicroRNAs Following Ionising Radiation and Hydroxyurea Treatment in Breast Cancer Cells

5.1 Introduction

Cells have evolved a diverse range of mechanisms to detect, repair, and tolerate DNA damage (Blackford & Jackson, 2017). The DNA damage response (DDR) comprises a set of signalling pathways that lead to cell cycle checkpoint activation, DNA repair, and modulation of chromatin structure and transcriptional activity. The DDR varies as a function of exposure time and the type of stress or damage encountered. Failure to properly coordinate cell cycle arrest and activate or maintain the appropriate protective response results in genome instability (Hanahan & Weinberg, 2000).

Various research groups have characterised mRNA (Choudhary et al., 2020; Rashi-Elkeles et al., 2014; Ray, Yunis, Chen, & Rocke, 2012; Travesa et al., 2012) and protein expression (Bruckbauer et al., 2020; Hurst et al., 2021) changes in response to replication stress (hydroxyurea) or DNA damage (ionising radiation), while expression profiling of miRNAs under different conditions remains largely unexplored. As previously described, microRNAs regulate diverse biological and metabolic processes by targeting the 3' untranslated regions of target-mRNAs for their degradation or translational repression. Expression levels of >60% of human protein-coding genes, including that of many transcription factors coordinating the cellular responses to stress, are under the control of miRNAs (Friedman et al., 2009).

The integrated analysis of miRNA and mRNA expression profiles allows for the identification of specific DNA damage- or replication stress-dependent miRNA-mRNA interaction pairs.

These miRNA-guided transcriptome changes could function to improve stress tolerance or restore cellular homeostasis. Furthermore, as miRNAs are stably expressed in human blood and plasma, the monitoring of early miRNA expression changes that coordinate the responses to chemo- or radiation therapy, could help identify novel biomarker candidates (Mitchell et al., 2008).

Therefore, I used NGS techniques, together with gene expression analysis tools, such as DESeq2 and *miRNAtap*, to integrate miRNA and gene expression data in the early response to γ-irradiation-induced DNA damage or hydroxyurea (HU)-induced replication stress in the human HCC1806 breast cancer cell line. Furthermore, I characterised the roles of both SETD2 and the miR-106b/25 cluster in regulating mRNA target expression following HU- or IR-treatment and evaluated how alterations in the expression levels of these factors impacted on radiosensitivity. Using this integrated approach, I aimed to improve our understanding of how miRNAs regulate and fine-tune the cellular stress response to prevent propagation of damaged or under-replicated DNA.

5.2 Extraction and Quality Control of RNA samples

Before preparation of the sequencing libraries for NGS, the quality of RNA samples was evaluated using the Agilent 2100 Bioanalyser. For mRNA-sequencing, samples satisfied quality control requirements when the total amount of RNA was ≥0.8 μg with an RNA integrity number (RIN) ≥ 6.8. For sRNA-sequencing, samples satisfied quality control requirements when the total amount of RNA was ≥4 μg and RIN ≥ 7.5. A representative electropherogram is shown in Figure 5.1.

RNA integrity and degradation products were further evaluated on a 1% (w/v) agarose gel, followed by staining with ethidium bromide and visualisation under UV light (Figure 5.2). Figure 5.2 shows intact RNA with a 28S:18S rRNA ratio of approximately 2:1.

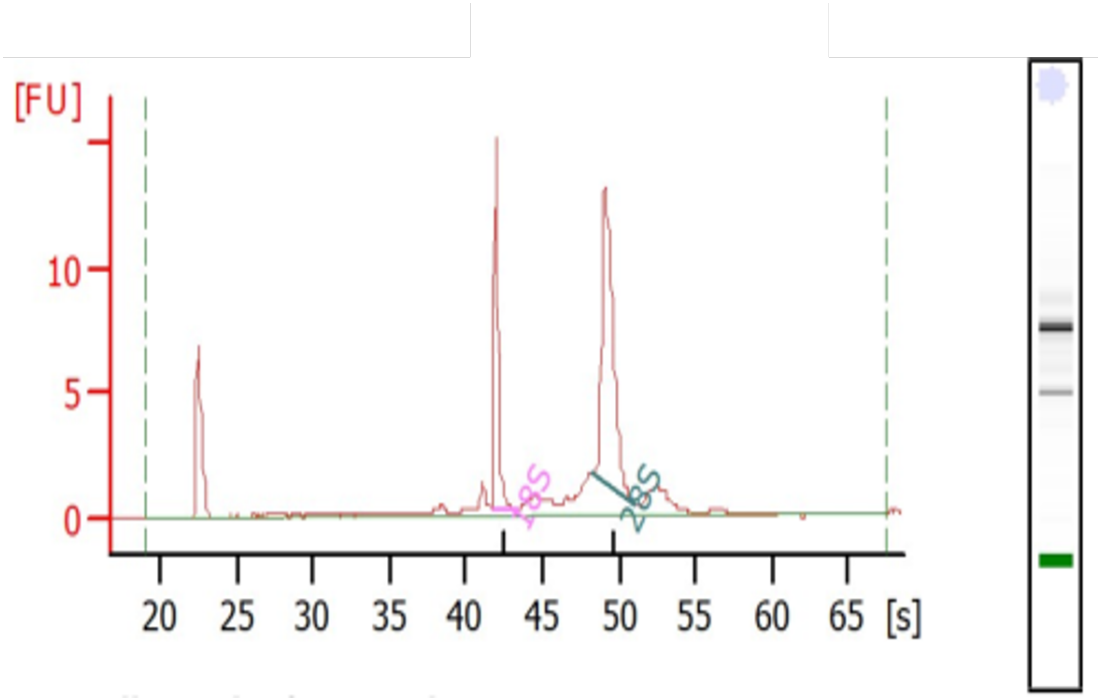

Figure 5.1. ***Quality of isolated RNA was analysed using the Agilent 2100 Bioanalyser****. Representative image of total RNA extracted from untreated HCC1806 cells. All samples were assigned a RIN number between 8 and 10, indicative of high-quality RNA.*

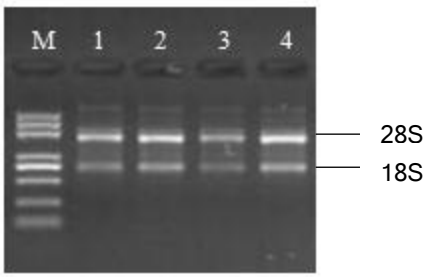

Figure 5.2. ***Gel electrophoresis of total RNA extracted from HCC1806 cells.*** *Analysis of total RNA isolated from four different samples. M: Trans 2K Plus DNA ladder, 1: control, 2: 4 hours post-HU treatment (2 mM), 3: 2 hours post-γ-irradiation (10 Gy), and 4: 6 hours post-γ-irradiation (10 Gy). The presence of sharp and distinct 28S and 18S rRNA bands and absence of smears verified the integrity of RNA (Repeat 1).*

5.3 Sequencing and Annotation of miRNAs in HCC1806 Cells

To explore early miRNA expression changes in response to γ-irradiation or hydroxyurea treatment, small RNA sequencing (sRNA-seq) experiments were performed by Novogene Company Ltd. on the Illumina NovaSeq 6000 with single-end (SE) 50-bp reads (Q30>85%). Reads were trimmed and reads without 3' adaptors, reads with 5' primer contaminants, and reads for which > 50% of bases had a base quality score of no more than 5, were dropped. Finally, microRNA candidates were detected using the Chimira web interface from the EBI institute, and to improve confidence of our findings, reads with fewer than five read counts in at least one sample were removed. In total, I identified 1,646 miRNA species (out of 1,917 miRBase entries), ranging from five to 859,928 reads (Figure 5.3A) (Vitsios & Enright, 2015).

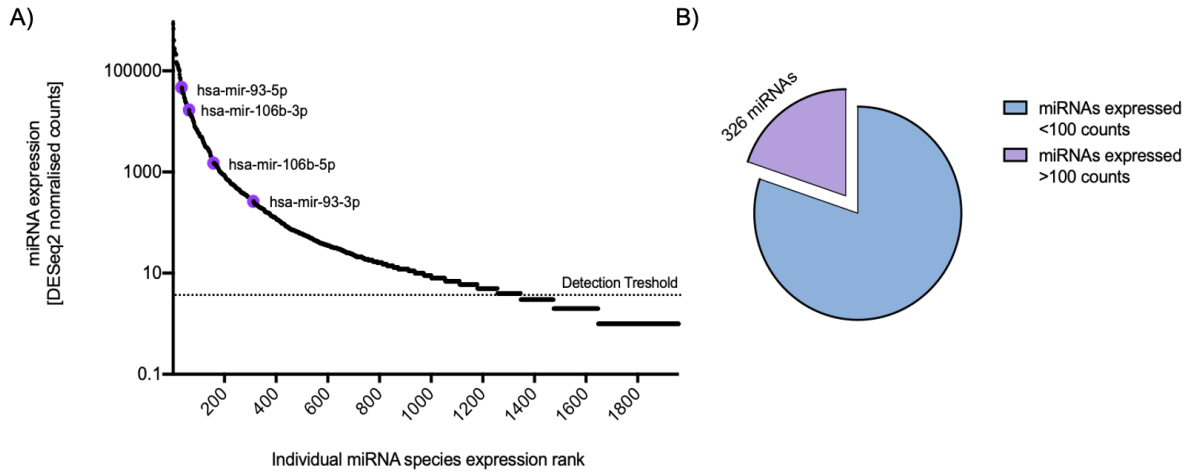

Figure 5.3. ***Highly expressed microRNAs in HCC1806 cells.*** *A) Graph (DESeq2-normalised counts) showing all miRNAs detected in HCC1806 cells across 4 different treatment conditions using Chimira (n=2). Purple dots represent miR-93 and miR-106b, members of the miR-106b/25 cluster of microRNAs. B) Out of 1646 mapped miRNAs (>2 counts), 326 were expressed at over 100 counts per million reads in at least one of the 4 samples. These miRNAs are termed "highly expressed" miRNAs.*

326 miRNAs (19.81%) were found to be expressed at substantial levels in HCC1806 cells (>100 counts per million reads in at least one sample type; untreated, post-γ-irradiation, or post-HU treatment) (Figure 5.3B). The list of most abundant miRNAs included members of the let-7 family of miRNAs, such as let-7d-5p and let-7c-5p, and members of the oncogenic miR-106b/25 cluster (Figure 5.3A, purple dots). Elevated miR-106b/25 expression levels were also found in our miRNA microarray data (Figure 3.8), in accordance with *AGO2* CNA in HCC1806 cells, as presented in Chapter 3 (Section 3.5)

Next, differential expression analysis was performed to evaluate the early impact of γ-irradiation [2 hours (T2) and 6 hours (T6)] (Section 5.4) and hydroxyurea treatment [4 hours (T4)] (Section 5.5) on miRNA and mRNA expression profiles. The first aim was to identify DNA damage-inducible miRNAs and explore the effects of differentially regulated miRNAs on their target-mRNAs, with a focus on pathways involved in the regulation of cell cycle progression and DNA damage repair.

5.4 Impact of γ-irradiation on the Transcriptomic Profile of HCC1806 cells

5.4.1 Changes in Global miRNA Expression in Response to γ-Irradiation

To determine the transcriptome profile of microRNAs in HCC1806 breast cancer cells following radiotherapy treatment, I conducted an integrated analysis to evaluate the early impact of γ-irradiation (10 Gy) [2 hours (T2) and 6 hours (T6)] on miRNA expression. To perform differential expression analysis, *DESeq2* was used (Love et al., 2014). Differentially expressed microRNAs were defined as miRNAs with a Log_2 Fold Change (LFC) of ≥1.0 and p-values (pval) ≤0.05 (n=2). Comparison of normalised miRNA expression under the different conditions (Control, T2, and T6) was investigated using the Log_2-ratio and scatter plots (Figure 5.4). Figure 5.4 reveals an overall similarity between the miRNA expression profiles of

untreated and IR-treated HCC1806 cells. The scatter plots also indicate that more microRNAs are differentially expressed at T2 than at T6 (as evident by greater deviation from the trend line) (Figure 5.4).

Another study exploring miRNA expression patterns in response to ionising radiation in two breast cancer cell lines, MDA-MB-231 and T47D, recently identified two miRNAs, miR-23b-3p and miR-16-5p, that were significantly upregulated 24 hours post γ-irradiation (2 Gy). (Choudhary et al., 2020). In our analysis, neither of those miRNAs came up as significantly differentially regulated, suggesting a clear separation of the timing of the response, with early- and late-induced miRNA clusters.

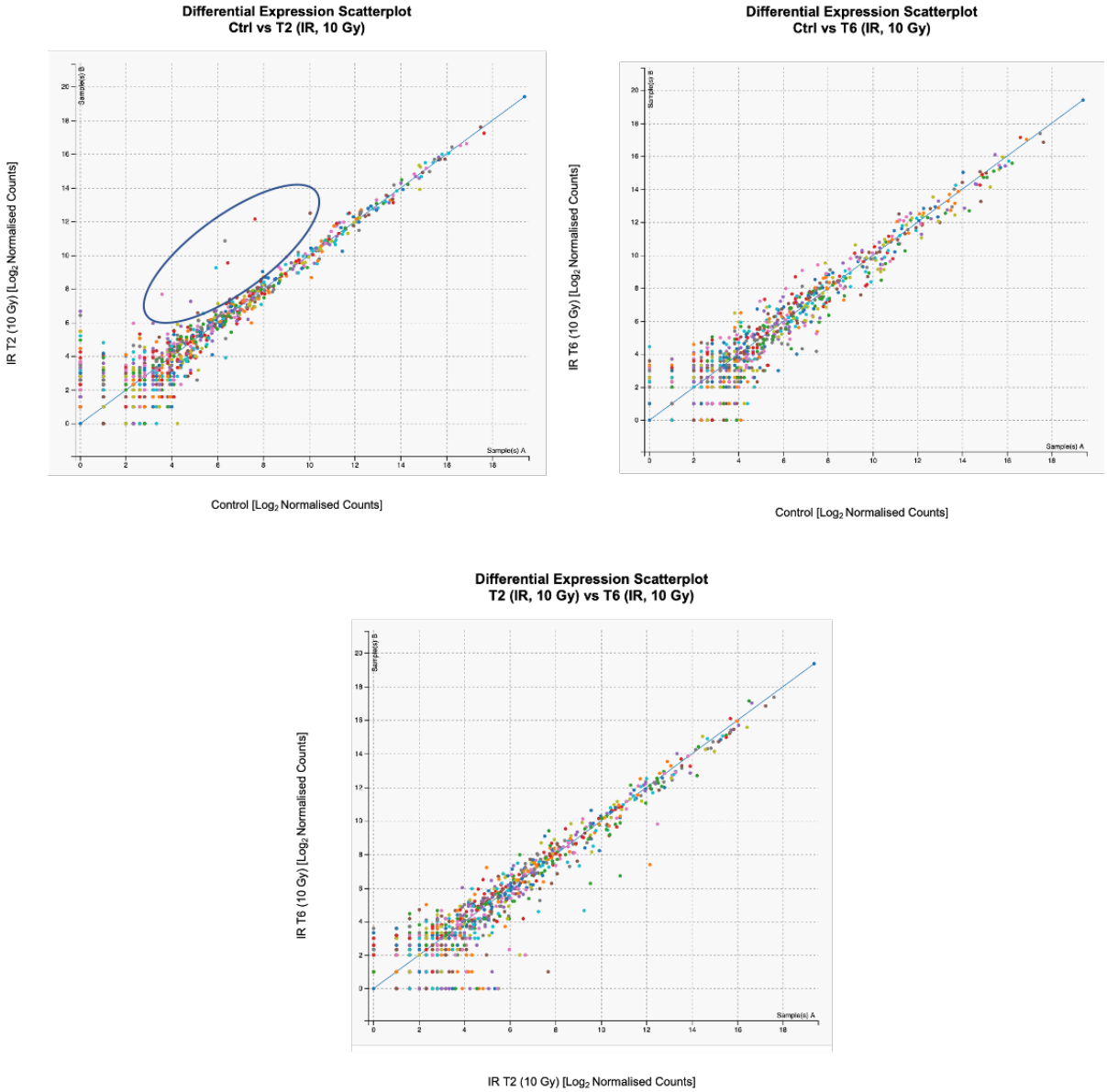

Figure 5.4. ***Scatter plots of the differential expression levels of microRNAs between the control, 2 hours post-IR (T2) and 6 hours post-IR (T6) HCC1806 samples.*** *Each coloured dot represents a microRNA. Dots above the blue line are overexpressed, dots below the line are downregulated. The normalised count levels (DESeq2, Log_2) of the irradiated samples are indicated on the Y axis, the control sample on the X axis.*

Therefore, to better understand the role of miRNAs in the early response to ionising radiation, I proceeded to perform differential expression analysis using *DESeq2*. A number of differentially expressed miRNAs were identified both 2 and 6 hours post-γ-irradiation when compared to the untreated cells. 18 microRNAs showed significant levels of differential expression between the T2 γ-irradiated (10 Gy) and untreated HCC1806 cells (LFC ≥ |1|; pval ≤ 0.05) (Figure 5.5A). Seventeen of these miRNAs (such as hsa-mir-1-3p, hsa-mir-519d-3p, hsa-mir-516b-5p, hsa-mir-516a-5p, hsa-mir-451a, hsa-mir-517b-3p, and hsa-mir-190a-5p) were significantly upregulated 2 hours post-irradiation when compared to the untreated condition, whereas only one miRNA, hsa-miR-223-5p, was downregulated at T2 (Figure 5.5A). Interestingly, six of these 17 upregulated miRNAs [hsa-mir-516a-5p, hsa-mir-516b-5p, hsa-mir-517b-3p, hsa-mir-518a-3p, hsa-mir-519d-3p, and hsa-mir-520h] are clustered miRNAs and belong to the largest human miRNA cluster (chromosome 19 miRNA cluster, C19MC), which extends over a ~100kb genomic region (Bentwich et al., 2005). No significant expression changes were found for *DICER1, AGO2*, or *PABPC1* at T2 when compared to the control cells, suggesting these early miRNA changes were largely driven by altered pri-miRNA transcription.

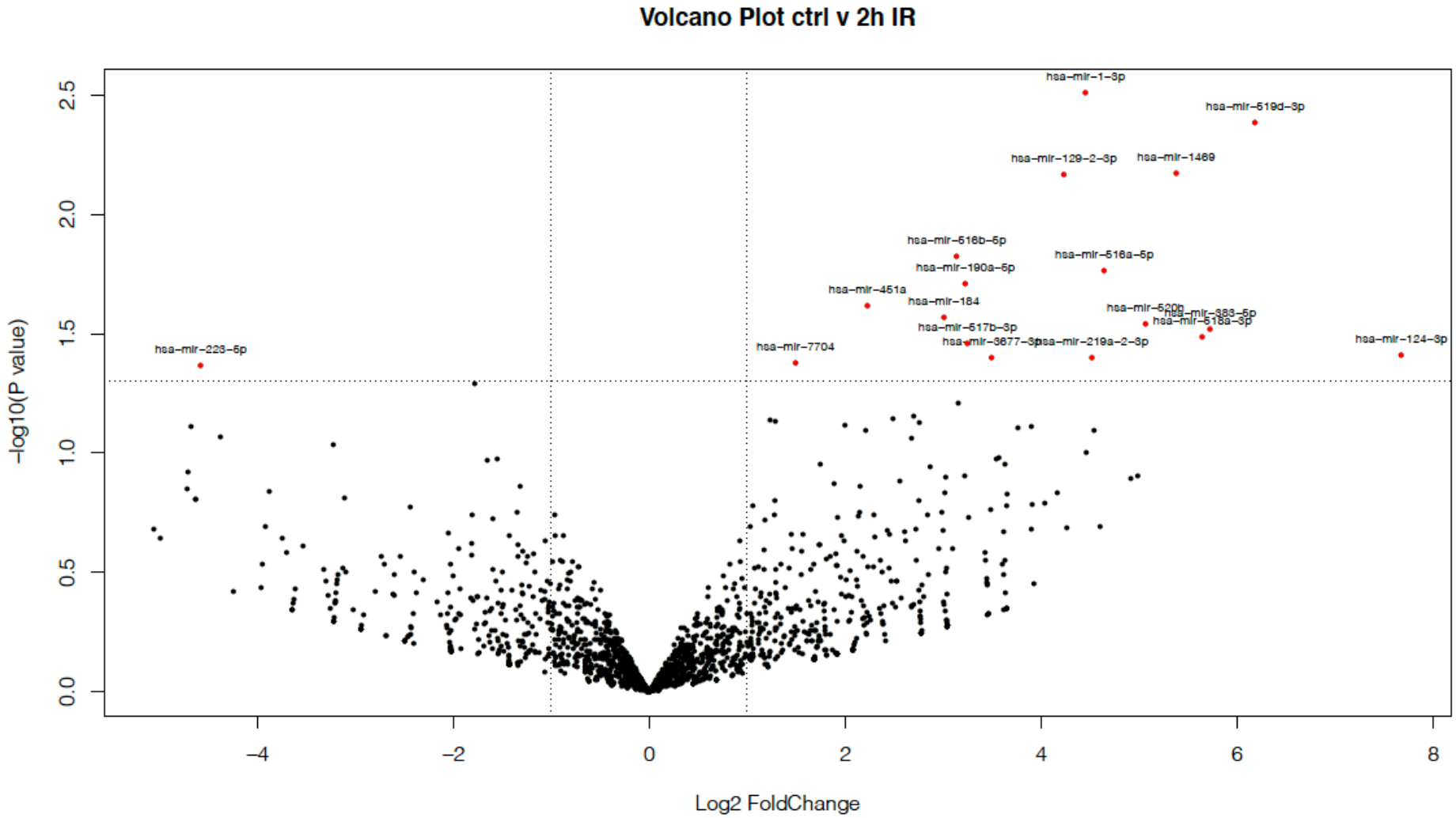

Figure 5.5. ***Differential microRNA expression, with fold difference between log_2 normalised expression in A) control and T2 (2 hours post-IR treatment) and HCC1806 cells plotted versus $-log_{10}$ P-value (n=2).*** *Each dot represents a microRNA. Red coloured dots were classed as Log_2 Fold Change $\geq |1|$ and p-value ≤ 0.05.*

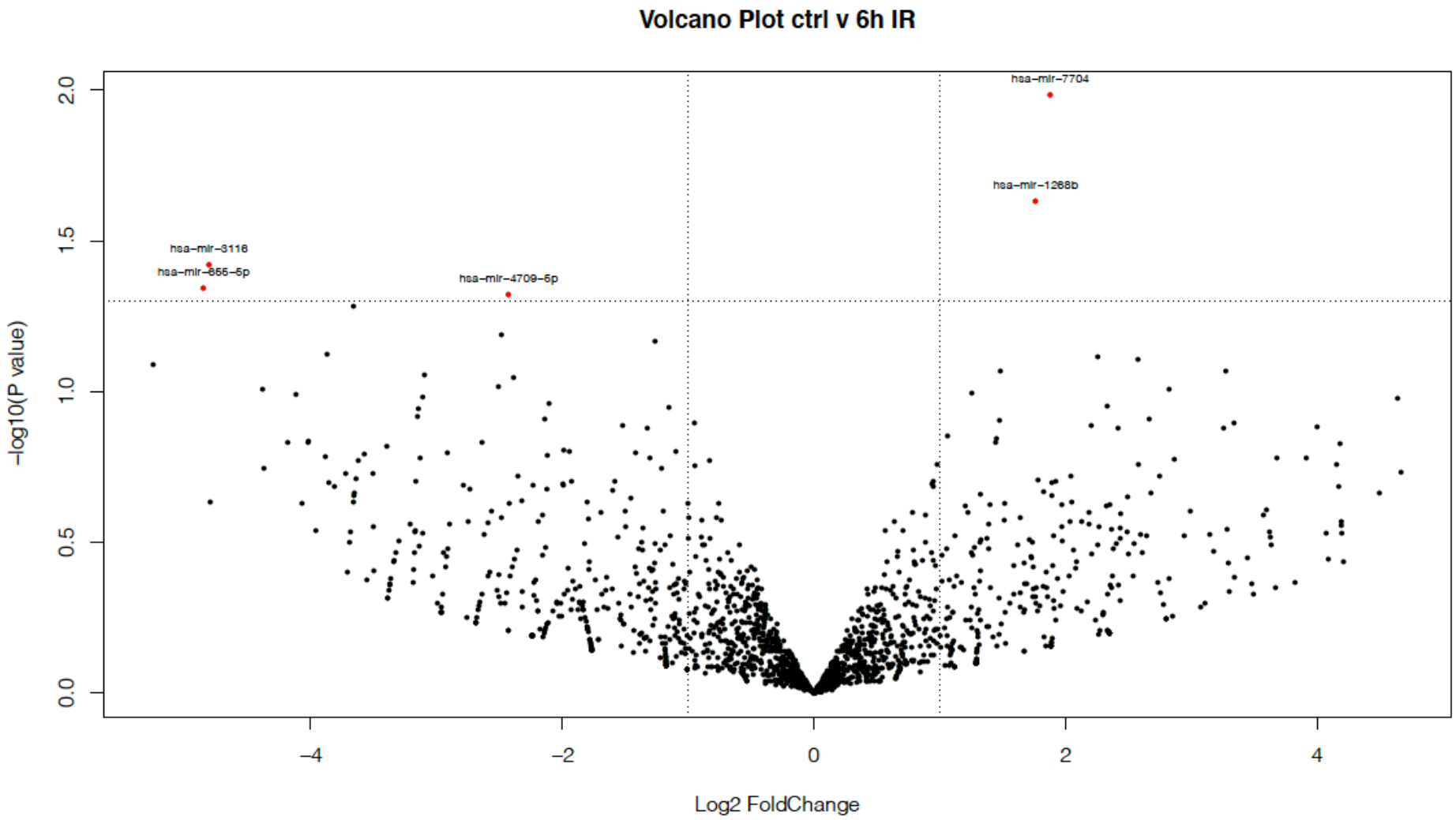

Figure 5.5 – Continued. ***Differential microRNA expression, with fold difference between log_2 normalised expression in B) control and T6 (6 hours post-IR treatment) HCC1806 cells plotted versus $-log_{10}$ P-value (n=2).*** *Each dot represents a microRNA. Red coloured dots were classed as Log_2 Fold Change $\geq |1|$ and p-value ≤ 0.05.*

Analysis of miRNA expression at later time points post-IR (T6) revealed a smaller number of differentially expressed miRNAs than at T2. When miRNA expression profiles obtained 6 hours post-IR treatment (T6) were compared with the untreated cells, only 5 differentially expressed miRNAs were identified, including hsa-mir-1268b, hsa-mir-3116, hsa-mir-4709-5p, hsa-mir-655-5p, and hsa-mir-7704 (Figure 5.5B). Interestingly, only one miRNA, miR-7704, showed consistent upregulation at both 2- and 6 hours post γ-irradiation when compared to the control cells (Figure 5.6). Previously, ultraviolet B (UV(B)) was also shown to cause upregulation of miR-7704 expression in exosomes secreted by melanocytes (Shen, Sun, Shao, & Xu, 2020). Even though cytotoxicity induced by γ-irradiation results primarily from the generation of DNA DSBs, whereas cytotoxicity induced by UV(B) radiation results from the formation of pyrimidine dimers, both damages are potent inducers of p53 protein activity and its downstream signalling pathways (Giaccia & Kastan, 1998). This data could therefore suggest that miR-7704 plays a global role in regulating the cellular response to genotoxic stresses from a variety of sources.

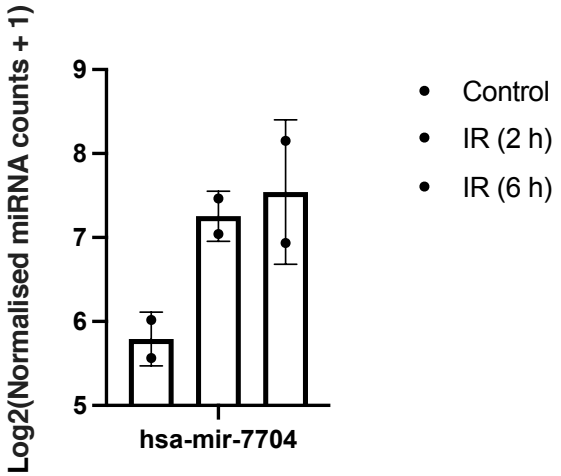

Figure 5.6. ***Elevated miR-7704 expression in response to γ-irradiation in HCC1806 cells.*** *Normalised hsa-mir-7704 expression values (normalised miRNA counts + 1) were log2 transformed and plotted for the different treatment conditions (n=2).*

5.4.2 Changes in Global mRNA Expression in Response to γ-Irradiation

In order to identify alterations in the expression of protein-coding genes following exposure to ionising radiation, mRNA-sequencing of HCC1806 cells was used to evaluate the early impact of γ-irradiation [2 hours (T2) and 6 hours (T6)] on largely overlapping samples as used for sRNA-seq. The cDNA libraries for mRNA sequencing were sequenced on the Illumina NovaSeq 6000 platform with paired-end (2 x 150 nucleotide) reads (Q30>80%) and yielded an average of 27 million reads per sample, with mappable reads ranging from 82.4-85.3%. Reads from each library were contiguously aligned to the appropriate transcriptome using *kallisto* (GRCh38-Ensembl 96 Archive, April 2019) and *DESeq2* was used to identify genes that were differentially expressed (N. L. Bray et al., 2016; Love et al., 2014). A gene was defined as expressed if the expression estimates in at least one of the samples were >= 5 normalised read counts. Volcano plots in Figure 5.7 visualise the number of differentially expressed genes (DEGs) at T2 and T6 (versus untreated HCC1806 cells). The horizontal dashed line indicates the pre-set statistical threshold corresponding to a p-value of < 0.05, with the red dots representing the significantly differentially regulated genes.

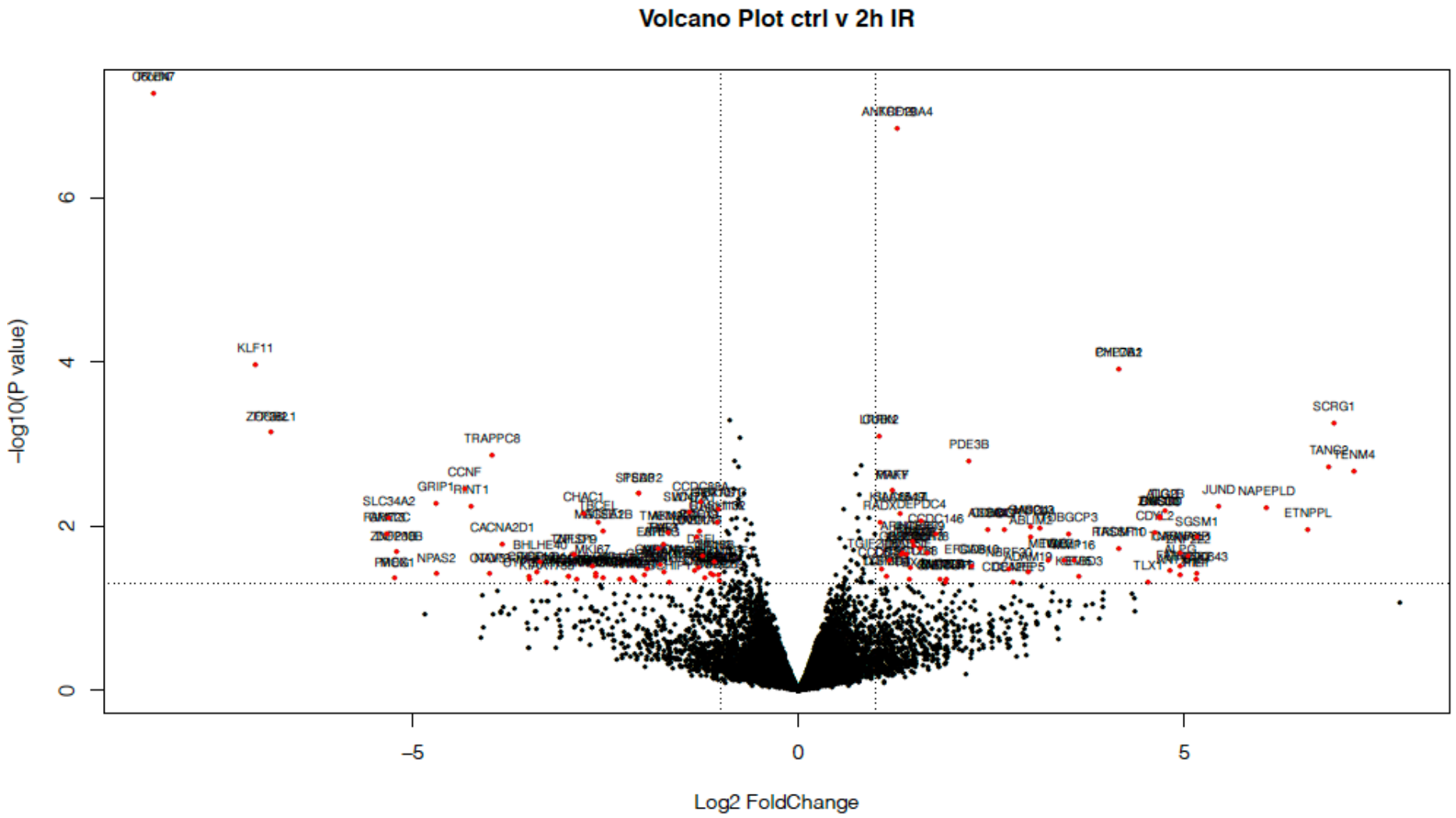

Figure 5.7. ***Differential mRNA expression, with fold difference between log₂ normalised expression in A) control and T2 (2 hours post-IR treatment) and HCC1806 cells plotted versus −log₁₀ P-value (n=2).*** *Each dot represents a transcript. Red coloured dots were classed as Log₂ Fold Change ≥ \|1\| and p-value ≤ 0.05.*

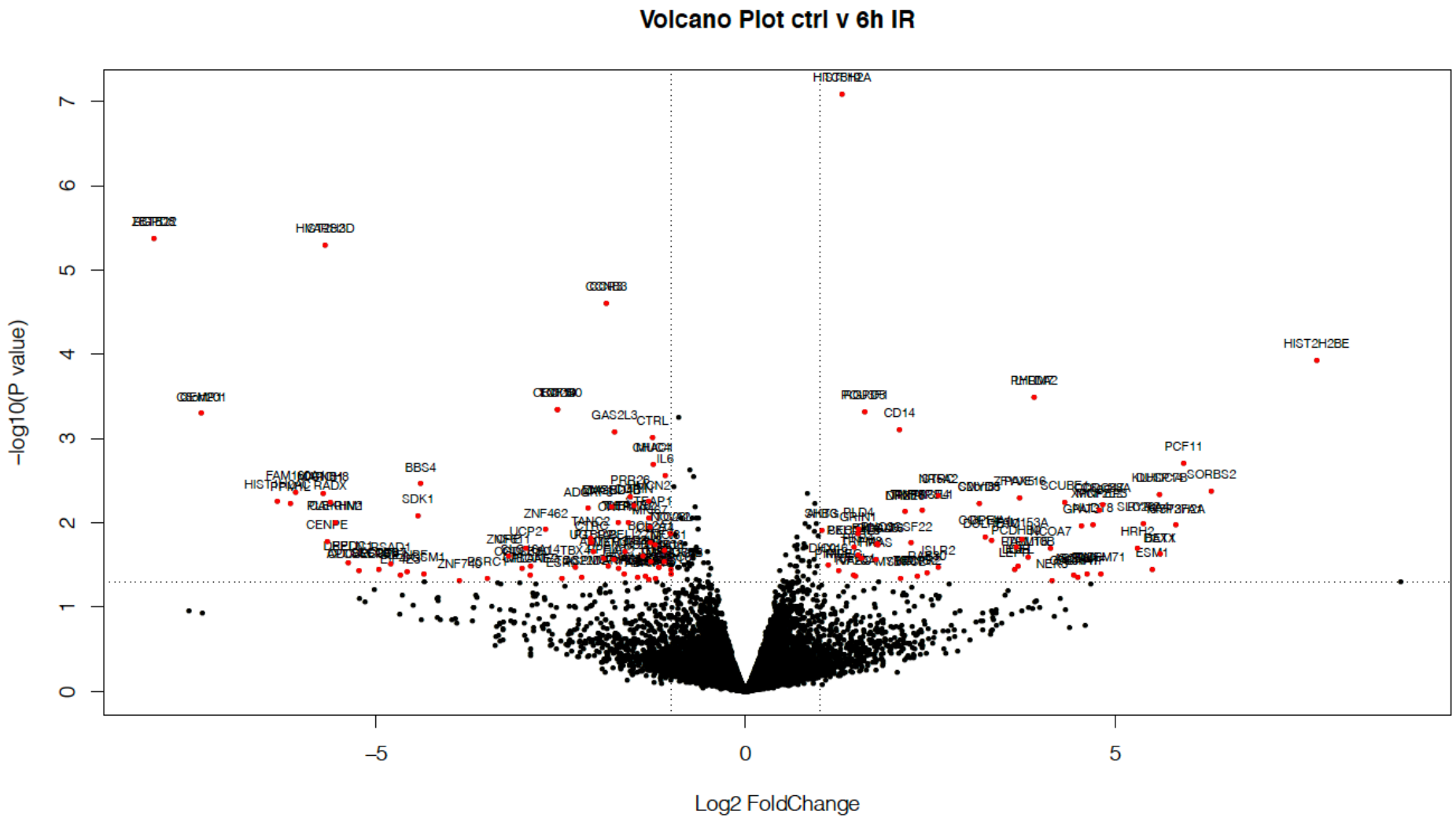

Figure 5.7 – Continued. ***Differential mRNA expression, with fold difference between log₂ normalised expression in B) control and T6 (6 hours post-IR treatment) HCC1806 cells plotted versus −log₁₀ P-value (n=2).*** *Each dot represents a transcript. Red coloured dots were classed as Log₂ Fold Change ≥ \|1\| and p-value ≤ 0.05.*

Differential expression analysis between the T2 γ-irradiated (10 Gy) and untreated cells revealed 175 differentially expressed genes (LFC ≥ |1|, pval < 0.05) (Figure 5.7A), which were annotated using Gene Ontology (GO) terms. GO terms capture functional annotations of genes, or genetic elements, in different ontologies (such as their molecular function or biological processes). Among the 98 downregulated genes were multiple cyclins (*CCNF, CCNG2),* centromere proteins (*CENPE, CENPA*), and other genes involved in cell cycle regulation and proliferation, such as *PTEN, WEE1,* and *MKI67*. In accordance with this, GO BP enrichment analysis for the downregulated DEGs revealed significant enrichment for biological processes such as "Regulation of cyclin-dependent protein serine/threonine kinase activity" (FDR =7.8E-02) and "Mitotic cell cycle" (FDR=7.8E-02). The 77 upregulated DEGs at T2 were enriched for GO biological processes such as "Regulation of transcription by RNA polymerase II", which was reflected in upregulation of multiple zinc-finger transcription factors (*ZNF733, ZNF222, ZNF180, ZNF280B*) and other transcriptional regulators, such as *JUND, KLF11, POU3F1,* and *KLF4*.

Next, I compared mRNA expression levels between the T6 γ-irradiated (10 Gy) and untreated cells. At this later time point, 178 differentially expressed genes (LFC ≥ |1|, pval < 0.05) were identified when compared to untreated cells (Figure 5.7B). GO BP enrichment analysis for the downregulated DEGs revealed a strong enrichment for processes related to "Cell division" (FDR = 2.6E-08). Downregulated genes 6 hours post-IR included *CENPE* and *CENPF*, but also the B-type cyclins, *CCNB1* and *CCNB3*. Previous work demonstrated that repression of *cyclin B1* and CDK1 by p53 enforces a G_2-M arrest (Taylor et al., 2017) and our data therefore indicates that the DNA damage checkpoint is active 6 hours post γ-irradiation treatment in HCC1806 cells.

To identify transcripts whose expression levels were consistently altered across the entire early response (both at T2 and T6 post γ-irradiation), the overlap between DEGs (both up- and downregulated) at the two different time points was analysed (Figure 5.8). As shown in Figure 5.8A, the expression of 19 genes was reduced at both time points (including *MKI67*, encoding the proliferation marker Ki-67, *G2E3*, a G_2/M phase-specific E3 ubiquitin-protein ligase, *GAS2L3*, a target gene of the DREAM complex required for cytokinesis and genomic stability (Wolter et al., 2012), *GTSE1*, a cytoskeletal protein required for cell migration (Scolz et al., 2012), *RADX*, which regulates activity of RAD51 (Dungrawala et al., 2017), and *CENPE,* a kinetochore-associated kinesin-like motor protein required for proper chromosome segregation (Yao, Anderson, & Cleveland, 1997).

When the same analysis was performed for the upregulated DEGs, I found that the expression of 20 genes was increased at both T2 and T6 post γ-irradiation (Figure 5.8B). This included genes such as *PLD4*, a ssDNA exonuclease which regulates cytokine responses via nucleic acid degradation (Gavin et al., 2018), *IL6*, a DNA-damage responsive cytokine with an important role in the inflammatory response and radioprotective roles (Neta, Perlstein, Vogel, Ledney, & Abrams, 1992), and *CCR3*, a chemokine receptor.

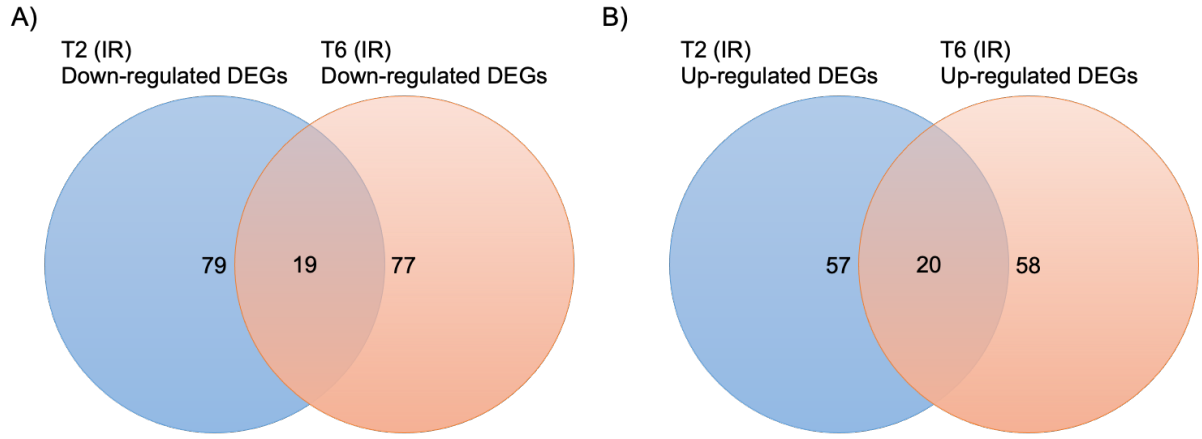

Figure 5.8. ***Venn diagram depicting common up- and downregulated DEGs in HCC1806 cells 2 hours post-IR (T2) and 6 hours post-IR (T6).*** *Differentially expressed genes fulfilled combined criteria of LFC ≥ |1| and p-value < 0.05).*

Transcription factors (TFs) and microRNAs (miRNAs) are two of the major regulatory factors that can alter RNA function at the transcriptional and post-transcriptional level, respectively. To investigate whether any of the described γ-irradiation-dependent transcriptome changes could be driven by altered TF-binding, the list of the DEGs (at both T2 and T6) was searched for predicted TF-motif enrichments in the promoter regions of these genes. This analysis was performed using the ShinyGO v0.66 web interface (Ge et al., 2020), which uses information derived from the hundreds of ChIP-seq experiments from the ENCODE Consortium (Dunham et al., 2012) to perform TF factor enrichment analysis (TFEA).

Using this approach, I identified only one significantly enriched transcription factor, *FOXM1* (FDR = 1.2E-07), which emerged as a potential regulator of these differentially expressed early IR-response genes. In an unperturbed cell cycle, ATR gets inactivated after completion of DNA replication, repressing the FOXM1-dependent transcriptional programme to facilitate transcription of genes required for mitotic entry, including *PLK1, CENPE*, and *CENPF* (Saldivar et al., 2018). Our data suggests that IR-induced DNA damage can lead to inhibition of FOXM1-mediated G_2-M transcription and subsequent cell cycle arrest. I did not find any significant changes in FOXM1 expression at T2 or T6, and therefore predict that reduced FOXM1 target expression at T2 and T6 could be a result of decreased FOXM1 phosphorylation, which is mediated through both CDK1 and CHK2 (Liao et al., 2018; Saldivar et al., 2018).

5.4.3 miRNA Target Transcript Predictions in Response to γ-Irradiation

Next, differentially expressed miRNAs (Section 5.4.1) were linked to changing levels of putative target transcripts. For this analysis, only the five most strongly upregulated miRNAs

per condition (T2 and T6 versus untreated cells) were considered (p-value < 0.05, baseMean > 10 (mean of normalised miRNA counts) (Table 5.1 and 5.2).

Table 5.1. ***Top 5 most upregulated miRNAs 2 hours post-IR (T2 vs control).***

id	***baseMean***	***Log_2 Fold Change***	***LFC SE***	***p-value***
hsa-mir-124-3p	19.41605	7.673087	3.716464	0.038958930
hsa-mir-519d-3p	17.12066	6.181860	2.154298	0.004110608
hsa-mir-516a-5p	22.12846	4.640505	1.947008	0.017153408
hsa-mir-1-3p	662.29728	4.451564	1.504680	0.003091613
hsa-mir-129-3p	10.05628	4.230032	1.564001	0.006838199

Table 5.2. ***Top 5 most upregulated miRNAs 6 hours post-IR (T6 vs control).***

id	***baseMean***	***Log_2 Fold Change***	***LFC SE***	***p-value***
hsa-mir-7704	119.6375	1.879671	0.7333338	0.01037166
hsa-mir-1268b	394.7425	1.761173	0.7763629	0.02329925

To determine whether these upregulated miRNAs shared common target-mRNAs, the *miRNAtap* package (version 1.14.0) was used to integrate "Predicted Targets" of each of those miRNAs from five different resources (TargetScan (Friedman et al., 2009), DIANA (Reczko, Maragkakis, Alexiou, Papadopoulos, & Hatzigeorgiou, 2012), miRanda (John et al., 2005), PicTar (Lall et al., 2006), and miRDB (Wong & Wang, 2015)). Next, building on the principle that increased miRNA expression impacts on target gene expression, I used our mRNA-sequencing data to validate those computational predictions and find "True Targets". To this end, only those "Predicted Targets" for which the mRNA fold change was significantly correlated with the miRNA upregulation were selected, and thus considered to be "True Targets". I used the commonly used fold change (FC) cut-off value of 1.5 (|LFC| = 0.58) (Dalman, Deeter, Nimishakavi, & Duan, 2012), irrespective of the direction of change, to perform those validations. This approach enabled me to explore significant miRNA-mRNA

interactions involving the differentially expressed miRNAs as shown in Table 5.1 and 5.2 and could therefore reveal novel genes that are repressed in a miRNA-driven manner following ionising radiation treatment.

As shown in Figure 5.9, a total of 875 unique predicted targets (|LFC| > 0.58) was obtained for the five upregulated miRNAs at T2. Overlapping mRNA targets that were common to four of the top five most upregulated miRNAs (namely, hsa-miR-124-3p, hsa-miR-519d-3p, hsa-miR-1-3p, and hsa-miR-129-3p) are displayed in Figure 5.9B and included the genes *RORA (*LFC = -0.855), *ABCG8 (*LFC = -0.1.29)*, SIK* (LFC = 1.359), and *WEE1 (*LFC = -0.707). SIK1, which seems to be stabilised by these miRNAs, as shown by its upregulation, has previously been shown to interact with p53 and positively regulate its transcriptional activity, thus facilitating oxidative phosphorylation (Ponnusamy & Manoharan, 2021). As previously described, WEE1 plays a key role in cell cycle regulation through modulation of the activity of CDK1 and CDK2.

I proceeded to analyse the mRNA targets of the upregulated miRNAs at T6, namely miR-7704 and miR-1268b (Figure 5.9A). I was interested in the predicted target-mRNAs of these differentially regulated miRNAs as they were much more strongly and consistently upregulated than those at T2, and secondly, their upregulation, especially that of miR-7704, was specific to ionising radiation and not detected in response to hydroxyurea treatment. For those two miRNAs up regulated at T6, I only obtained a total of 11 unique predicted targets (|LFC| > 1.5). Amongst these downregulated mRNA targets was *KDM6B/JMJD3*, which catalyses demethylation of the histone marks H3K27me2 and H3K27me3 and interacts with the tumour suppressor protein p53 (Hong et al., 2007; Williams et al., 2014).

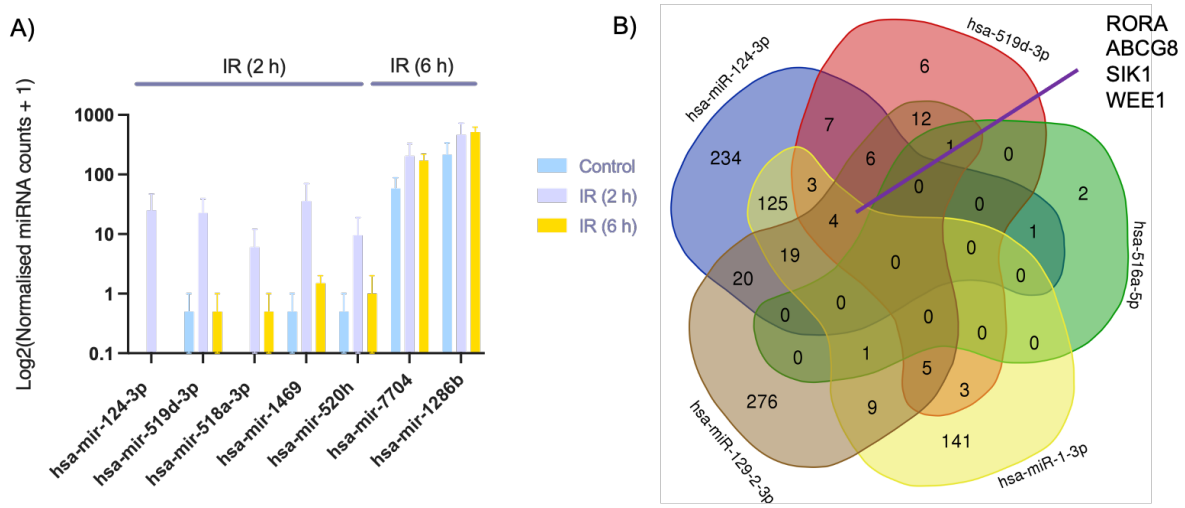

Figure 5.9. ***Upregulated miRNAs 2-hours post-IR target cell cycle kinases WEE1 and SIK1.*** *A) Expression levels (normalised microRNA read counts) for the 5 microRNAs with the largest log fold change values 2- or 6-hours post-irradiation (10 Gy). B) Venn diagram of five miRNAs, which covers the majority of the predicted target genes. The Venn diagram shows common predicted mRNA targets among five miRNAs (hsa-miR-124-3p, hsa-miR-519d-3p, hsa-miR-516a-5p, hsa-miR-1-3p and hsa-miR-129-2-3p). Different colours represent different miRNAs. The number in the intersection represents the number of common predicted mRNA target genes among the miRNAs.*

5.4.4 Roles of SETD2 and the miR-106b/25 Cluster in Response to γ-Irradiation

As this thesis has a particular focus on characterising the roles of both SETD2 and the miR-106b/25 cluster in the DNA damage and replication stress responses, I next asked whether *SETD2* mRNA levels, or mature miRNA levels of members of the miR-106b/25 cluster, were differentially regulated following IR-treatment in HCC1806 cells.

First, normalised counts for miRNAs of the miR-106b/25 cluster were extracted from our sRNA-sequencing dataset (Figure 5.10A). Hsa-miR-25-3p, hsa-miR-93-3p, and hsa-miR-93-5p expression levels showed a downward trend in response to 10 Gy of IR (both at T2 and T6). In contrast, expression levels of miR-106b-5p, and to a lesser extent miR-106b-3p, were upregulated in response to γ-irradiation treatment in this cell line (Figure 5.10A). Next, TaqMan™ qPCR assays were used to validate changes in mature miR-106b/25 expression levels in IR-treated cells. In accordance with observations made from the sRNA-seq data,

expression levels of miR-106b-3p and miR-106b-5p were significantly elevated in response to IR (10 Gy) in HCC1806 cells, whereas mature miR-93-3p levels decreased following IR treatment (Figure 5.10B).

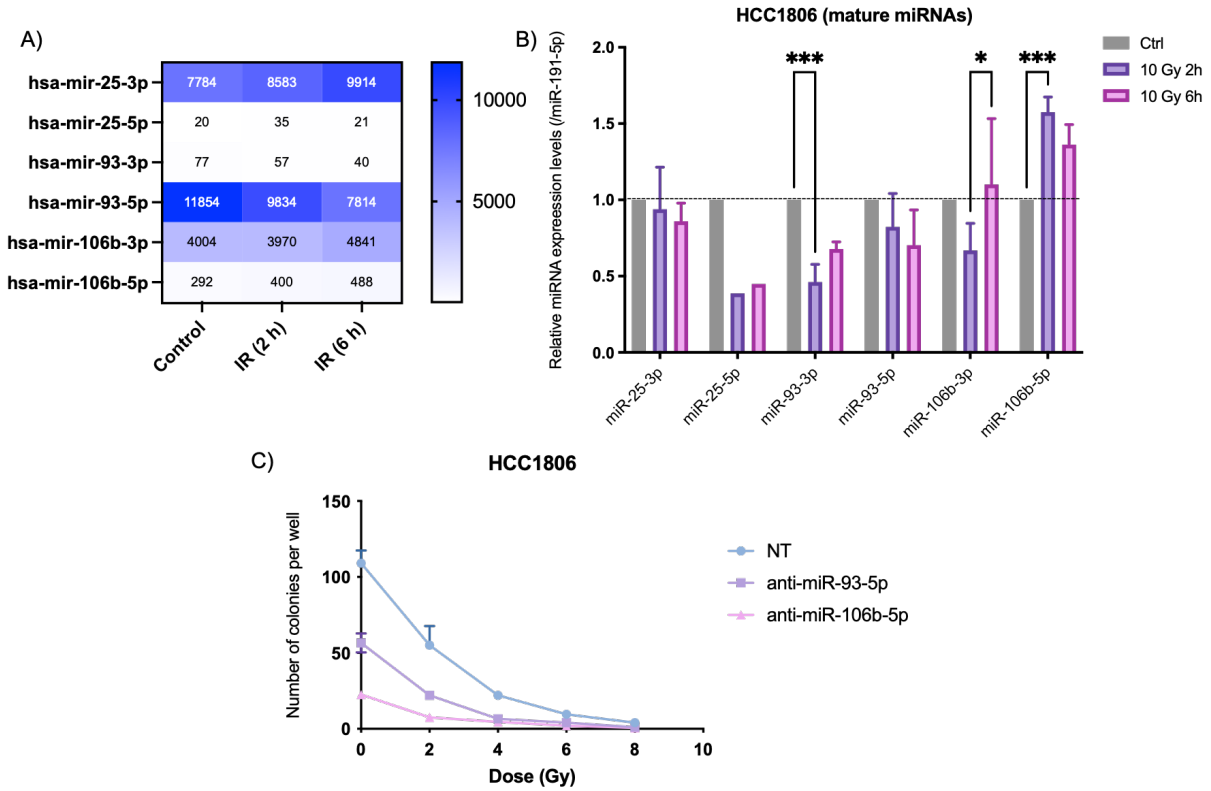

Figure 5.10. ***hsa-miR-93-3p and hsa-miR-93-5p expression in HCC1806 cells decrease following irradiation (10 Gy dose), in contrast to miR-106b-3p and miR-106b-5p levels, which show increased expression.*** *A) Normalised read counts for microRNAs of the miR-106b/25 cluster in untreated HCC1806 cells, 2-, or 6-hours post-irradiation (10 Gy) from sRNA-sequencing data. B) Validation of expression changes in the miR-106b/25 cluster in response to IR in HCC1806 using qRT-PCR. Significance calculated with a two-way ANOVA. Data represented as mean ± SEM (n=3). C) HCC1806 cells were plated and exposed to 2, 4, 6, or 8 Gy of IR (or were mock exposed). After 10 days of colony growth, the cells were stained, and colonies were counted manually (n=3).*

Next, I evaluated the impact of altered miR-93-5p and miR-106b-5p levels on radiosensitivity (Figure 5.10C). To do this, anti-miR-93-5p and anti-miR-106b-5p oligonucleotides were transfected into HCC1806 cells, those cells were exposed to different doses of radiation (2, 4, 6, or 8 Gy), and clonogenic assays were used to determine relative survival. Even though reduced colony formation was observed following both miR-93-5p and miR-106b-5p inhibition in the absence of IR, anti-miR-93-5p or anti-miR-106b-5p transfection did not cause further radiosensitisation (Figure 5.10C). MicroRNAs of the miR-106b/25 cluster therefore mediate the cellular response to IR without impacting on radiosensitivity.

As I have previously shown a correlation between miR-106b-5p expression levels and *SETD2*, *E2F1*, and *MCM7* mRNA levels (Chapter 4), I tested whether expression levels of these transcripts were altered in response to γ-irradiation treatment. From our mRNA-sequencing data, no significant changes in *SETD2* or *MCM7* expression could be detected at either T2 or T6 when compared to the untreated cells (Figure 5.11A). Elevated levels of *E2F1* were observed 2-hours post IR treatment (LFC = 0.456, p-value = 0.088), but this change was not significant, and only temporary, as E2F1 expression levels were restored to baseline levels at T6 (Figure 5.11A). We therefore predicted that upregulation of miR-106b-5p, which targets both SETD2 and E2F1, might keep E2F1-dependent transcription low in response to ionising radiation.

To validate these findings using qRT-PCR, HCC1806 cells were exposed to 10 Gy of IR, and samples were harvested at the indicated time-points. Even though no significant changes in *MCM7* expression levels were identified in the early-response to IR (Figure 5.11B), *E2F1* mRNA levels were found to be elevated at T6. Furthermore, *SETD2* mRNA levels were lower at T2 and T6 but were restored to normal after 24 hours (Figure 5.11B).

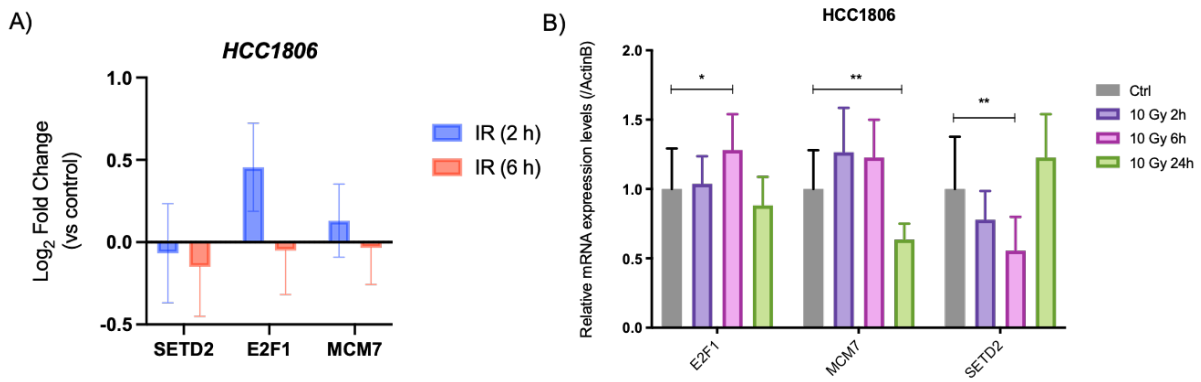

Figure 5.11. ***SETD2, E2F1 and MCM7 expression levels in response to γ-irradiation treatment in HCC1806 cells.*** *A) Log_2 Fold Change of SETD2, E2F1, and MCM7 expression levels 2- and 6-hours post IR treatment (10 Gy) when compared to control cells from mRNA-sequencing data (n=2). B) Relative mRNA expression levels of E2F1, MCM7, and SETD2 as measured by qRT-PCR of cells collected 2, 6, or 24 hours after 10 Gy of IR. Data expressed as mean ± 95% confidence interval (CI (n=3). Significance calculated with a two-way ANOVA.*

Given the decreased *SETD2* mRNA levels 2- and 6-hours post-IR, I tested whether any concomitant changes in the levels of H3K36me3 could be observed. To this end, asynchronous U2OS cells were treated with a lower dose of IR (4 Gy) and cell lysates were collected at the indicated time points (Figure 5.12A). I could not detect any differences in total H3K36me3 levels either 2, 6, or 24 hours post IR-treatment in U2OS cells. Previous work, however, demonstrated a role for SETD2 in the cellular response to DNA damage, as SETD2 promotes DNA DSB-end resection and homologous recombination repair through recruitment of CtIP (Pfister et al., 2014). In accordance with those previous reports, SETD2 knockdown in U2OS cells significantly reduced survival after treatment with ionising radiation when compared to the non-targeting controls as measured by clonogenic survival assays (Figure 5.12C).

We can therefore conclude that constitutive H3K36me3 facilitates DNA damage repair, as previously described (Pfister et al., 2014), and that SETD2 plays an important role in regulating survival in response to radiation treatment, even though expression levels of *SETD2* or H3K36me3 were not induced following γ-irradiation treatment in this cell line. This suggests

that signalling of SETD2 for DNA repair is regulated through post-translational mechanisms, or through differential recruitment to the chromatin.

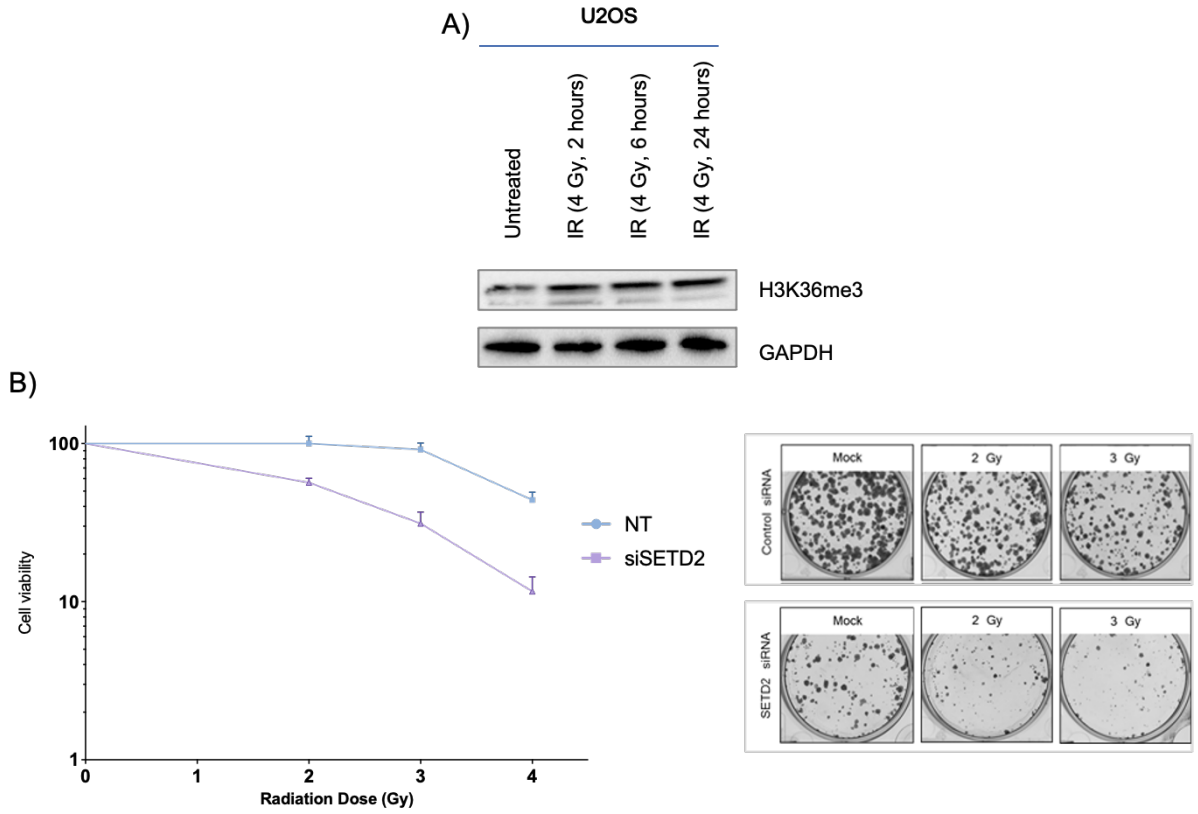

Figure 5.12. ***Knockdown of SETD2 sensitises U2OS cells to ionising radiation.*** *A) Western Blot of H3K36me3 and GAPDH in U2OS cells 2, 4, or 24 hours after IR-treatment (4 Gy). B) U2OS cells were plated and then exposed to 2, 3, or 4 Gy of ionising radiation or were mock-exposed (0 Gy). After 10 days of colony growth, the cells were stained, and colonies were counted manually. Data points and bars represent the mean and SEM of ≥ three independent experiments. Images show representative colony formation assays after the exposure of the siNT and siSETD2-treated U2OS cells to 0, 2, and 3 Gy of IR.*

5.5 Impact of Hydroxyurea on the Transcriptomic Profile of HCC1806 Cells

5.5.1 Changes in Global miRNA Expression in Response to Hydroxyurea

Following analysis of miRNA and mRNA expression changes in response to ionising radiation (Section 5.4), I next evaluated transcriptomic alterations in the presence of the replication-stress inducing agent hydroxyurea. To this end, differential expression analysis between untreated HCC1806 cells and HCC1806 cells exposed to 2 mM hydroxyurea for 4 hours was performed using *DESeq2*. Differential microRNA analysis, using our sRNA-sequencing data, revealed 14 microRNAs that showed significant levels of differential expression between the HU-treated and untreated HCC1806 cells (LFC $\geq |1|$; pval ≤ 0.05) (Figure 5.13).

Interestingly, 11 of these 14 miRNAs overlapped with miRNAs that were also upregulated 2 hours post γ-irradiation, and included hsa-miR-1-3p, hsa-miR-124-3p, hsa-mir-129-2-3p, hsa-miR-383-5p, hsa-451a, hsa-mir-516a-5p, hsa-mir-516b-5p, hsa-miR-517b-3p, hsa-miR-518a-3p, hsa-519d-3p, and hsa-miR-520h. This enabled the validation of significant interactions involving those miRNAs as identified in the previous section.

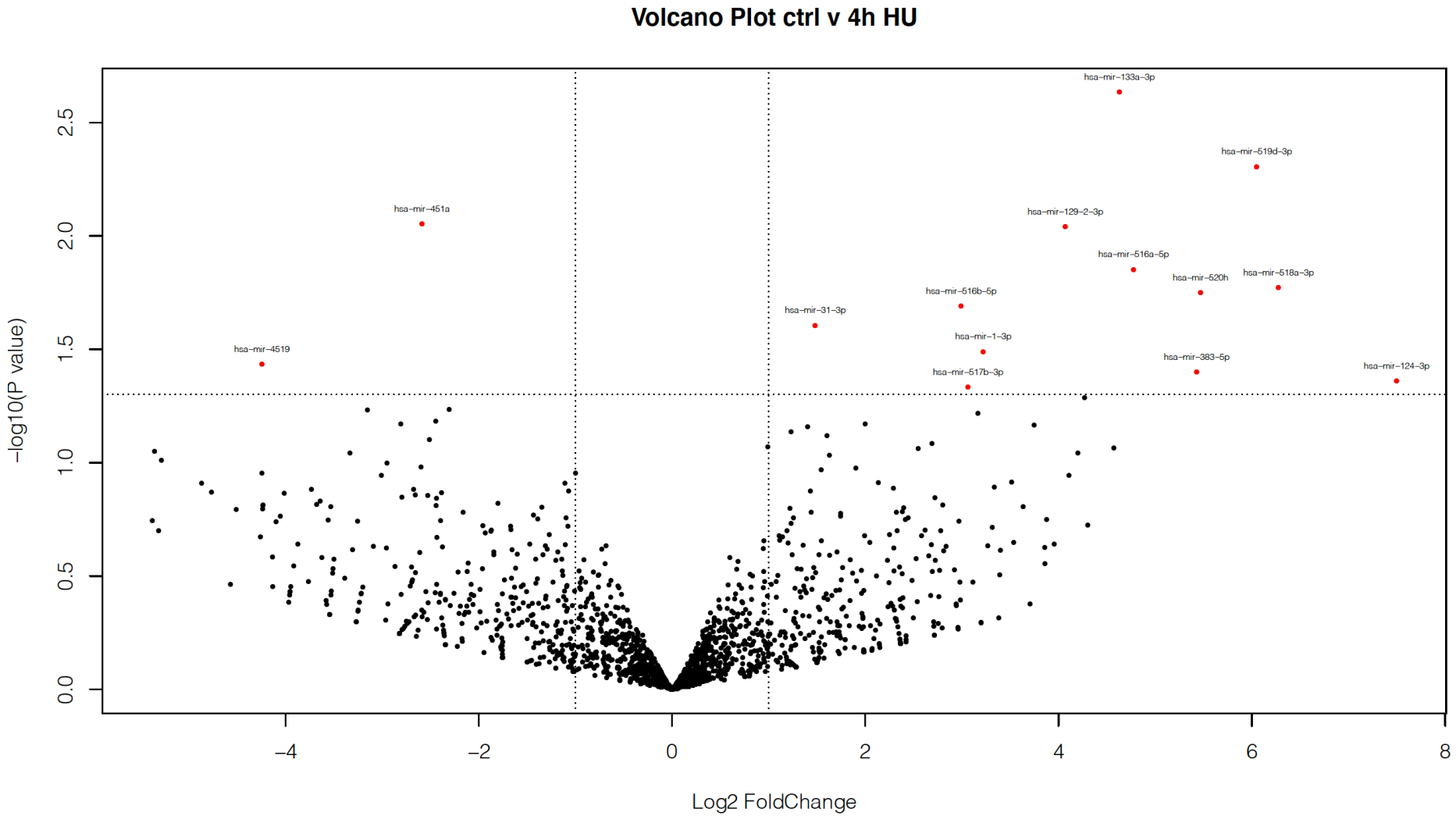

Figure 5.13. ***Differential microRNA expression, with fold difference between log_2 normalised expression in control and hydroxyurea (2 mM) treated HCC1806 cells plotted versus $-log_{10}$ P-value (n=2).*** *Each dot represents a transcript. Red coloured dots were classed as Log_2 Fold Change $\geq |1|$ and p-value ≤ 0.05.*

5.5.2 Changes in Global mRNA Expression in Response to Hydroxyurea

Next, I identified alterations in the expression of protein-coding genes following exposure to hydroxyurea (2 mM) for 4 hours, on largely overlapping samples as used for sRNA-seq (i.e., both sRNA and mRNA were extracted from a single cell pellet). The methods used were identical to those described in Section 5.4.2. The Volcano Plot in Figure 5.14 visualises the number of differentially expressed genes at T4 post-HU treatment (versus untreated HCC1806 cells). The horizontal dashed line indicates the pre-set statistical threshold corresponding to a p-value of < 0.05, with the red dots representing the significantly differentially regulated genes. When gene expression 4 hours (T4) post hydroxyurea treatment was compared with the untreated conditions, I found 1,407 genes that fulfilled our combined criterion for significant up- or downregulation (Log_2 FC $\geq |1|$, pval < 0.05) (Figure 5.14). Among these, 550 significantly downregulated DEGs and 857 significantly upregulated DEGs were identified.

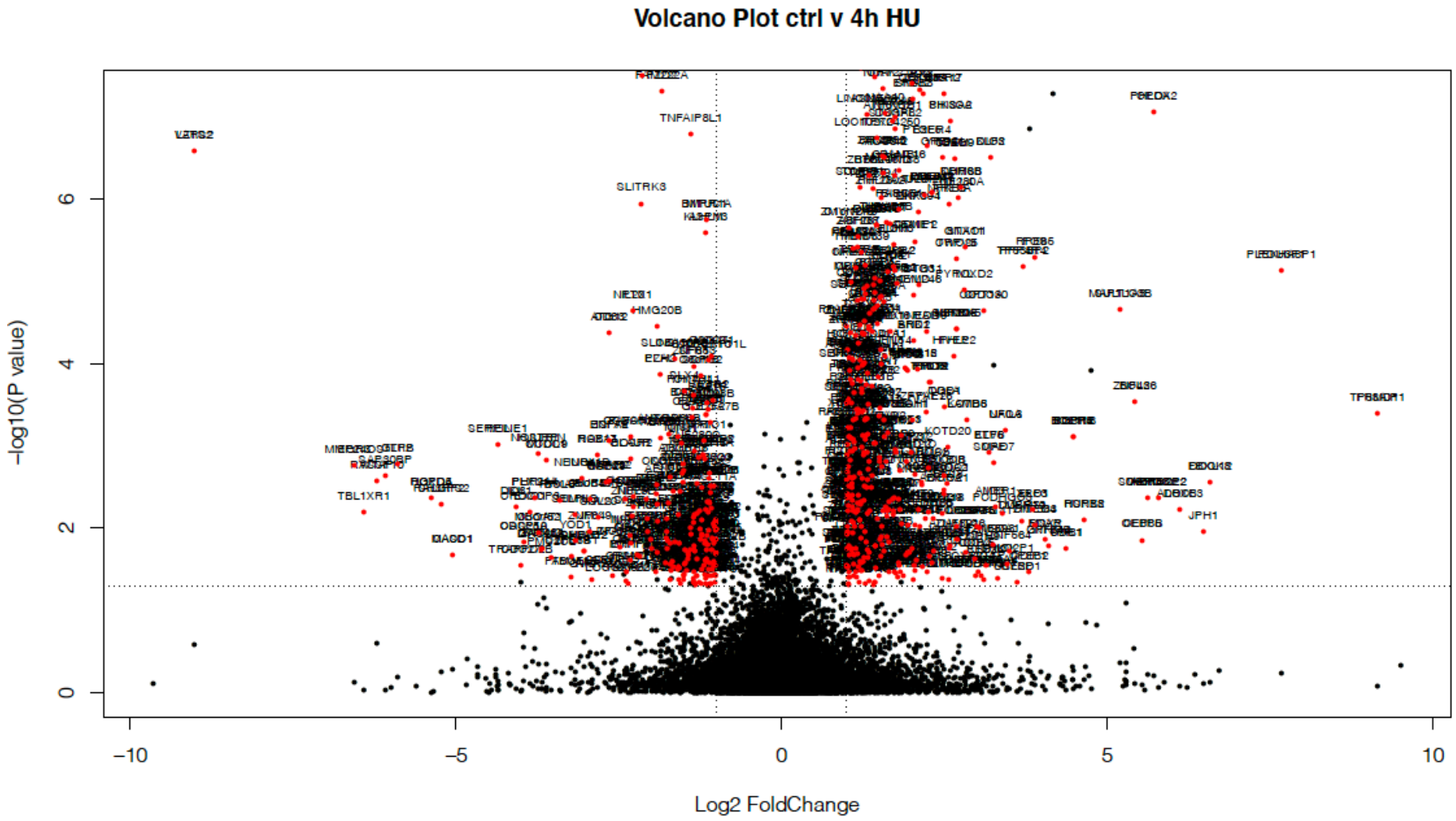

Figure 5.14. ***Differential mRNA expression, with fold difference between log$_2$ normalised expression in control and hydroxyurea (2 mM) treated HCC1806 cells plotted versus −log$_{10}$ P-value (n=2).*** *Each dot represents a transcript. Red coloured dots were classed as Log$_2$ Fold Change ≥ \|1\| and p-value ≤ 0.05.*

When GO BP enrichment analysis was performed for the downregulated DEGs, I found significant depletion for processes including "Neurogenesis" (FDR = 3.3E-06) and "Cell Division" (FDR = 1.5E-04) in response to HU-treatment. The comparative transcriptomic analysis between HU-treated and untreated HCC1806 cells confirmed the downregulation of putative regulators of nervous system development and neuron differentiation, such as *FOXA1, DNMT3B, HOXA2* and *YAP1*. Previous research has indeed shown that the self-renewal capacity of stem-cells, particularly neural stem cells, is significantly impaired by hydroxyurea treatment, leading to compromised neuronal differentiation and a decreased proportion of neurons (Dong et al., 2014). Furthermore, I also identified significant downregulation of cell cycle-related genes including *CCNF*, which controls E2F1 ubiquitylation and degradation during the G_2/M transition (Burdova et al., 2019), *CCNA2,* and *BUB1* and *BUB1B*, central components of the spindle assembly checkpoint (Jia, Li, & Yu, 2016).

GO BP enrichment analysis for the upregulated DEGs at T4 (post-HU treatment) revealed enrichment for processes such as "Regulation of RNA metabolic process" (FDR = 5.2E-50), "Regulation of nucleic acid-templated transcription" (FDR = 9.8E-48), and "Regulation of biosynthetic process" (FDR = 1.3E-47). Significantly upregulated DEGs associated with these processes included previously identified HU-induced genes, such as the activating E2Fs and their target genes (e.g., *E2F1, E2F2, E2F3, CCNE1)* (Bertoli, Klier, Mcgowan, Wittenberg, & De Bruin, 2013; Bertoli, Klier, McGowan, et al., 2013), the catalytic subunit of the dNTP biosynthesis enzyme ribonucleotide reductase (*RRM2)* (Zhang et al., 2009), as well as factors involved in proteasome-mediated protein degradation, such as *UBAP2* and *UBE2D1,* which promote repair of broken replication forks by HR (Schmidt et al., 2015).

Furthermore, I identified upregulation of chromatin remodellers and modifiers, such as *HDAC9, KDM6B,* and *INO80,* DNA repair factors, such and *BRCA2*, and checkpoint signalling proteins, such as *CDKN1A* and *TP53INP2.* The increase in repair and proteasome components parallels the recently reported yeast chromatome changes observed after exposure to hydroxyurea (Hurst et al., 2021) or oxidative damage (Challa et al., 2021).

5.5.3 MicroRNA Target Transcript Predictions in Response to Hydroxyurea

Next, the most strongly upregulated miRNAs were identified (p-value < 0.05, baseMean > 10) (HU- versus untreated HCC1806 cells) (Table 5.3). As in Section 5.4.3, the *miRNAtap* v1.14.0 package was used to predict whether these upregulated miRNAs had any common target genes. Only those target genes for which the mRNA fold change was significantly correlated with the miRNA upregulation were selected (Dalman et al., 2012). This approach enabled us to explore significant miRNA-mRNA interactions involving the differentially expressed miRNAs as shown in Table 5.3.

Table 5.3. ***Top 5 most upregulated miRNAs 4 hours post-HU (T4 vs control).***

id	***baseMean***	***Log_2 FoldChange***	***LFC SE***	***p-value***
hsa-mir-124-3p	19.416050	7.495928	3.715732	0.043659096
hsa-mir-518a-3p	6.573710	6.273850	2.627752	0.016961803
hsa-mir-519d-3p	17.120662	6.048490	2.152644	0.004957284
hsa-mir-520h	9.614768	5.467981	2.307853	0.017822112
hsa-mir-516a-5p	22.128458	4.774097	1.944450	0.014078955

As several miRNAs were commonly upregulated at both the T2 (2 hours post-IR) and T4 (4 hours post-HU) time-points when compared to the untreated condition, despite the different sources of stress, their expression levels (normalised log_2 miRNA counts) were plotted for the various conditions (untreated cells, 2- and 6-hours post-IR, and 4-hours post HU) (Figure

5.15A). MicroRNA expression levels at these early time-points, especially 2 hours post-IR (T2) and 4 hours post-HU treatment, indeed showed very similar patterns of regulation.

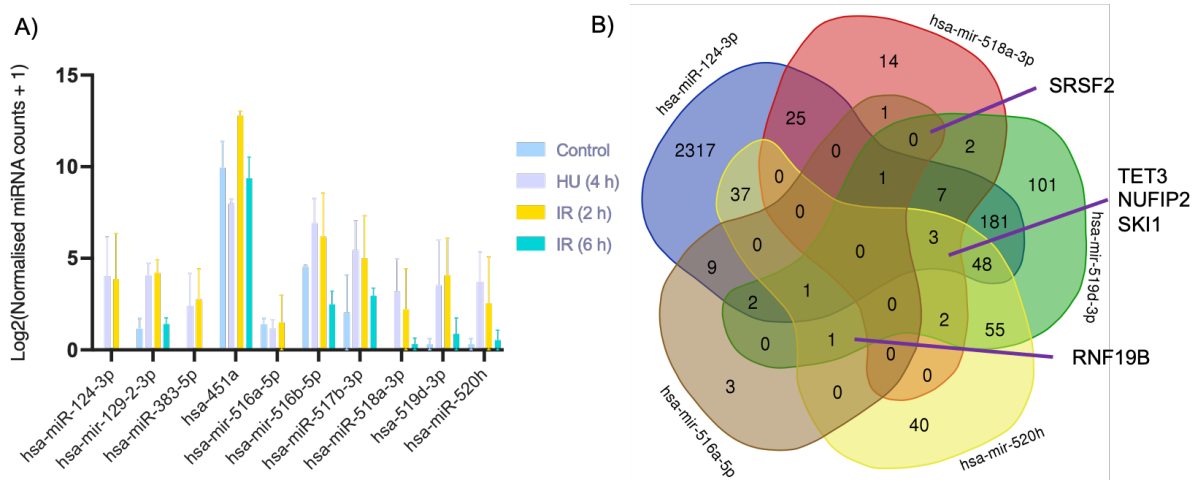

Figure 5.15. ***Upregulated miRNAs 4 hours post-HU treatment with their target-mRNAs.*** *A) Normalised microRNA read counts for overlapping upregulated microRNAs in response to HU or IR (T2). B) Venn diagram of five miRNAs, which covers the majority of the predicted target genes. The Venn diagram shows common predicted mRNA targets among five miRNAs (hsa-miR-124-3p, hsa-miR-518a-3p, hsa-miR-519d-3p, hsa-miR-520h and hsa-miR-516a-5p). Different colours represent different miRNAs. The number in the intersection represents the number of common predicted mRNA target genes among the miRNAs.*

As shown in Figure 5.15B, a total of 2,850 unique predicted targets (|LFC| > 0.58) was obtained for the upregulated miRNAs 4 hours post-hydroxyurea treatment. Overlapping mRNA targets that were common to four of the top five most upregulated miRNAs included *SKI* (LFC = 0.377), which was also identified post γ-irradiation treatment, but also a number of additional targets, including *SRSF2* (LFC = 0.394), *TET3* (LFC = 0.384), *NUFIP2* (LFC = 0.435) and *RNF19B* (LFC = 0.906).

Next, I wanted to examine the recurrence of the above associations (between the upregulated miRNAs and their target-mRNAs) across the different treatment conditions. For this analysis, I focused on hsa-124-3p, as this miRNA was upregulated in response to both IR (2 hours) and hydroxyurea. To do this, I extracted the list of miRNA-mRNA interactions and found a number

of predicted hsa-miR-124-3p mRNA-targets that were consistently downregulated across those two conditions when compared to untreated cells. These included a number of mRNAs involved in microtubule cytoskeleton organisation, such as *AURKA*, *CCDC88A*, *KNSTRN, BORA*, *TBCEL*, *PSRC1 ASPM*, *SPRY1*, *WEE1*, *CENPA*, and *FSIP2* (Figure 5.16).

To validate this bioinformatically, I explored the correlation between hsa-miR-124-3p and these predicted targets in the invasive breast carcinoma (BRCA) clinical dataset (TCGA) using StarBase v2.0 (Li et al., 2014). Indeed, when MirTarPathway was used to analyse the KEGG enriched pathways of miRNA hsa-miR-124-3p, I found enrichment of KEGG "Pathways in Cancer" (Log_{10}[FDR] = -12.57) and "Regulation of Actin Cytoskeleton" (Log_{10}[FDR]= -9.35). Bioengineered miR-124-3p was recently shown to inhibit effectively lung cancer metastasisation, partly due to the selective downregulation of proteins that form the cytoskeleton and cell-cell junctions (Deng et al., 2021). Therefore, we conclude that miR-124-3p could have an important role in preventing mitotic onset and altering cytoskeleton organisation, both in response to replication stress and DNA damage.

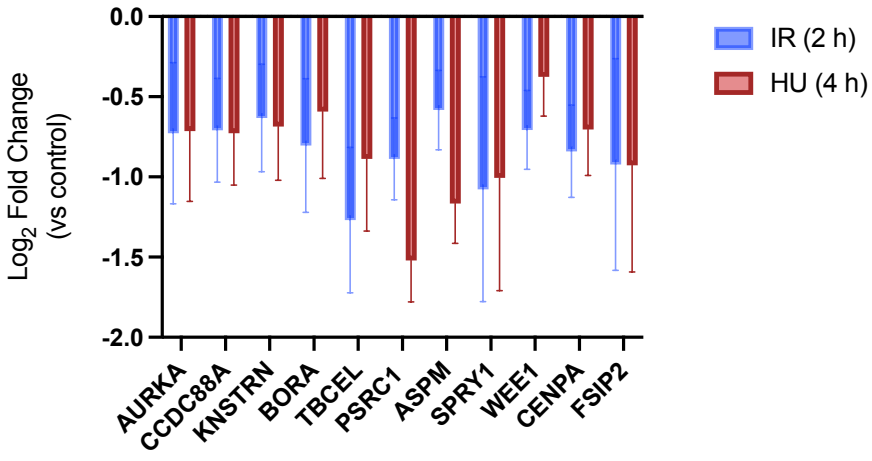

Figure 5.16. ***Expression changes of hsa-miR-124-3p-target genes involved in Microtubule Cytoskeleton Organisation following HU- or IR-treatment.*** *Log_2 Fold Changes 4 hours post HU treatment or 2 hours post-IR (T2) treatment when compared to untreated cells from mRNA-sequencing data.*

5.5.4 Roles of SETD2 and the miR-106b/25 Cluster in the Replication Stress Response

Finally, I evaluated the possible roles of SETD2 and the oncomiR-1 cluster in the DNA replication stress response. To do this, normalised microRNA counts for miRNAs of the miR-106b/25 cluster were extracted from our sRNA-sequencing data and compared between the control and HU-treated HCC1806 cells (Figure 5.17A). Here, I found that hsa-miR-25-3p, miR-93-3p, and hsa-miR-93-5p expression levels showed an upward trend in response to hydroxyurea treatment, whereas miR-106b-3p and miR-106b-5p levels were unaffected (Figure 5.17A). This contrasts with IR-induced changes, as elevated hsa-miR-25-3p, miR-93-3p, and hsa-miR-93-5p levels were found both 2- and 6-hours post IR.

To test whether the observed differences in miR-106b/25 expression levels could be a result of HU-induced cell cycle changes, miRNA levels of miR-106b/25 cluster members were measured at different stages of the cell cycle. To this end, T98G cells were synchronised using serum starvation in G_0/G_1 and subsequently released into the cell cycle using medium containing 10% FBS (Figure 5.17B). Even though miR-106b-3p levels remained stable throughout the cell cycle, I found slightly increased miR-106b-5p levels in late-G_1. Previous works established a proapoptotic role for E2F1 after DNA damage checkpoint activation (Pediconi et al., 2003; Stevens, Smith, & La Thangue, 2003) and I therefore speculated that high miR-106b-5p levels at the G_1-to-S transition might keep E2F1 activity in check during the normal physiological cell cycle to prevent E2F1-induced apoptosis.

Next, mature miR-106b/25 expression changes post-HU treatment were validated using qRT-PCR, and our observations from the sRNA-seq were confirmed. Mature miR-93-3p levels increased in the presence of HU, whereas no changes were observed for other oncomiR-1 cluster members (Figure 5.17D). I also found that the changes in miR-93-3p levels were

unlikely to result from changes in levels of its precursor miRNA (Figure 5.17C), as pre-miR-93 levels were not significantly altered.

Finally, I evaluated changes in *SETD2* mRNA levels and the E2F-dependent transcriptional response following hydroxyurea treatment in HCC1806 cells. Previous work has already shown that the G_1/S transcriptional program can get reactivated through the DNA replication checkpoint (Bertoli, Klier, McGowan, et al., 2013). Indeed, hydroxyurea-induced replication stress induced the activating E2Fs, *E2F1* and *E2F3*, and several E2F-target genes, including *CDT1, CDC6, RRM2* and *MCM2-7* (Figure 5.18A). Increased E2F-dependent transcription in response to DNA replication stress could additionally be validated using qRT-PCR (Figure 5.18B). In this cell line, no changes in *SETD2* expression were observed in response to HU-induced replication stress.

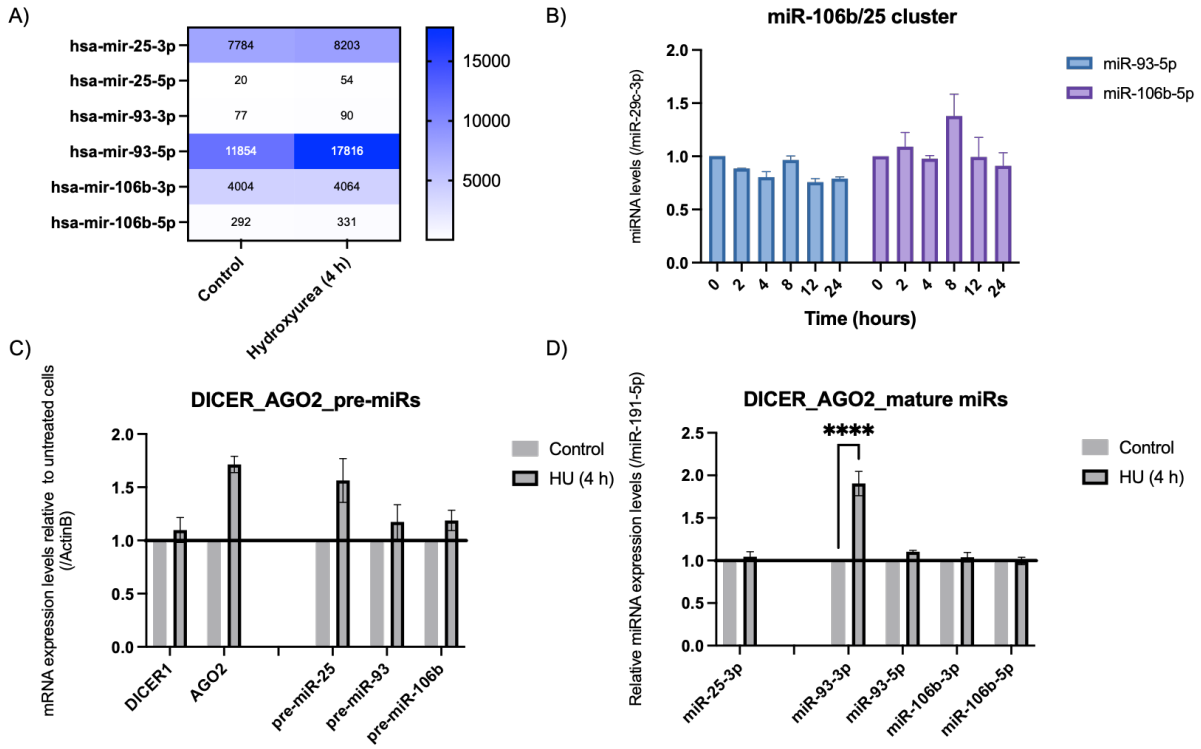

Figure 5.17. ***Upregulation of miR-93-3p in response to hydroxyurea treatment.*** *A) Expression levels (normalised microRNA read counts) for microRNAs of the miR-106b/25 cluster in untreated or HU-treated (2 mM, 4 hours) HCC1806 cells from the sRNA-sequencing data. B) Quantification of miR-106b-3p and miR-106b-5p levels at different time points following cell-cycle re-entry using qRT-PCR. To obtain cells in the different phases of the cell cycle, the starved T98G cells were incubated with serum-containing medium and collected at the indicated time points. C-D) Validation of expression changes in the precursor (C) and mature miRNA levels (D) of members of the oncomiR-1 cluster in response to HU treatment in HCC1806 using qRT-PCR. Significance calculated with a two-way ANOVA. Data represented as mean ± SEM (n=3).*

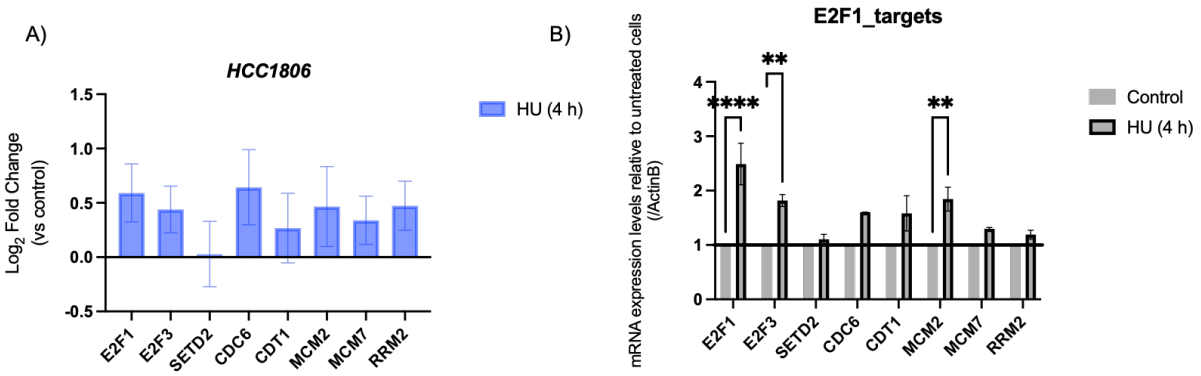

Figure 5.18. ***E2F-dependent transcription in response to hydroxyurea treatment****. A) Log₂ Fold Change of SETD2, E2F1, E2F3, MCM2, MCM7, CDT1, CDC6, and RRM2 expression levels 4 hours post HU treatment when compared to untreated cells from mRNA-sequencing data. B) qRT-PCR validation of (A). Data represented as mean ± SEM (n=3).*

5.6 Chapter Discussion

The cellular responses to both DNA damage and replication stress are complex and multi-step, involving the transcriptional and post-transcriptional regulation of genes involved in cell cycle regulation and DNA repair. Even though previous studies have demonstrated the involvement of miRNAs in the DDR (Wang & Taniguchi, 2013), there are fewer reports on whether, and how, miRNAs can regulate or fine-tune the transcriptional response to differentiate between different types of insults.

Our results demonstrate that the early miRNA responses to DNA damage and replication stress are markedly similar, with overlapping differentially expressed miRNAs in IR- and HU-treated HCC1806 cells when compared to untreated cells. Multiple shared upregulated miRNAs between IR (T2) and HU were identified, such as hsa-miR-124-3p, which targets multiple genes involved in cytoskeleton organisation. Its upregulation was previously shown to cause cell cycle arrest and the induction of apoptosis (Nolan et al., 2020). Our data therefore suggests that the initial cellular response to external stress-inducing factors is universal and mostly involves the inhibition of cell cycle progression, whereas the fraction of miRNAs and genes that respond to all stresses diminishes over time, instead shifting toward the expression of stress-specific miRNAs and genes.

One such example is miR-7704, which was upregulated in response to IR (T6), but not following HU-induced replication stress. We found a negative miRNA-mRNA correlation between miR-7704 and *KDM6B*, which encodes a histone H3K27 demethylase (Hong et al., 2007). This recurrent miRNA-mRNA interaction was identified across the different treatment conditions, with on the one hand, high miR-7704 and low *KDM6B* levels in response to IR, and on the other, unchanged miR-7704 and elevated *KDM6B* levels in the presence of

hydroxyurea-induced replication stress. Recently, a *BioRxiv* paper suggested that KDM6B can promote E2F-dependent transcription via H3K27me3-dependent enhancer-promoter interactions (D'Oto et al., 2020). If this were confirmed in our system, the miR-7704-KDM6B axis, and its consequent epigenetic reprogramming, could underlie differential gene expression changes, especially of the CDK4/6-pRB-E2F pathway, in response to different sources of damage.

We do indeed show that E2F-dependent G_1/S transcription is maintained in response to HU-induced replication stress, but not in response to DNA damage, in accordance with previous reports (Bertoli, Klier, McGowan, et al., 2013; Travesa et al., 2012). This was evidenced by elevated expression levels of the activating E2Fs, E2F1-3, and their targets, including genes involved in DNA repair and nucleotide synthesis, following HU treatment. Interestingly, aside from its possible correlation with hsa-mir-7704, we find that the absence of an E2F-dependent transcriptional response in the presence of DNA damage was also accompanied by upregulation of miR-106b-5p, whose levels were shown to correlate with E2F1 expression levels in the previous chapter. Upregulation of miR-106b-5p and miR-7704 in response to ionising radiation could therefore prevent the induction of E2F1 activity and thereby the expression of specific pro-apoptotic genes at early time-points, to allow for repair before signalling programmed cell death.

When transcriptome changes in response to IR-inflicted DNA damage were further characterised, I identified the downregulation of FOXM1-mediated transcripts, including *CCNB1, CENPF* and *PLK1,* in response to IR. This is in accordance with a recent study performed in glioblastoma (Choudhary et al., 2020), where FOXM1 was identified as a master-regulator of radiation-induced transcriptome changes. FOXM1 facilitates transcription of

mitotic genes (Laoukili et al., 2005), under direct control of both CDK1 and DNA damage checkpoint proteins. Previous studies have found that ATR prevents untimely cyclin B expression in S-phase, to counter premature activation of the FOXM1-driven promitotic programme (Saldivar et al., 2018). One could therefore predict that FOXM1-mediated downregulation of these mitotic transcripts prevents premature mitotic entry and subsequent DNA damage in the presence of DNA damage.

In summary, the key findings of this chapter are:

- The early miRNA responses to HU and IR are remarkably similar, with shared upregulation of miR-124-3p, which targets the actin cytoskeleton.
- IR-induced transcriptional changes are largely governed by reduced activity of the pro-mitotic transcription factor FOXM1.
- Replication stress causes more widespread changes to the transcriptome, with nearly 8% of all quantified genes, including E2F-dependent transcripts, significantly changed in abundance.

Chapter 6

SETD2-dependent H3K36me3 Regulates E2F-dependent Transcription as Part of the DNA Replication Stress Checkpoint Response

6.1 Introduction

Entry into S-phase is accompanied by increased transcription of *RRM2*, the regulatory subunit of ribonucleotide reductase (RNR), which catalyses dNTP production and facilitates DNA synthesis in S-phase (Chabes et al., 2004; DeGregori et al., 1995). Previous studies from our group have demonstrated that transcription of *RRM2* requires the SETD2-catalysed epigenetic mark H3K36me3 (Pfister et al., 2015). In Chapter 4, the positive correlation between *SETD2* and *RRM2* expression levels was confirmed in a panel of breast cancer cell lines. However, the mechanism by which SETD2, or SETD2-dependent H3K36me3, regulates *RRM2* expression levels in mammalian cells is not yet understood.

Studies in fission yeast have shown a role for Set2-dependent H3K36 methylation in promoting MluI cell-cycle box (MCB) binding factor (MBF)-complex-dependent transcription (Pai et al., 2017). Loss of Set2 in *S. pombe* leads to reduced MBF-dependent expression of RNR, of which *cdc22* is the large subunit, and consequently, reduced deoxyribonucleoside triphosphate (dNTP) synthesis (Pai et al., 2017). Reduced dNTP pools cause S-phase delays and alter DNA replication origin firing. In mammalian cells, transcription of *RRM2* is dependent on the transcription factor E2F1 (Chabes et al., 2004; DeGregori et al., 1995), which is functionally analogous to the MBF complex in *S. pombe*. Hence, I asked whether the role for SETD2-dependent H3K36 trimethylation in facilitating E2F-dependent cell cycle transcription could be conserved across species.

DNA replication stress, arising from both endogenous (e.g., oncogene amplification) and exogenous (e.g., ribonucleotide reductase inhibitors, such as hydroxyurea) sources can cause RF slowing or stalling (Zeman & Cimprich, 2014). Impediments of RF progression during DNA synthesis can lead to exposure of extended lengths of ssDNA, which can act as a platform for RPA binding and activation of ATR- and CHK1- dependent signalling. Activation of this S-phase checkpoint, also referred to as the replication stress checkpoint, results in arrest and stabilisation of ongoing RFs to prevent their collapse and the subsequent generation of DNA damage (Iyer & Rhind, 2017), prohibits cell cycle progression, and inhibits global origin firing to prevent the duplication and segregation of under-replicated DNA. Furthermore, the S-phase checkpoint actively maintains E2F-dependent transcription in the presence of replication stress via CHK1-dependent phosphorylation and inactivation of E2F6 (Bertoli, Klier, McGowan, et al., 2013; Bertoli, Skotheim, et al., 2013). The ability of cells to activate G_1/S transcription under these conditions is crucial for survival because E2F-targets include proteins that prevent RF collapse and DNA damage, those that allow replication to resume after the arrest (e.g., CtIP and RAD51), and those that allow for dNTP production for DNA synthesis, such as *RRM2* (Choi and Kim, 2019). Therefore, induction of E2F-dependent transcription, both at the G_1-to-S transition, and under replication stress conditions, is essential to ensure faithful completion of DNA replication before the onset of mitosis.

In this chapter, I therefore addressed the following questions:

- Can SETD2-dependent H3K36me3 facilitate E2F-dependent transcription in mammalian cells?
- Does SETD2 promote the transcriptional checkpoint response in the presence of hydroxyurea-induced replication stress?

- Could a role for SETD2-dependent H3K36me3 in maintaining E2F-dependent transcription in S-phase be attributed to a function for SETD2 in modulating checkpoint activation?

6.2 SETD2-depletion Causes Altered Transcription Factor Binding

To determine whether SETD2 modulates gene expression of a specific subset of (co-regulated) genes, we compared the expression profiles of *SETD2*-deficient cells with their wild-type counterparts. RNA-sequencing of asynchronous parental U2OS cells and two *SETD2* CRISPR KO U2OS clonal lines was performed previously (Armfield, 2019), and revealed very distinct transcriptional profiles with over 1300 differentially expressed genes (DEGs) between *SETD2* KO and *SETD2* wild-type U2OS cells. A total of 726 upregulated and 575 downregulated DEGs were extracted and, to infer the biological significance of SETD2-driven gene expression changes and their potential modes of regulation, I then tested both the up- and downregulated DEGs for statistical overrepresentation of GO terms using ShinyGO v0.66 (Ge et al., 2020).

GO Molecular Function (MF) enrichment analysis for the downregulated DEGs in the *SETD2*-depleted (KO) cells when compared to the parental cell line, revealed enriched GO-terms of MF such as “Kinase Binding” (Enrichment FDR value of 3.3E-05), “TF Binding” (Enrichment FDR value = 1.6E-06), and “Chromatin Binding” (Enrichment FDR value of 2.1E-03) (Figure 6.1A). GO MF enrichment analysis for the upregulated DEGs (Figure 6.1B) showed that these genes were enriched for different MFs, including “Metal Ion Binding” (Enrichment FDR value = 4.4E-04), “Extracellular Matrix Structural Constituents” (Enrichment FDR value = 6.4E-04), and “Proteoglycan Binding” (Enrichment FDR value = 4.4E-04) (Figure 6.1B).

Recent studies have identified Fibrillin 1 (*FBN1*), which is an important glycoprotein component of the extracellular matrix (Sakai, Keene, & Engvall, 1986), as a novel cellular target of SETD2 (Schuhmacher et al., 2020). *SETD2* KO cells showed significantly increased expression levels of *FBN1* when compared to *SETD2* WT U2OS cells (LFC = 1.03504, p-value = 0.00035). Our data therefore supports the notion that SETD2 plays an important role in regulating cell-cell adhesion and extracellular matrix composition, perhaps through methylation of Fibrillin 1, or other yet undiscovered pathways.

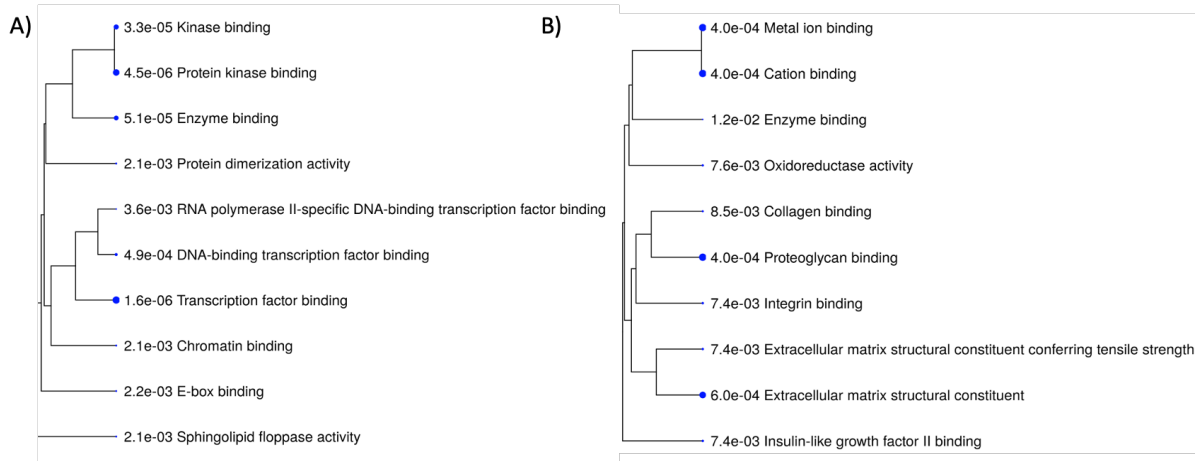

Figure 6.1. ***Downregulated genes in the SETD2-depleted cells were enriched for molecular functions, such as transcription factor binding.*** *GO Molecular Function overrepresentation analysis for the downregulated (A) and upregulated (B) DEGs in SETD2-deficient U2OS cells when compared to the control cells. Enrichment FDR values shown in figure.*

SETD2 modulates chromatin structure via co-catalysis of H3K36me3 over gene bodies during transcriptional elongation (Edmunds et al., 2008; Kizer et al., 2005; Li et al., 2003). Recently, however, SETD2 was also shown to bind to gene promoter regions (Bhattacharya, Levy, et al., 2021), where it could control gene expression via the recruitment of other TFs or RNAPII directly. Consistent with this potential role for SETD2 as transcriptional activator, I further characterised the DEGs that were downregulated in the absence of SETD2 (i.e., those that were likely to be under positive control of SETD2). As the most significantly enriched categories for the downregulated DEGs by GO MF were related to TF binding, or RNAPII-specific TF

binding (Figure 6.1A), I explored whether this subset of genes was under the control of a particular transcription factor (TF) or a set of TFs. To do this, TF factor enrichment analysis (TFEA) was performed using information derived from the hundreds of ChIP-seq experiments from the ENCODE Consortium (Dunham et al., 2012). 455 out of 575 significantly downregulated genes, including *E2F1* and *E2F2* themselves, were putative E2F6 target genes (Figure 6.2A, enrichment FDR = 8.9e-44). E2F6 is a repressor of E2F-dependent G_1/S transcription and therefore shares many of its targets with E2F1-3 (Giangrande et al., 2004). Furthermore, 463 out of 575 downregulated DEGs were KDM4A targets, which has previously been shown to enhance E2F1 chromatin binding and transcriptional activity (Wang et al., 2016).

A)

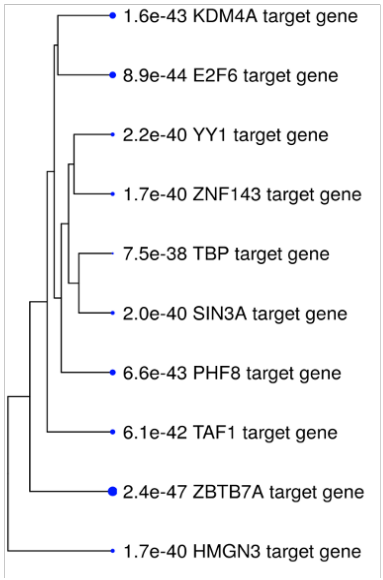

B)

Enrichment FDR	Genes in list	Total genes	Functional Category
6.2E-31	569	15100	TBP target gene
6.7E-28	570	15437	SIN3A target gene
3.2E-27	538	14134	PHF8 target gene
3.0E-26	560	15172	MXI1 target gene
6.4E-25	550	14876	CHD2 target gene

Figure 6.2. ***TFEA for down- and upregulated DEGs in SETD2 CRISPR KO U2OS cells.*** *Downregulated (A) and upregulated (B) DEGs in SETD2 CRISPR KO cells when compared to the wild-type cells were analysed using the ShinyGO tool for Encode Transcription Factor (TF) targets. Putative TFs showing enrichment are listed based on their FDR. Enrichment FDR values shown in figure.*

Additionally, TFEA analysis for the upregulated DEGs in the *SETD2*-depleted cells revealed enrichment for predicted TATA-box-binding protein (TBP) targets (Figure 6.2B, FDR = 6.2E-31). TBP binds to conserved TATA box DNA sequences to ensure accurate transcription initiation by RNAPII (Tora & Timmers, 2010). Previous studies have already proposed that

H3K36me3 might recruit histone deacetylase complexes (HDACs) and prevent histone exchange to maintain a repressive chromatin environment to limit cryptic transcription from these TATA-like elements (Difiore et al., 2020). I subsequently cross-validated these results using the ChIP Enrichment Analysis (ChEA) software, which uses genome-wide transcription-factor ChIP-X experiments to further predict TF binding (Lachmann et al., 2010). Interestingly, TBP targets did not come up as significantly enriched. Instead, ChEA analysis identified a significant enrichment for *NFE2L2*-targets (Enrichment FDR value of 4.9E-07), a transcription factor that regulates the cellular response to toxins and oxidative stress (Ma, 2013). Furthermore, upregulated DEGs were significantly enriched for *TP53* targets (Enrichment FDR value of 1.1E-07). Upregulation of p53 and its target genes is typically indicative of the presence of DNA lesions and our findings therefore suggest that loss of *SETD2* causes elevated levels of endogenous DNA damage.

6.3 Loss of SETD2 Causes Reduced Expression of E2F-dependent Transcripts

As I identified enrichment for E2F6- and KDM4A-TF activity among the downregulated DEGs between *SETD2* CRISPR KO U2OS and *SETD2* wild-type cells (Figure 6.2), I asked whether epigenetic and transcriptional control of the G_1-to-S boundary was conserved from fission yeast into human cells. Analogously to a function for Set2 in promoting MBF-transcription activation in *S. pombe* (Pai et al., 2017), it was hypothesised that human SETD2 could facilitate E2F-dependent transcription in mammalian cells.

First, expression levels of all transcripts were extracted as normalised FPKM (Fragments Per Kilobase of transcript per Million mapped reads) values. Next, the log-transformed $\log_2$(FPKM + 1) values of selected E2F-target genes showing differential expression (p-value<0.05) were plotted for each condition, i.e., for *SETD2* wild-type U2OS cells (P_1) and the *SETD2* KO

U2OS cells (SET2_1) (n=2) (Figure 6.3A). As seen in Figure 6.3A, loss of *SETD2* caused reduced expression levels of the activating E2F transcription factors, *E2F1* and *E2F2*, and many of their target genes, including *CDT1*, *MCM4*, and *RRM2*. E2F6 transcript levels were unaffected (not shown).

Next, I tested whether these mRNA expression changes caused consequent changes in protein expression. To this end, Western Blot analysis of H3K36me3, H3, E2F1, and minichromosome maintenance 2 (MCM2) levels was performed using protein extracts from asynchronous *SETD2* WT and *SETD2* KO U2OS cells (Figure 6.3B). I confirmed that *SETD2* KO U2OS cells displayed strongly reduced levels of H3K36me3, consistent with previously published data (Pfister et al., 2015). However, I did find there was some H3K36me3 remaining, suggesting there might either be more copies of *SETD2* in this cell line, or that other methyltransferases, such as PRDM9, can catalyse H3K36me3 in the absence of *SETD2* (Eram et al., 2014). Further, I found that loss of *SETD2* caused a reduction in the protein levels of E2F1 and one of its targets, MCM2 (Figure 6.3B).

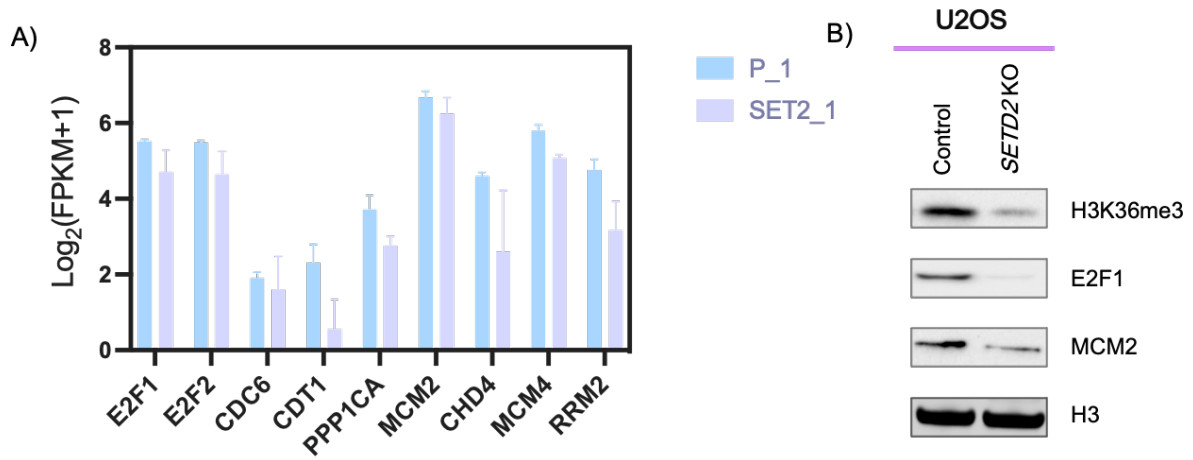

Figure 6.3. ***E2F-target genes are downregulated in SETD2 CRISPR KO U2OS cells when compared to SETD2 WT U2OS cells.*** *A) Graph showing log_2(1 + FPKM, Fragments Per Kilobase of transcript per Million) values for significantly differentially expressed E2F-target genes in Parental (P_1) and SETD2 KO U2OS cells (SET2_1). B) Western blot analysis of H3K36me3, E2F1, MCM2, and Total H3 protein levels in SETD2 WT and SETD2 CRISPR KO U2OS (Pfister et al., 2015) cells.*

As we know that transcription of E2F-target genes is strongly cell-cycle regulated (Bertoli, Skotheim, et al., 2013), it was important to exclude the possibility that these observed mRNA and protein expression changes were an artefact of differential *SETD2* WT and *SETD2* CRISPR KO cell cycle profiles. This analysis has already been performed by another student, and thus fall beyond the scope of this thesis. They found, however, consistent decreases in mRNA and protein levels of E2F1 and E2F2, as well as E2F-target genes CDC6, CDT1, and RRM2 both in G_1-synchronised *SETD2* CRISPR KO U2OS cells when compared to the parental U2OS cells and following siRNA-mediated depletion of SETD2 in G_1-synchronised T98G cells (Armfield, 2019). We can therefore conclude that SETD2-dependent regulation of E2F-target gene expression is independent of SETD2's role in cell cycle progression and DNA damage-induced p53 activation (Carvalho et al., 2014). Our findings, therefore, suggest a universal role for SETD2 in facilitating transcription of E2F-target genes under physiological conditions in human cells, and functionally equivalent MBF-target genes in fission yeast.

6.4 SETD2-dependent H3K36me3 Mediates E2F1-binding to its Target Genes in G_1

Next, I asked whether the role for SETD2 and H3K36me3 in facilitating E2F-dependent transcription was mediated by altered E2F1 transcription factor activity directly, or via other, more indirect mechanisms. To do this, the effect of *SETD2* depletion on the DNA binding ability of E2F1 to the endogenous promoters of well-described E2F1-target genes including *CDC6*, *MCM2*, and *CDT1* was examined by ChIP. T98G cells were transfected with control siRNA or siRNA targeting SETD2 and synchronised in G_1 by serum starvation (for 48 hours). We performed ChIP-qPCR in G_1-synchronised T98G cells, as we know from previous work in fission yeast (Pai et al., 2017) and mammalian cells (Armfield, 2019), that loss of *SETD2* causes problems during S-phase entry and progression.

First, siRNA-mediated depletion of SETD2 was validated in T98G cells using western blot analysis for the histone mark H3K36me3 (Figure 6.4A). Knockdown of SETD2 in T98G cells caused a reduction in H3K36me3 (Figure 6.4A), whereas total H3 levels remained unchanged.

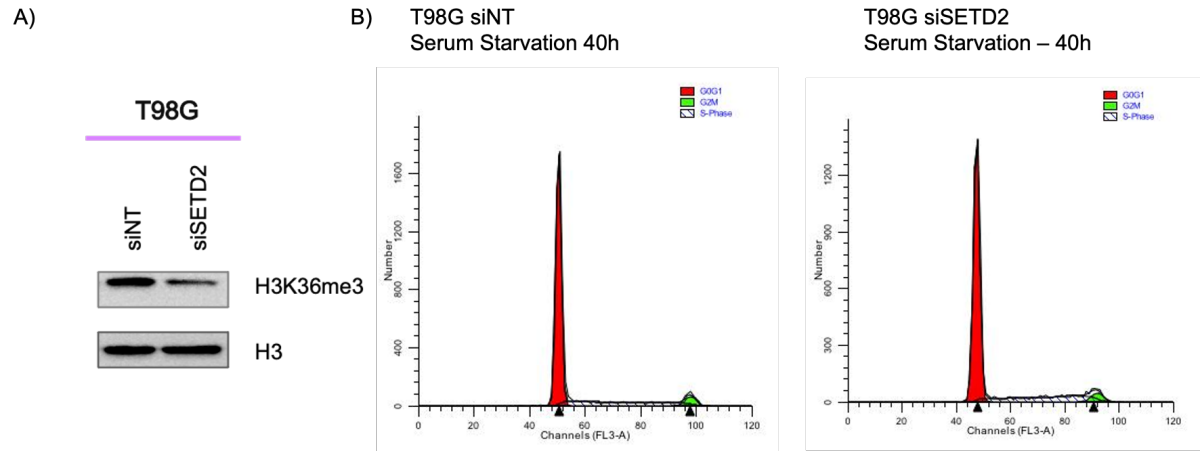

Figure 6.4. ***Knockdown of SETD2 in synchronised T98G cells was confirmed using WB for H3K36me3.*** *A) Western blot analysis of H3K36me3 and H3 protein levels in T98G cells 48 hours transfection with a non-targeting control siRNA or SETD2 siRNA. B) FACS cell cycle profile (using propidium iodide) of synchronised T98G cells, transfected with an siRNA targeting SETD2 or a control siRNA. The data shown are from a single representative experiment out of three repeats.*

I also analysed the cell cycle profiles of synchronised T98G cells (T= 0 hours post-release) using FACS and propidium iodide staining (PI) and found that the large majority of T98G cells were rendered quiescent by serum starvation (T98G siNT: 86.25% G_1 cells and T98G siSETD2: 85.56% G_1 cells) (Figure 6.4B).

Next, we analysed binding of E2F1 to the promoter regions of a subset of genes, including *CDC6*, *MCM2*, and *CDT1* following siNT or SETD2 siRNA transfection in synchronised T98G cells. As shown in Figure 6.5, E2F1 binding to the *CDC6* and *MCM2* promoter regions was significantly reduced following SETD2 knockdown (Figure 6.5), indicating that the

observed reduction in E2F-target expression is due to reduced binding of E2F1 to the endogenous promoters of these genes.

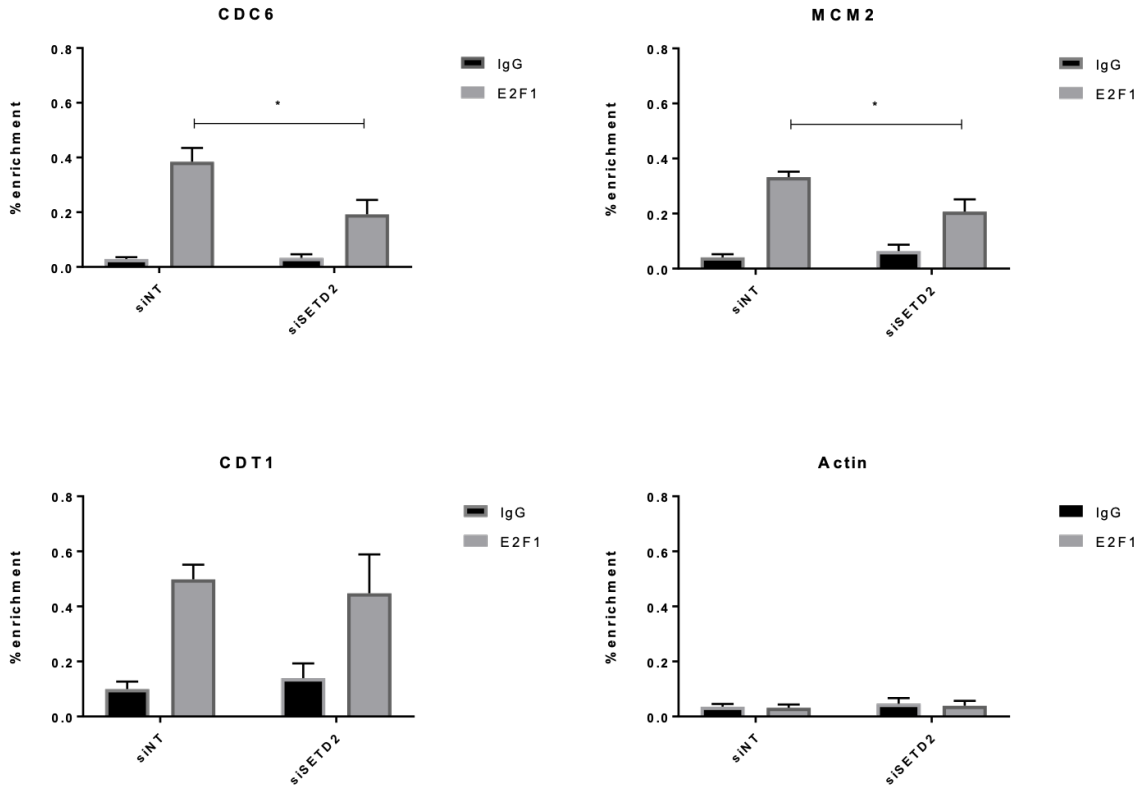

Figure 6.5. ***ChIP-qPCR analysis of E2F1 occupancy on CDC6, CDT1, and MCM2 promoters in T98G cells treated with siNT or siSETD2 using IgG or anti-E2F1 antibodies****. ChIP DNAs were analysed by qPCR with primers that amplify promoter regions for each gene. Data represented as mean ± SEM (n=3). *ChIP analysis was performed with the help of Simon Carr.*

6.5 SETD2 and H3K36me3 Levels Peak Prior to Entry into S-phase

The activating E2Fs (E2F1-3) induce transcription of their target genes, including *RRM2*, *CCNE2* (S-phase-specific cyclin E2), and *MCM7* (component of the CMG helicase for DNA replication) at the G_1-to-S transition to facilitate DNA synthesis (Bertoli, Skotheim, et al., 2013). Previous studies in both fission yeast and human cells have shown histone H3K36 trimethylation to be similarly cell-cycle regulated, with H3K36me3 levels peaking at the G_1-to-S transition (Li et al., 2013; Pai et al., 2014).

I therefore wanted to test whether deposition of H3K36me3 and induction of E2F-target gene expression occurred simultaneously and asked whether cellular oscillations of *SETD2* mRNA and H3K36me3 protein levels occurred, as previously reported, in our T98G cell system. To this end, T98G cells were synchronised in G_0 using serum starvation, released back into the cell cycle after serum addition, and collected at the indicated time-points for qRT-PCR analysis (T= 0-, 2-, 4-, 8-, 12- and 24-hours post-FBS addition) (Figure 6.6A). Expression levels of *CCNB1* (Cyclin B1), which is induced in late S-phase and peaks in late G_2 or early mitosis (Fung & Poon, 2005), Polo-Like Kinase 2 (*PLK2*), which functions as regulator of G_1 progression in cycling cells (Ma, Charron, & Erikson, 2003), and Geminin (*GMNN*) and Proliferating Cell Nuclear Antigen (*PCNA*), both important for DNA replication, were utilised to determine the cell cycle phase of T98G cells.

As shown in Figure 6.6A, cells induced expression of *PLK2* upon addition of serum as they re-entered the cell cycle. They subsequently entered S-phase between 8-12 hours post-serum addition, as shown by increased *PCNA* and *GMNN* transcription. At 24 hours post-release, cells were in late-S- or early G_2-phase, as shown by high *CCNB1*, and decreasing *GMNN* expression levels (Figure 6.6A). Next, expression levels of these cell cycle markers were used to determine *E2F1* and *SETD2* levels throughout the cell cycle, at the same time-points post-G_0-release. Here, we found that *E2F1* and *MCM7* mRNA levels increased at 8 hours and peaked at 12 hours post-serum addition, in accordance with S-phase entry (Figure 6.6B). Interestingly, however, *SETD2* mRNA levels peaked in quiescent cells (T= 0 hours), then decreased in G_1, and further decreased upon S-phase entry (Figure 6.6B).

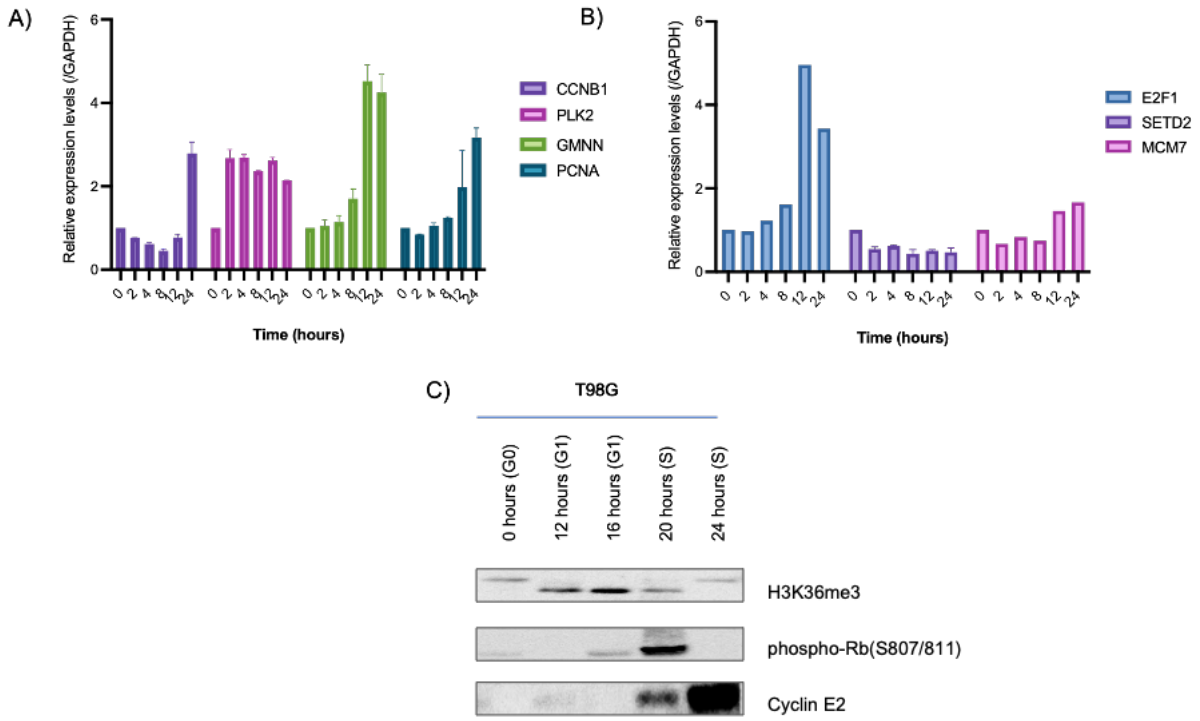

Figure 6.6. ***Levels of H3K36me3 peak at the G_1-to-S transition and decrease in S-phase.*** *To obtain cells in the different phases of the cell cycle, the starved T98G cells were incubated with serum-containing medium and collected at the indicated time points. A) Quantification of CCNB1, PLK2, GMNN, PCNA, and B) E2F1, SETD2, and MCM7 transcript levels at different time points following cell-cycle re-entry using qRT-PCR, normalised to GAPDH expression levels. Data represented as mean ± SEM (n=3). C) Western Blotting was used to test the expression of H3K36me3, p-Rb and Cyclin E2.*

Next, I investigated protein levels of H3K36me3 and the *RB1* gene product pRB, which, in its phosphorylated state, releases the E2F transcription factors to induce S-phase transcription, using the same T98G block and release experiment (Figure 6.6C). Here, I found that synchronised T98G cells entered S-phase between 16 and 20 hours, as evidenced by increased p-Rb and cyclin E2 levels (Figure 6.6C). Similar to previously published data (Li et al., 2013; Pai et al., 2014), I found that H3K36me3 levels peak at the G_1.S transition, when RB is inactivated to allow for full activation of E2F transcription (Figure 6.6C), and significantly decline in middle and late S-phase. Interestingly, however, the α-H3K36me3 antibody detected two different band sizes for H3K36me3, which seem to be cell-cycle regulated (Figure 6.6C).

The appearance of higher bands could correspond with increasingly modified H3, possibly as a result of DNA replication-coupled phosphorylation (e.g., H3S10ph) (Crosio et al., 2002) or acetylation (e.g., H3K56ac) (Kaplan et al., 2008) events, and would therefore explain complete loss of lower bands. Together, these results further support that SETD2-dependent H3K36 trimethylation regulates the binding of E2F1 to its target genes during the G_1/S transition, thereby regulating their expression.

6.6 SETD2 Mediates E2F1-Target Expression in Response to Replication Stress

Under normal conditions, phosphorylation by CDK2-cyclin A removes activating E2Fs (E2F1-3) from target gene promoters upon S-phase entry to prevent expression of E2F-target genes during S-phase, which may lead to re-replication (Xu, Sheppard, Peng, Yee, & Piwnica-Worms, 1994). As described in the introduction, however, E2F transcription can be actively maintained throughout S-phase in the presence of replication stress, via CHK1-dependent phosphorylation and inactivation of E2F6 (Bertoli, Klier, Mcgowan, et al., 2013; Giangrande et al., 2004). Therefore, I hypothesised SETD2 and H3K36me3 might not only be required for expression of E2F-target genes under normal physiological conditions, but also in S-phase following hydroxyurea-induced replication stress.

To test this, replication stress was induced in asynchronous U2OS cells treated with siNT or siSETD2 by treatment with 2 mM hydroxyurea (HU) for 4 hours (Figure 6.7A), after which RNA was extracted and subjected to mRNA-sequencing analysis. From the mRNA-seq, I observed HU-induced upregulation of 138 genes (Figure 6.7A), including E2F1-target genes, such as *CCNE2*, *PCNA*, and *CDC25A*. HU-induced genes were enriched for Reactome pathways including "*TP53* Regulates Transcription of Cell Cycle Genes" (FDR = 5.43E-05) and "Transcriptional Regulation by *TP53*" (FDR = 0.000123) (Figure 6.7B). To test whether

SETD2 was required to induce p53- and E2F1-targets in the presence of HU, I also looked at RNA-seq data from cells treated with 2 mM HU for 4 hours in U2OS cells where SETD2 was depleted using siRNA-based methods (Figure 6.8A). In accordance with previously published ChIP data, where HU-induced upregulation of E2F-target genes *RAD51, CtIP,* and *RRM2* was found to be accompanied by increased H3K36me3 levels (Armfield, 2019), I found that HU treatment failed to induce a similar transcriptional response in U2OS cells transfected with siSETD2. In U2OS cells transfected with siSETD2 and treated with HU for 4 hours, I found only 61 upregulated DEGs (Figure 6.8B), and no significantly enriched Reactome Pathways (FDR cut-off value of 0.05). Previously, we had already shown that, while a strong upregulation of E2F1-dependent transcripts was observed in *SETD2* wild-type cells, SETD2-depleted T98G cells (using an siRNA targeting SETD2) showed significantly decreased levels of E2F1 target gene induction after hydroxyurea-induced replication stress (Armfield, 2019).

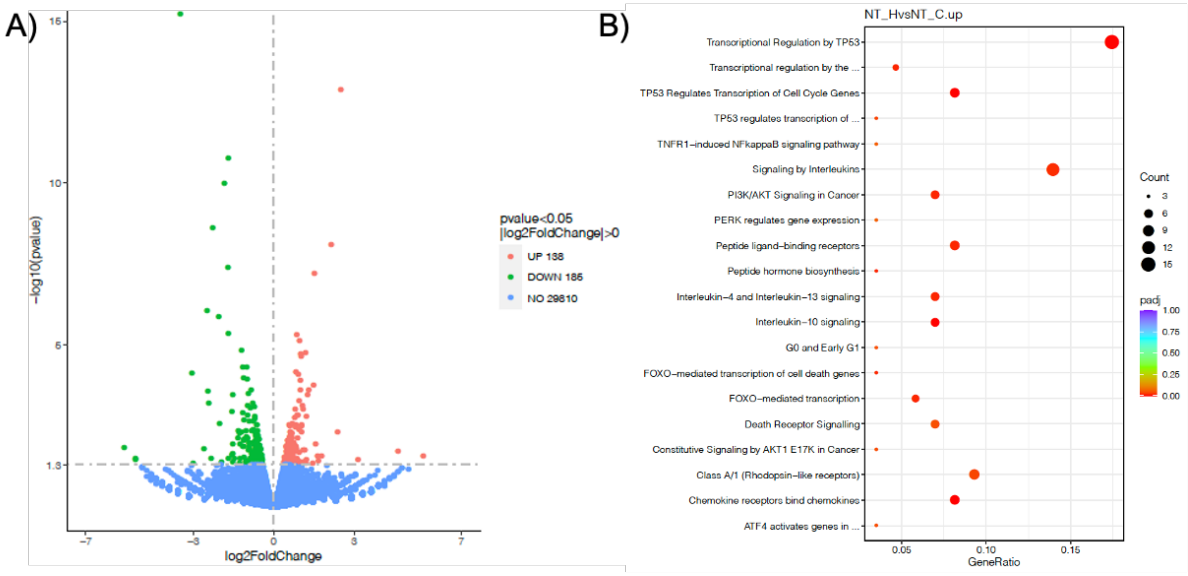

Figure 6.7. ***Transcriptional response to HU-induced replication stress.*** *A) mRNA sequencing volcano plot of differentially expressed genes (DEGs) after 4 hours of hydroxyurea treatment (2 mM) when compared to control cells. Non DEG, blue; upregulated DEGs; pink; downregulated DEGs, green. B) Gene set enrichment analysis (GSEA) was used to compare gene expression profiles of untreated cells and cells treated with hydroxyurea (4 hours, 2 mM). Significantly enriched Reactome Pathways are shown with their ratio and adjusted p-value.*

Next, I was interested in exploring the relationship between SETD2 and E2F6, as previous work has shown that E2F6 plays an important role in repressing E2F-dependent transcription during G_1-and S-phases (Bertoli, Klier, McGowan, et al., 2013). Furthermore, I found that the genes downregulated following loss of *SETD2* were enriched for predicted E2F6 TF-binding (Figure 6.2). This led me to hypothesise that inactivation of E2F6, in response to intra-S checkpoint activation and its CHK1-dependent phosphorylation, might de-repress E2F-dependent transcription in S-phase via SETD2 and H3K36me3.

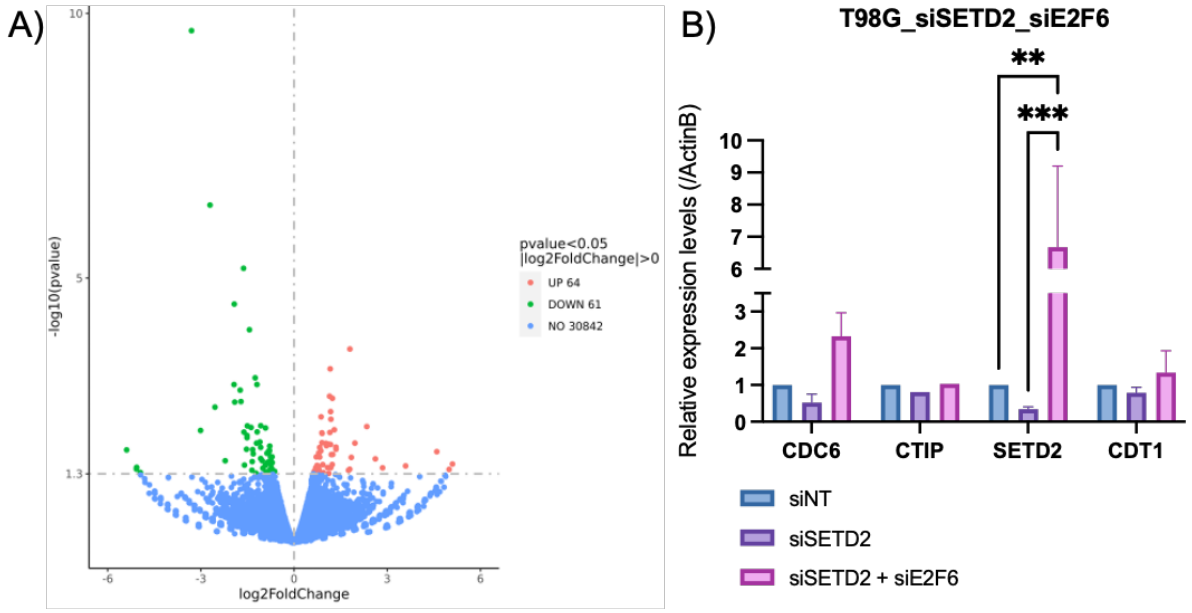

Figure 6.8. ***SETD2 and inactivation of E2F6 are required for expression of E2F-dependent transcripts****. A) mRNA sequencing volcano plot of differentially expressed genes (DEGs) 4 hours after hydroxyurea treatment (2 mM) in cells treated with siSETD2 when compared to non-treated siSETD2 cells. Non DEG, blue; upregulated DEGs; pink; downregulated DEGs, green. B) Expression levels of CDC6, CtIP, SETD2, and CDT1 in T98G cells transfected with siNT (control siRNA), SETD2 siRNA, or E2F6 and SETD2 siRNA as measured by qRT-PCR analysis. Data represented as mean ± SEM (n=3). Significance calculated with a two-way ANOVA.*

I observed, as previously shown, that siRNA-mediated depletion of SETD2 caused reduced expression of E2F-dependent transcripts, such as *CDC6* and *CDT1* at 72 hours post-transfection (Figure 6.8B). Interestingly, however, we found that co-depletion of E2F6 caused

both a very strong increase in *SETD2* mRNA levels (Figure 6.8B) and a concomitant repression of E2F-targets. This suggests that E2F6 and SETD2 might cooperate to repress E2F-targets in response to replication stress, possibly in response to ATR- and CHK1-dependent checkpoint signalling.

6.7 Complementation of *SETD2* KO U2OS Cells with SETD2-FL cDNA Restores H3K36me3 and E2F1 Expression Levels

To confirm that loss of SETD2 was the cause of reduced E2F-mediated transcription in *SETD2* KO U2OS cells, a rescue experiment was performed. *E2F1, MCM2* and *RRM2* expression were measured in *SETD2* KO U2OS cells rescued with wildtype full-length (FL)-SETD2 and a SETD2 mutant lacking the SRI domain, which mediates the interaction of SETD2 with the C-terminal domain of RNAPII, and is required for transcriptional coupled-SETD2 activity (Bhattacharya, Levy, et al., 2021) (Figure 1.5). Complementation of *SETD2* KO U2OS cells with the full-length SETD2 construct almost restored H3K36me3 levels to wild type levels, whereas SETD2 in which the SRI domain was deleted only resulted in a small increase in the levels of H3K36me3 (Figure 6.9A).

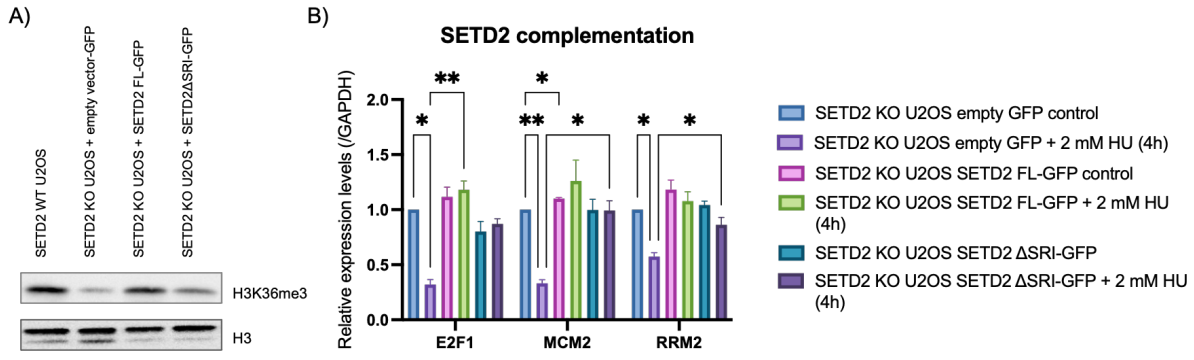

Figure 6.9. ***Expression of wild-type SETD2 restored H3K36me3 levels and expression of E2F1 and its target genes.*** *A) Western blot with of whole-cell lysates of KO cells expressing full length SETD2 (SETD2-FL) or a SETD2 mutant (SETD2ΔSRI-FL).* ***B)*** *Fold change of E2F1, MCM2 and RRM2 expression levels measured by qRT-PCR relative to empty vector. Data represented as mean ± SEM (n=3).*

In accordance with this, rescue of *SETD2* CRISPR KO U2OS with full-length SETD2 increased expression of *E2F1,* and its target genes *RRM2* and *MCM2,* 24 hours post-transfection, whereas expression of SETD2 lacking the SRI domain (SETD2ΔSRI) caused only a partial restoration of *E2F1* expression levels (Figure 6.9B). Similarly, the expression of *E2F1* and its targets genes *RRM2* and *MCM2* could be rescued following hydroxyurea-induced replication stress using a full-length SETD2 and partly using a SETD2 construct lacking the SRI domain in *SETD2* CRISPR KO cells (Figure 6.9B).

6.8 HU-induced Replication Stress Causes a Global Re-distribution of Total H3 and H3K36me3 Levels

The data presented so far suggests that SETD2-mediated H3K36me3 is required for the recruitment of E2F1 to target-gene promoters under replication stress conditions. Therefore, we wanted to test whether SETD2 regulates E2F-dependent transcription in response to replication stress through redistribution of H3K36me3. As treatment with hydroxyurea induces replication stress and therefore activates the checkpoint kinase ATR and its downstream effector CHK1, we also asked whether the redistribution of H3K36me3 was dependent on intra-S-checkpoint signalling, as was previously shown for E2F-dependent transcription (Bertoli, Klier, McGowan, et al., 2013).

First, I confirmed that 4 hours of hydroxyurea (HU) treatment (2 mM) induced RF stalling and DNA replication stress, using p-RPA32(S33), a marker of ssDNA, and phosphorylation and subsequent activation of downstream effector kinase CHK1 as a readout (Figure 6.10A and B). Only short exposures to HU were used, as previous work has shown that RFs can restart after short replication blocks (2-6 hours) but become inactivated and collapse following long

replication blocks (>16 hours) (Petermann, Orta, Issaeva, Schultz, & Helleday, 2010). This dosage and timing of HU therefore allows us to study replication stress only, without having our findings confounded by the presence of DNA DSBs.

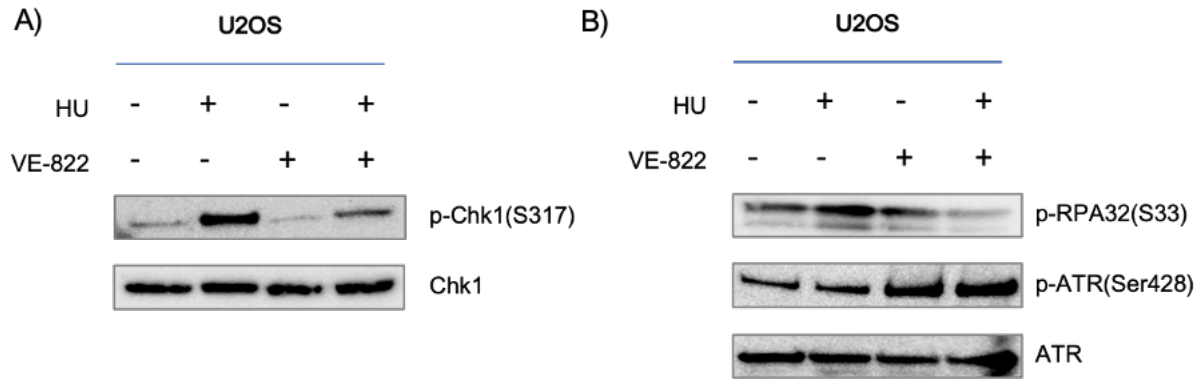

Figure 6.10. ***ATR inhibitor (VE-822) treatment partly impairs HU-induced checkpoint signalling in U2OS cells.*** *Western Blot of (A) p-Chk1(S317) and Chk1 levels and (B) p-RPA32(S33), p-ATR(S428) and total ATR levels in U2OS cells after 4 hours of HU (2 mM) and/or VE-822 (2 uM) treatment.*

Further, I studied phosphorylation changes of ATR at S428, which is not critical for CHK1 activation (Liu et al., 2011), but instead reflects a CDK1-mediated phosphorylation event that functions to promote the formation of *trans*-ATR (Hilton et al., 2015; Makinwa et al., 2020). *Trans*-ATR is activated in the nucleus to initiate DNA damage signalling and checkpoint activation, and in accordance with a role for ATR in suppressing CDK1 activity, I also showed increased p-ATR(S428) in the presence of VE-822, a specific ATR kinase inhibitor (Figure 6.10B).

Next, once I confirmed that VE-822 treatment selectively attenuated ATR/CHK1 signalling in response to HU-induced replication stress in U2OS cells (Figure 6.10A), we proceeded with mononucleosome-sequencing (mNUC-seq) to study global H3K36me3 re-distribution. In mNUC-sequencing, chromatin DNA is precipitated by histone-specific antibodies, such as

H3K36me3, followed by selection of mononucleosome-sized DNA fragments and sequencing (Nojima et al., 2018). An alternative control for the mNUC-seq of H3K36 trimethylation is an anti-H3 antibody IP, as this gives a better measure of the enrichment of a histone mark relative to the presence of the histone, in our case, histone H3. This is especially important if an antibody for a specific histone modification has a slight affinity for the histone, irrespective of its modifications.

U2OS cells were treated with 2 mM of hydroxyurea for 4 hours, or with hydroxyurea and VE-822 (ATRi), and mNUC-seq for H3K36me3 and H3 was performed alongside RNA-sequencing to quantify expression changes. First, I studied the genomic profile of total histone H3 levels along the DNA using mNUC-seq and plotted the signal for all genes (expressed and non-expressed) (Figure 6.11A). Notably, H3K36me3 is exclusive to protein-coding genes with introns and mRNA-like lincRNA, as shown previously (Nojima et al., 2018), so we also limited our analysis to a subset of highly expressed genes (i.e., those displaying high levels of the activating H3K36me3 mark) (n=6,090) (Figure 6.11B). These plots showed a number of predicted patterns, with higher H3 coverage in highly expressed genes, as previously shown (Flensburg, Kinkel, Keniry, Blewitt, & Oshlack, 2014). Furthermore, I found a dip for H3 at the transcription start site (TSS) of genes, which is consistent with nucleosome depletion across the region (Ozsolak, Song, Liu, & Fisher, 2007).

Next, we compared the impact of different treatments on the genomic H3 profiles (Figure 6.11A and 6.11B). Previous work from other groups has shown that fork stalling, induced by exogenous replication stress-inducing agents, generates ssDNA and accumulation of H3 evicted from the chromatin (Jasencakova et al., 2010). In accordance with this, we found reduced levels of H3 across the genome in response to HU-induced replication stress (red vs.

blue). Interestingly, however, we found that pre-treatment of these cells with the ATR-inhibitor VE-822 completely abrogated this effect, and even caused enrichment of histone H3 levels across the gene bodies of genes, and past the transcription-end site (TES) (purple vs. red) (Figure 6.11A and 6.11B).

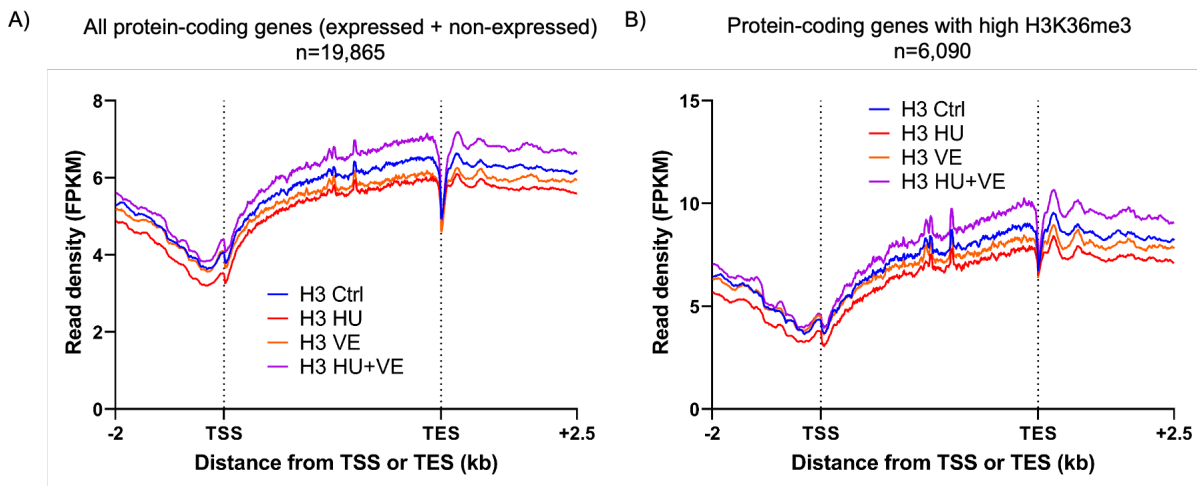

Figure 6.11. ***Meta-analysis of reads density for mNUC-seq H3 signal over gene bodies*** *of all A) protein coding genes (n=19,685) or B) protein-coding genes with high H3K36me3 (n=6,090) following hydroxyurea and or ATR inhibitor treatment for 4 hours. HU = hydroxyurea (2 mM), VE = VE-822, ATR inhibitor (2 uM). *mNUC-seq analysis was performed with the help of Michael Tellier.*

Next, we plotted the H3K36me3 signal with H3 normalisation across the U2OS cell genome (Figure 6.12A and 6.12B). As hypothesised, following HU treatment, I saw a global redistribution of H3K36me3 normalised to H3 (Figure 6.12A), with a higher H3K36me3/H3 ratio throughout the gene bodies of a number of protein-coding genes, such as *MCM9*, REV1, *SETX*, and *TOP2A*, when compared to the untreated control. Furthermore, comparison of the H3K36me3/H3 ratio over the promoter region of protein coding genes revealed an increased H3K36me3/H3 ratio both ±500 bp downstream of the TSS as well as upstream of the TSS (Figure 6.12B). These data suggest that despite high rates of H3 eviction, levels of H3K36me3 on the remaining histones increase following hydroxyurea treatment in U2OS cells.

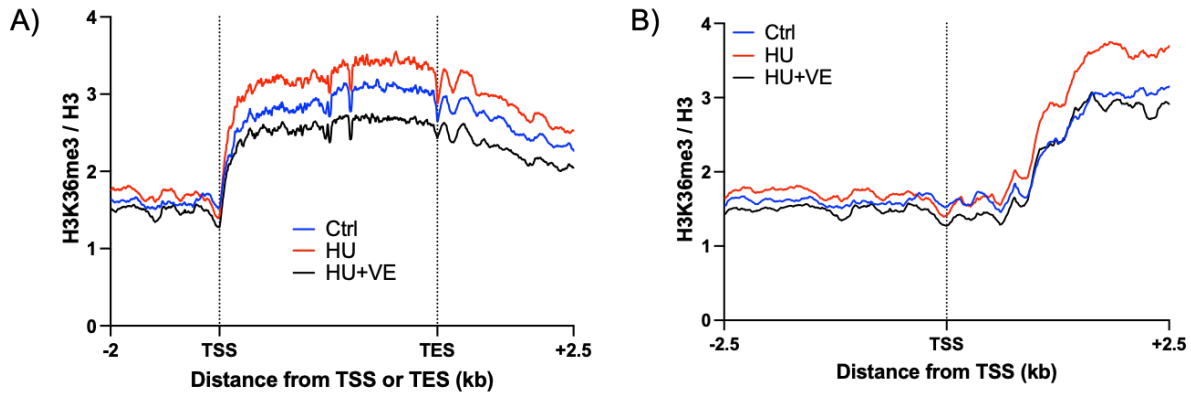

Figure 6.12. ***SETD2 facilitates the transcriptional checkpoint response to HU-induced replication stress in an ATR-dependent manner.*** *Meta-analysis of reads density for mNuc-seq H3K36me3/H3 signals over gene bodies (A) and promoter regions (B) of protein-coding genes with high H3K36me3 (n=6,090) following hydroxyurea and or ATR inhibitor treatment for 4 hours. HU = hydroxyurea (2 mM), VE = VE-822, ATR inhibitor (2 uM). *mNUC-seq analysis was performed with the help of Michael Tellier.*

6.9 H3K36me3 Re-distribution and E2F-dependent Transcription Following HU is Dependent on Intra-S checkpoint Signalling

Next, I asked whether the re-distribution of the H3K36me3 was dependent on ATR-dependent checkpoint activation. We found that the increased ratio of H3K36me3 over H3 on both the TSS and protein coding gene bodies following HU-induced replication stress was abrogated following pre-treatment with the ATR inhibitor, VE-822 (Figure 6.12A and 6.12B).

Next, I compared our mNUC-seq data, particularly the H3K36me3/H3 signal ratios over different genomic regions, with the corresponding RNA-sequencing data. I found that only 72 of 324 H3K36me3-enriched genes from the mNUC-seq (following HU only) still had enriched H3K36me3 peaks over gene bodies following combined HU and ATR-inhibitor treatment (Figure 6.13A) and only 52 of 138 HU-induced genes (Figure 6.7A) from the RNA-seq were still upregulated when cells were pre-treated with the ATRi before RS induction (Figure 6.13B), of which only 16 were predicted p53- or E2F-targets. Instead, most of these 52

overlapping genes were involved in regulation of programmed cell death and apoptotic processes, but not in the stress or transcriptional response, suggesting that the H3K36me3 changes were dependent on intra-S checkpoint signalling. When GO term enrichment analysis was performed for the DEGs between the U2OS cells treated with HU only and those treated with a combination of HU and the ATR-inhibitor VE-822 (Figure 6.13C), I found an enrichment for processes related to mitotic nuclear division, and surprisingly, organismal homeostasis and cellular development (including that of the skin and the renal system).

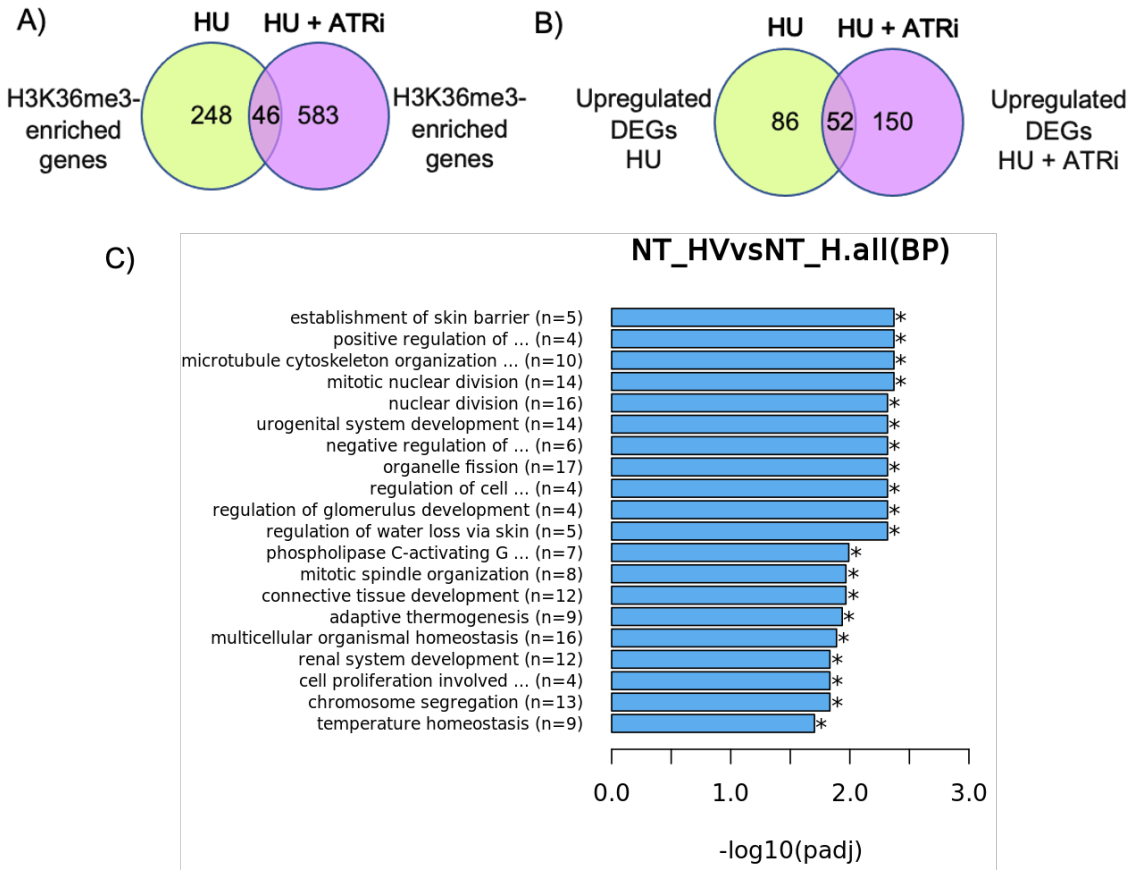

Figure 6.13. ***Transcriptional response to replication stress is dependent on ATR signalling****. A) Overlap between H3K36me3-enriched genes following treatment with hydroxyurea or a combination of hydroxyurea and the ATR inhibitor VE-822. B) Overlap between DEGs from the RNA-seq following treatment of U2OS cells with hydroxyurea or a combination of hydroxyurea and the ATR inhibitor VE-822. C) GO term overrepresentation analysis for the DEGs between cells treated with HU alone, or those treated with a combination of HU and VE-822 (NT_HV = siNT transfected, treated with HU and VE-822, NT_H = siNT transfected, treated with HU only).*

6.10 ATR and CHK1 Inhibition Prevent Expression of H3K36me3 in Response to Replication Stress

Given the observed changes in chromatin-bound H3K36me3 following HU and/or ATR inhibitor treatment, I investigated whether the role for ATR-mediated checkpoint activation in facilitating expression of E2F-targets was mediated through SETD2-dependent H3K36 trimethylation more globally. First, I treated unsynchronised U2OS cells with hydroxyurea for 4 hours, with or without 1 hour of VE-822 pre-treatment, and extracted the total protein from these cells. Western Blot analysis was subsequently performed for levels of H3K36me3 and total histone H3 (Figure 6.14A). Global levels of H3K36me3 were not induced in response to hydroxyurea treatment in unsynchronised cells, but levels of H3K36me3 were reduced in response to VE-822 treatment, even in the presence of HU (Figure 6.14A, H3K36me3 levels after siSETD2 transfection shown for comparison).

As I was particularly interested in exploring the role of H3K36me3 in facilitating the induction of E2F-dependent transcription as part of the transcriptional checkpoint response, I also looked at H3K36me3 levels in response to replication stress in the different cell cycle phases. To do this, T98G cells were synchronised in G_0, released into G_1 (Figure 6.14B) or S-phase (Figure 6.14C) and then treated with HU and/or the ATR inhibitor, VE-822. In synchronised T98G cells, I found an increase in H3K36me3 levels in both G_1- and S-phase cells in response to HU-induced replication stress (Figure 6.14B and 6.14C). HU-induced increases in H3K36me3 were impaired when G_1-cells were pre-treated with the ATR inhibitor (Figure 6.14B), and fully abrogated in the presence of the ATR inhibitor in S-phase cells (Figure 6.14C), consistent with roles for ATR in both the G_1- and S-phases of the cell cycle (Bøe, Håland, Boye, Syljuåsen, & Grallert, 2018; Shechter, Costanzo, & Gautier, 2004). Cells were also unable to increase

H3K36me3 levels in response to HU-induced RS in the presence of the CHK1 inhibitor UCN-01, suggesting checkpoint activation is essential for changes in H3K36me3 deposition to facilitate transcriptional changes in S-phase.

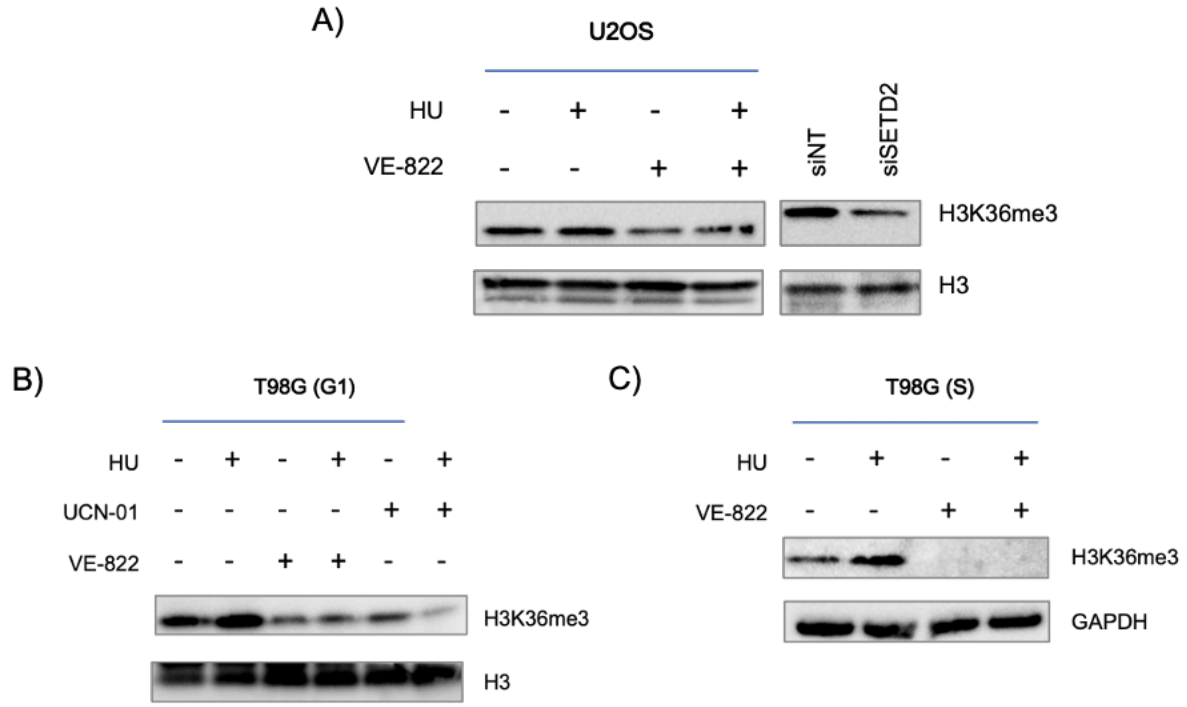

Figure 6.14. ***H3K36me3 induction in response to replication stress in S-phase is dependent on ATR- and CHK1-signalling.*** *A) Western Blot of H3K36me3 and total H3 levels in unsynchronised U2OS cells after 4 hours of HU (2 mM) and/or VE-822 (2 uM) treatment. B) Western Blot of H3K36me3 and total H3 levels in G_1-synchronised T98G cells after 4 hours of HU (2mM) and/or VE-822 (2 uM) or UCN-01 (500 nM) treatment. C) Western Blot of H3K36me3 and GAPDH levels in S-phase synchronised T98G cells after 4 hours of HU (2mM) and/or VE-822 (2 uM) treatment.*

Finally, I analysed the cell-cycle phases of T98G cells treated with HU and/or the ATR inhibitor ensure the observed changes in H3K36me3 levels between treatment conditions were not a result of differential cell cycle profiles, as H3K36me3 was previously shown to be cell-cycle regulated (Figure 6.6). Even though 4 hours of HU-treatment caused a slight increase in S- and G_2/M phase cells, and this effect was abrogated following co-treatment with the ATR inhibitor (Figure 6.15), those changes were only minor and were therefore unlikely to have caused the observed changes.

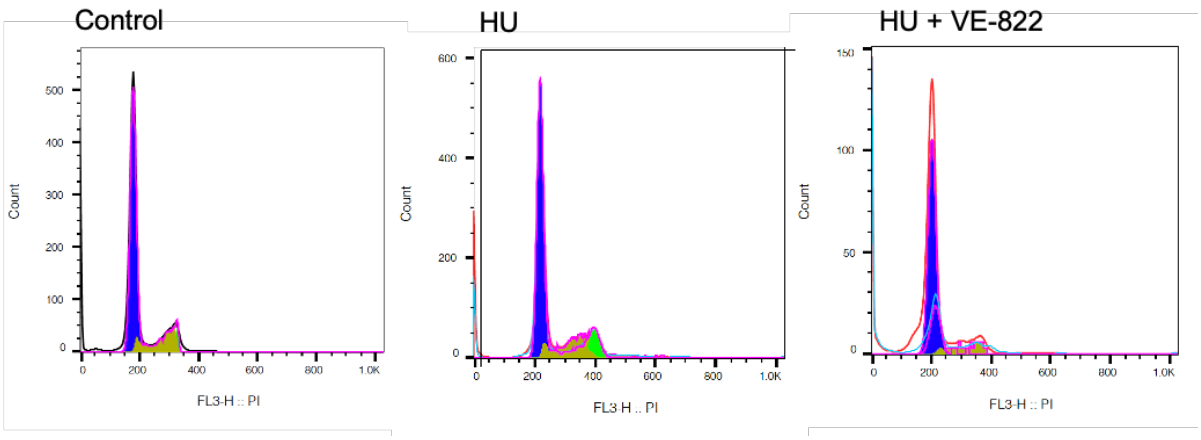

Figure 6.15. ***FACS analysis of synchronised T98G cells treated with 2 mM hydroxyurea, 2 uM VE-822, or both for 4 hours.*** *FACS cell cycle profile (using propidium iodide) of synchronised T98G cells after treatment with 2 mM HU, 2 uM VE-822, or both for 4 hours. The data shown are from a single representative experiment out of three repeats.*

Together, our data suggest that *E2F*- and *p53*- -target gene expression following hydroxyurea-induced replication fork stalling requires ATR/CHK1-dependent H3K36 trimethylation.

6.11 E2F- and p53-Target Gene Expression Requires ATR-dependent H3K36me3

Finally, I tested whether the presence of active ATR signalling could have a more global role in maintaining active transcription of DNA replication stress response genes. To study this, I conducted analysis of gene expression patterns after HU-treatment, with or without the ATR inhibitor (VE-822), in the presence or absence of *SETD2*, and identified four distinct clusters of genes that exhibit distinct patterns of expression.

One cluster of genes, 'cluster 3' (Figure 6.16A) demonstrated a very strong dependency on active ATR-signalling. This cluster included p53-target genes *CDKN1A*, encoding the CDK inhibitor p21, and *RRM2B*, encoding p53-controlled ribonucleotide reductase (p53R2) (Figure 6.16B). Treatment with VE-822 did not further reduce the levels of *RRM2B,* which is a p53- and E2F1-target (Qi et al., 2015), in the absence of SETD2, suggesting ATR and SETD2/H3K36me3 are epistatic. In yeast, previous studies have shown that Set2 is epistatic

with DNA damage checkpoint factors, including Rad3 (*S. pombe* ATR homolog) and Chk1, in DNA damage repair pathways (Lim, Nguyen, Li, Yeo, & Chen, 2018). However, other studies have shown that loss of SETD2 is synthetic lethal with ATRi (Pfister et al., 2015) and that *rad3Δ* in *S. pombe* suppresses the slow entry into and progression through S-phase in *set2*Δ cells (Pai et al., 2017), suggesting ATR might perform additional functions that are not epistatic to SETD2. Hence, we wanted to explore whether the altered expression of genes in "cluster 3" following HU, with or without the ATR inhibitor, was indeed dependent on altered H3K36me3 levels on the gene bodies of these genes.

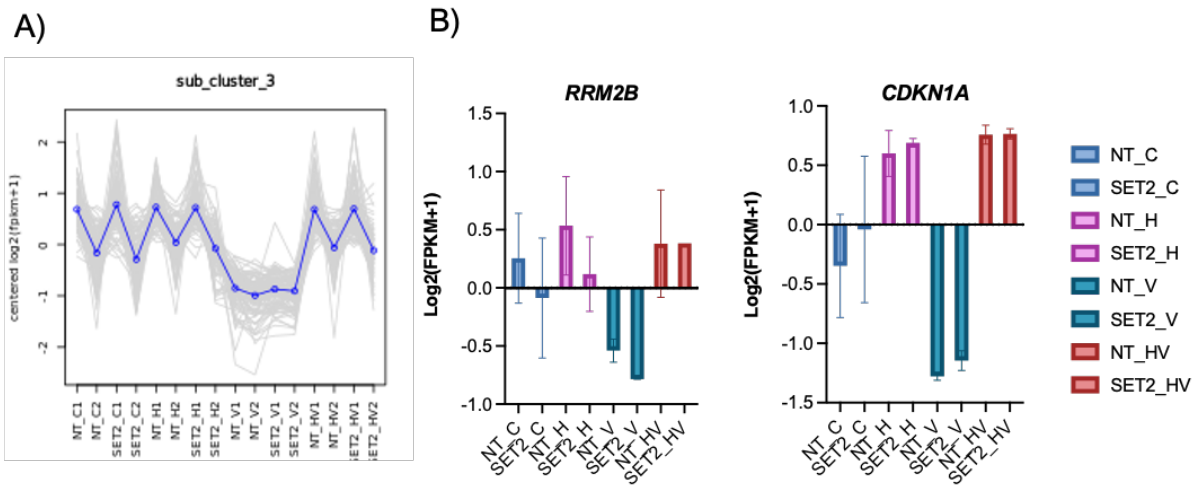

Figure 6.16. ***Expression changes of E2F- and p53-target genes in response to HU and/or ATR inhibitor treatment in the presence and absence of SETD2.*** *A) Expression profile of genes in cluster "3". The intensity of expression, as determined from the average difference values is expressed as centred Log_2(FPKM)+1, showing a clear decrease following ATR inhibitor treatment.* ***B)*** *Representative example of expression profile of RRM2B and CDKN1A of cluster "3". The average expression value (with SEM) in Log_2(FPKM)+1 after each drug treatment (NT = siNT, SET = siSETD2, C = control, H = HU, V = VE-822, HV = HU + VE-822) is plotted for each gene.*

To do this, the mNUC-seq signal ratio of H3K36me3 to H3 was plotted for the *CDKN1A* and *RRM2B* gene loci and the intensity of the signal was compared between different treatment conditions (control shown in blue, HU in red, VE-822 in violet and HU + VE-822 in orange). As shown in Figure 6.17, the relative peak sizes clearly demonstrate that hydroxyurea treatment causes an increase of the H3K36me3 mark along the gene bodies of these genes (red vs. blue).

These HU-induced increases in H3K36me3 along the gene body could not be observed, however, when the cells were pre-treated with VE-822 (orange vs. blue) or VE-822 alone (purple vs. blue) (Figure 6.17).

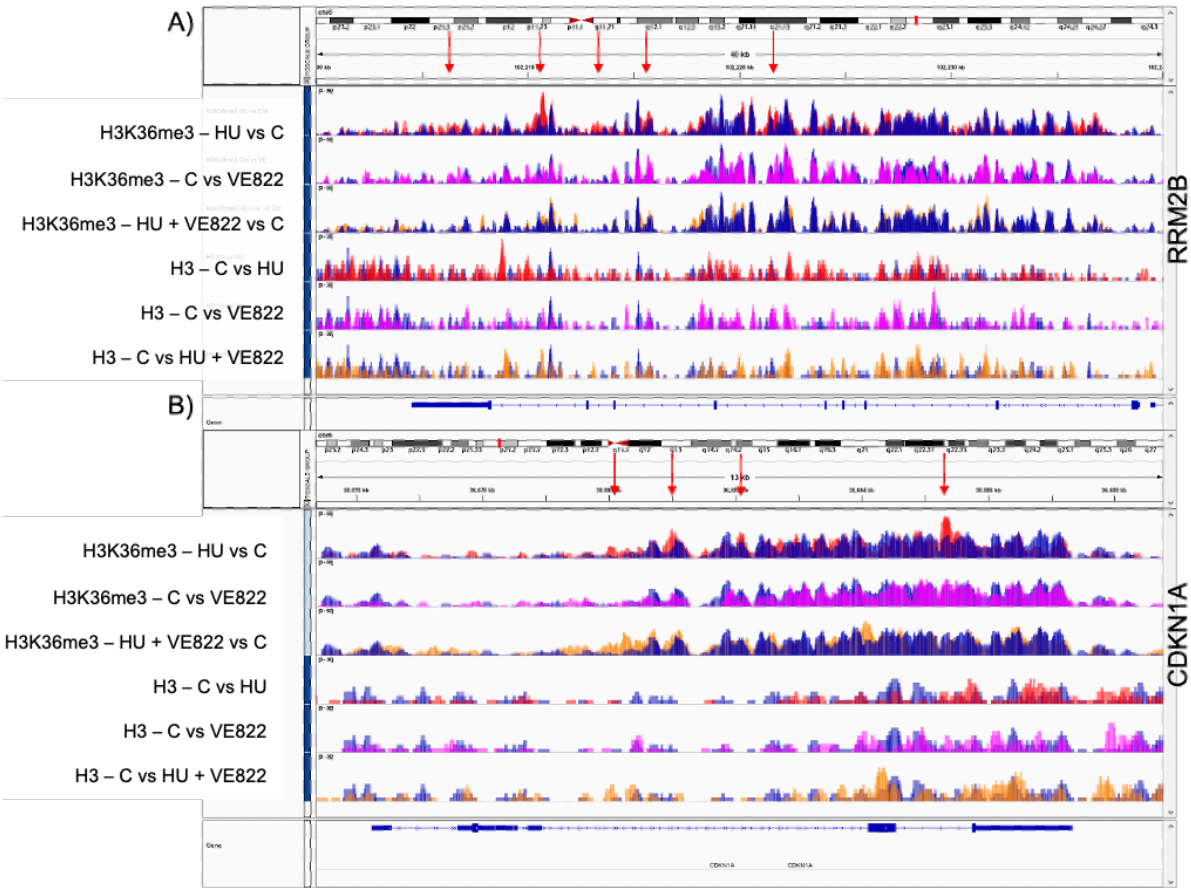

Figure 6.17. ***mNUC-seq signal of H3K36me3/H3 on RRM2B and CDKN1A gene loci of HU-, VE822- or HU- and VE822-treated samples compared to control.*** *Control shown in blue, HU in red, VE-822 in violet and HU + VE-822 in orange. *mNUC-seq analysis was performed with the help of Michael Tellier.*

Given that we observed a correlation between ATR activity and H3K36me3 levels on *RRM2B* and *CDKN1A,* with reduced levels of the activating H3K36me3 mark following ATR inhibition (Figure 6.17), I asked whether there was a more general effect of checkpoint activation and cell cycle regulation on chromatin modifications.

First, I performed differential expression analysis to extract the list of genes whose expression levels were significantly altered upon ATR inhibition by VE-822. 1874 downregulated and 1959 upregulated DEGs were identified when comparing VE-822 treated U2OS cells with the control cells (Figure 6.18A). Next, I compared the H3K36me3/H3 ratio over the up- and downregulated DEGs following VE-822 treatment. Interestingly, quantification of mNUC-seq signal ratio of H3K36me3 to H3 showed that levels of H3K36me3 specifically decreased on the downregulated protein coding genes after ATR inhibitor treatment (Figure 6.18B), whereas this decrease was less apparent for the upregulated DEGs (Figure 6.18C). This suggests that ATR signalling functions to promote SETD2-dependent H3K36me3 changes, to facilitate transcription of both p53- and E2F-dependent transcripts.

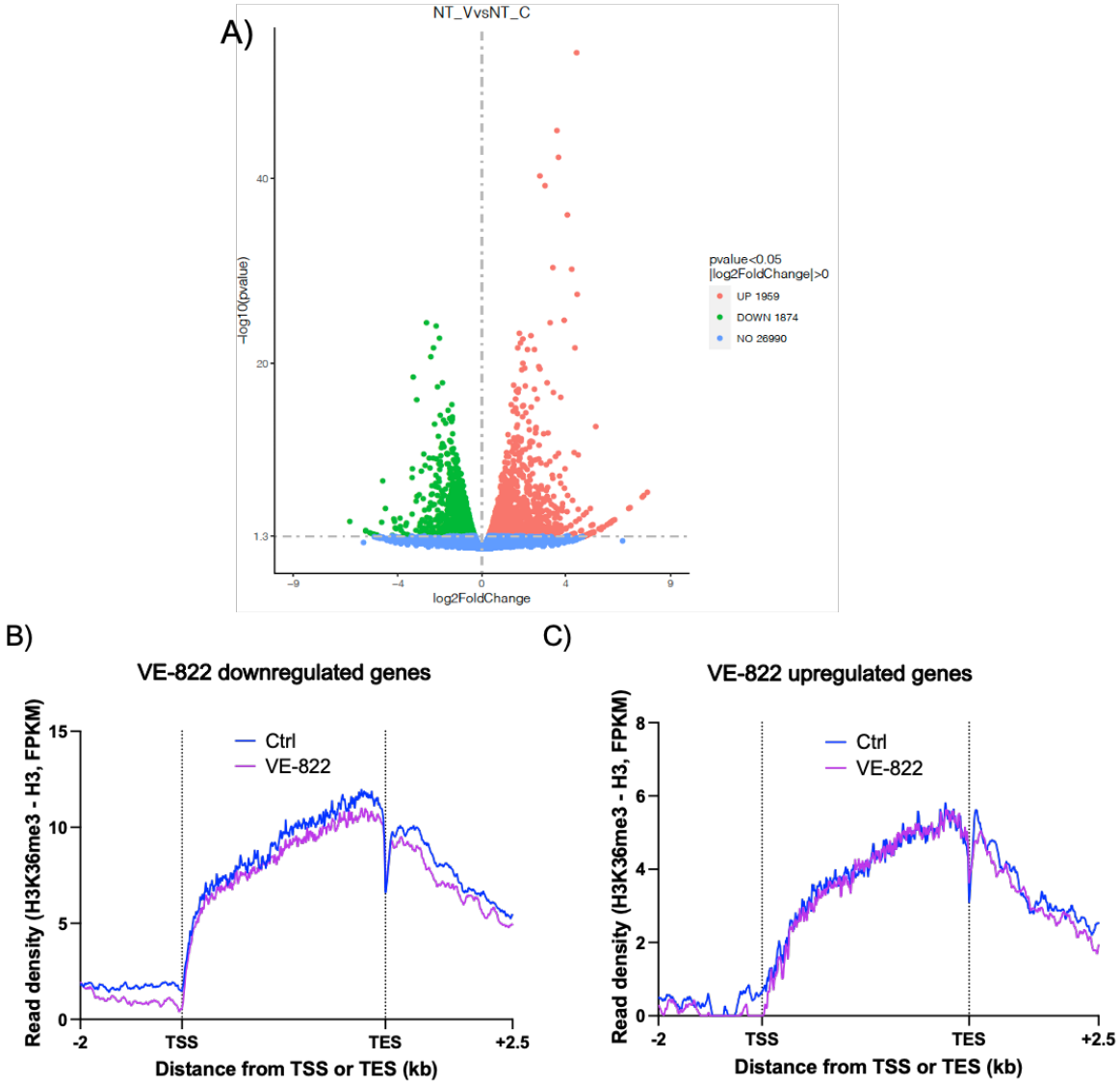

Figure 6.18. ***ATR inhibition causes H3K36me3 re-distribution and subsequent expression changes.*** *A) mRNA sequencing volcano plot of differentially expressed genes (DEGs) after 4 hours of VE-822 treatment (2 uM) in U2OS cells when compared to control (untreated) cells. Non DEG, blue; upregulated DEGs; pink; downregulated DEGs, green. B and C) Meta-analysis of reads density for mNuc-seq H3K36me3/H3 signals over the protein coding gene bodies of downregulated DEGs (B) and upregulated DEGs (C) following ATR inhibitor treatment. *mNUC-seq analysis was performed with the help of Michael Tellier.*

6.12 Conclusion

In this study, we identify a novel role for SETD2-dependent H3K36me3 in coordinating the transcriptional response to DNA replication stress. I show that, in the presence of hydroxyurea, SETD2 can act as an effector of the ATR- and CHK1-mediated checkpoint by promoting the redistribution of the active histone mark H3K36me3 on p53- and E2F-responsive promoters and gene bodies to maintain p53- and E2F-dependent transcription in S-phase, thereby preventing the formation of replication stress-induced DNA damage.

Although the biological mechanisms that couple intra-S checkpoint activation and SETD2-dependent H3K36 trimethylation are not yet fully understood, I propose two pathways through which this might occur:

i. Depletion of E2F6 resulted in elevated S*ETD2* mRNA levels and concomitant repression of E2F-dependent transcription, in accordance with previously published data (Bertoli, Klier, McGowan, et al., 2013). Recent studies, using IP coupled with mass spectrometry (MS), revealed a putative interaction between E2F6 and SETD2 in embryonic stem cells (Dahlet et al., 2021). One could therefore predict that, under conditions of replication stress, CHK1-dependent phosphorylation of E2F6 causes its dissociation from the *SETD2* promoter, leading to elevated SETD2-dependent H3K36 trimethylation and consequently, increased E2F-dependent transcription.

ii. Set2 was recently identified as an HU-induced phospho-target in a proteomic screen performed in budding yeast (Hurst et al., 2021). This raises the possibility that ATR or its downstream effector kinase CHK1 directly phosphorylate SETD2 in the presence of DNA replication stress, thereby causing changes in its stability or transferase activity.

In budding yeast, Set2-mediated H3K36me is required for activation of the Rad53 (yeast homologue of mammalian Chk2)-dependent DNA damage checkpoint in response to phleomycin treatment (Jha & Strahl, 2014). While Chk2 activation has not been reported to be dependent on SETD2 in mammalian cells, recent work did show that SETD2 gets recruited to the chromatin in the presence of HU-induced replication stress (Zhu et al., 2021). There, SETD2-mediated H3K14me3 is thought to serve as a dock to recruit the RPA complex to chromatin to promote ATR signalling in response to replication stress (Zhu et al., 2021).

Our findings therefore collectively suggest the existence of an important feedback loop, where SETD2 promotes ATR activation via H3K14me3, which subsequently facilitates the redistribution of SETD2-dependent H3K36me3 to promote the E2F-dependent transcriptional checkpoint response, either via E2F6, or via direct ATR-CHK1-mediated phosphorylation events (Figure 6.19). The cooperative role of the intra-S checkpoint and SETD2 provides the first evidence of a chromatin-based link for cell cycle and replication stress tolerance through maintenance of transcriptional activity, and expands the function of SETD2 in maintaining genome integrity beyond its previously described roles in DNA damage repair (Pfister et al., 2014) and nucleotide synthesis (Pfister et al., 2015).

Previous studies in both fission yeast and human cells have shown histone H3K36 methylation to be cell-cycle regulated, with H3K36me3 levels peaking at the G_1/S transition (Li et al., 2013; Pai et al., 2014). This timing correlates strongly with the initiation of E2F-dependent transcription in mammalian cells, with expression of these genes, together with H3K36me3, decreasing upon replication initiation. Involvement of SETD2 in cell-cycle regulation of transcription is consistent with previously published work in fission yeast (Pai et al., 2017), where H3K36 methylation was found to facilitate efficient DNA replication through induction

of MBF-target genes. Interestingly, while the MBF and E2F genes are functionally analogous, they have no conserved sequence homology. Despite this, the role of H3K36me3 in both DNA replication and in the response to replication stress appears to be highly evolutionarily conserved.

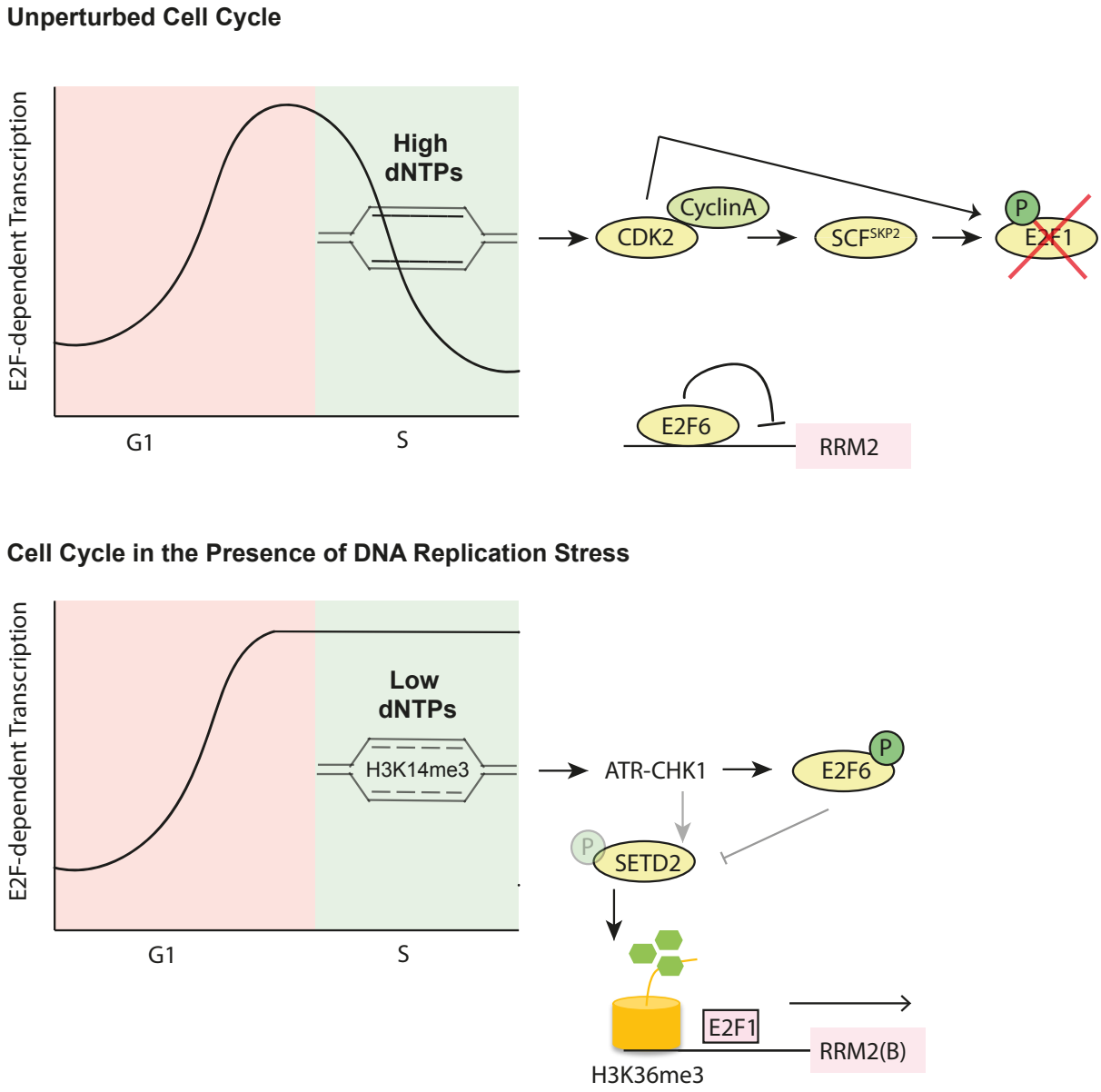

Figure 6.19. ***Graphical Abstract: Role for SETD2 in the Transcriptional Checkpoint Response.***

In summary, the key findings of this chapter are:

- Loss of *SETD2* results in reduced expression of a subset of E2F-target genes due to decreased occupancy of E2F1 on its target gene promoters.
- H3K36 trimethylation peaks at the G_1-to S transition, which is consistent with a role in facilitating E2F-dependent transcription.
- Replication stress results in elevated levels of H3K36me3 in S-phase, which subsequently facilitates global increases in E2F- and p53-dependent gene expression in an ATR-checkpoint dependent manner.

Chapter 7
General Discussion

Mechanisms underlying breast cancer development are widely varied and generally poorly understood; however, much effort has recently been directed at delineating the genomic alterations that occur during breast tumour formation and progression (Curtis et al., 2012; Nik-Zainal et al., 2016; Paul et al., 2020). Hereditary and genetic factors, including mutations in tumour suppressor genes, such as *BRCA1*, *BRCA2*, *CDH1*, and *TP53*, are considered to be the major drivers in approximately 10% of breast cancer cases (reviewed in Shiovitz & Korde, 2015). Here, a novel, subtype-specific, driver pathway involving amplification-dependent overexpression of *AGO2* and miR-106b/25 was identified. Moreover, tumour suppressive roles for SETD2 beyond the control of HRR repair (Pfister et al., 2014) and nucleotide synthesis (Pfister et al., 2015) were characterised. Broadly, the work presented in this thesis has described a role for the miRNA regulatory network, via the oncogenic miR-106b/25 cluster, and histone modifications, via tumour suppressive actions of SETD2-dependent H3K36me3, in regulating E2F-dependent gene expression changes during the G_1/S transition and as part of the DNA replication stress response in cancer.

7.1 Non-canonical miRNA Biogenesis Pathways and Oncogenic MicroRNA Production in Breast Cancer

The canonical processing of primary- and precursor-miRNAs is typically dependent on sequential DROSHA/DGCR8 and DICER action (Graves & Zeng, 2012). However, miRNA biogenesis pathways demonstrate a high degree of plasticity, allowing cells to adapt to selective pressures during tumourigenesis and to counter external threats to genome stability,

particularly during DNA damage or replication stress (Wan et al., 2013; Zhang, Wan, Berger, He, & Lu, 2011).

Recurrent DNA copy number losses of the miRNA master regulators *DICER* and *DROSHA* (Dedes et al., 2011; Grelier et al., 2009; Khoshnaw et al., 2012) were previously associated with global disruption of the miRNA transcriptome in breast tumours. First, deletion of *DICER1* was shown to reduce the efficiency of miRNA production via the canonical miRNA biogenesis pathway (Kim et al., 2016). Second, cancers harbouring *DICER1* copy number losses or mutations in *DICER1* RNaseIIIa/b hotspot domains presented impairments in DICER-mediated cleavage of the 5p arm of pre-miRNAs, leading to asymmetric distribution of miRNA abundance and a global downregulation of 5p-miRNAs (Galka-Marciniak, Urbanek-Trzeciak, Nawrocka, & Kozlowski, 2021).

Together with insights from studies that have characterised the mechanisms underlying non-canonical miRNA biogenesis (Cheloufi et al., 2010; Kim et al., 2016), this work proposes that amplification-dependent overexpression of *AGO2* and *PABPC1* promotes usage of a non-canonical miRNA biogenesis pathway in breast cancer. This alternative miRNA biogenesis pathway relies on AGO2 endonuclease activity for cleavage of the pre-miRNA (Cheloufi et al., 2010; Cifuentes et al., 2010) and could function to compensate for reduced efficiency of miRNA biogenesis in the absence of *DICER1* (Galka-Marciniak et al., 2021; Kim et al., 2016). To date, only one miRNA, miR-451, has been shown to employ this alternative pathway for its production (Yang et al., 2010), but the analysis of miRNA abundance in the absence of *DICER1* suggests that *AGO2* activity alone is sufficient to maintain canonical miRNA production. Moreover, the analysis of mature: immature miRNA ratios shows that *AGO2* copy

number amplification can promote the preferential maturation of miRNAs of the miR-106b/25 cluster.

MiR-106b-5p, a miR-106b/25 cluster member, was recently identified as an important regulator of breast cancer aggressiveness and prognosis, with elevated expression levels in both mouse and human malignant breast tissue when compared to adjacent healthy tissue (Farré et al., 2021). In accordance with this, I found a role for miR-106b-5p in promoting breast cancer tumour spheroid growth. Taken together, this work highlights the development of non-canonical AGO2-dependent oncomiR processing as a novel driver pathway during breast cancer evolution.

7.2 MiR-106b-5p Levels Predict the Response to WEE1 inhibition

Even though miRNAs often only have moderate effects on the expression levels of individual target-mRNAs, the simultaneous targeting of parallel pathways can result in phenotypic alterations (Iorio et al., 2007). Here, I demonstrate that miR-106b-5p represses several key genes that function in the G_1/S transition, such as *CDKN1A* and *E2F1*, and to a lesser extent, *SETD2*, in breast cancer cell lines, which is in accordance with previously published work in other cancer types (Ivanovska et al., 2008; Shalgi et al., 2007; Trompeter et al., 2011; Xiang et al., 2015). Two of those genes (*CDKN1A* and *SETD2*) have been shown to play important tumour suppressive roles in breast cancer, as illustrated by the frequency of their disruption and associations with poor outcomes (Al Sarakbi et al., 2009; Schmidt et al., 2020). Previous studies have additionally shown that the miR-106b/25 and miR-17/92 polycistrons are transcriptionally repressed by p53 in breast cancers (Brosh et al., 2008), further supporting the tumour-promoting role of the miR-106b/25 polycistron, especially in *TP53*-mutated cancers. The work presented in this thesis therefore suggests that the genomic switch from DICER1-

dependent to AGO2-dependent and DICER1-independent miRNA biogenesis upregulates select oncogenic miRNA species to promote silencing of various TSGs, including p21 and SETD2, during cancer progression.

I propose that miR-106b-5p, aside from playing an oncogenic role in *AGO2*-amplified breast cancers, can also be used as a prognostic marker for WEE1 kinase inhibitor sensitivity. Elevated levels of miR-106b-5p promote S-phase entry, through downregulation of p21 and consequent increases in CDK1 activity, impair cell cycle arrest and programmed cell death (Petrocca et al., 2008), and increase the levels of endogenous replication stress, through loss of SETD2 and reduced E2F-dependent transcription (Armfield, 2019). These features collectively cause cells to display sensitivity to WEE1 kinase inhibitor treatment, as recently shown in clinical studies (Seligmann et al., 2021), and miR-106b-5p could therefore be utilised as a biomarker for AZD1775-sensitivity in a clinical setting.

Recent studies have also suggested a role for miR-106b-5p in mediating the cellular response to CDK4/6 inhibition (Andrikopoulou et al., 2021). High levels of RB have previously been associated with increased CDK4/6 inhibitor-sensitivity (DeMichele et al., 2015) and gene signatures of RB loss-of-function could identify palbociclib-resistant cell lines (Malorni et al., 2016). In response to CDK4/6 inhibitor treatment, miR-106b expression levels are significantly repressed through modulation of *MCM7* expression via the RB/E2F pathway (Thangavel et al., 2013), exclusively in *RB*-wild type cancers. Reduced miR-106b-5p expression levels could therefore help identify cancers that display complex alterations of the RB/E2F pathway. Taken together, my data suggests that miR-106b-5p expression could be a helpful tool for patient stratification; it predicts activity of the RB/E2F pathway, both before and after treatment, and could therefore predict patient responses to both WEE1- and CDK4/6-inhibitor treatment.

7.3 Conserved Role for SETD2-dependent H3K36me3 in The Transcriptional Checkpoint Response

Studies in fission yeast have previously demonstrated a role for Set2-dependent H3K36 methylation in promoting MluI cell-cycle box (MCB) binding factor (MBF)-complex-dependent transcription (Pai et al., 2017). In accordance with a high degree of functional conservation of the mechanisms of G_1/S transcriptional activation from yeast to humans (Cross et al., 2011), this work similarly identified a role for SETD2-dependent H3K36me3 in promoting E2F-dependent transcription, in an ATR/CHK1-dependent manner, to prevent the formation of replication stress-induced DNA damage (Armfield, 2019).

Recent chromatome and phosphoproteomic screens in *S. cerevisiae* revealed that HU-induced replication stress caused a $Mec1^{ATR}$-dependent reduction of the large RNAPII subunit Rbp1, but increased chromatin occupancy of both Set2, the yeast homolog of SETD2, and dNTP biosynthesis enzyme ribonucleotide reductase subunits (Rnr2, Rnr3, and Rnr4) (Hurst et al., 2021). This suggests that, in the presence of DNA replication stress, H3K36me3 deposition might occur in a an uncharacteristic transcription-independent manner. In accordance with this, I found that expression of a SETD2 mutant lacking the SRI domain, which mediates the interaction of SETD2 with the CTD of RNAPII (Kizer et al., 2005), could partially rescue E2F-target gene expression in *SETD2* KO cells under replication stress conditions.

Furthermore, we observed increased H3K36me3/H3 ratios not only within gene bodies, but also around promoter elements of p53- and E2F-responsive genes, such as *CDKN1A* and *RRM2B.* Our data therefore suggests that SETD2 does not only function to maintain cell cycle checkpoints in response to genotoxic agents (Zhu et al., 2021), but also to facilitate ATR-

dependent H3K36 trimethylation changes on the promoter regions of stress-responsive genes. These changes could subsequently induce E2F- and p53-target gene expression, as shown here, and may also promote H3K36me3-coupled alternative splicing events. Recent studies have found that the SETD2 SHI domain mediates the interaction of SETD2 with RNA and numerous RNA processing proteins, including Med23 and hnRNP (Bhattacharya, Levy, et al., 2021; Bhattacharya, Wang, et al., 2021). The SETD2-hnRNP interactions occurs even without the RNAPII interaction domain (SRI), and mediates AS- and alternative cleavage and polyadenylation (APA) events (Huang et al., 2012). Future research must therefore determine whether HU-induced H3K36me3 deposition changes are RNAPII-dependent, and whether increased H3K36me3, and potentially hnRNP, at the promoters of target genes leads to significant changes in alternative splicing events.

7.4 Future Directions

We have previously demonstrated a conserved synthetic lethal interaction between loss of SETD2-dependent H3K36me3 and WEE1 inhibition (Pai et al., 2019; Pfister et al., 2015). This observation has been taken into clinical trials to target SETD2-deficient cancers (clinicaltrals.gov; NCT03284385), where the use of miR-106b-5p as a predictive biomarker for WEE1 inhibitor response could be explored further. The identification of SETD2-dependent H3K36me3 as an effector of the ATR- and CHK1-checkpoint pathway, described here, is consistent with the observation that both ATR and CHK1 are synthetic lethal with WEE1 inhibition in both fission yeast and human cells (al-Khodairy & Carr, 1992; Bukhari et al., 2019; Enoch, Carr, & Nurse, 1992; Nam et al., 2020). However, we have also observed a synthetic lethality between loss of SETD2-dependent H3K36me3 and ATR or CHK1 inhibition (Pfister et al., 2015), suggesting that ATR performs additional functions that are not epistatic to SETD2.

The main question that remains is how ATR/CHK1-dependent intra-S checkpoint activation causes elevated H3K36me3 on the promoter regions of p53- and E2F-responsive genes. We have had multiple hypotheses, including a role for ATR and/or CHK1 in directly targeting SETD2 or KDM4A-D (H3K36me3 demethylases) for phosphorylation or altered ubiquitin-mediated degradation. Furthermore, recent studies have shown that SETD2 is a substrate for SPOP (Zhu et al., 2017), a key subunit of the CUL3 ubiquitin E3 ligase complex, which is under direct control of the ATR/CHK1 axis (Tang et al., 2021). In the absence of ATR activity, CDK1-SPOP signalling could therefore lead to the degradation of SETD2 protein and low H3K36me3-driven gene expression during S-phase. Alternatively, CHK1-dependent phosphorylation of E2F6 could lead to its dissociation from the SETD2 promoter, causing global changes in H3K36me3 at the promoter regions of E2F-target genes. Further delineation of the functional relationship between SETD2 and these cell cycle checkpoint kinases, ATR and CHK1, together with the upstream and downstream factors described here, will be an important goal, and one which may provide further clinical opportunities.

Bibliography

Abbas, T., & Dutta, A. (2009). p21 in cancer: intricate networks and multiple activities. *Nature Reviews. Cancer*, *9*(6), 400–414. https://doi.org/10.1038/nrc2657

Abdel-Fatah, T. M. A., Arora, A., Alsubhi, N., Agarwal, D., Moseley, P. M., Perry, C., … Madhusudan, S. (2014). Clinicopathological Significance of ATM-Chk2 Expression in Sporadic Breast Cancers: a Comprehensive Analysis in Large Cohorts. *Neoplasia*, *16*(11), 982–991. https://doi.org/10.1016/J.NEO.2014.09.009

Adams, K. E., Medhurst, A. L., Dart, D. A., & Lakin, N. D. (2006). Recruitment of ATR to sites of ionising radiation-induced DNA damage requires ATM and components of the MRN protein complex. *Oncogene 2006 25:28*, *25*(28), 3894–3904. https://doi.org/10.1038/sj.onc.1209426

Akoglu, H. (2018). User's guide to correlation coefficients. *Turkish Journal of Emergency Medicine*, *18*(3), 91. https://doi.org/10.1016/J.TJEM.2018.08.001

al-Khodairy, F., & Carr, A. M. (1992). DNA repair mutants defining G2 checkpoint pathways in Schizosaccharomyces pombe. *The EMBO Journal*, *11*(4), 1343–1350. https://doi.org/10.1002/J.1460-2075.1992.TB05179.X

Al Sarakbi, W., Sasi, W., Jiang, W., Roberts, T., Newbold, R., & Mokbel, K. (2009). The mRNA expression of SETD2 in human breast cancer: correlation with clinico-pathological parameters. *BMC Cancer 2009 9:1*, *9*(1), 1–7. https://doi.org/10.1186/1471-2407-9-290

Allemani, C., Weir, H. K., Carreira, H., Harewood, R., Spika, D., Wang, X. S., … Miles, S. A. (2015). Global surveillance of cancer survival 1995–2009: analysis of individual data for 25 676 887 patients from 279 population-based registries in 67 countries (CONCORD-2). *The Lancet*, *385*(9972), 977–1010. https://doi.org/10.1016/S0140-6736(14)62038-9

Anda, S., Rothe, C., Boye, E., & Grallert, B. (2016). Consequences of abnormal CDK activity in S phase. *Cell Cycle*, *15*(7), 963–973. https://doi.org/10.1080/15384101.2016.1152423

Andrikopoulou, A., Shalit, A., Zografos, E., Koutsoukos, K., Korakiti, A. M., Liontos, M., … Zagouri, F. (2021). MicroRNAs as Potential Predictors of Response to CDK4/6 Inhibitor Treatment. *Cancers 2021, Vol. 13, Page 4114*, *13*(16), 4114. https://doi.org/10.3390/CANCERS13164114

Armfield, L. (2019). The role of histone H3K36me3 in mammalian cell cycle regulation and genome stability.

Arya, G., & Schlick, T. (2009). A tale of tails: how histone tails mediate chromatin compaction in different salt and linker histone environments. *Journal of Physical Chemistry A*, *113*(16), 4045–4059. https://doi.org/10.1021/jp810375d

Aymard, F., Bugler, B., Schmidt, C. K., Guillou, E., Caron, P., Briois, S., … Legube, G. (2014). Transcriptionally active chromatin recruits homologous recombination at DNA double-strand breaks. *Nature Structural & Molecular Biology*, *21*(4), 366–374. https://doi.org/10.1038/nsmb.2796

Baldin, V., Lukas, J., Marcote, M. J., Pagano, M., & Draetta, G. (1993). Cyclin D1 is a nuclear protein required for cell cycle progression in G1. *Genes Dev*, *7*(5), 812–821. https://doi.org/10.1101/gad.7.5.812

Bamford, S., Dawson, E., Forbes, S., Clements, J., Pettett, R., Dogan, A., … Wooster, R. (2004). The COSMIC (Catalogue of Somatic Mutations in Cancer) database and website. *British Journal of Cancer*. https://doi.org/10.1038/sj.bjc.6601894

Banerjee, S., Kalyani Yabalooru, S. R., & Karunagaran, D. (2020). Identification of mRNA and non-coding RNA hubs using network analysis in organ tropism regulated triple negative breast cancer metastasis. *Computers in Biology and Medicine*, *127*, 104076. https://doi.org/10.1016/J.COMPBIOMED.2020.104076

Bannister, A. J., Schneider, R., Myers, F. A., Thorne, A. W., Crane-Robinson, C., & Kouzarides, T. (2005). Spatial distribution of di- and tri-methyl lysine 36 of histone H3 at active genes. *Journal of Biological Chemistry*, *280*(18), 17732–17736. https://doi.org/10.1074/jbc.M500796200

Barretina, J., Caponigro, G., Stransky, N., Venkatesan, K., Margolin, A. A., Kim, S., … Garraway, L. A. (2012). The Cancer Cell Line Encyclopedia enables predictive modelling of anticancer drug

sensitivity. *Nature 2012 483:7391*, *483*(7391), 603–607. https://doi.org/10.1038/nature11003
Bartel, D. P. (2009). MicroRNAs: Target Recognition and Regulatory Functions. *Cell*. https://doi.org/10.1016/j.cell.2009.01.002
Baskerville, S., & Bartel, D. P. (2005). Microarray profiling of microRNAs reveals frequent coexpression with neighboring miRNAs and host genes. *RNA*. https://doi.org/10.1261/rna.7240905
Baubec, T., Colombo, D. F., Wirbelauer, C., Schmidt, J., Burger, L., Krebs, A. R., … Schu, D. (2015). Genomic profilingofDNAmethyltransferases reveals a role for DNMT3B in genic methylation. *Nature*, *520*(7546), 243–247. https://doi.org/10.1038/nature14176
Beck, H., Nähse-Kumpf, V., Larsen, M. S. Y., O'Hanlon, K. A., Patzke, S., Holmberg, C., … Sorensen, C. S. (2012). Cyclin-Dependent Kinase Suppression by WEE1 Kinase Protects the Genome through Control of Replication Initiation and Nucleotide Consumption. *Molecular and Cellular Biology*, *32*(20), 4226–4236. https://doi.org/10.1128/MCB.00412-12
Beck, H., Nähse, V., Larsen, M. S. Y., Groth, P., Clancy, T., Lees, M., … Sørensen, C. S. (2010). Regulators of cyclin-dependent kinases are crucial for maintaining genome integrity in S phase. *Journal of Cell Biology*, *188*(5), 629–638. https://doi.org/10.1083/JCB.200905059
Benjamini, Y., & Hochberg, Y. (1995). Controlling the False Discovery Rate: A Practical and Powerful Approach to Multiple Testing. *Journal of the Royal Statistical Society: Series B (Methodological)*, *57*(1), 289–300. https://doi.org/10.1111/J.2517-6161.1995.TB02031.X
Bensimon, A., Schmidt, A., Ziv, Y., Elkon, R., Wang, S.-Y., Chen, D. J., … Shiloh, Y. (2010). ATM-Dependent and -Independent Dynamics of the Nuclear Phosphoproteome After DNA Damage. *Science Signaling*, *3*(151). https://doi.org/10.1126/SCISIGNAL.2001034
Bentwich, I., Avniel, A., Karov, Y., Aharonov, R., Gilad, S., Barad, O., … Bentwich, Z. (2005). Identification of hundreds of conserved and nonconserved human microRNAs. *Nature Genetics 2005 37:7*, *37*(7), 766–770. https://doi.org/10.1038/ng1590
Bertoli, C., Klier, S., Mcgowan, C., Wittenberg, C., & De Bruin, R. A. M. (2013). Chk1 keeps cell cycle transcription active in response to replication stress by interfering with E2F6-dependent repression. https://doi.org/10.1016/j.cub.2013.06.063
Bertoli, C., Klier, S., McGowan, C., Wittenberg, C., & De Bruin, R. A. M. (2013). Chk1 inhibits E2F6 repressor function in response to replication stress to maintain cell-cycle transcription. *Current Biology*, *23*(17), 1629–1637. https://doi.org/10.1016/j.cub.2013.06.063
Bertoli, C., Skotheim, J. M., & De Bruin, R. A. M. (2013, August). Control of cell cycle transcription during G1 and S phases. *Nature Reviews Molecular Cell Biology*. Nat Rev Mol Cell Biol. https://doi.org/10.1038/nrm3629
Besson, A., Dowdy, S. F., & Roberts, J. M. (2008). CDK Inhibitors: Cell Cycle Regulators and Beyond. *Developmental Cell*. https://doi.org/10.1016/j.devcel.2008.01.013
Betancur, J. G., & Tomari, Y. (2012). Dicer is dispensable for asymmetric RISC loading in mammals. *RNA*, *18*(1), 24–30. https://doi.org/10.1261/RNA.029785.111
Bhattacharya, S., Levy, M. J., Zhang, N., Li, H., Florens, L., Washburn, M. P., & Workman, J. L. (2021). The methyltransferase SETD2 couples transcription and splicing by engaging mRNA processing factors through its SHI domain. *Nature Communications 2021 12:1*, *12*(1), 1–16. https://doi.org/10.1038/s41467-021-21663-w
Bhattacharya, S., Wang, S., Reddy, D., Shen, S., Zhang, Y., Zhang, N., … Li, F. (2021). Structural basis of the interaction between SETD2 methyltransferase and hnRNP L paralogs for governing co-transcriptional splicing. *Nature Communications 2021 12:1*, *12*(1), 1–15. https://doi.org/10.1038/s41467-021-26799-3
Black, J. C., Van Rechem, C., & Whetstine, J. R. (2012). Histone Lysine Methylation Dynamics: Establishment, Regulation, and Biological Impact. *Molecular Cell*. https://doi.org/10.1016/j.molcel.2012.11.006
Blackford, A. N., & Jackson, S. P. (2017). ATM, ATR, and DNA-PK: The Trinity at the Heart of the DNA Damage Response. *Molecular Cell*. https://doi.org/10.1016/j.molcel.2017.05.015
Bland, J. M., & Altman, D. G. (2004). Statistics Notes: The logrank test. *BMJ : British Medical Journal*, *328*(7447), 1073. https://doi.org/10.1136/BMJ.328.7447.1073

Bøe, C. A., Håland, T. W., Boye, E., Syljuåsen, R. G., & Grallert, B. (2018). A novel role for ATR/Rad3 in G1 phase. *Scientific Reports 2018 8:1*, *8*(1), 1–12. https://doi.org/10.1038/s41598-018-25238-6

Bolger, A. M., Lohse, M., & Usadel, B. (2014). Trimmomatic: a flexible trimmer for Illumina sequence data. *Bioinformatics*, *30*(15), 2114–2120. https://doi.org/10.1093/BIOINFORMATICS/BTU170

Booher, R. N., Holman, P. S., & Fattaey, A. (1997). Human Myt1 is a cell cycle-regulated kinase that inhibits Cdc2 but not Cdk2 activity. *Journal of Biological Chemistry*, *272*(35), 22300–22306. https://doi.org/10.1074/jbc.272.35.22300

Boos, D., Frigola, J., & Diffley, J. F. X. (2012). Activation of the replicative DNA helicase: breaking up is hard to do. *Current Opinion in Cell Biology*, *24*(3), 423–430. https://doi.org/10.1016/J.CEB.2012.01.011

Borchert, G. M., Lanier, W., & Davidson, B. L. (2006). RNA polymerase III transcribes human microRNAs. *Nature Structural and Molecular Biology*. https://doi.org/10.1038/nsmb1167

Brandsma, I., Fleuren, E. D. G., Williamson, C. T., & Lord, C. J. (2017). Directing the use of DDR kinase inhibitors in cancer treatment. *Https://Doi.Org/10.1080/13543784.2017.1389895*, *26*(12), 1341–1355. https://doi.org/10.1080/13543784.2017.1389895

Brase, J. C., Wuttig, D., Kuner, R., & Sültmann, H. (2010). Serum microRNAs as non-invasive biomarkers for cancer. *Molecular Cancer*. https://doi.org/10.1186/1476-4598-9-306

Braun, J. E., Huntzinger, E., Fauser, M., & Izaurralde, E. (2011). GW182 proteins directly recruit cytoplasmic deadenylase complexes to miRNA targets. *Molecular Cell*, *44*(1), 120–133. https://doi.org/10.1016/J.MOLCEL.2011.09.007/ATTACHMENT/3949DB29-31EC-4662-A807-D7C1B6317D67/MMC1.PDF

Bray, F., Ferlay, J., Soerjomataram, I., Siegel, R. L., Torre, L. A., & Jemal, A. (2018). Global cancer statistics 2018: GLOBOCAN estimates of incidence and mortality worldwide for 36 cancers in 185 countries. *CA: A Cancer Journal for Clinicians*, *68*(6), 394–424. https://doi.org/10.3322/CAAC.21492

Bray, N. L., Pimentel, H., Melsted, P., & Pachter, L. (2016). Near-optimal probabilistic RNA-seq quantification. *Nature Biotechnology*. https://doi.org/10.1038/nbt.3519

Brosh, R., Shalgi, R., Liran, A., Landan, G., Korotayev, K., Nguyen, G. H., … Rotter, V. (2008). p53-repressed miRNAs are involved with E2F in a feed-forward loop promoting proliferation. *Molecular Systems Biology*, *4*(1), 229. https://doi.org/10.1038/MSB.2008.65

Bruckbauer, S. T., Minkoff, B. B., Yu, D., Cryns, V. L., Cox, M. M., & Sussman, M. R. (2020). Ionizing Radiation-induced Proteomic Oxidation in Escherichia coli. *Molecular & Cellular Proteomics : MCP*, *19*(8), 1375. https://doi.org/10.1074/MCP.RA120.002092

Bueno, M. J., Gómez de Cedrón, M., Laresgoiti, U., Fernández-Piqueras, J., Zubiaga, A. M., & Malumbres, M. (2010). Multiple E2F-Induced MicroRNAs Prevent Replicative Stress in Response to Mitogenic Signaling. *Molecular and Cellular Biology*, *30*(12), 2983–2995. https://doi.org/10.1128/MCB.01372-09

Bukhari, A. B., Lewis, C. W., Pearce, J. J., Luong, D., Chan, G. K., & Gamper, A. M. (2019). Inhibiting Wee1 and ATR kinases produces tumor-selective synthetic lethality and suppresses metastasis. *The Journal of Clinical Investigation*, *129*(3), 1329–1344. https://doi.org/10.1172/JCI122622

Bunz, F., Dutriaux, A., Lengauer, C., Waldman, T., Zhou, S., Brown, J. P., … Vogelstein, B. (1998). Requirement for p53 and p21 to Sustain G2 Arrest After DNA Damage. *Science*, *282*(5393), 1497–1501. https://doi.org/10.1126/SCIENCE.282.5393.1497

Burdova, K., Yang, H., Faedda, R., Hume, S., Chauhan, J., Ebner, D., … D'Angiolella, V. (2019). E2F1 proteolysis via SCF-cyclin F underlies synthetic lethality between cyclin F loss and Chk1 inhibition. *The EMBO Journal*, *38*(20). https://doi.org/10.15252/EMBJ.2018101443

Caetano, C., Klier, S., & Bruin, R. A. M. de. (2011). Phosphorylation of the MBF Repressor Yox1p by the DNA Replication Checkpoint Keeps the G1/S Cell-Cycle Transcriptional Program Active. *PLOS ONE*, *6*(2), e17211. https://doi.org/10.1371/JOURNAL.PONE.0017211

Calin, G. A., Sevignani, C., Dumitru, C. D., Hyslop, T., Noch, E., Yendamuri, S., … Croce, C. M.

(2004). Human microRNA genes are frequently located at fragile sites and genomic regions involved in cancers. *Proceedings of the National Academy of Sciences of the United States of America*. https://doi.org/10.1073/pnas.0307323101

Campbell, P. J., Getz, G., Korbel, J. O., Stuart, J. M., Jennings, J. L., Stein, L. D., … Zhang, J. (2020). Pan-cancer analysis of whole genomes. *Nature 2020 578:7793*, *578*(7793), 82–93. https://doi.org/10.1038/s41586-020-1969-6

Cappell, S. D., Chung, M., Jaimovich, A., Spencer, S. L., & Meyer, T. (2016). Irreversible APCCdh1 Inactivation Underlies the Point of No Return for Cell-Cycle Entry. *Cell*, *166*(1), 167. https://doi.org/10.1016/J.CELL.2016.05.077

Carvalho, S., Raposo, A. C., Martins, F. B., Grosso, A. R., Sridhara, S. C., Rino, J., … De Almeida, S. F. (2013). Histone methyltransferase SETD2 coordinates FACT recruitment with nucleosome dynamics during transcription. *Nucleic Acids Research*, *41*(5), 2881–2893. https://doi.org/10.1093/nar/gks1472

Carvalho, S., Vítor, A. C., Sridhara, S. C., Filipa, B. M., Ana, C. R., Desterro, J. M. P., … de Almeida, S. F. (2014). SETD2 is required for DNA double-strand break repair and activation of the p53-mediated checkpoint. *ELife*, *2014*(3), 1–19. https://doi.org/10.7554/eLife.02482

Cerami, E., Gao, J., Dogrusoz, U., Gross, B. E., Sumer, S. O., Aksoy, B. A., … Schultz, N. (2012). The cBio Cancer Genomics Portal: An Open Platform for Exploring Multidimensional Cancer Genomics Data. *Cancer Discovery*, *2*(5), 401–404. https://doi.org/10.1158/2159-8290.CD-12-0095

Chabes, A. L., Björklund, S., & Thelander, L. (2004). S Phase-specific Transcription of the Mouse Ribonucleotide Reductase R2 Gene Requires Both a Proximal Repressive E2F-binding Site and an Upstream Promoter Activating Region *. *Journal of Biological Chemistry*, *279*(11), 10796–10807. https://doi.org/10.1074/JBC.M312482200

Chaitanya, G. V., Alexander, J. S., & Babu, P. P. (2010). PARP-1 cleavage fragments: signatures of cell-death proteases in neurodegeneration. *Cell Communication and Signaling : CCS*, *8*, 31. https://doi.org/10.1186/1478-811X-8-31

Challa, K., Schmid, C. D., Kitagawa, S., Cheblal, A., Iesmantavicius, V., Seeber, A., … Gasser, S. M. (2021). Damage-induced chromatome dynamics link Ubiquitin ligase and proteasome recruitment to histone loss and efficient DNA repair. *Molecular Cell*, *81*(4), 811-829.e6. https://doi.org/10.1016/J.MOLCEL.2020.12.021

Chang, T. C., Yu, D., Lee, Y. S., Wentzel, E. A., Arking, D. E., West, K. M., … Mendell, J. T. (2008). Widespread microRNA repression by Myc contributes to tumorigenesis. *Nature Genetics*. https://doi.org/10.1038/ng.2007.30

Chellappan, S. P., Hiebert, S., Mudryj, M., Horowitz, J. M., & Nevins, J. R. (1991). The E2F transcription factor is a cellular target for the RB protein. *Cell*, *65*(6), 1053–1061. https://doi.org/10.1016/0092-8674(91)90557-F

Cheloufi, S., Dos Santos, C. O., Chong, M. M. W., & Hannon, G. J. (2010). A dicer-independent miRNA biogenesis pathway that requires Ago catalysis. *Nature*. https://doi.org/10.1038/nature09092

Chen, X., Low, K.-H., Alexander, A., Jiang, Y., Karakas, C., Hess, K. R., … Keyomarsi, K. (2018). Cyclin E Overexpression Sensitizes Triple-Negative Breast Cancer to Wee1 Kinase Inhibition. *Clinical Cancer Research : An Official Journal of the American Association for Cancer Research*, *24*(24), 6594. https://doi.org/10.1158/1078-0432.CCR-18-1446

Chendrimada, T. P., Gregory, R. I., Kumaraswamy, E., Norman, J., Cooch, N., Nishikura, K., & Shiekhattar, R. (2005). TRBP recruits the Dicer complex to Ago2 for microRNA processing and gene silencing. *Nature 2005 436:7051*, *436*(7051), 740–744. https://doi.org/10.1038/nature03868

Chiruvella, K. K., Liang, Z., & Wilson, T. E. (2013). Repair of Double-Strand Breaks by End Joining. *Cold Spring Harbor Perspectives in Biology*, *5*(5), a012757. https://doi.org/10.1101/CSHPERSPECT.A012757

Choi, E.-H., & Kim, K. P. (2019). E2F1 facilitates DNA break repair by localizing to break sites and enhancing the expression of homologous recombination factors. *Experimental & Molecular*

Medicine 2019 51:9, *51*(9), 1–12. https://doi.org/10.1038/s12276-019-0307-2
Choudhary, S., Burns, S. C., Mirsafian, H., Li, W., Vo, D. T., Qiao, M., … Penalva, L. O. (2020). Genomic analyses of early responses to radiation in glioblastoma reveal new alterations at transcription, splicing, and translation levels. *Scientific Reports 2020 10:1*, *10*(1), 1–12. https://doi.org/10.1038/s41598-020-65638-1
Chow, J. P. H., & Poon, R. Y. C. (2012). The CDK1 inhibitory kinase MYT1 in DNA damage checkpoint recovery. *Oncogene 2013 32:40*, *32*(40), 4778–4788. https://doi.org/10.1038/onc.2012.504
Chu, S., Liu, G., Xia, P., Chen, G., Shi, F., Yi, T., & Zhou, H. (2017). miR-93 and PTEN: Key regulators of doxorubicin-resistance and EMT in breast cancer. *Oncology Reports*, *38*(4), 2401–2407. https://doi.org/10.3892/OR.2017.5859
Chu, Z., Li, J., Eshaghi, M., Peng, X., Karuturi, R. K. M., & Liu, J. (2007). Modulation of Cell Cycle–specific Gene Expressions at the Onset of S Phase Arrest Contributes to the Robust DNA Replication Checkpoint Response in Fission Yeas. *Https://Doi.Org/10.1091/Mbc.E06-10-0928*, *18*(5), 1756–1767. https://doi.org/10.1091/MBC.E06-10-0928
Ciccia, A., & Elledge, S. J. (2010). The DNA Damage Response: Making It Safe to Play with Knives. *Molecular Cell*, *40*(2), 179–204. https://doi.org/10.1016/J.MOLCEL.2010.09.019
Cifuentes, D., Xue, H., Taylor, D. W., Patnode, H., Mishima, Y., Cheloufi, S., … Giraldez, A. J. (2010). A Novel miRNA Processing Pathway Independent of Dicer Requires Argonaute2 Catalytic Activity. *Science*, *328*(5986), 1694–1698. https://doi.org/10.1126/SCIENCE.1190809
Cooper, G. M., & Hausman, R. E. (2007). *The Cell: A Molecular Approach 2nd Edition*. *Sinauer Associates*.
Corcoran, D. L., Pandit, K. V., Gordon, B., Bhattacharjee, A., Kaminski, N., & Benos, P. V. (2009). Features of mammalian microRNA promoters emerge from polymerase II chromatin immunoprecipitation data. *PLoS ONE*. https://doi.org/10.1371/journal.pone.0005279
Costa, A., Ilves, I., Tamberg, N., Petojevic, T., Nogales, E., Botchan, M. R., & Berger, J. M. (2011). The structural basis for MCM2–7 helicase activation by GINS and Cdc45. *Nature Structural & Molecular Biology 2011 18:4*, *18*(4), 471–477. https://doi.org/10.1038/nsmb.2004
Coverley, D., Laman, H., & Laskey, R. A. (2002). Distinct roles for cyclins E and A during DNA replication complex assembly and activation. *Nature Cell Biology*, *4*(7), 523–528. https://doi.org/10.1038/ncb813
Crosio, C., Fimia, G. M., Loury, R., Kimura, M., Okano, Y., Zhou, H., … Sassone-Corsi, P. (2002). Mitotic Phosphorylation of Histone H3: Spatio-Temporal Regulation by Mammalian Aurora Kinases. *Molecular and Cellular Biology*, *22*(3), 874–885. https://doi.org/10.1128/MCB.22.3.874-885.2002
Cross, F. R., Buchler, N. E., & Skotheim, J. M. (2011). Evolution of networks and sequences in eukaryotic cell cycle control. *Philosophical Transactions of the Royal Society B: Biological Sciences*, *366*(1584), 3532–3544. https://doi.org/10.1098/RSTB.2011.0078
Cullen, B. R. (2004). Transcription and processing of human microRNA precursors. *Molecular Cell*. https://doi.org/10.1016/j.molcel.2004.12.002
Curtis, C., Shah, S. P., Chin, S.-F., Turashvili, G., Rueda, O. M., Dunning, M. J., … Aparicio, S. (2012). The genomic and transcriptomic architecture of 2,000 breast tumours reveals novel subgroups. *Nature 2012 486:7403*, *486*(7403), 346–352. https://doi.org/10.1038/nature10983
D'Angiolella, V., Donato, V., Forrester, F. M., Jeong, Y. T., Pellacani, C., Kudo, Y., … Pagano, M. (2012). Cyclin F-mediated degradation of ribonucleotide reductase M2 controls genome integrity and DNA repair. *Cell*, *149*(5), 1023–1034. https://doi.org/10.1016/j.cell.2012.03.043
D'Oto, A., Fang, J., Jin, H., Xu, B., Singh, S., Mullasseril, A., … Yang, J. (2020). KDM6B promotes oncogenic CDK4/6-pRB-E2F pathway via maintaining enhancer activation in high-risk neuroblastoma. *BioRxiv*, 2020.07.02.184986. https://doi.org/10.1101/2020.07.02.184986
Dahlet, T., Truss, M., Frede, U., Al Adhami, H., Bardet, A. F., Dumas, M., … Weber, M. (2021). E2F6 initiates stable epigenetic silencing of germline genes during embryonic development. *Nature Communications 2021 12:1*, *12*(1), 1–14. https://doi.org/10.1038/s41467-021-23596-w
Dalman, M. R., Deeter, A., Nimishakavi, G., & Duan, Z.-H. (2012). Fold change and p-value cutoffs

significantly alter microarray interpretations. *BMC Bioinformatics*, *13*(Suppl 2), S11. https://doi.org/10.1186/1471-2105-13-S2-S11
Daugaard, M., Baude, A., Fugger, K., Povlsen, L. K., Beck, H., Sørensen, C. S., … Jäättelä, M. (2012). LEDGF (p75) promotes DNA-end resection and homologous recombination. *Nature Structural & Molecular Biology*, *19*(8), 803–810. https://doi.org/10.1038/nsmb.2314
Davis, M. P. A., van Dongen, S., Abreu-Goodger, C., Bartonicek, N., & Enright, A. J. (2013). Kraken: A set of tools for quality control and analysis of high-throughput sequence data. *Methods*, *63*(1), 41–49. https://doi.org/10.1016/J.YMETH.2013.06.027
de Bruin, R. A. M., Kalashnikova, T. I., Chahwan, C., McDonald, W. H., Wohlschlegel, J., Yates, J., … Wittenberg, C. (2006). Constraining G1-Specific Transcription to Late G1 Phase: The MBF-Associated Corepressor Nrm1 Acts via Negative Feedback. *Molecular Cell*, *23*(4), 483–496. https://doi.org/10.1016/J.MOLCEL.2006.06.025
de Rinaldis, E., Gazinska, P., Mera, A., Modrusan, Z., Fedorowicz, G. M., Burford, B., … Tutt, A. (2013). Integrated genomic analysis of triple-negative breast cancers reveals novel microRNAs associated with clinical and molecular phenotypes and sheds light on the pathways they control. *BMC Genomics 2013 14:1*, *14*(1), 1–19. https://doi.org/10.1186/1471-2164-14-643
Dedes, K. J., Natrajan, R., Lambros, M. B., Geyer, F. C., Lopez-Garcia, M. A., Savage, K., … Reis-Filho, J. S. (2011). Down-regulation of the miRNA master regulators Drosha and Dicer is associated with specific subgroups of breast cancer. *European Journal of Cancer*, *47*(1), 138–150. https://doi.org/10.1016/J.EJCA.2010.08.007
Deegan, T. D., & Diffley, J. F. X. (2016). MCM: one ring to rule them all. *Current Opinion in Structural Biology*, *37*, 145–151. https://doi.org/10.1016/J.SBI.2016.01.014
DeGregori, J., Kowalik, T., & Nevins, J. R. (1995). Cellular targets for activation by the E2F1 transcription factor include DNA synthesis- and G1/S-regulatory genes. *Molecular and Cellular Biology*, *15*(8), 4215. https://doi.org/10.1128/MCB.15.8.4215
Demczuk, A., Gauthier, M. G., Veras, I., Kosiyatrakul, S., Schildkraut, C. L., Busslinger, M., … Norio, P. (2012). Regulation of DNA Replication within the Immunoglobulin Heavy-Chain Locus During B Cell Commitment. *PLOS Biology*, *10*(7), e1001360. https://doi.org/10.1371/JOURNAL.PBIO.1001360
DeMichele, A., Clark, A. S., Tan, K. S., Heitjan, D. F., Gramlich, K., Gallagher, M., … O'Dwyer, P. (2015). CDK 4/6 Inhibitor palbociclib (PD0332991) in Rb^+ advanced breast cancer: Phase II activity, safety, and predictive biomarker assessment. *Clinical Cancer Research*. https://doi.org/10.1158/1078-0432.CCR-14-2258
Deng, L., Petrek, H., Tu, M.-J., Batra, N., Yu, A.-X., & Yu, A.-M. (2021). Bioengineered miR-124-3p prodrug selectively alters the proteome of human carcinoma cells to control multiple cellular components and lung metastasis in vivo. *Acta Pharmaceutica Sinica B*. https://doi.org/10.1016/J.APSB.2021.07.027
Dephoure, N., Zhou, C., Villén, J., Beausoleil, S. A., Bakalarski, C. E., Elledge, S. J., & Gygi, S. P. (2008). A quantitative atlas of mitotic phosphorylation. *Proceedings of the National Academy of Sciences*, *105*(31), 10762–10767. https://doi.org/10.1073/PNAS.0805139105
Dewar, J. M., Budzowska, M., & Walter, J. C. (2015). The mechanism of DNA replication termination in vertebrates. *Nature 2015 525:7569*, *525*(7569), 345–350. https://doi.org/10.1038/nature14887
Dhawan, A., Scott, J. G., Harris, A. L., & Buffa, F. M. (2018). Pan-cancer characterisation of microRNA across cancer hallmarks reveals microRNA-mediated downregulation of tumour suppressors. *Nature Communications*. https://doi.org/10.1038/s41467-018-07657-1
Di Leva, G., Garofalo, M., & Croce, C. M. (2014). MicroRNAs in cancer. *Annual Review of Pathology: Mechanisms of Disease*. https://doi.org/10.1146/annurev-pathol-012513-104715
Difiore, J. V, Ptacek, T. S., Wang, Y., Li, B., Simon, J. M., & Strahl, B. D. (2020). Unique and Shared Roles for Histone H3K36 Methylation States in Transcription Regulation Functions. https://doi.org/10.1016/j.celrep.2020.107751
Dobin, A., Davis, C. A., Schlesinger, F., Drenkow, J., Zaleski, C., Jha, S., … Gingeras, T. R. (2013). STAR: ultrafast universal RNA-seq aligner. *Bioinformatics*, *29*(1), 15–21.

https://doi.org/10.1093/BIOINFORMATICS/BTS635
Dong, C.-M., Wang, X.-L., Wang, G.-M., Zhang, W.-J., Zhu, L., Gao, S., … Xu, J. (2014). A stress-induced cellular aging model with postnatal neural stem cells. *Cell Death & Disease 2014 5:3*, *5*(3), e1116–e1116. https://doi.org/10.1038/cddis.2014.82
Dulic, V., Lees, E., & Reed, S. (1992). Association of human cyclin E with a periodic G1-S phase protein kinase. *Science*, *257*(5078), 1958–1961. https://doi.org/10.1126/SCIENCE.1329201
Dungrawala, H., Bhat, K. P., Meur, R. Le, Chazin, W. J., Ding, X., Sharan, S. K., … Cortez, D. (2017). RADX promotes genome stability and modulates chemosensitivity by regulating RAD51 at replication forks. *Molecular Cell*, *67*(3), 374. https://doi.org/10.1016/J.MOLCEL.2017.06.023
Dunham, I., Kundaje, A., Aldred, S. F., Collins, P. J., Davis, C. A., Doyle, F., … Lochovsky, L. (2012). An integrated encyclopedia of DNA elements in the human genome. *Nature*, *489*(7414), 57–74. https://doi.org/10.1038/nature11247
Duns, G., van den Berg, E., van Duivenbode, I., Osinga, J., Hollema, H., Hofstra, R. M. W., & Kok, K. (2010). Histone methyltransferase gene SETD2 is a novel tumor suppressor gene in clear cell renal cell carcinoma. *Cancer Research*, *70*(11), 4287–4291. https://doi.org/10.1158/0008-5472.CAN-10-0120
Dvinge, H., Git, A., Gräf, S., Salmon-Divon, M., Curtis, C., Sottoriva, A., … Caldas, C. (2013). The shaping and functional consequences of the microRNA landscape in breast cancer. *Nature 2013 497:7449*, *497*(7449), 378–382. https://doi.org/10.1038/nature12108
Edmunds, J. W., Mahadevan, L. C., & Clayton, A. L. (2008). Dynamic histone H3 methylation during gene induction: HYPB/Setd2 mediates all H3K36 trimethylation. *The EMBO Journal*, *27*, 406–420. https://doi.org/10.1038/
El-Shemerly, M., Hess, D., Pyakurel, A. K., Moselhy, S., & Ferrari, S. (2008). ATR-dependent pathways control hEXO1 stability in response to stalled forks. *Nucleic Acids Research*, *36*(2), 511–519. https://doi.org/10.1093/NAR/GKM1052
Elbæk, C. R., Petrosius, V., & Sørensen, C. S. (2020). WEE1 kinase limits CDK activities to safeguard DNA replication and mitotic entry. *Mutation Research/Fundamental and Molecular Mechanisms of Mutagenesis*, *819–820*, 111694. https://doi.org/10.1016/J.MRFMMM.2020.111694
Elledge, S. J., Zhou, Z., & Allen, J. B. (1992). Ribonucleotide reductase: regulation, regulation, regulation. *Trends in Biochemical Sciences*, *17*(3), 119–123. https://doi.org/10.1016/0968-0004(92)90249-9
Endogenous Controls for Real-Time Quantitation of miRNA Using TaqMan® MicroRNA Assays. (2007, August). Retrieved 14 September 2021, from https://www.gene-quantification.de/AB-microRNA-endog-controls.pdf
Enoch, T., Carr, A. M., & Nurse, P. (1992). Fission yeast genes involved in coupling mitosis to completion of DNA replication. *Genes and Development*, *6*(11), 2035–2046. https://doi.org/10.1101/gad.6.11.2035
Eram, M. S., Bustos, S. P., Lima-Fernandes, E., Siarheyeva, A., Senisterra, G., Hajian, T., … Vedadi, M. (2014). Trimethylation of Histone H3 Lysine 36 by Human Methyltransferase PRDM9 Protein *. *Journal of Biological Chemistry*, *289*(17), 12177–12188. https://doi.org/10.1074/JBC.M113.523183
Farazi, T. A., ten Hoeve, J. J., Brown, M., Mihailovic, A., Horlings, H. M., van de Vijver, M. J., … Wessels, L. F. A. (2014). Identification of distinct miRNA target regulation between breast cancer molecular subtypes using AGO2-PAR-CLIP and patient datasets. *Genome Biology*. https://doi.org/10.1186/gb-2014-15-1-r9
Farré, P. L., Duca, R. B., Massillo, C., Dalton, G. N., Graña, K. D., Gardner, K., … Siervi, A. De. (2021). MiR-106b-5p: A Master Regulator of Potential Biomarkers for Breast Cancer Aggressiveness and Prognosis. *International Journal of Molecular Sciences 2021, Vol. 22, Page 11135*, *22*(20), 11135. https://doi.org/10.3390/IJMS222011135
Filipów, S., & Łaczmański, Ł. (2019). Blood Circulating miRNAs as Cancer Biomarkers for Diagnosis and Surgical Treatment Response. *Frontiers in Genetics*, *10*(FEB).

https://doi.org/10.3389/FGENE.2019.00169
Filippov, V., Solovyev, V., Filippova, M., & Gill, S. S. (2000). A novel type of RNase III family proteins in eukaryotes. *Gene*, *245*(1), 213–221. https://doi.org/10.1016/S0378-1119(99)00571-5
Flensburg, C., Kinkel, S. A., Keniry, A., Blewitt, M. E., & Oshlack, A. (2014). A comparison of control samples for ChIP-seq of histone modifications. *Frontiers in Genetics*, *0*(SEP), 329. https://doi.org/10.3389/FGENE.2014.00329
Fontebasso, A. M., Schwartzentruber, J., Khuong-Quang, D.-A., Liu, X.-Y., Sturm, D., Korshunov, A., … Majewski, J. (2013). Mutations in SETD2 and genes affecting histone H3K36 methylation target hemispheric high-grade gliomas. *Acta Neuropathologica 2013 125:5*, *125*(5), 659–669. https://doi.org/10.1007/S00401-013-1095-8
Franken, N. A. P., Rodermond, H. M., Stap, J., Haveman, J., & van Bree, C. (2006). Clonogenic assay of cells in vitro. *Nature Protocols 2006 1:5*, *1*(5), 2315–2319. https://doi.org/10.1038/nprot.2006.339
Friedman, R. C., Farh, K. K. H., Burge, C. B., & Bartel, D. P. (2009). Most mammalian mRNAs are conserved targets of microRNAs. *Genome Research*. https://doi.org/10.1101/gr.082701.108
Fu, Y. V., Yardimci, H., Long, D. T., Ho, V., Guainazzi, A., Bermudez, V. P., … Walter, J. C. (2011). Selective Bypass of a Lagging Strand Roadblock by the Eukaryotic Replicative DNA Helicase. *Cell*, *146*(6), 931–941. https://doi.org/10.1016/J.CELL.2011.07.045
Fu, Z., Malureanu, L., Huang, J., Wang, W., Li, H., Deursen, J. M. van, … Chen, J. (2008). Plk1-dependent phosphorylation of FoxM1 regulates a transcriptional programme required for mitotic progression. *Nature Cell Biology*, *10*(9), 1076. https://doi.org/10.1038/NCB1767
Fukuda, T., Yamagata, K., Fujiyama, S., Matsumoto, T., Koshida, I., Yoshimura, K., … Kato, S. (2007). DEAD-box RNA helicase subunits of the Drosha complex are required for processing of rRNA and a subset of microRNAs. *Nature Cell Biology 2007 9:5*, *9*(5), 604–611. https://doi.org/10.1038/ncb1577
Fung, T. K., & Poon, R. Y. C. (2005). A roller coaster ride with the mitotic cyclins. *Seminars in Cell & Developmental Biology*, *16*(3), 335–342. https://doi.org/10.1016/J.SEMCDB.2005.02.014
Galka-Marciniak, P., Urbanek-Trzeciak, M. O., Nawrocka, P. M., & Kozlowski, P. (2021). A pan-cancer atlas of somatic mutations in miRNA biogenesis genes. *Nucleic Acids Research*, *49*(2), 601. https://doi.org/10.1093/NAR/GKAA1223
Gao, J., Aksoy, B. A., Dogrusoz, U., Dresdner, G., Gross, B., Sumer, S. O., … Schultz, N. (2013). Integrative Analysis of Complex Cancer Genomics and Clinical Profiles Using the cBioPortal. *Science Signaling*, *6*(269). https://doi.org/10.1126/SCISIGNAL.2004088
Garzon, R., Calin, G. A., & Croce, C. M. (2009). MicroRNAs in cancer. *Annual Review of Medicine*. https://doi.org/10.1146/annurev.med.59.053006.104707
Gavet, O., & Pines, J. (2010). Progressive activation of CyclinB1-Cdk1 coordinates entry to mitosis. *Developmental Cell*, *18*(4), 533. https://doi.org/10.1016/J.DEVCEL.2010.02.013
Gavin, A. L., Huang, D., Huber, C., Mårtensson, A., Tardif, V., Skog, P. D., … Nemazee, D. (2018). PLD3 and PLD4 are single-stranded acid exonucleases that regulate endosomal nucleic-acid sensing. *Nature Immunology 2018 19:9*, *19*(9), 942–953. https://doi.org/10.1038/s41590-018-0179-y
Ge, S. X., Jung, D., Jung, D., & Yao, R. (2020). ShinyGO: A graphical gene-set enrichment tool for animals and plants. *Bioinformatics*, *36*(8), 2628–2629. https://doi.org/10.1093/bioinformatics/btz931
Ge, X. Q., Jackson, D. A., & Blow, J. J. (2007). Dormant origins licensed by excess Mcm2–7 are required for human cells to survive replicative stress. *Genes & Development*, *21*(24), 3331–3341. https://doi.org/10.1101/GAD.457807
Geng, Y., Eaton, E. N., Picón, M., Roberts, J. M., Lundberg, A. S., Gifford, A., … Weinberg, R. A. (1996). Regulation of cyclin E transcription by E2Fs and retinoblastoma protein. *Oncogene*, *12*(6), 1173–1180.
Gerlinger, M., Rowan, A. J., Horswell, S., Larkin, J., Endesfelder, D., Gronroos, E., … Swanton, C. (2012). Intratumor heterogeneity and branched evolution revealed by multiregion sequencing. *The New England Journal of Medicine*, *366*(10), 883–892.

https://doi.org/10.1056/NEJMoa1113205
Ghandi, M., Huang, F. W., Jané-Valbuena, J., Kryukov, G. V., Lo, C. C., McDonald, E. R., … Sellers, W. R. (2019). Next-generation characterization of the Cancer Cell Line Encyclopedia. *Nature*. https://doi.org/10.1038/s41586-019-1186-3
Giaccia, A. J., & Kastan, M. B. (1998). The complexity of p53 modulation: emerging patterns from divergent signals. *Genes & Development*, *12*(19), 2973–2983. https://doi.org/10.1101/GAD.12.19.2973
Giangrande, P. H., Zhu, W., Schlisio, S., Sun, X., Mori, S., Gaubatz, S., & Nevins, J. R. (2004). A role for E2F6 in distinguishing G1/S- and G2/M-specific transcription. *Genes & Development*, *18*(23), 2941–2951. https://doi.org/10.1101/GAD.1239304
Gillett, C., Fantl, V., Smith, R., Fisher, C., Bartek, J., Dickson, C., … Peters, G. (1994). Amplification and Overexpression of Cyclin D1 in Breast Cancer Detected by Immunohistochemical Staining. *Cancer Research*, *54*(7).
Gong, C., Qu, S., Liu, B., Pan, S., Jiao, Y., Nie, Y., … Song, E. (2013). MiR-106b expression determines the proliferation paradox of TGF-β in breast cancer cells. *Oncogene 2015 34:1*, *34*(1), 84–93. https://doi.org/10.1038/onc.2013.525
Gorecki, L., Andrs, M., & Korabecny, J. (2021). Clinical Candidates Targeting the ATR–CHK1–WEE1 Axis in Cancer. *Cancers 2021, Vol. 13, Page 795*, *13*(4), 795. https://doi.org/10.3390/CANCERS13040795
Gottesman, M. M. (2002). Mechanisms of cancer drug resistance. *Annual Review of Medicine*. https://doi.org/10.1146/annurev.med.53.082901.103929
Graham, T. G. W., Walter, J. C., & Loparo, J. J. (2016). Two-Stage Synapsis of DNA Ends during Non-homologous End Joining. *Molecular Cell*, *61*(6), 850–858. https://doi.org/10.1016/J.MOLCEL.2016.02.010
Graves, P., & Zeng, Y. (2012). Biogenesis of Mammalian MicroRNAs: A Global View. *Genomics, Proteomics and Bioinformatics*. https://doi.org/10.1016/j.gpb.2012.06.004
Grelier, G., Voirin, N., Ay, A.-S., Cox, D. G., Chabaud, S., Treilleux, I., … Moyret-Lalle, C. (2009). Prognostic value of Dicer expression in human breast cancers and association with the mesenchymal phenotype. *British Journal of Cancer*, *101*(4), 673. https://doi.org/10.1038/SJ.BJC.6605193
Griffiths-Jones, S., Grocock, R. J., van Dongen, S., Bateman, A., & Enright, A. J. (2006). miRBase: microRNA sequences, targets and gene nomenclature. *Nucleic Acids Research*. https://doi.org/10.1093/nar/gkj112
Gruener, R. F., Ling, A., Chang, Y.-F., Morrison, G., Geeleher, P., Greene, G. L., & Huang, R. S. (2021). Facilitating Drug Discovery in Breast Cancer by Virtually Screening Patients Using In Vitro Drug Response Modeling. *Cancers 2021, Vol. 13, Page 885*, *13*(4), 885. https://doi.org/10.3390/CANCERS13040885
Gu, Y., Rosenblatt, J., & Morgan, D. O. (1992). Cell cycle regulation of CDK2 activity by phosphorylation of Thr160 and Tyr15. *The EMBO Journal*, *11*(11), 3995–4005. https://doi.org/10.1002/J.1460-2075.1992.TB05493.X
Guarente, L. (1993). Synthetic enhancement in gene interaction: a genetic tool come of age. *Trends in Genetics*, *9*(10), 362–366. https://doi.org/10.1016/0168-9525(93)90042-G
Guiley, K. Z., Stevenson, J. W., Lou, K., Barkovich, K. J., Kumarasamy, V., Wijeratne, T. U., … Rubin, S. M. (2019). P27 allosterically activates cyclin-dependent kinase 4 and antagonizes palbociclib inhibition. *Science*, *366*(6471). https://doi.org/10.1126/SCIENCE.AAW2106/SUPPL_FILE/AAW2106_GUILEY_SM.PDF
Gulyaeva, L. F., & Kushlinskiy, N. E. (2016). Regulatory mechanisms of microRNA expression. *Journal of Translational Medicine*, *14*(1), 1–10. https://doi.org/10.1186/S12967-016-0893-X/FIGURES/1
Guo, J., Liu, H., & Zheng, J. (2016). SynLethDB: synthetic lethality database toward discovery of selective and sensitive anticancer drug targets. *Nucleic Acids Research*, *44*(Database issue), D1011. https://doi.org/10.1093/NAR/GKV1108
Hakimi, A. A., Ostrovnaya, I., Reva, B., Schultz, N., Chen, Y. B., Gonen, M., … Hsieh, J. J. (2013).

Adverse outcomes in clear cell renal cell carcinoma with mutations of 3p21 epigenetic regulators BAP1 and SETD2: A report by MSKCC and the KIRC TCGA research network. *Clinical Cancer Research*, *19*(12), 3259–3267. https://doi.org/10.1158/1078-0432.CCR-12-3886

Haldar, S., Roy, A., & Banerjee, S. (2014). Differential regulation of MCM7 and its intronic miRNA cluster miR-106b-25 during megakaryopoiesis induced polyploidy. *RNA Biology*, *11*(9), 1137. https://doi.org/10.4161/RNA.36136

Han, J., Lee, Y., Yeom, K. H., Nam, J. W., Heo, I., Rhee, J. K., … Kim, V. N. (2006). Molecular Basis for the Recognition of Primary microRNAs by the Drosha-DGCR8 Complex. *Cell*. https://doi.org/10.1016/j.cell.2006.03.043

Hanahan, D, & Weinberg, R. A. (2000). The hallmarks of cancer. *Cell*, *100*(1), 57–70. https://doi.org/10.1007/s00262-010-0968-0

Hanahan, Douglas, & Weinberg, R. A. (2011). Hallmarks of cancer: The next generation. *Cell*. https://doi.org/10.1016/j.cell.2011.02.013

Harbour, J. W., Luo, R. X., Dei Santi, A., Postigo, A. A., & Dean, D. C. (1999). Cdk phosphorylation triggers sequential intramolecular interactions that progressively block Rb functions as cells move through G1. *Cell*, *98*(6), 859–869. https://doi.org/10.1016/S0092-8674(00)81519-6

Harper, J. V, & Brooks, G. (2004). The Mammalian Cell Cycle. In *Cell Cycle Control: Mechanisms and Protocols* (Vol. 296, pp. 113–153). https://doi.org/10.1385/1-59259-857-9:113

Hartwell, L., & Weinert, T. (1989). Checkpoints: controls that ensure the order of cell cycle events. *Science*, *246*(4930), 629–634. https://doi.org/10.1126/science.2683079

Hayashi, K., Yoshida, K., & Matsui, Y. (2005). A histone H3 methyltransferase controls epigenetic events required for meiotic prophase. *Nature 2005 438:7066*, *438*(7066), 374–378. https://doi.org/10.1038/nature04112

He, C., Chen, H., Liu, Y., Li, X., Zhang, C., Qin, Q., & Pang, Q. (2020). miR-106b-5p promotes cell proliferation and cell cycle progression by directly targeting CDKN1A in osteosarcoma. *Experimental and Therapeutic Medicine*, *19*(5), 3203. https://doi.org/10.3892/ETM.2020.8574

He, L., Thomson, J. M., Hemann, M. T., Hernando-Monge, E., Mu, D., Goodson, S., … Hammond, S. M. (2005). A microRNA polycistron as a potential human oncogene. *Nature 2005 435:7043*, *435*(7043), 828–833. https://doi.org/10.1038/nature03552

Hiebert, S. W., Srikumar, /, Chellappan, P., Horowitz, J. M., & Nevins^, J. R. (1992). The interaction of RB with E2F coincides with an inhibition of the transcriptional activity of E2F.

Hilton, B. A., Li, Z., Musich, P. R., Wang, H., Cartwright, B. M., Serrano, M., … Zou, Y. (2015). ATR Plays a Direct Antiapoptotic Role at Mitochondria, which Is Regulated by Prolyl Isomerase Pin1. *Molecular Cell*, *60*(1), 35–46. https://doi.org/10.1016/J.MOLCEL.2015.08.008

Ho, T. H., Kapur, P., Joseph, R. W., Serie, D. J., Eckel-Passow, J. E., Tong, P., … Parker, A. S. (2015). Loss of histone H3 lysine 36 trimethylation is associated with an increased risk of renal cell carcinoma-specific death. *Modern Pathology 2016 29:1*, *29*(1), 34–42. https://doi.org/10.1038/modpathol.2015.123

Hong, S., Cho, Y.-W., Yu, L.-R., Yu, H., Veenstra, T. D., & Ge, K. (2007). Identification of JmjC domain-containing UTX and JMJD3 as histone H3 lysine 27 demethylases. *Proceedings of the National Academy of Sciences*, *104*(47), 18439–18444. https://doi.org/10.1073/PNAS.0707292104

Horn, P. J., & Peterson, C. L. (2002). Chromatin higher order folding: wrapping up transcription. *Science*, *297*(5588), 1824–1827. https://doi.org/10.1126/science.1074200

Horvath, J. E., Bailey, J. a, Locke, D. P., & Eichler, E. E. (2001). Lessons from the human genome: transitions between euchromatin and heterochromatin. *Human Molecular Genetics*, *10*(20), 2215–2223. https://doi.org/10.1093/hmg/10.20.2215

Howard, A., & Pelc, S. R. (1953). Synthesis of Desoxyribonucleic Acid in Normal and Irradiated Cells and Its Relation to Chromosome Breakage. *Http://Dx.Doi.Org/10.1080/09553008514552501*, *49*(2), 207–218. https://doi.org/10.1080/09553008514552501

Hsieh, C.-L. (1994). Dependence of transcriptional repression on CpG methylation density. *Molecular and Cellular Biology*, *14*(8), 5487–5494. https://doi.org/10.1128/MCB.14.8.5487-5494.1994

Huang, K. K., McPherson, J. R., Tay, S. T., Das, K., Tan, I. B., Ng, C. C. Y., … Tan, P. (2016). SETD2 histone modifier loss in aggressive GI stromal tumours. *Gut*, *65*(12), 1960–1972. https://doi.org/10.1136/GUTJNL-2015-309482

Huang, Y., Li, W., Yao, X., Lin, Q. jiang, Yin, J. wen, Liang, Y., … Wang, G. (2012). Mediator Complex Regulates Alternative mRNA Processing via the MED23 Subunit. *Molecular Cell*, *45*(4), 459–469. https://doi.org/10.1016/J.MOLCEL.2011.12.022/ATTACHMENT/EFCE4851-4CC3-44EE-96F0-A8EEF1E369D4/MMC1.PDF

Hurst, V., Challa, K., Jonas, F., Forey, R., Sack, R., Seebacher, J., … Poli, J. (2021). A regulatory phosphorylation site on Mec1 controls chromatin occupancy of RNA polymerases during replication stress. *The EMBO Journal*, e108439. https://doi.org/10.15252/EMBJ.2021108439

Hussmann, J. A., Ling, J., Ravisankar, P., Yan, J., Cirincione, A., Xu, A., … Adamson, B. (2021). Mapping the genetic landscape of DNA double-strand break repair. *Cell*, *184*(22), 5653-5669.e25. https://doi.org/10.1016/J.CELL.2021.10.002/ATTACHMENT/E8524C8B-A725-472B-8067-36E661D8D662/MMC7.XLSX

Hutvagner, G., & Simard, M. J. (2008). Argonaute proteins: Key players in RNA silencing. *Nature Reviews Molecular Cell Biology*. https://doi.org/10.1038/nrm2321

Ilves, I., Petojevic, T., Pesavento, J. J., & Botchan, M. R. (2010). Activation of the MCM2-7 Helicase by Association with Cdc45 and GINS Proteins. *Molecular Cell*, *37*(2), 247–258. https://doi.org/10.1016/J.MOLCEL.2009.12.030

Iorio, M. V., Visone, R., Di Leva, G., Donati, V., Petrocca, F., Casalini, P., … Croce, C. M. (2007). MicroRNA signatures in human ovarian cancer. *Cancer Research*. https://doi.org/10.1158/0008-5472.CAN-07-1936

Ivanovska, I., Ball, A. S., Diaz, R. L., Magnus, J. F., Kibukawa, M., Schelter, J. M., … Cleary, M. A. (2008). MicroRNAs in the miR-106b family regulate p21/CDKN1A and promote cell cycle progression. *Molecular and Cellular Biology*, *28*(7), 2167–2174. https://doi.org/10.1128/MCB.01977-07

Iyer, D. R., & Rhind, N. (2017, February 17). The intra-S checkpoint responses to DNA damage. *Genes*. MDPI AG. https://doi.org/10.3390/genes8020074

Jackson, D. A., & Pombo, A. (1998). Replicon Clusters Are Stable Units of Chromosome Structure: Evidence That Nuclear Organization Contributes to the Efficient Activation and Propagation of S Phase in Human Cells. *Journal of Cell Biology*, *140*(6), 1285–1295. https://doi.org/10.1083/JCB.140.6.1285

Jacobsen, A., Silber, J., Harinath, G., Huse, J. T., Schultz, N., & Sander, C. (2013). Analysis of microRNA-target interactions across diverse cancer types. *Nature Structural & Molecular Biology 2013 20:11*, *20*(11), 1325–1332. https://doi.org/10.1038/nsmb.2678

Jasencakova, Z., Scharf, A. N. D., Ask, K., Corpet, A., Imhof, A., Almouzni, G., & Groth, A. (2010). Replication Stress Interferes with Histone Recycling and Predeposition Marking of New Histones. *Molecular Cell*, *37*(5), 736–743. https://doi.org/10.1016/J.MOLCEL.2010.01.033

Jazayeri, A., Falck, J., Lukas, C., Bartek, J., Smith, G. C. M., Lukas, J., & Jackson, S. P. (2005). ATM- and cell cycle-dependent regulation of ATR in response to DNA double-strand breaks. *Nature Cell Biology 2005 8:1*, *8*(1), 37–45. https://doi.org/10.1038/ncb1337

Jenuwein, T., Laible, G., Dorn, R., & Reuter, G. (1998). SET domain proteins modulate chromatin domains in eu- and heterochromatin. *Cellular and Molecular Life Sciences*. https://doi.org/10.1007/s000180050127

Jha, D. K., & Strahl, B. D. (2014). An RNA polymerase II-coupled function for histone H3K36 methylation in checkpoint activation and DSB repair. *Nature Communications 2014 5:1*, *5*(1), 1–13. https://doi.org/10.1038/ncomms4965

Jia, L., Li, B., & Yu, H. (2016). The Bub1-Plk1 kinase complex promotes spindle checkpoint signalling through Cdc20 phosphorylation. *Nature Communications*, *7*, 10818. https://doi.org/10.1038/ncomms10818

Jiang, C., & Pugh, B. F. (2009). Nucleosome positioning and gene regulation: advances through genomics. *Nature Reviews Genetics*, *10*(3), 161–172. https://doi.org/10.1038/nrg2522

Jin, J., Fang, H., Yang, F., Ji, W., Guan, N., Sun, Z., … Guan, X. (2018). Combined Inhibition of

ATR and WEE1 as a Novel Therapeutic Strategy in Triple-Negative Breast Cancer. *Neoplasia*, *20*(5), 478–488. https://doi.org/10.1016/J.NEO.2018.03.003

Jin, W., Lei, Z., Xu, S., Fachen, Z., Yixiang, Z., Shilei, Z., … Chundong, G. (2021). Genetic Mutation Analysis in Small Cell Lung Cancer by a Novel NGS-Based Targeted Resequencing Gene Panel and Relation with Clinical Features. *BioMed Research International*, *2021*. https://doi.org/10.1155/2021/3609028

John, B., Enright, A. J., Aravin, A., Tuschl, T., Sander, C., & Marks, D. S. (2005). Correction: Human MicroRNA Targets. *PLoS Biology*. https://doi.org/10.1371/journal.pbio.0030264

Johnson, D. G., & Schneider-Broussard, R. (1998). Role of E2F in cell cycle control and cancer. *Front Biosci*, *3*, d447-8. Retrieved from http://www.ncbi.nlm.nih.gov/entrez/query.fcgi?cmd=Retrieve&db=PubMed&dopt=Citation&list_uids=9556498

Kan, T., Sato, F., Ito, T., Matsumura, N., David, S., Cheng, Y., … Meltzer, S. J. (2009). The miR-106b-25 Polycistron, Activated by Genomic Amplification, Functions as an Oncogene by Suppressing p21 and Bim. *Gastroenterology*, *136*(5), 1689–1700. https://doi.org/10.1053/j.gastro.2009.02.002

Kaplan, T., Liu, C. L., Erkmann, J. A., Holik, J., Grunstein, M., Kaufman, P. D., … Rando, O. J. (2008). Cell Cycle– and Chaperone-Mediated Regulation of H3K56ac Incorporation in Yeast. *PLOS Genetics*, *4*(11), e1000270. https://doi.org/10.1371/JOURNAL.PGEN.1000270

Kastan, M. B., & Bartek, J. (2004). Cell-cycle checkpoints and cancer. *Nature 2004 432:7015*, *432*(7015), 316–323. https://doi.org/10.1038/nature03097

Kato, J., Matsushime, H., Hiebert, S. W., Ewen, M. E., & Sherr, C. J. (1993). Direct binding of cyclin D to the retinoblastoma gene product (pRb) and pRb phosphorylation by the cyclin D-dependent kinase CDK4. *Genes and Development*, *7*(3), 331–342. https://doi.org/10.1101/GAD.7.3.331

Katsuno, Y., Suzuki, A., Sugimura, K., Okumura, K., Zineldeen, D. H., Shimada, M., … Nakanishi, M. (2009). Cyclin A–Cdk1 regulates the origin firing program in mammalian cells. *Proceedings of the National Academy of Sciences*, *106*(9), 3184–3189. https://doi.org/10.1073/PNAS.0809350106

Kawai, S., & Amano, A. (2012). BRCA1 regulates microRNA biogenesis via the DROSHA microprocessor complex. *The Journal of Cell Biology*, *197*(2), 201. https://doi.org/10.1083/JCB.201110008

Kenny, F. S., Hui, R., Musgrove, E. A., Gee, J. M. W., Blamey, R. W., Nicholson, R. I., … Robertson, J. F. R. (1999). Overexpression of Cyclin D1 Messenger RNA Predicts for Poor Prognosis in Estrogen Receptor-positive Breast Cancer 1.

Khoshnaw, S. M., Rakha, E. A., Abdel-Fatah, T. M., Nolan, C. C., Hodi, Z., Macmillan, D. R., … Green, A. R. (2012). Loss of Dicer expression is associated with breast cancer progression and recurrence. *Breast Cancer Research and Treatment 2012 135:2*, *135*(2), 403–413. https://doi.org/10.1007/S10549-012-2169-3

Khvorova, A., Reynolds, A., & Jayasena, S. D. (2003). Functional siRNAs and miRNAs exhibit strand bias. *Cell*. https://doi.org/10.1016/S0092-8674(03)00801-8

Kim, V. N., Han, J., & Siomi, M. C. (2009). Biogenesis of small RNAs in animals. *Nature Reviews Molecular Cell Biology*. https://doi.org/10.1038/nrm2632

Kim, Y. K., Kim, B., & Kim, V. N. (2016). Re-evaluation of the roles of DROSHA, Exportin 5, and DICER in microRNA biogenesis. *Proceedings of the National Academy of Sciences of the United States of America*. https://doi.org/10.1073/pnas.1602532113

Kizer, K. O., Phatnani, H. P., Shibata, Y., Hall, H., Greenleaf, A. L., & Strahl, B. D. (2005). A Novel Domain in Set2 Mediates RNA Polymerase II Interaction and Couples Histone H3 K36 Methylation with Transcript Elongation. *Molecular and Cellular Biology*, *25*(8), 3305–3316. https://doi.org/10.1128/MCB.25.8.3305-3316.2005

Knudsen, E. S., & Zacksenhaus, E. (2018). The vulnerability of RB loss in breast cancer: Targeting a void in cell cycle control. *Oncotarget*, *9*(57), 30940. https://doi.org/10.18632/ONCOTARGET.25797

Koboldt, D. C., Fulton, R. S., McLellan, M. D., Schmidt, H., Kalicki-Veizer, J., McMichael, J. F., …

Palchik, J. D. (2012). Comprehensive molecular portraits of human breast tumours. *Nature 2012 490:7418*, *490*(7418), 61–70. https://doi.org/10.1038/nature11412
Kohn, E. A., Ruth, N. D., Brown, M. K., Livingstone, M., & Eastman, A. (2002). Abrogation of the S Phase DNA Damage Checkpoint Results in S Phase Progression or Premature Mitosis Depending on the Concentration of 7-Hydroxystaurosporine and the Kinetics of Cdc25C Activation *. *Journal of Biological Chemistry*, *277*(29), 26553–26564. https://doi.org/10.1074/JBC.M202040200
Kolasinska-Zwierz, P., Down, T., Latorre, I., Liu, T., Liu, X. S., & Ahringer, J. (2009). Differential chromatin marking of introns and expressed exons by H3K36me3. *Nature Genetics*, *41*(3), 376–381. https://doi.org/10.1038/ng.322.Differential
Kong, A., & Mehanna, H. (2021). WEE1 Inhibitor: Clinical Development. *Current Oncology Reports*, *23*(9). https://doi.org/10.1007/S11912-021-01098-8
Koniaras, K., Cuddihy, A. R., Christopoulos, H., Hogg, A., & O'Connell, M. J. (2001). Inhibition of Chk1-dependent G2 DNA damage checkpoint radiosensitizes p53 mutant human cells. *Oncogene 2001 20:51*, *20*(51), 7453–7463. https://doi.org/10.1038/sj.onc.1204942
Koppenhafer, S. L., Goss, K. L., Terry, W. W., & Gordon, D. J. (2020). Inhibition of the ATR–CHK1 Pathway in Ewing Sarcoma Cells Causes DNA Damage and Apoptosis via the CDK2-Mediated Degradation of RRM2. *Molecular Cancer Research*, *18*(1), 91–104. https://doi.org/10.1158/1541-7786.MCR-19-0585
Kornberg, R. D. (1974). Chromatin Structure: A Repeating Unit of Histones and DNA. *Science*, *184*(4139), 868–871. https://doi.org/10.1126/SCIENCE.184.4139.868
Kotsantis, P., Petermann, E., & Boulton, S. J. (2018). Mechanisms of Oncogene-Induced Replication Stress: Jigsaw Falling into Place. *Cancer Discovery*, *8*(5), 537–555. https://doi.org/10.1158/2159-8290.CD-17-1461
Kovacs, L. A. S., Orlando, D. A., & Haase, S. B. (2008). Transcription network and cyclin/CDKs: The yin and yang of cell cycle oscillators. *Http://Dx.Doi.Org/10.4161/Cc.7.17.6515*, *7*(17), 2626–2629. https://doi.org/10.4161/CC.7.17.6515
Krell, J., Stebbing, J., Carissimi, C., Dabrowska, A. F., Giorgio, A. de, Frampton, A. E., … Castellano, L. (2016). TP53 regulates miRNA association with AGO2 to remodel the miRNA–mRNA interaction network. *Genome Research*, *26*(3), 331. https://doi.org/10.1101/GR.191759.115
Kretov, D. A., Walawalkar, I. A., Mora-Martin, A., Shafik, A. M., Moxon, S., & Cifuentes, D. (2020). Ago2-Dependent Processing Allows miR-451 to Evade the Global MicroRNA Turnover Elicited during Erythropoiesis. *Molecular Cell*, *78*(2), 317-328.e6. https://doi.org/10.1016/J.MOLCEL.2020.02.020
Krol, J., Loedige, I., & Filipowicz, W. (2010). The widespread regulation of microRNA biogenesis, function and decay : Abstract : Nature Reviews Genetics. *Nature Reviews. Genetics*. https://doi.org/10.1038/nrg2843
Kumar, M. S., Pester, R. E., Chen, C. Y., Lane, K., Chin, C., Lu, J., … Jacks, T. (2009). Dicer1 functions as a haploinsufficient tumor suppressor. *Genes and Development*. https://doi.org/10.1101/gad.1848209
Kunz-Schughart, L. A., Kreutz, M., & Knuechel, R. (1998). Multicellular spheroids: a three-dimensional in vitro culture system to study tumour biology. *International Journal of Experimental Pathology*, *79*(1), 1–23. https://doi.org/10.1046/J.1365-2613.1998.00051.X
Kwak, P. B., & Tomari, Y. (2012). The N domain of Argonaute drives duplex unwinding during RISC assembly. *Nature Structural & Molecular Biology 2012 19:2*, *19*(2), 145–151. https://doi.org/10.1038/nsmb.2232
Laake, K., Launonen, V., Niederacher, D., Gudlaugsdottir, S., Seitz, S., Rio, P., … Børresen-Dale, A.-L. (1999). Loss of Heterozygosity at 11q23.1 and Survival in Breast Cancer: Results of a Large European Study. *Genes Chromosomes Cancer*, *25*, 212–221. https://doi.org/10.1002/(SICI)1098-2264(199907)25:3
Lachmann, A., Xu, H., Krishnan, J., Berger, S. I., Mazloom, A. R., & Ma'ayan, A. (2010). ChEA: transcription factor regulation inferred from integrating genome-wide ChIP-X experiments.

Bioinformatics, *26*(19), 2438. https://doi.org/10.1093/BIOINFORMATICS/BTQ466
Lagos-Quintana, M., Rauhut, R., Lendeckel, W., & Tuschl, T. (2001). Identification of novel genes coding for small expressed RNAs. *Science*. https://doi.org/10.1126/science.1064921
Lai, E. C. (2002). Micro RNAs are complementary to 3′ UTR sequence motifs that mediate negative post-transcriptional regulation. *Nature Genetics*. https://doi.org/10.1038/ng865
Lall, S., Grün, D., Krek, A., Chen, K., Wang, Y. L., Dewey, C. N., … Rajewsky, N. (2006). A genome-wide map of conserved MicroRNA targets in C. elegans. *Current Biology*. https://doi.org/10.1016/j.cub.2006.01.050
Laoukili, J., Kooistra, M. R. H., Brás, A., Kauw, J., Kerkhoven, R. M., Morrison, A., … Medema, R. H. (2005). FoxM1 is required for execution of the mitotic programme and chromosome stability. *Nature Cell Biology 2005 7:2*, *7*(2), 126–136. https://doi.org/10.1038/ncb1217
Lee, Y., Jeon, K., Lee, J. T., Kim, S., & Kim, V. N. (2002). MicroRNA maturation: stepwise processing and subcellular localization. *The EMBO Journal*, *21*(17), 4663–4670. https://doi.org/10.1093/EMBOJ/CDF476
Lee, Y., Kim, M., Han, J., Yeom, K. H., Lee, S., Baek, S. H., & Kim, V. N. (2004). MicroRNA genes are transcribed by RNA polymerase II. *EMBO Journal*. https://doi.org/10.1038/sj.emboj.7600385
Leek, R., Grimes, D. R., Harris, A. L., & McIntyre, A. (2016). Methods: Using Three-Dimensional Culture (Spheroids) as an In Vitro Model of Tumour Hypoxia. *Advances in Experimental Medicine and Biology*, *899*, 167–196. https://doi.org/10.1007/978-3-319-26666-4_10
Lew, D. J., Dulić, V., & Reed, S. I. (1991). Isolation of three novel human cyclins by rescue of G1 cyclin (cln) function in yeast. *Cell*, *66*(6), 1197–1206. https://doi.org/10.1016/0092-8674(91)90042-W
Lewis, C. W., Jin, Z., Macdonald, D., Wei, W., Qian, X. J., Choi, W. S., … Chan, G. (2017). Prolonged mitotic arrest induced by Wee1 inhibition sensitizes breast cancer cells to paclitaxel. *Oncotarget*, *8*(43), 73705. https://doi.org/10.18632/ONCOTARGET.17848
Li, Bing, Howe, L., Anderson, S., Yates, J. R., & Workman, J. L. (2003). The Set2 histone methyltransferase functions through the phosphorylated carboxyl-terminal domain of RNA polymerase II. *The Journal of Biological Chemistry*, *278*(11), 8897–8903. https://doi.org/10.1074/jbc.M212134200
Li, Bo, & Dewey, C. N. (2011). RSEM: accurate transcript quantification from RNA-Seq data with or without a reference genome. *BMC Bioinformatics 2011 12:1*, *12*(1), 1–16. https://doi.org/10.1186/1471-2105-12-323
Li, F., Mao, G., Tong, D., Huang, J., Gu, L., Yang, W., & Li, G.-M. (2013). The Histone Mark H3K36me3 Regulates Human DNA Mismatch Repair through Its Interaction with MutSα. *Cell*, *153*(3), 590–600. https://doi.org/10.1016/J.CELL.2013.03.025
Li, H., Handsaker, B., Wysoker, A., Fennell, T., Ruan, J., Homer, N., … Subgroup, 1000 Genome Project Data Processing. (2009). The Sequence Alignment/Map format and SAMtools. *Bioinformatics*, *25*(16), 2078–2079. https://doi.org/10.1093/BIOINFORMATICS/BTP352
Li, J. H., Liu, S., Zhou, H., Qu, L. H., & Yang, J. H. (2014). StarBase v2.0: Decoding miRNA-ceRNA, miRNA-ncRNA and protein-RNA interaction networks from large-scale CLIP-Seq data. *Nucleic Acids Research*. https://doi.org/10.1093/nar/gkt1248
Li, N., Miao, Y., Shan, Y., Liu, B., Li, Y., Zhao, L., & Jia, L. (2017). MiR-106b and miR-93 regulate cell progression by suppression of PTEN via PI3K/Akt pathway in breast cancer. *Cell Death & Disease 2017 8:5*, *8*(5), e2796–e2796. https://doi.org/10.1038/cddis.2017.119
Liao, G.-B., Li, X.-Z., Zeng, S., Liu, C., Yang, S.-M., Yang, L., … Bai, J.-Y. (2018). Regulation of the master regulator FOXM1 in cancer. *Cell Communication and Signaling : CCS*, *16*(1). https://doi.org/10.1186/S12964-018-0266-6
Lim, K. K., Nguyen, T. T. T., Li, A. Y., Yeo, Y. P., & Chen, E. S. (2018). Histone H3 lysine 36 methyltransferase mobilizes NER factors to regulate tolerance against alkylation damage in fission yeast. *Nucleic Acids Research*, *46*(10), 5061–5074. https://doi.org/10.1093/NAR/GKY245
Lim, L. P., Lau, N. C., Garrett-Engele, P., Grimson, A., Schelter, J. M., Castle, J., … Johnson, J. M.

(2005). Microarray analysis shows that some microRNAs downregulate large numbers of-target mRNAs. *Nature*. https://doi.org/10.1038/nature03315

Lin, A. B., McNeely, S. C., & Beckmann, R. P. (2017). Achieving Precision Death with Cell-Cycle Inhibitors that Target DNA Replication and Repair. *Clinical Cancer Research*, *23*(13), 3232–3240. https://doi.org/10.1158/1078-0432.CCR-16-0083

Liu, F., Stanton, J. J., Wu, Z., & Piwnica-Worms, H. (1997). The human Myt1 kinase preferentially phosphorylates Cdc2 on threonine 14 and localizes to the endoplasmic reticulum and Golgi complex. *Molecular and Cellular Biology*, *17*(2), 571. https://doi.org/10.1128/MCB.17.2.571

Liu, J., Carmell, M. A., Rivas, F. V., Marsden, C. G., Thomson, J. M., Song, J.-J., … Hannon, G. J. (2004). Argonaute2 Is the Catalytic Engine of Mammalian RNAi. *Science*, *305*(5689), 1437–1441. https://doi.org/10.1126/SCIENCE.1102513

Liu, S., Shiotani, B., Lahiri, M., Maréchal, A., Tse, A., Leung, C. C. Y., … Zou, L. (2011). ATR Autophosphorylation as a Molecular Switch for Checkpoint Activation. *Molecular Cell*, *43*(2), 192. https://doi.org/10.1016/J.MOLCEL.2011.06.019

Liu, W., Fu, Q., An, H., Chang, Y., Zhang, W., Zhu, Y., … Xu, J. (2015). Decreased Expression of SETD2 Predicts Unfavorable Prognosis in Patients With Nonmetastatic Clear-Cell Renal Cell Carcinoma. *Medicine*, *94*(45), e2004. https://doi.org/10.1097/MD.0000000000002004

Lopes, M., Cotta-Ramusino, C., Pellicioli, A., Liberi, G., Plevani, P., Muzi-Falconi, M., … Foiani, M. (2001). The DNA replication checkpoint response stabilizes stalled replication forks. *Nature 2001 412:6846*, *412*(6846), 557–561. https://doi.org/10.1038/35087613

Love, M. I., Huber, W., & Anders, S. (2014). Moderated estimation of fold change and dispersion for RNA-seq data with DESeq2. *Genome Biology 2014 15:12*, *15*(12), 1–21. https://doi.org/10.1186/S13059-014-0550-8

Luco, R. F., Pan, Q., Tominaga, K., Blencowe, B. J., Pereira-Smith, O. M., & Misteli, T. (2010). Regulation of alternative splicing by histone modifications. *Science (New York, N.Y.)*, *327*(5968), 996–1000. https://doi.org/10.1126/science.1184208

Luger, K., Mäder, A. W., Richmond, R. K., Sargent, D. F., & Richmond, T. J. (1997). Crystal structure of the nucleosome core particle at 2.8 A resolution. *Nature*, *389*(6648), 251–260. https://doi.org/10.1038/38444

Lundberg, A. S., & Weinberg, R. A. (1998). Functional Inactivation of the Retinoblastoma Protein Requires Sequential Modification by at Least Two Distinct Cyclin-cdk Complexes. *Molecular and Cellular Biology*, *18*(2), 753–761. https://doi.org/10.1128/MCB.18.2.753

Ma, Q. (2013). Role of Nrf2 in Oxidative Stress and Toxicity. *Annual Review of Pharmacology and Toxicology*, *53*, 401. https://doi.org/10.1146/ANNUREV-PHARMTOX-011112-140320

Ma, S., Charron, J., & Erikson, R. L. (2003). Role of Plk2 (Snk) in Mouse Development and Cell Proliferation . *Molecular and Cellular Biology*, *23*(19), 6936–6943. https://doi.org/10.1128/MCB.23.19.6936-6943.2003

Major, M. L., Lepe, R., & Costa, R. H. (2004). Forkhead Box M1B Transcriptional Activity Requires Binding of Cdk-Cyclin Complexes for Phosphorylation-Dependent Recruitment of p300/CBP Coactivators. *Molecular and Cellular Biology*, *24*(7), 2649–2661. https://doi.org/10.1128/MCB.24.7.2649-2661.2004/ASSET/F3AF6578-33CE-4FC2-A153-BDC55DCD1D0C/ASSETS/GRAPHIC/ZMB0070412650008.JPEG

Mak, T. W. (2000). DNA damage-induced activation of p53 by the checkpoint kinase Chk2. *Science*, *287*(5459), 1824–1827. https://doi.org/10.1126/SCIENCE.287.5459.1824

Makinwa, Y., Cartwright, B. M., Musich, P. R., Li, Z., Biswas, H., & Zou, Y. (2020). PP2A Regulates Phosphorylation-Dependent Isomerization of Cytoplasmic and Mitochondrial-Associated ATR by Pin1 in DNA Damage Responses. *Frontiers in Cell and Developmental Biology*, *8*, 813. https://doi.org/10.3389/FCELL.2020.00813

Malorni, L., Piazza, S., Ciani, Y., Guarducci, C., Bonechi, M., Biagioni, C., … Migliaccio, I. (2016). A gene expression signature of retinoblastoma loss-of-function is a predictive biomarker of resistance to palbociclib in breast cancer cell lines and is prognostic in patients with ER positive early breast cancer. *Oncotarget*, *7*(42), 68012–68022. https://doi.org/10.18632/ONCOTARGET.12010

Malumbres, M. (2014). Cyclin-dependent kinases. *Genome Biology 2014 15:6*, *15*(6), 1–10. https://doi.org/10.1186/GB4184
Maric, M., Maculins, T., De Piccoli, G., & Labib, K. (2014). Cdc48 and a ubiquitin ligase drive disassembly of the CMG helicase at the end of DNA replication. *Science*, *346*(6208). https://doi.org/10.1126/SCIENCE.1253596
Martin, M. (2011). Cutadapt removes adapter sequences from high-throughput sequencing reads. *EMBnet.Journal*, *17*(1), 10–12. https://doi.org/10.14806/EJ.17.1.200
Mathys, H., Basquin, J. Ô., Ozgur, S., Czarnocki-Cieciura, M., Bonneau, F., Aartse, A., … Filipowicz, W. (2014). Structural and Biochemical Insights to the Role of the CCR4-NOT Complex and DDX6 ATPase in MicroRNA Repression. *Molecular Cell*, *54*(5), 751–765. https://doi.org/10.1016/J.MOLCEL.2014.03.036
Matthews, H. K., Bertoli, C., & de Bruin, R. A. M. (2021). Cell cycle control in cancer. *Nature Reviews Molecular Cell Biology 2021*, 1–15. https://doi.org/10.1038/s41580-021-00404-3
McGowan, C H, & Russell, P. (1993). Human Wee1 kinase inhibits cell division by phosphorylating p34cdc2 exclusively on Tyr15. *The EMBO Journal*, *12*(1), 75. Retrieved from /pmc/articles/PMC413177/?report=abstract
McGowan, Clare H., & Russell, P. (2004). The DNA damage response: sensing and signaling. *Current Opinion in Cell Biology*, *16*(6), 629–633. https://doi.org/10.1016/J.CEB.2004.09.005
Mehlich, D., Garbicz, F., & Włodarski, P. K. (2018). The emerging roles of the polycistronic miR-106b∼25 cluster in cancer – A comprehensive review. *Biomedicine and Pharmacotherapy*. https://doi.org/10.1016/j.biopha.2018.08.097
Meister, G. (2013). Argonaute proteins: functional insights and emerging roles. *Nature Reviews Genetics 2013 14:7*, *14*(7), 447–459. https://doi.org/10.1038/nrg3462
Meister, G., Landthaler, M., Patkaniowska, A., Dorsett, Y., Teng, G., & Tuschl, T. (2004). Human Argonaute2 mediates RNA cleavage targeted by miRNAs and siRNAs. *Molecular Cell*. https://doi.org/10.1016/j.molcel.2004.07.007
Melo, S. A., Moutinho, C., Ropero, S., Calin, G. A., Rossi, S., Spizzo, R., … Esteller, M. (2010). A genetic defect in exportin-5 traps precursor MicroRNAs in the nucleus of cancer cells. *Cancer Cell*. https://doi.org/10.1016/j.ccr.2010.09.007
Mermel, C. H., Schumacher, S. E., Hill, B., Meyerson, M. L., Beroukhim, R., & Getz, G. (2011). GISTIC2.0 facilitates sensitive and confident localization of the targets of focal somatic copy-number alteration in human cancers. *Genome Biology 2011 12:4*, *12*(4), 1–14. https://doi.org/10.1186/GB-2011-12-4-R41
Mitchell, P. S., Parkin, R. K., Kroh, E. M., Fritz, B. R., Wyman, S. K., Pogosova-Agadjanyan, E. L., … Tewari, M. (2008). Circulating microRNAs as stable blood-based markers for cancer detection. *Proceedings of the National Academy of Sciences of the United States of America*. https://doi.org/10.1073/pnas.0804549105
Mitchison, J. M. (1971). *The biology of the cell cycle*. Cambridge University Press.
Moiseeva, T., Hood, B., Schamus, S., O'Connor, M. J., Conrads, T. P., & Bakkenist, C. J. (2017). ATR kinase inhibition induces unscheduled origin firing through a Cdc7-dependent association between GINS and And-1. *Nature Communications 2017 8:1*, *8*(1), 1–11. https://doi.org/10.1038/s41467-017-01401-x
Moiseeva, T. N., Yin, Y., Calderon, M. J., Qian, C., Schamus-Haynes, S., Sugitani, N., … Bakkenist, C. J. (2019). An ATR and CHK1 kinase signaling mechanism that limits origin firing during unperturbed DNA replication. *Proceedings of the National Academy of Sciences*, *116*(27), 13374–13383. https://doi.org/10.1073/PNAS.1903418116
Morgan, D. O. (1995). Principles of CDK regulation. *Nature*, *374*(6518), 131–134. https://doi.org/10.1038/374131a0
Morlando, M., Ballarino, M., Gromak, N., Pagano, F., Bozzoni, I., & Proudfoot, N. J. (2008). Primary microRNA transcripts are processed co-transcriptionally. *Nature Structural and Molecular Biology*. https://doi.org/10.1038/nsmb.1475
Musselman, C. A., Khorasanizadeh, S., & Kutateladze, T. G. (2014). Towards understanding methyllysine readout. *Biochimica et Biophysica Acta - Gene Regulatory Mechanisms*.

https://doi.org/10.1016/j.bbagrm.2014.04.001
Myers, J. S., & Cortez, D. (2006). Rapid Activation of ATR by Ionizing Radiation Requires ATM and Mre11 *. *Journal of Biological Chemistry*, *281*(14), 9346–9350. https://doi.org/10.1074/JBC.M513265200
Nam, A.-R., Jin, M.-H., Bang, J.-H., Oh, K.-S., Seo, H.-R., Oh, D.-Y., & Bang, Y.-J. (2020). Inhibition of ATR Increases the Sensitivity to WEE1 Inhibitor in Biliary Tract Cancer. *Cancer Res Treat*, *52*(3). https://doi.org/10.4143/crt.2020.080
Narasimha, A. M., Kaulich, M., Shapiro, G. S., Choi, Y. J., Sicinski, P., & Dowdy, S. F. (2014). Cyclin D activates the Rb tumor suppressor by mono-phosphorylation. *ELife*, *3*. https://doi.org/10.7554/ELIFE.02872
Neri, F., Rapelli, S., Krepelova, A., Incarnato, D., Parlato, C., Basile, G., … Oliviero, S. (2017). Intragenic DNA methylation prevents spurious transcription initiation. *Nature*. https://doi.org/10.1038/nature21373
Neta, R., Perlstein, R., Vogel, S. N., Ledney, G. D., & Abrams, J. (1992). Role of interleukin 6 (IL-6) in protection from lethal irradiation and in endocrine responses to IL-1 and tumor necrosis factor. *Journal of Experimental Medicine*, *175*(3), 689–694. https://doi.org/10.1084/JEM.175.3.689
Nik-Zainal, S., Davies, H., Staaf, J., Ramakrishna, M., Glodzik, D., Zou, X., … Stratton, M. R. (2016). Landscape of somatic mutations in 560 breast cancer whole-genome sequences. *Nature 2016 534:7605*, *534*(7605), 47–54. https://doi.org/10.1038/nature17676
Nishikura, K. (2015). A-to-I editing of coding and non-coding RNAs by ADARs. *Nature Reviews Molecular Cell Biology 2015 17:2*, *17*(2), 83–96. https://doi.org/10.1038/nrm.2015.4
Nojima, T., Tellier, M., Foxwell, J., Ribeiro de Almeida, C., Tan-Wong, S., Dhir, S., … Proudfoot, N. (2018). Deregulated Expression of Mammalian lncRNA through Loss of SPT6 Induces R-Loop Formation, Replication Stress, and Cellular Senescence. *Molecular Cell*, *72*(6), 970-984.e7. https://doi.org/10.1016/J.MOLCEL.2018.10.011
Nolan, J. C., Salvucci, M., Carberry, S., Barat, A., Segura, M. F., Fenn, J., … Piskareva, O. (2020). A Context-Dependent Role for MiR-124-3p on Cell Phenotype, Viability and Chemosensitivity in Neuroblastoma in vitro. *Frontiers in Cell and Developmental Biology*, *0*, 1396. https://doi.org/10.3389/FCELL.2020.559553
Norbury, C., Blow, J., & Nurse, P. (1991). Regulatory phosphorylation of the p34cdc2 protein kinase in vertebrates. *The EMBO Journal*, *10*(11), 3321. Retrieved from /pmc/articles/PMC453058/?report=abstract
Nurse, P., & Thuriaux, P. (1980). REGULATORY GENES CONTROLLING MITOSIS IN THE FISSION YEAST SCHIZOSACCHAROMYCES POMBE. *Genetics*, *96*(3), 627–637. https://doi.org/10.1093/GENETICS/96.3.627
O'Connell, M. J., Walworth, N. C., & Carr, A. M. (2000). The G2-phase DNA-damage checkpoint. *Trends in Cell Biology*, *10*(7), 296–303. https://doi.org/10.1016/S0962-8924(00)01773-6
O'Donnell, K. A., Wentzel, E. A., Zeller, K. I., Dang, C. V., & Mendell, J. T. (2005). c-Myc-regulated microRNAs modulate E2F1 expression. *Nature*. https://doi.org/10.1038/nature03677
O'Leary, B., Finn, R. S., & Turner, N. C. (2016). Treating cancer with selective CDK4/6 inhibitors. *Nature Reviews Clinical Oncology 2016 13:7*, *13*(7), 417–430. https://doi.org/10.1038/nrclinonc.2016.26
Oberley, M. J., Inman, D. R., & Farnham, P. J. (2003). E2F6 Negatively Regulates BRCA1 in Human Cancer Cells without Methylation of Histone H3 on Lysine 9 *. *Journal of Biological Chemistry*, *278*(43), 42466–42476. https://doi.org/10.1074/JBC.M307733200
Ohshima, K., Hatakeyama, K., Nagashima, T., Watanabe, Y., Kanto, K., Doi, Y., … Yamaguchi, K. (2017). Integrated analysis of gene expression and copy number identified potential cancer driver genes with amplification-dependent overexpression in 1,454 solid tumors. *Scientific Reports 2017 7:1*, *7*(1), 1–13. https://doi.org/10.1038/s41598-017-00219-3
Oliveira, F. M. B. de, Harris, M. R., Brazauskas, P., Bruin, R. A. M. de, & Smolka, M. B. (2012). Linking DNA replication checkpoint to MBF cell-cycle transcription reveals a distinct class of G1/S genes. *The EMBO Journal*, *31*(7), 1798–1810. https://doi.org/10.1038/EMBOJ.2012.27

Ortega, S., Malumbres, M., & Barbacid, M. (2002). Cyclin D-dependent kinases, INK4 inhibitors and cancer. *Biochimica et Biophysica Acta - Reviews on Cancer*. https://doi.org/10.1016/S0304-419X(02)00037-9

Ozsolak, F., Song, J. S., Liu, X. S., & Fisher, D. E. (2007). High-throughput mapping of the chromatin structure of human promoters. *Nature Biotechnology 2007 25:2*, *25*(2), 244–248. https://doi.org/10.1038/nbt1279

Pagano, M., Pepperkok, R., Lukas, J., Baldin, V., Ansorge, W., Bartek, J., & Draetta, G. (1993). Regulation of the cell cycle by the cdk2 protein kinase in cultured human fibroblasts. *The Journal of Cell Biology*, *121*(1), 101–111.

Pai, C.-C., Deegan, R. S., Subramanian, L., Gal, C., Sarkar, S., Blaikley, E. J., … Humphrey, T. C. (2014). A histone H3K36 chromatin switch coordinates DNA double-strand break repair pathway choice. *Nature Communications 2014 5:1*, *5*(1), 1–11. https://doi.org/10.1038/ncomms5091

Pai, C.-C., Kishkevich, A., Deegan, R. S., Keszthelyi, A., Folkes, L., Kearsey, S. E., … Humphrey, T. C. (2017). Set2 Methyltransferase Facilitates DNA Replication and Promotes Genotoxic Stress Responses through MBF-Dependent Transcription. *Cell Reports*, *20*(11), 2693–2705. https://doi.org/10.1016/j.celrep.2017.08.058

Pai, C. C., Hsu, K. F., Durley, S. C., Keszthelyi, A., Kearsey, S. E., Rallis, C., … Humphrey, T. C. (2019). An essential role for dNTP homeostasis following CDK-induced replication stress. *Journal of Cell Science*. https://doi.org/10.1242/jcs.226969

Pardee, a B. (1974). A restriction point for control of normal animal cell proliferation. *Proceedings of the National Academy of Sciences of the United States of America*, *71*(4), 1286–1290. https://doi.org/10.1073/pnas.71.4.1286

Park, I. Y., Powell, R. T., Tripathi, D. N., Dere, R., Ho, T. H., Blasius, T. L., … Walker, C. L. (2016). Dual Chromatin and Cytoskeletal Remodeling by SETD2. *Cell*, *166*(4), 950–962. https://doi.org/10.1016/j.cell.2016.07.005

Parker, L. L., & Piwnica-Worms, H. (1992). Inactivation of the p34cdc2-Cyclin B Complex by the Human WEE1 Tyrosine Kinase. *Science*, *257*(1989), 1955–1957. https://doi.org/10.1126/science.1384126

Pasero, P., & Schwob, E. (2000). Think global, act local — how to regulate S phase from individual replication origins. *Current Opinion in Genetics & Development*, *10*(2), 178–186. https://doi.org/10.1016/S0959-437X(00)00067-8

Paul, M. R., Pan, T. C., Pant, D. K., Shih, N. N. C., Chen, Y., Harvey, K. L., … Chodosh, L. A. (2020). Genomic landscape of metastatic breast cancer identifies preferentially dysregulated pathways and targets. *The Journal of Clinical Investigation*, *130*(8), 4252–4265. https://doi.org/10.1172/JCI129941

Pediconi, N., Ianari, A., Costanzo, A., Belloni, L., Gallo, R., Cimino, L., … Levrero, M. (2003). Differential regulation of E2F1 apoptotic target genes in response to DNA damage. *Nature Cell Biology 2003 5:6*, *5*(6), 552–558. https://doi.org/10.1038/ncb998

Peng, Y., & Croce, C. M. (2016). The role of microRNAs in human cancer. *Signal Transduction and Targeted Therapy*. https://doi.org/10.1038/sigtrans.2015.4

Perou, C. M., Sørlie, T., Eisen, M. B., van de Rijn, M., Jeffrey, S. S., Rees, C. A., … Botstein, D. (2000). Molecular portraits of human breast tumours. *Nature 2000 406:6797*, *406*(6797), 747–752. https://doi.org/10.1038/35021093

Petermann, E., Orta, M. L., Issaeva, N., Schultz, N., & Helleday, T. (2010). Hydroxyurea-Stalled Replication Forks Become Progressively Inactivated and Require Two Different RAD51-Mediated Pathways for Restart and Repair. *Molecular Cell*, *37*(4), 492. https://doi.org/10.1016/J.MOLCEL.2010.01.021

Petermann, E., Woodcock, M., & Helleday, T. (2010). Chk1 promotes replication fork progression by controlling replication initiation. *Proceedings of the National Academy of Sciences*, *107*(37), 16090–16095. https://doi.org/10.1073/PNAS.1005031107

Petrocca, F., Visone, R., Onelli, M. R., Shah, M. H., Nicoloso, M. S., de Martino, I., … Vecchione, A. (2008). E2F1-Regulated MicroRNAs Impair TGFβ-Dependent Cell-Cycle Arrest and Apoptosis

in Gastric Cancer. *Cancer Cell*. https://doi.org/10.1016/j.ccr.2008.02.013
Pfister, S. X., Ahrabi, S., Zalmas, L. P., Sarkar, S., Aymard, F., Bachrati, C. Z., … Humphrey, T. C. (2014). SETD2-Dependent Histone H3K36 Trimethylation Is Required for Homologous Recombination Repair and Genome Stability. *Cell Reports*, *7*(6), 2006–2018. https://doi.org/10.1016/j.celrep.2014.05.026
Pfister, S. X., Markkanen, E., Jiang, Y., Sarkar, S., Woodcock, M., Orlando, G., … Humphrey, T. C. (2015). Inhibiting WEE1 Selectively Kills Histone H3K36me3-Deficient Cancers by dNTP Starvation. *Cancer Cell*, *28*(5), 557–568. https://doi.org/10.1016/j.ccell.2015.09.015
Pines, J. (1995). Cyclins and cyclin-dependent kinases: a biochemical view. *Biochemical Journal*, *308*(3), 697–711. https://doi.org/10.1042/bj3080697
Pines, Jonathon, & Hunter, T. (1989). Isolation of a human cyclin cDNA: Evidence for cyclin mRNA and protein regulation in the cell cycle and for interaction with p34cdc2. *Cell*, *58*(5), 833–846. https://doi.org/10.1016/0092-8674(89)90936-7
Poli, J., Tsaponina, O., Crabbé, L., Keszthelyi, A., Pantesco, V., Chabes, A., … Pasero, P. (2012). dNTP pools determine fork progression and origin usage under replication stress. *The EMBO Journal*, *31*(4), 883–894. https://doi.org/10.1038/emboj.2011.470
Ponnusamy, L., & Manoharan, R. (2021). Distinctive role of SIK1 and SIK3 isoforms in aerobic glycolysis and cell growth of breast cancer through the regulation of p53 and mTOR signaling pathways. *Biochimica et Biophysica Acta (BBA) - Molecular Cell Research*, *1868*(5), 118975. https://doi.org/10.1016/J.BBAMCR.2021.118975
Prioleau, M.-N., & MacAlpine, D. M. (2016). DNA replication origins—where do we begin? *Genes & Development*, *30*(15), 1683–1697. https://doi.org/10.1101/GAD.285114.116
Qi, J. J., Liu, L., Cao, J. X., An, G. S., Li, S. Y., Li, G., … Ni, J. H. (2015). E2F1 regulates p53R2 gene expression in p53-deficient cells. *Molecular and Cellular Biochemistry*, *399*(1–2), 179–188. https://doi.org/10.1007/s11010-014-2244-7
Quinlan, A. R., & Hall, I. M. (2010). BEDTools: a flexible suite of utilities for comparing genomic features. *Bioinformatics*, *26*(6), 841–842. https://doi.org/10.1093/BIOINFORMATICS/BTQ033
Ramalingam, P., Palanichamy, J. K., Singh, A., Das, P., Bhagat, M., Kassab, M. A., … Chattopadhyay, P. (2014). Biogenesis of intronic miRNAs located in clusters by independent transcription and alternative splicing. *RNA*, *20*(1), 76–87. https://doi.org/10.1261/RNA.041814.113
Ramírez, F., Ryan, D. P., Grüning, B., Bhardwaj, V., Kilpert, F., Richter, A. S., … Manke, T. (2016). deepTools2: a next generation web server for deep-sequencing data analysis. *Nucleic Acids Research*, *44*(W1), W160–W165. https://doi.org/10.1093/NAR/GKW257
Rao, H., Li, X., Liu, M., Liu, J., Feng, W., Tang, H., … Li, L. (2021). Multilevel Regulation of β-Catenin Activity by SETD2 Suppresses the Transition from Polycystic Kidney Disease to Clear Cell Renal Cell Carcinoma. *Cancer Research*, *81*(13), 3554–3567. https://doi.org/10.1158/0008-5472.CAN-20-3960
Rashi-Elkeles, S., Warnatz, H.-J., Elkon, R., Kupershtein, A., Chobod, Y., Paz, A., … Shiloh, Y. (2014). Parallel Profiling of the Transcriptome, Cistrome, and Epigenome in the Cellular Response to Ionizing Radiation. *Science Signaling*, *7*(325). https://doi.org/10.1126/SCISIGNAL.2005032
Ray, M., Yunis, R., Chen, X., & Rocke, D. M. (2012). Comparison of low and high dose ionising radiation using topological analysis of gene coexpression networks. *BMC Genomics 2012 13:1*, *13*(1), 1–17. https://doi.org/10.1186/1471-2164-13-190
Rebehmed, J., Revy, P., Faure, G., De Villartay, J. P., & Callebaut, I. (2014). Expanding the SRI domain family: A common scaffold for binding the phosphorylated C-terminal domain of RNA polymerase II. *FEBS Letters*, *588*(23), 4431–4437. https://doi.org/10.1016/j.febslet.2014.10.014
Reczko, M., Maragkakis, M., Alexiou, P., Papadopoulos, G. L., & Hatzigeorgiou, A. G. (2012). Accurate microRNA target prediction using detailed binding site accessibility and machine learning on proteomics data. *Frontiers in Genetics*. https://doi.org/10.3389/fgene.2011.00103
Ricketts, C. J., & Linehan, W. M. (2014). Intratumoral heterogeneity in kidney cancer. *Nature Genetics*, *46*(3), 214–215. https://doi.org/10.1038/ng.2904

Ritchie, M. E., Phipson, B., Wu, D., Hu, Y., Law, C. W., Shi, W., & Smyth, G. K. (2015). limma powers differential expression analyses for RNA-sequencing and microarray studies. *Nucleic Acids Research*, *43*(7), e47–e47. https://doi.org/10.1093/NAR/GKV007

Rosenfeld, N., Aharonov, R., Meiri, E., Rosenwald, S., Spector, Y., Zepeniuk, M., … Barshack, I. (2008). MicroRNAs accurately identify cancer tissue origin. *Nature Biotechnology*. https://doi.org/10.1038/nbt1392

Ruby, J. G., Jan, C. H., & Bartel, D. P. (2007). Intronic microRNA precursors that bypass Drosha processing. *Nature*. https://doi.org/10.1038/nature05983

Ruthenburg, A. J., Li, H., Patel, D. J., & David Allis, C. (2007). Multivalent engagement of chromatin modifications by linked binding modules. *Nature Reviews Molecular Cell Biology*, *8*(12), 983–994. https://doi.org/10.1038/nrm2298

Sadeghi, H., Kamal, A., Ahmadi, M., Najafi, H., Zarchi, A. S., Haddad, P., … Totonchi, M. (2021). A novel panel of blood-based microRNAs capable of discrimination between benign breast disease and breast cancer at early stages. *Https://Doi.Org/10.1080/15476286.2021.1989218*, 1–10. https://doi.org/10.1080/15476286.2021.1989218

Saito, Y., Liang, G., Egger, G., Friedman, J. M., Chuang, J. C., Coetzee, G. A., & Jones, P. A. (2006). Specific activation of microRNA-127 with downregulation of the proto-oncogene BCL6 by chromatin-modifying drugs in human cancer cells. *Cancer Cell*. https://doi.org/10.1016/j.ccr.2006.04.020

Sakai, L. Y., Keene, D. R., & Engvall, E. (1986). Fibrillin, a new 350-kD glycoprotein, is a component of extracellular microfibrils. *The Journal of Cell Biology*, *103*(6), 2499. https://doi.org/10.1083/JCB.103.6.2499

Saldivar, J. C., Hamperl, S., Bocek, M. J., Chung, M., Bass, T. E., Cisneros-Soberanis, F., … Cimprich, K. A. (2018). An intrinsic S/G2 checkpoint enforced by ATR. *Science*, *361*(6404), 806–810. https://doi.org/10.1126/SCIENCE.AAP9346

Sanidas, I., Morris, R., Fella, K. A., Rumde, P. H., Boukhali, M., Tai, E. C., … Dyson, N. J. (2019). A Code of Mono-phosphorylation Modulates the Function of RB. *Molecular Cell*, *73*(5), 985-1000.e6. https://doi.org/10.1016/J.MOLCEL.2019.01.004

Schmidt, A.-K., Pudelko, K., Boekenkamp, J.-E., Berger, K., Kschischo, M., & Bastians, H. (2020). The p53/p73 - p21CIP1 tumor suppressor axis guards against chromosomal instability by restraining CDK1 in human cancer cells. *Oncogene 2020 40:2*, *40*(2), 436–451. https://doi.org/10.1038/s41388-020-01524-4

Schmidt, C. K., Galanty, Y., Sczaniecka-Clift, M., Coates, J., Jhujh, S., Demir, M., … Jackson, S. P. (2015). Systematic E2 screening reveals a UBE2D–RNF138–CtIP axis promoting DNA repair. *Nature Cell Biology 2015 17:11*, *17*(11), 1458–1470. https://doi.org/10.1038/ncb3260

Schmidt, M. F., Korb, O., & Abell, C. (2013). MicroRNA-Specific Argonaute 2 Protein Inhibitors. *ACS Chemical Biology*, *8*(10), 2122–2126. https://doi.org/10.1021/CB400246K

Schuhmacher, M. K., Beldar, S., Khella, M. S., Bröhm, A., Ludwig, J., Tempel, W., … Jeltsch, A. (2020). Sequence specificity analysis of the SETD2 protein lysine methyltransferase and discovery of a SETD2 super-substrate. *Communications Biology 2020 3:1*, *3*(1), 1–13. https://doi.org/10.1038/s42003-020-01223-6

Scolz, M., Widlund, P. O., Piazza, S., Bublik, D. R., Reber, S., Peche, L. Y., … Bird, A. W. (2012). GTSE1 Is a Microtubule Plus-End Tracking Protein That Regulates EB1-Dependent Cell Migration. *PLOS ONE*, *7*(12), e51259. https://doi.org/10.1371/JOURNAL.PONE.0051259

Scott, G. K., Mattie, M. D., Berger, C. E., Benz, S. C., & Benz, C. C. (2006). Rapid alteration of microRNA levels by histone deacetylase inhibition. *Cancer Research*. https://doi.org/10.1158/0008-5472.CAN-05-3632

Seligmann, J. F., Fisher, D. J., Brown, L. C., Adams, R. A., Graham, J., Quirke, P., … Investigators, on behalf of the F. T. (2021). Inhibition of WEE1 Is Effective in TP53- and RAS-Mutant Metastatic Colorectal Cancer: A Randomized Trial (FOCUS4-C) Comparing Adavosertib (AZD1775) With Active Monitoring. *Https://Doi.Org/10.1200/JCO.21.01435*, JCO.21.01435. https://doi.org/10.1200/JCO.21.01435

Shahbandi, A., Nguyen, H. D., & Jackson, J. G. (2020). TP53 Mutations and Outcomes in Breast

Cancer: Reading beyond the Headlines. *Trends in Cancer*, *6*(2), 98–110. https://doi.org/10.1016/J.TRECAN.2020.01.007
Shalgi, R., Lieber, D., Oren, M., & Pilpel, Y. (2007). Global and Local Architecture of the Mammalian microRNA–Transcription Factor Regulatory Network. *PLOS Computational Biology*, *3*(7), e131. https://doi.org/10.1371/JOURNAL.PCBI.0030131
Shechter, D., Costanzo, V., & Gautier, J. (2004). ATR and ATM regulate the timing of DNA replication origin firing. *Nature Cell Biology*, *6*(7), 648–655. https://doi.org/10.1038/ncb1145
Shen, Z., Sun, J., Shao, J., & Xu, J. (2020). Ultraviolet B irradiation enhances the secretion of exosomes by human primary melanocytes and changes their exosomal miRNA profile. *PLOS ONE*, *15*(8), e0237023. https://doi.org/10.1371/JOURNAL.PONE.0237023
Sherr, C. J., & Roberts, J. M. (1995). Inhibitors of mammalian G1 cyclin-dependent kinases. *Genes and Development*. https://doi.org/10.1101/gad.9.10.1149
Shilatifard, A. (2006). Chromatin Modifications by Methylation and Ubiquitination : Implications in the Regulation of Gene Expression. *Gene Expression*, *75*, 243–272. https://doi.org/10.1146/annurev.biochem.75.103004.142422
Shimura, T., Torres, M. J., Martin, M. M., Rao, V. A., Pommier, Y., Katsura, M., … Aladjem, M. I. (2008). Bloom's Syndrome Helicase and Mus81 are Required to Induce Transient Double-strand DNA Breaks in Response to DNA Replication Stress. *Journal of Molecular Biology*, *375*(4), 1152–1164. https://doi.org/10.1016/j.jmb.2007.11.006
Shiovitz, S., & Korde, L. A. (2015). Genetics of breast cancer: a topic in evolution. *Annals of Oncology*, *26*(7), 1291. https://doi.org/10.1093/ANNONC/MDV022
Si, W., Shen, J., Zheng, H., & Fan, W. (2019). The role and mechanisms of action of microRNAs in cancer drug resistance. *Clinical Epigenetics*. https://doi.org/10.1186/s13148-018-0587-8
Smith, B. C., & Denu, J. M. (2009). Chemical mechanisms of histone lysine and arginine modifications. *Biochimica et Biophysica Acta - Gene Regulatory Mechanisms*. https://doi.org/10.1016/j.bbagrm.2008.06.005
Smith, H. L., Southgate, H., Tweddle, D. A., & Curtin, N. J. (2020). DNA damage checkpoint kinases in cancer. *Expert Reviews in Molecular Medicine*, *22*. https://doi.org/10.1017/ERM.2020.3
Soneson, C., Love, M. I., & Robinson, M. D. (2016). Differential analyses for RNA-seq: transcript-level estimates improve gene-level inferences. *F1000Research 2016 4:1521*, *4*, 1521. https://doi.org/10.12688/f1000research.7563.2
Sorenson, M. R., Jha, D. K., Ucles, S. A., Flood, D. M., Strahl, B. D., Stevens, S. W., & Kress, T. L. (2016). Histone H3K36 methylation regulates pre-mRNA splicing in *Saccharomyces cerevisiae*. *RNA Biology*, *13*(4), 412–426. https://doi.org/10.1080/15476286.2016.1144009
Spencer, S. L., Cappell, S. D., Tsai, F. C., Overton, K. W., Wang, C. L., & Meyer, T. (2013). The Proliferation-Quiescence Decision Is Controlled by a Bifurcation in CDK2 Activity at Mitotic Exit. *Cell*, *155*(2), 369–383. https://doi.org/10.1016/J.CELL.2013.08.062
Srihari, S., Singla, J., Wong, L., & Ragan, M. A. (2015). Inferring synthetic lethal interactions from mutual exclusivity of genetic events in cancer. *Biology Direct*, *10*(1). https://doi.org/10.1186/S13062-015-0086-1
Stahlhut, C., & Slack, F. J. (2013). MicroRNAs and the cancer phenotype: profiling, signatures and clinical implications. *Genome Medicine*. https://doi.org/10.1186/gm516
Stallaert, W., Kedziora, K. M., Taylor, C. D., Zikry, T. M., Sobon, H. K., Taylor, S. R., … Purvis, J. E. (2021). The Structure of the Human Cell Cycle. *SSRN Electronic Journal*. https://doi.org/10.2139/SSRN.3821952
Stevens, C., Smith, L., & La Thangue, N. B. (2003). Chk2 activates E2F-1 in response to DNA damage. *Nature Cell Biology 2003 5:5*, *5*(5), 401–409. https://doi.org/10.1038/ncb974
Sun, X. J., Wei, J., Wu, X. Y., Hu, M., Wang, L., Wang, H. H., … Chen, Z. (2005). Identification and characterization of a novel human histone H3 lysine 36-specific methyltransferase. *J Biol Chem*, *280*(42), 35261–35271. https://doi.org/M504012200 [pii] 10.1074/jbc.M504012200
Sundarraj, J., Taylor, G. C. A., Kriegsheim, A. von, & Pradeepa, M. M. (2017). H3K36me3 and PSIP1/LEDGF associate with several DNA repair proteins, suggesting their role in efficient DNA repair at actively transcribing loci. *Wellcome Open Research*, *2*, 83.

https://doi.org/10.12688/WELLCOMEOPENRES.11589.4
Swift, M., Morrell, D., Massey, R. B., & Chase, C. L. (2010). Incidence of Cancer in 161 Families Affected by Ataxia–Telangiectasia. *Http://Dx.Doi.Org/10.1056/NEJM199112263252602*, *325*(26), 1831–1836. https://doi.org/10.1056/NEJM199112263252602
Symeonidou, I. E., Taraviras, S., & Lygerou, Z. (2012). Control over DNA replication in time and space. *FEBS Letters*, *586*(18), 2803–2812. https://doi.org/10.1016/J.FEBSLET.2012.07.042
Szmyd, R., Niska-Blakie, J., Diril, M. K., Renck Nunes, P., Tzelepis, K., Lacroix, A., … Kaldis, P. (2018). Premature activation of Cdk1 leads to mitotic events in S phase and embryonic lethality. *Oncogene 2018 38:7*, *38*(7), 998–1018. https://doi.org/10.1038/s41388-018-0464-0
Takahashi, Y., Rayman, J. B., & Dynlacht, B. D. (2000). Analysis of promoter binding by the E2F and pRB families in vivo: distinct E2F proteins mediate activation and repression. *Genes & Development*, *14*(7), 804–816. https://doi.org/10.1101/GAD.14.7.804
Tang, Z., Pilié, P. G., Geng, C., Manyam, G. C., Yang, G., Park, S., … Thompson, T. C. (2021). ATR Inhibition Induces CDK1–SPOP Signaling and Enhances Anti–PD-L1 Cytotoxicity in Prostate Cancer. *Clinical Cancer Research*, *27*(17), 4898–4909. https://doi.org/10.1158/1078-0432.CCR-21-1010
Taylor, W. R., DePrimo, S. E., Agarwal, A., Agarwal, M. L., Schönthal, A. H., Katula, K. S., & Stark, G. R. (2017). Mechanisms of G2 Arrest in Response to Overexpression of p53. *Https://Doi.Org/10.1091/Mbc.10.11.3607*, *10*(11), 3607–3622. https://doi.org/10.1091/MBC.10.11.3607
Thangavel, C., Boopathi, E., Ertel, A., Lim, M., Addya, S., Fortina, P., … Knudsen, E. S. (2013). Regulation of miR106b cluster through the RB pathway: Mechanismand functional targets. *Cell Cycle*, *12*(1), 98–111. https://doi.org/10.4161/CC.23029/SUPPL_FILE/KCCY_A_10923029_SM0001.ZIP
Thomson, J. M., Newman, M., Parker, J. S., Morin-Kensicki, E. M., Wright, T., & Hammond, S. M. (2006). Extensive post-transcriptional regulation of microRNAs and its implications for cancer. *Genes and Development*. https://doi.org/10.1101/gad.1444406
Tian, Y., Simanshu, D. K., Ma, J. B., & Patel, D. J. (2011). Structural basis for piRNA 2′-O-methylated 3′-end recognition by Piwi PAZ (Piwi/Argonaute/Zwille) domains. *Proceedings of the National Academy of Sciences of the United States of America*, *108*(3), 903–910. https://doi.org/10.1073/PNAS.1017762108/-/DCSUPPLEMENTAL
Toledo, L. I., Altmeyer, M., Rask, M. B., Lukas, C., Larsen, D. H., Povlsen, L. K., … Lukas, J. (2013). ATR Prohibits Replication Catastrophe by Preventing Global Exhaustion of RPA. *Cell*, *155*(5), 1088–1103. https://doi.org/10.1016/J.CELL.2013.10.043
Tora, L., & Timmers, H. T. M. (2010). The TATA box regulates TATA-binding protein (TBP) dynamics in vivo. *Trends in Biochemical Sciences*, *35*(6), 309–314. https://doi.org/10.1016/J.TIBS.2010.01.007
Travesa, A., Kuo, D., Bruin, R. A. M. de, Kalashnikova, T. I., Guaderrama, M., Thai, K., … Wittenberg, C. (2012). DNA replication stress differentially regulates G1/S genes via Rad53-dependent inactivation of Nrm1. *The EMBO Journal*, *31*(7), 1811–1822. https://doi.org/10.1038/EMBOJ.2012.28
Treiber, T., Treiber, N., & Meister, G. (2018). Regulation of microRNA biogenesis and its crosstalk with other cellular pathways. *Nature Reviews Molecular Cell Biology 2018 20:1*, *20*(1), 5–20. https://doi.org/10.1038/s41580-018-0059-1
Trenz, K., Smith, E., Smith, S., & Costanzo, V. (2006). ATM and ATR promote Mre11 dependent restart of collapsed replication forks and prevent accumulation of DNA breaks. *The EMBO Journal*, *25*(8), 1764–1774. https://doi.org/10.1038/SJ.EMBOJ.7601045
Treré, D., Brighenti, E., Donati, G., Ceccarelli, C., Santini, D., Taffurelli, M., … Derenzini, M. (2009). High prevalence of retinoblastoma protein loss in triple-negative breast cancers and its association with a good prognosis in patients treated with adjuvant chemotherapy. *Annals of Oncology*, *20*(11), 1818–1823. https://doi.org/10.1093/ANNONC/MDP209
Trompeter, H.-I., Abbad, H., Iwaniuk, K. M., Hafner, M., Renwick, N., Tuschl, T., … Wernet, P. (2011). MicroRNAs MiR-17, MiR-20a, and MiR-106b Act in Concert to Modulate E2F Activity

on Cell Cycle Arrest during Neuronal Lineage Differentiation of USSC. *PLOS ONE*, *6*(1), e16138. https://doi.org/10.1371/JOURNAL.PONE.0016138

Tsai, K. Y., Hu, Y., Macleod, K. F., Crowley, D., Yamasaki, L., & Jacks, T. (1998). Mutation of E2f-1 Suppresses Apoptosis and Inappropriate S Phase Entry and Extends Survival of Rb-Deficient Mouse Embryos. *Molecular Cell*, *2*(3), 293–304. https://doi.org/10.1016/S1097-2765(00)80274-9

Urbanek-Trzeciak, M. O., Galka-Marciniak, P., Nawrocka, P. M., Kowal, E., Szwec, S., Giefing, M., & Kozlowski, P. (2020). Pan-cancer analysis of somatic mutations in miRNA genes. *EBioMedicine*, *61*. https://doi.org/10.1016/J.EBIOM.2020.103051/ATTACHMENT/30B199BB-C7E3-44F0-9703-B326B8F1A327/MMC17.XLSX

van Bijsterveldt, L., Durley, S. C., Maughan, T. S., & Humphrey, T. C. (2021). The Challenge of Combining Chemo- and Radiotherapy with Checkpoint Kinase Inhibitors. *Clinical Cancer Research*, *27*(4), 937 LP – 962. https://doi.org/10.1158/1078-0432.CCR-20-3358

van den Beucken, T., Koch, E., Chu, K., Rupaimoole, R., Prickaerts, P., Adriaens, M., … Wouters, B. G. (2014). Hypoxia promotes stem cell phenotypes and poor prognosis through epigenetic regulation of DICER. *Nature Communications 2014 5:1*, *5*(1), 1–13. https://doi.org/10.1038/ncomms6203

van den Heuvel, S., & Harlow, E. (1993). Distinct roles for cyclin-dependent kinases in cell cycle control. *Science (New York, N.Y.)*, *262*(5142), 2050–2054. https://doi.org/10.1126/science.8266103

Van Rechem, C., Ji, F., Chakraborty, D., Black, J. C., Sadreyev, R. I., & Whetstine, J. R. (2021). Collective regulation of chromatin modifications predicts replication timing during cell cycle. *Cell Reports*, *37*(1), 109799. https://doi.org/10.1016/J.CELREP.2021.109799

Vassilopoulos, A., Tominaga, Y., Kim, H.-S., Lahusen, T., Li, B., Yu, H., … Deng, C.-X. (2014). WEE1 murine deficiency induces hyper-activation of APC/C and results in genomic instability and carcinogenesis. *Oncogene 2015 34:23*, *34*(23), 3023–3035. https://doi.org/10.1038/onc.2014.239

Vasudevan, S., Tong, Y., & Steitz, J. A. (2007). Switching from repression to activation: MicroRNAs can up-regulate translation. *Science*. https://doi.org/10.1126/science.1149460

Venkatesh, S., & Workman, J. L. (2015). Histone exchange, chromatin structure and the regulation of transcription. *Nature Reviews Molecular Cell Biology 2015 16:3*, *16*(3), 178–189. https://doi.org/10.1038/nrm3941

Vitale, I., Galluzzi, L., Castedo, M., & Kroemer, G. (2011). Mitotic catastrophe: a mechanism for avoiding genomic instability. *Nature Reviews Molecular Cell Biology 2011 12:6*, *12*(6), 385–392. https://doi.org/10.1038/nrm3115

Vitsios, D. M., & Enright, A. J. (2015). Chimira: Analysis of small RNA sequencing data and microRNA modifications. *Bioinformatics*. https://doi.org/10.1093/bioinformatics/btv380

Vouzas, A. E., & Gilbert, D. M. (2021). Mammalian DNA Replication Timing. *Cold Spring Harbor Perspectives in Biology*, *13*(7), a040162. https://doi.org/10.1101/CSHPERSPECT.A040162

Walter, D. M., Venancio, O. S., Buza, E. L., Tobias, J. W., Deshpande, C., Gudiel, A. A., … Feldser, D. M. (2017). Systematic In Vivo Inactivation of Chromatin-Regulating Enzymes Identifies Setd2 as a Potent Tumor Suppressor in Lung Adenocarcinoma. *Cancer Research*, *77*(7), 1719–1729. https://doi.org/10.1158/0008-5472.CAN-16-2159

Wan, G., Zhang, X., Langley, R. R., Liu, Y., Hu, X., Han, C., … Lu, X. (2013). DNA-Damage-Induced Nuclear Export of Precursor MicroRNAs Is Regulated by the ATM-AKT Pathway. *Cell Reports*. https://doi.org/10.1016/j.celrep.2013.05.038

Wang, H., Ach, R. A., & Curry, B. O. (2007). Direct and sensitive miRNA profiling from low-input total RNA. *RNA*. https://doi.org/10.1261/rna.234507

Wang, L. Y., Hung, C. L., Chen, Y. R., Yang, J. C., Wang, J., Campbell, M., … Kung, H. J. (2016). KDM4A Coactivates E2F1 to Regulate the PDK-Dependent Metabolic Switch between Mitochondrial Oxidation and Glycolysis. *Cell Reports*, *16*(11), 3016–3027. https://doi.org/10.1016/j.celrep.2016.08.018

Wang, Yemin, & Taniguchi, T. (2013). MicroRNAs and DNA damage response: Implications for

cancer therapy. *Cell Cycle*, *12*(1), 32. https://doi.org/10.4161/CC.23051
Wang, Yuli, Decker, S. J., & Sebolt-Leopold, J. (2003). Knockdown of Chk1, Wee1 and Myt1 by RNA Interference Abrogates G2 Checkpoint and Induces Apoptosis. *Http://Dx.Doi.Org/10.4161/Cbt.3.3.697*, *3*(3), 305–313. https://doi.org/10.4161/CBT.3.3.697
Weber, B., Stresemann, C., Brueckner, B., & Lyko, F. (2007). Methylation of human MicroRNA genes in normal and neoplastic cells. *Cell Cycle*. https://doi.org/10.4161/cc.6.9.4209
Weinstat-Saslow, D., Merino, M. J., Manrow, R. E., Lawrence, J. A., Bluth, R. F., Wittenbel, K. D., … Steeg, P. S. (1995). Overexpression of cyclin D mRNA distinguishes invasive and in situ breast carcinomas from non-malignant lesions. *Nature Medicine 1995 1:12*, *1*(12), 1257–1260. https://doi.org/10.1038/nm1295-1257
Weinstein, J. N., Collisson, E. A., Mills, G. B., Shaw, K. R. M., Ozenberger, B. A., Ellrott, K., … Kling, T. (2013). The cancer genome atlas pan-cancer analysis project. *Nature Genetics*. https://doi.org/10.1038/ng.2764
Weintraub, S. J., Prater, C. A., & Dean, D. C. (1992). Retinoblastoma protein switches the E2F site from positive to negative element. *Nature 1992 358:6383*, *358*(6383), 259–261. https://doi.org/10.1038/358259a0
Wettersten, H. I., Hwang, S. H., Li, C., Shiu, E. Y., Wecksler, A. T., Hammock, B. D., & Weiss, R. H. (2013). A novel p21 attenuator which is structurally related to sorafenib. *Cancer Biology and Therapy*, *14*(3), 278–285. https://doi.org/10.4161/cbt.23374
Williams, K., Christensen, J., Rappsilber, J., Nielsen, A. L., Johansen, J. V., & Helin, K. (2014). The Histone Lysine Demethylase JMJD3/KDM6B Is Recruited to p53 Bound Promoters and Enhancer Elements in a p53 Dependent Manner. *PLOS ONE*, *9*(5), e96545. https://doi.org/10.1371/JOURNAL.PONE.0096545
Winchester, L., van Bijsterveldt, L., Dhawan, A., Wigfield, S., Triantafyllidis, C., Haider, S., … Buffa, F. M. (2021). Dicer-to-Argonaute switch controls biogenesis of oncogenic miRNA. *BioRxiv*, 2021.08.30.458145. https://doi.org/10.1101/2021.08.30.458145
Winter, J., & Diederichs, S. (2011). Argonaute proteins regulate microRNA stability: Increased microRNA abundance by Argonaute proteins is due to microRNA stabilization. *Http://Dx.Doi.Org/10.4161/Rna.8.6.17665*, *8*(6), 1149–1157. https://doi.org/10.4161/RNA.8.6.17665
Wolter, P., Schmitt, K., Fackler, M., Kremling, H., Probst, L., Hauser, S., … Gaubatz, S. (2012). GAS2L3, a target gene of the DREAM complex, is required for proper cytokinesis and genomic stability. *Journal of Cell Science*, *125*(10), 2393–2406. https://doi.org/10.1242/JCS.097253
Wong, N., & Wang, X. (2015). miRDB: An online resource for microRNA target prediction and functional annotations. *Nucleic Acids Research*. https://doi.org/10.1093/nar/gku1104
Wu, H., Sun, S., Tu, K., Gao, Y., Xie, B., Krainer, A. R., & Zhu, J. (2010). A Splicing-Independent Function of SF2/ASF in MicroRNA Processing. *Molecular Cell*, *38*(1), 67. https://doi.org/10.1016/J.MOLCEL.2010.02.021
Xiang, W., He, J., Huang, C., Chen, L., Tao, D., Wu, X., … Jiang, G. (2015). miR-106b-5p targets tumor suppressor gene SETD2 to inactive its function in clear cell renal cell carcinoma. *Oncotarget*, *6*(6), 4066–4079. https://doi.org/10.18632/oncotarget.2926
Xiao, C., Fan, T., Tian, H., Zheng, Y., Zhou, Z., Li, S., … He, J. (2021). H3K36 trimethylation-mediated biological functions in cancer. *Clinical Epigenetics 2021 13:1*, *13*(1), 1–19. https://doi.org/10.1186/S13148-021-01187-2
Xiong, Y., Connolly, T., Futcher, B., & Beach, D. (1991). Human D-type cyclin. *Cell*, *65*(4), 691–699. https://doi.org/10.1016/0092-8674(91)90100-D
Xu, M., Sheppard, K. A., Peng, C. Y., Yee, A. S., & Piwnica-Worms, H. (1994). Cyclin A/CDK2 binds directly to E2F-1 and inhibits the DNA-binding activity of E2F-1/DP-1 by phosphorylation. *Molecular and Cellular Biology*, *14*(12), 8420–8431. https://doi.org/10.1128/mcb.14.12.8420-8431.1994
Xu, Q., Xiang, Y., Wang, Q., Wang, L., Brind'Amour, J., Bogutz, A. B., … Xie, W. (2019). SETD2 regulates the maternal epigenome, genomic imprinting and embryonic development. *Nature Genetics 2019 51:5*, *51*(5), 844–856. https://doi.org/10.1038/s41588-019-0398-7

Yang, J.-S., Maurin, T., Robine, N., Rasmussen, K. D., Jeffrey, K. L., Chandwani, R., … Lai, E. C. (2010). Conserved vertebrate mir-451 provides a platform for Dicer-independent, Ago2-mediated microRNA biogenesis. *Proceedings of the National Academy of Sciences*, *107*(34), 15163–15168. https://doi.org/10.1073/PNAS.1006432107

Yao, X., Anderson, K. L., & Cleveland, D. W. (1997). The Microtubule-dependent Motor Centromere–associated Protein E (CENP-E) Is an Integral Component of Kinetochore Corona Fibers That Link Centromeres to Spindle Microtubules. *The Journal of Cell Biology*, *139*(2), 435. https://doi.org/10.1083/JCB.139.2.435

Young, L. A., O'Connor, L. O., Renty, C. de, Veldman-Jones, M. H., Dorval, T., Wilson, Z., … O'Connor, M. J. (2019). Differential Activity of ATR and WEE1 Inhibitors in a Highly Sensitive Subpopulation of DLBCL Linked to Replication Stress. *Cancer Research*, *79*(14), 3762–3775. https://doi.org/10.1158/0008-5472.CAN-18-2480

Zeman, M. K., & Cimprich, K. A. (2014). Causes and consequences of replication stress. *Nature Cell Biology*, *16*(1), 2–9. https://doi.org/10.1038/ncb2897

Zhang, B., Tang, C., Yao, Y., Chen, X., Zhou, C., Wei, Z., … Liu, Q. (2021). The tumor therapy landscape of synthetic lethality. *Nature Communications 2021 12:1*, *12*(1), 1–11. https://doi.org/10.1038/s41467-021-21544-2

Zhang, H., Sheng, C., Yin, Y., Wen, S., Yang, G., Cheng, Z., & Zhu, Q. (2015). PABPC1 interacts with AGO2 and is responsible for the microRNA mediated gene silencing in high grade hepatocellular carcinoma. *Cancer Letters*, *367*(1), 49–57. https://doi.org/10.1016/J.CANLET.2015.07.010

Zhang, J., Cavallaro, M., & Hebenstreit, D. (2021). Timing RNA polymerase pausing with TV-PRO-seq. *Cell Reports Methods*, *1*(6), None. https://doi.org/10.1016/J.CRMETH.2021.100083

Zhang, L., Huang, J., Yang, N., Greshock, J., Megraw, M. S., Giannakakis, A., … Coukos, G. (2006). microRNAs exhibit high frequency genomic alterations in human cancer. *Proceedings of the National Academy of Sciences of the United States of America*. https://doi.org/10.1073/pnas.0508889103

Zhang, X., Wan, G., Berger, F. G., He, X., & Lu, X. (2011). The ATM Kinase Induces MicroRNA Biogenesis in the DNA Damage Response. *Molecular Cell*, *41*(4), 371–383. https://doi.org/10.1016/J.MOLCEL.2011.01.020

Zhang, Y., Liu, T., Meyer, C. A., Eeckhoute, J., Johnson, D. S., Bernstein, B. E., … Liu, X. S. (2008). Model-based Analysis of ChIP-Seq (MACS). *Genome Biology 2008 9:9*, *9*(9), 1–9. https://doi.org/10.1186/GB-2008-9-9-R137

Zhang, Y. W., Jones, T. L., Martin, S. E., Caplen, N. J., & Pommier, Y. (2009). Implication of checkpoint kinase-dependent up-regulation of ribonucleotide reductase R2 in DNA damage response. *Journal of Biological Chemistry*. https://doi.org/10.1074/jbc.M109.003020

Zhao, Z.-M., Yost, S. E., Hutchinson, K. E., Li, S. M., Yuan, Y.-C., Noorbakhsh, J., … Yuan, Y. (2019). CCNE1 amplification is associated with poor prognosis in patients with triple negative breast cancer. *BMC Cancer 2019 19:1*, *19*(1), 1–11. https://doi.org/10.1186/S12885-019-5290-4

Zhu, K., Lei, P. J., Ju, L. G., Wang, X., Huang, K., Yang, B., … Wu, M. (2017). SPOP-containing complex regulates SETD2 stability and H3K36me3-coupled alternative splicing. *Nucleic Acids Research*, *45*(1), 92. https://doi.org/10.1093/NAR/GKW814

Zhu, Q., Yang, Q., Lu, X., Wang, H., Tong, L., Li, Z., … Zhu, W.-G. (2021). SETD2-mediated H3K14 trimethylation promotes ATR activation and stalled replication fork restart in response to DNA replication stress. *Proceedings of the National Academy of Sciences*, *118*(23), 2021. https://doi.org/10.1073/PNAS.2011278118

Zhu, X., He, F., Zeng, H., Ling, S., Chen, A., Wang, Y., … Wang, Q. (2014). Identification of functional cooperative mutations of SETD2 in human acute leukemia. *Nature Genetics 2014 46:3*, *46*(3), 287–293. https://doi.org/10.1038/ng.2894

Ziebarth, J. D., Bhattacharya, A., & Cui, Y. (2012). Integrative Analysis of Somatic Mutations Altering MicroRNA Targeting in Cancer Genomes. *PLoS ONE*. https://doi.org/10.1371/journal.pone.0047137

Zou, L., & Elledge, S. J. (2003). Sensing DNA Damage Through ATRIP Recognition of RPA-ssDNA

Complexes. *Science*, *300*(5625), 1542–1548. https://doi.org/10.1126/SCIENCE.1083430